JAERI-M
94-015

UCLA-FNT-75
UCLA-ENG-93-85

PHASE III EXPERIMENTS OF THE JAERI/USDOE COLLABORATIVE PROGRAM ON FUSION BLANKET NEUTRONICS

—— LINE SOURCE AND ANNULAR BLANKET EXPERIMENTS ——

VOLUME I : EXPERIMENT

February 1994

Yukio OYAMA
Chikara KONNO
Yujiro IKEDA
Fujio MAEKAWA
Kazuaki KOSAKO
Tomoo NAKAMURA
Hiroshi MAEKAWA
Mahmoud Z. YOUSSEF
Anil KUMAR
Mohamed A. ABDOU
Yoichi WATANABE
Edgar F. BENNETT

日 本 原 子 力 研 究 所
Japan Atomic Energy Research Institute

JAERI-Mレポートは，日本原子力研究所が不定期に公刊している研究報告書です。
入手の問合わせは，日本原子力研究所技術情報部情報資料課（〒319-11茨城県那珂郡東海村）あて，お申しこしください。なお，このほかに財団法人原子力弘済会資料センター（〒319 11 茨城県那珂郡東海村日本原子力研究所内）で複写による実費頒布をおこなっております。

JAERI-M reports are issued irregularly.
Inquiries about availability of the reports should be addressed to Information Division Department of Technical Information, Japan Atomic Energy Research Institute, Tokai-mura, Naka-gun, Ibaraki-ken 319-11, Japan.

©Japan Atomic Energy Research Institute, 1994

編集兼発行　日本原子力研究所
印　　刷　いばらき印刷㈱

JAERI-M 94-015

UCLA-FNT-75

UCLA-ENG-93-85

Phase III Experiments of the JAERI/USDOE Collaborative Program on Fusion Blanket Neutronics*

- Line Source and Annular Blanket Experiments - Volume I: Experiment

JAERI

Yukio OYAMA, Chikara KONNO
Yujiro IKEDA, Fujio MAEKAWA
Kazuaki KOSAKO*1, Tomoo NAKAMURA
Hiroshi MAEKAWA

U.S.A.

Mahmoud Z. YOUSSEF(UCLA+)
Anil KUMAR (UCLA)
Mohamed A. ABDOU (UCLA)
Yoichi WATANABE*2 (UCLA)
Edgar F. BENNETT (ANL++)

Edited by Yukio OYAMA

Department of Reactor Engineering
Tokai Research Establishment
Japan Atomic Energy Research Institute
Tokai-mura, Naka-gun, Ibaraki-ken

(Received January 20, 1994)

A pseudo-line source has been realized by using an accelerator based D-T point neutron source. The pseudo-line source is obtained by time averaging of continuously moving point source or by superposition of

---

* Program Managers: H. Maekawa (JAERI), M. Abdou (USA)

+ Mechanical, Aerospace, and Nuclear Engineering Department, School of Engineering and Applied Science, University of California at Los Angeles, Los Angeles, CA 90024

++ Fusion Power Program-Bldg.205, Argonne National Laboratory, 9700 South Cass Avenue Argonne, Illinois 60439

*1 Nuclear Energy Data Center

*2 Innovative Nuclear Space Power Institute, University of Florida

finely distributed point sources. The line source is utilized for fusion blanket neutronics experiments with an annular geometry so as to simulate a part of a tokamak reactor. The source neutron characteristics were measured for two operational modes for the line source, continuous and step-wise modes, with the activation foil and the NE213 detectors, respectively. In order to give a source condition for a successive calculational analysis on the annular blanket experiment, the neutron source characteristics was calculated by a Monte Carlo code. The reliability of the Monte Carlo calculation was confirmed by comparison with the measured source characteristics. The shape of the annular blanket system was a rectangular (1300 × 1300 mm^2 square and 2040 mm length) with an inner cavity (425.5 × 425.5 mm^2 square). The annular blanket was consist of 15 mm-thick first wall (SS304) and 406 mm-thick breeder zone with Li_2O at inside and Li_2CO_3 at outside. The line source was produced at the center of the inner cavity by moving the annular blanket system in the span of 2 m. Three annular blanket configurations were examined; the reference blanket, the blanket covered with 25 mm thick graphite armor and the armor-blanket with a large opening (425.4 mm × 376 mm). The neutronics parameters of tritium production rate, neutron spectrum and activation reaction rate were measured with specially developed techniques such as multi-detector data acquisition system, spectrum weighting function method and ramp controlled high voltage system. The present experiment provides unique data for a higher step of benchmark to test a reliability of neutronics design calculation for a realistic tokamak reactor.

Keywords: Tokamak Reactor, Tritium Breeding Blanket, Integral Experiment, Line Source, Annular Blanket, Armor, Fusion Neutron

JAERI-M 94-015

UCLA-FNT-75
UCLA-ENG-93-85

核融合ブランケット中性子工学に関する原研／米国エネルギー省協力計画フェイズⅢ実験*

－線状線源と環状ブランケットについての実験と解析－
第一部：実験

日本原子力研究所東海研究所原子炉工学部

（編者）大山　幸夫

（原研）

大山　幸夫　　今野　　力
池田裕二郎　　前川　藤夫
小迫　和明*1　中村　知夫
前川　　洋

（米国）

Mahmoud Z. YOUSSEF(UCLA)
Anil KUMAR(UCLA)
Mohamed A. Abdou(UCLA)
Yoichi WATANABE(UCLA)*2
Edgar F. BENNETT(ANL)

（1994年1月20日受理）

加速器型点状Ｄ－Ｔ中性子源を用いて擬似線状線源を実現した。擬似線状線源は，連続的に動く点状線源を時間平均するか，または細かく分布した点状線源を重ね合わせることによって得られる。この線状線源はトカマク炉を部分模擬するために環状形状での核融合ブランケット中性子工学実験を行うのに用いられる。線源特性実験は連続とステップ状の２種類の運転モードに対して，各々放射化法とＮＥ213検出器を用いて行われた。これを用いて行う環状ブランケット実験の線源条件を与えるために，モンテカルロ計算で特性を求め，この計算の信頼性を実験と比較することで確認した。実験体系は内部に（425.5×425.5mm²角の）空洞を持つ直方体（外形1300×1300mm²角，2040mm長さ）である。試験ブランケットは15mm厚の第一壁（SS304）と406mm厚のトリチウム増殖層（内側Li_2O，外側Li_2CO_3）で環状ブランケットを２ｍにわたって動かすことで，線状線源を空洞の中心で発生した。３種類のブランケット配置について実験を行った。即ち，基準体系，25mm厚の黒鉛層によるアーマー体系及び425.4mm×376mmの大口径開口部のある体系である。多検出器データ収

東海研究所：〒319－11　茨城県那珂郡東海村白方字白根２－４

＊ 核融合炉ブランケット中性子工学に関する原研／米国ＤＯＥ協力計画
　　プログラムマネージャー：前川　洋（原研），M.A.Abdou（米国）

*1　原子力データセンター
*2　フロリダ大学

集システム，荷重関数法及び高電圧掃引方式の新たに開発した手法を用いて，これらの体系内でトリチウム生成率，中性子スペクトル，放射化反応率の測定を行った。この実験データは実際のトカマク炉の設計計算の信頼度を調べるのに適した，従来より高度なベンチマークデータを与える。

Contents

1. Introduction 1
2. Line Source Preparation 7
2.1 Introduction 7
2.2 Line Source System 7
2.2.1 Realization of Line Source 7
2.2.2 Design and Operation Control of Carriage Deck System 8
2.2.3 Long Tube Neutron Target and Neutron Monitor 10
2.3 Characteristics of the FNS Line Source 11
2.3.1 Experiment of Line Source Characteristics 11
2.3.1.1 Measurement for Stepwise Mode 12
2.3.1.2 Measurement for Continuous Mode 13
2.3.2 Calculation of Line Source Characteristics 15
2.3.2.1 Monte Carlo Calculation of the Long Tube Target 16
2.3.2.2 Reliability of the Line Source Model for Calculation . 17
2.4 Concluding Remarks 18
3. Annular Blanket Experiment 54
3.1 Introduction 54
3.2 Annular Blanket Assembly 55
3.2.1 Reference Test Blanket (Phase IIIA) 55
3.2.2 Armor Test Blanket (Phase IIIB) 56
3.2.3 Large Opening Test Blanket (Phase IIIC) 56
3.3 Measurements 57
3.3.1 Proton Recoil Gas Proportional Counter (PRC) 58
3.3.2 Li-glass Detector with Multi-detector Data Acquisition System 58
3.3.3 NE213 Detector with Spectrum Weighting Function Method .. 59
3.3.4 Activation Foil Detector 60
3.4 Experimental Results and Discussions 61
3.4.1 Neutron Spectrum 61
3.4.2 Tritium Production Rate 63
3.4.3 Activation Reaction Rate 64
3.5 Concluding Remarks 66
4. Summary 126
Acknowledgment 127
References 128

Appendix 1 Calculated Angle Dependent Neutron Spectra emitted from Long Tube Water Cooled Target Assembly 132
Appendix 2 Neutron Spectra for the Fixed Source Measured by PRC ... 151
Appendix 3 Results of Tritium Production Rates Measured by Li_2O Pellets 166
Appendix 4 Measurements of Gamma-ray Responses 178

目　　次

1. はじめに …… 1
2. 線状線源の整備 …… 7
2.1 序　論 …… 7
2.2 線状線源システム …… 7
2.2.1 線状線源の実現 …… 7
2.2.2 移動架台システムの設計と駆動制御 …… 8
2.2.3 長尺ターゲットと中性子モニター …… 10
2.3 FNS線状線源の特性 …… 11
2.3.1 線状線源特性実験 …… 11
2.3.1.1 ステップモードの実験 …… 12
2.3.1.2 連続モードの実験 …… 13
2.3.2 線状線源特性の計算 …… 15
2.3.2.1 長尺ターゲットのモンテカルロ計算 …… 16
2.3.2.2 計算の線状線源モデルの信頼性 …… 17
2.4 結　語 …… 18
3. 環状ブランケット実験体系 …… 54
3.1 序　論 …… 54
3.2 環状ブランケット実験体系 …… 55
3.2.1 基準試験ブランケット体系（Phase ⅢA） …… 55
3.2.2 アーマー試験ブランケット体系（Phase ⅢB） …… 56
3.2.3 大開口部付試験ブランケット体系（Phase ⅢC） …… 56
3.3 測　定 …… 57
3.3.1 反跳陽子比例計数管（PRC） …… 58
3.3.2 多検出器データ収集システムによるリチウムガラス検出器 …… 58
3.3.3 スペクトル荷重関数法によるNE213検出器 …… 59
3.3.4 放射化箔検出器 …… 60
3.4 実験結果と議論 …… 61
3.4.1 中性子スペクトル …… 61
3.4.2 トリチウム生成率 …… 63
3.4.3 放射化反応率 …… 64
3.5 結　語 …… 66
4. まとめ …… 126

謝　辞 …… 127
参考文献 …… 128
付録１　計算で得られた長尺水冷ターゲットから放出される角度依存中性子
　　エネルギースペクトル …… 132
付録２　PRCで測定された固定線源からの中性子スペクトル …… 151
付録３　Li_2Oペレットでのトリチウム生成率測定結果 …… 166
付録４　ガンマ線応答の測定 …… 178

List of Tables

Chapter 1

Table 1.1 Experimental features of JAERI/USDOE collaborative experiments on fusion blanket neutronics

Chapter 2

Table 2.3.1 Measured flux distributions around the long tube water cooled (LTWC) target assembly

Table 2.3.2 Superposed neutron flux distributions obtained from the NE213 measurement

Table 2.3.3 Activation reactions used in the source characteristics measurement

Table 2.3.4 Reaction rate distributions along the line source at a distance of 219 mm from the line source without blanket (distance is measured from beam drift tube side)

Table 2.3.5 Calculated neutron emission intensity for each emission angle; (a) Horizontal plane and (b) Vertical plane

Chapter 3

Table 3.2.1 Homogenized atomic densities of material used in the Phase III test blanket

Table 3.3.1 Techniques applied to nuclear parameter measurements in the annular blanket experiments Phase III

Table 3.3.2 Nuclear parameters of activation reactions used in the experiment

Table 3.4.1(a) Measured neutron flux by the NE213 spectrometer at the surface of Phase IIIA assembly

Table 3.4.1(b) Measured neutron flux by the NE213 spectrometer inside of Phase IIIA assembly

Table 3.4.1(c) Measured neutron flux by the NE213 spectrometer at the surface of Phase IIIB assembly

Table 3.4.1(d) Measured neutron flux by the NE213 spectrometer inside of Phase IIIB assembly

Table 3.4.2(a) Measured neutron flux by the PRC spectrometer at the surface of Phase IIIA assembly

Table 3.4.2(b) Measured neutron flux by the PRC spectrometer inside of Phase IIIA assembly

Table 3.4.2(c) Measured neutron flux by the PRC spectrometer at the surface of Phase IIIB assembly

Table 3.4.2(d) Measured neutron flux by the PRC spectrometer inside of Phase IIIB

assembly
Table 3.4.2(e) Measured neutron flux by the PRC spectrometer at the surface of Phase IIIC assembly (hole side)
Table 3.4.2(f) Measured neutron flux by the PRC spectrometer at the surface of Phase IIIC assembly (normal side)
Table 3.4.3 Tritium production rate of ^{7}Li for the line source measured by the NE213 detector (^{7}Li(n,n'α)^{3}T cross section from JENDL-3 was used)
Table 3.4.4 Tritium production rate of ^{6}Li for the line source measured by the Li-glass detector
Table 3.4.5 Reaction rate distributions along the line source at a distance of 219 mm from the line source for the reference test blanket (Phase IIIA)
Table 3.4.6 Reaction rate distribution along radial direction at central drawer (drawer B) for the reference (Phase IIIA) test blanket
Table 3.4.7 Reaction rate distribution along radial direction at off-central drawer (drawer C) for the reference (Phase IIIA) test blanket
Table 3.4.8 Reaction rate distributions along the line source at a distance of 187 mm from the line source for the armor test blanket (Phase IIIB)
Table 3.4.9 Reaction rate distribution along radial direction at central drawer (drawer B) for the armor (Phase IIIB) test blanket
Table 3.4.10 Reaction rate distribution along radial direction at off-central drawer (drawer C) for the armor (Phase IIIB) test blanket
Table 3.4.11 Reaction rate distributions along the line source at a distance of 187 mm from the source axis for the opening (Phase IIIC) test blanket (normal side)
Table 3.4.12 Reaction rate distributions along the line source at a distance of 187 mm from the source axis for the opening (Phase IIIC) test blanket (opening side)
Table 3.4.13 Reaction rate distributions along the line source for the opening (Phase IIIC) test blanket (inside of opening)
Table 3.4.14 Reaction rate distribution along radial direction at central drawer (drawer B) for the opening (Phase IIIC) test blanket
Table 3.4.15 Reaction rate distribution along radial direction in drawer D for the opening (Phase IIIC) test blanket

Appendix
Table A.1 Calculated angle dependent neutron spectra emitted from long tube water cooled target assembly (neutron/group/total emission)
Table A.2.1 Measured neutron flux by the PRC spectrometer at a distance of 300 mm from the line source axis (at a position of 0 mm from the position closest to the

source on the 300 mm axis)
Table A.2.2 Measured neutron flux by the PRC spectrometer at a distance of 300 mm from the line source axis (at a position of 500 mm forward from the position closest to the source on the 300 mm axis)
Table A.2.3 Measured neutron flux by the PRC spectrometer at a distance of 300 mm from the line source axis (at a position of 500 mm backward from the position closest to the source on the 300 mm axis)
Table A.2.4 Measured neutron flux by the PRC spectrometer at a surface of the Phase IIIA assembly (at a position of 0 mm from the position closest to the source on the surface)
Table A.2.5 Measured neutron flux by the PRC spectrometer at a surface of the Phase IIIA assembly (at a position of 500 mm forward from the position closest to the source on the surface)
Table A.2.6 Measured neutron flux by the PRC spectrometer at a surface of the Phase IIIA assembly (at a position of 500 mm backward from the position closest to the source on the surface)
Table A.2.7 Measured neutron flux by the PRC spectrometer inside of the Phase IIIA assembly (at a position of 0 mm from the position closest to the source on the surface)
Table A.2.8 Measured neutron flux by the PRC spectrometer inside of the Phase IIIA assembly (at a position of 500 mm forward from the position closest to the source on the surface)
Table A.2.9 Measured neutron flux by the PRC spectrometer inside of the Phase IIIA assembly (at a position of 500 mm backward from the position closest to the source on the surface)
Table A.3.1 Tritium production rate measured by the $^{6}Li_2O$ pellet
Table A.3.2 Tritium production rate measured by the $^{7}Li_2O$ pellet
Table A.3.3 Tritium production rate measured by the $^{n}Li_2O$ pellet
Table A.4.1 Calculated neutron response of TLDs
Table A.4.2 TLD results for the line source without assembly
Table A.4.3 TLD results for the reference test blanket
Table A.4.4 TLD results for the armor blanket

List of Figures

Chapter 1

Fig. 1.1 Stages for simulation of neutron source and blanket configuration in the integral experiments at FNS

Fig. 1.2 Strategy of the JAERI/USDOE collaborative program on fusion blanket neutronics to extrapolate test data to a fusion reactor environment

Chapter 2

Fig. 2.2.1 Concept of the FNS line source system

Fig. 2.2.2 Experimental room, moving deck and beam drift tube (top view)

Fig. 2.2.3 Experimental room, moving deck and beam drift tube (side view)

Fig. 2.2.4 Photograph of carriage-deck and annular blanket assembly

Fig. 2.2.5 Illustration of importance (adjoint flux) distribution for a detector location

Fig. 2.2.6 Long tube water cooled target (LTWC) assembly

Fig. 2.2.7 Typical record of neutron emission yield and deck position as a function of irradiation time

Fig. 2.3.1 Experimental setup for neutron flux distribution measurement around the target assembly using a miniature NE213 detectors

Fig. 2.3.2 Measured positions to obtain the line source characteristics. The 81 point data along the source axis were taken for one distance.

Fig. 2.3.3 Measured flux distributions at each distance from the line source axis

Fig. 2.3.4 Flux distribution for an ideal line source with uniform density and isotropic emission

Fig. 2.3.5 Superposed neutron flux for virtual line source of 2 m in length

Fig. 2.3.6 Comparison of the measured superposed flux to the calculation for ideal source with uniform and isotropic emission

Fig. 2.3.7 Dependence of superposed flux distribution on the interval of source step (comparison in the 5 cm step distribution)

Fig. 2.3.8 Correction factor of neutron flux variance at each foil position shown for the cases of three different decay times

Fig. 2.3.9 Foil locations for the source characteristics measurement with the continuous mode operation

Fig. 2.3.10 Measured reaction rate distributions at 219 mm distance from the present line source

Fig. 2.3.11 Asymmetry of reaction rate distribution. Ratios to the central value are plotted
Fig. 2.3.12 Geometrical model for MORSE-DD Monte Carlo code to calculate neutron emission spectrum from the LTWC target. (a) water cooling channel and cup-shaped tritium metal target, (b) water cover, (c) water feed pipe bended in parallel to the drift tube and (d) drift tube (target side)
Fig. 2.3.13 Angular dependence of neutron emission yield in vertical and horizontal planes
Fig. 2.3.14 Calculated neutron energy spectra for three directions emitted from the target
Fig. 2.3.15 Comparison of the calculated flux distribution along the target assembly with the experiment
Fig. 2.3.16 Comparison of the (n,2n) reactions to the calculations
Fig. 2.3.17 Comparison of the (n,p) reactions to the calculations
Fig. 2.3.18 Comparison of the lower threshold reactions to the calculations

Chapter 3
Fig. 3.1.1 Illustration of candidate blanket configurations with variations of asymmetry, heterogeneity and source condition
Fig. 3.2.1 Cross section of the reference configuration of annular test blanket assembly
Fig. 3.2.2 First wall surface with detector holes plugged by disks
Fig. 3.2.3 Photograph of the annular test blanket and the drift tube of long tube water cooled target assembly
Fig. 3.2.4 Armor test blanket. The 25 mm thick graphite layer is attached to the reference blanket
Fig. 3.2.5 Cross section of the armor test blanket and its dimensions
Fig. 3.2.6 Large opening test blanket assembly and dimensions
Fig. 3.2.7 Photograph of the opening in the Phase IIIC test blanket

Fig. 3.3.1 Multi-detector data acquisition system for simultaneous measurement of ^{7}Li and ^{6}Li glass detectors
Fig. 3.3.2 Virtual step response of the NE213 detector to act as an integral flux detector

Fig. 3.4.1 Comparison of source neutron spectra measured at the surface of test blanket between the point source experiment Phase II and the line source experiment Phase III
Fig. 3.4.2 Measured spectra at the surface and inside of the reference blanket by the NE213 and the PRC spectrometers

Fig. 3.4.3 Measured spectra inside the blanket for the reference (IIIA) and the armor (IIIB) test blankets

Fig. 3.4.4 Comparison of low energy spectra measured at both sides of the surface of the opening test blanket.

Fig. 3.4.5 Source position-wise profile of the energy integrated neutron flux measured by the PRC spectrometer (a) at the FW surface and (b) inside of the reference blanket (Phase IIIA)

Fig. 3.4.6 Source position-wise profile of the energy integrated neutron flux measured by the PRC spectrometer (a) at the graphite surface and (b) inside of the armor blanket (Phase IIIB)

Fig. 3.4.7 Source position-wise profile of the energy integrated neutron flux measured by the PRC spectrometer (a) at the opening side and (b) no-opening side of the graphite surfaces of the large opening test blanket (Phase IIIC)

Fig. 3.4.8 Source position-wise ^{7}Li tritium production rate (TPR) profile measured by the NE213 detector in the central drawer for three blankets of (a) Phase IIIA, (b) IIIB and (c) IIIC (reference, armor and opening)

Fig. 3.4.9 Source profile comparison of integrated fast neutron flux between the measurements at the positions with and without assembly

Fig. 3.4.10 Source position-wise ^{6}Li tritium production rate (TPR) profile measured by the Li-glass detector in the central drawer for three blankets of (a) Phase IIIA, (b) IIIB and (c) IIIC (reference, armor and opening)

Fig. 3.4.11 Effect of opening on the source position-wise ^{6}Li-TPR profile

Fig. 3.4.12 Superposed results of the source position-wise ^{7}Li tritium production rate (TPR) corresponding to the line source; (a) drawer A at a distance of -500 mm from the center (backward), (b) drawer B at the center and (c) drawer C at a distance of +500 mm from the center (forward).

Fig. 3.4.13 Superposed results of the source position-wise ^{6}Li tritium production rate (TPR) corresponding to the line source; (a) drawer B at the center and (b) drawer C at a distance of +500 mm from the center (forward).

Fig. 3.4.14 Activation reaction rate distribution along the line source at the first wall surface of the reference (IIIA) blanket

Fig. 3.4.15 Relative ratios of the reaction rates in the reference (IIIA) to in the source itself (source characteristics experiment)

Fig. 3.4.16 Radial distributions of activation reaction rates in the reference blanket ; (a) drawer B at the center and (b) drawer C at the forward

Fig. 3.4.17 Activation reaction rate distribution along the line source at the graphite surface of the armor (IIIB) blanket

Fig. 3.4.18 Radial distributions of activation reaction rates in the armor blanket ; (a) drawer B at the center and (b) drawer C at the forward

Fig. 3.4.19 Two foil arrangements in the drawer D to measure the distributions near the opening in the test blanket (IIIC)

Fig. 3.4.20 Distributions of reaction rates on the graphite surface of both sides with and without a opening; (a) $^{93}Nb(n,2n)^{92m}Nb$ reaction, (b) $^{115}In(n,n')^{115m}In$ reaction and (c) $^{197}Au(n,\gamma)^{198}Au$ reaction

Fig. 3.4.21 Radial distributions of activation reaction rates in the opening test blanket (drawer B at the center)

Fig. 3.4.22 Distributions of reaction rates inside of the opening; (a) $^{93}Nb(n,2n)^{92m}Nb$ reaction, (b) $^{115}In(n,n')^{115m}In$ reaction and (c) $^{197}Au(n,\gamma)^{198}Au$ reaction

Fig. 3.4.23 Radial distributions of activation reaction rates near the opening in the opening test blanket (drawer D)

Fig. 3.4.24 Comparisons of (a) radial distributions and (b) distributions along the line source of $^{197}Au(n,\gamma)^{198}Au$ activation reaction rates among the three test blankets

Fig. A.2.1 Relative position of the detector to the target

Fig. A.2.2 Measured neutron flux by the PRC spectrometer at a distance of 300 mm from the line source axis (at a position of 0 mm from the position closest to the source on the 300 mm axis)

Fig. A.2.3 Measured neutron flux by the PRC spectrometer at a distance of 300 mm from the line source axis (at a position of 500 mm forward from the position closest to the source on the 300 mm axis)

Fig. A.2.4 Measured neutron flux by the PRC spectrometer at a distance of 300 mm from the line source axis (at a position of 500 mm backward from the position closest to the source on the 300 mm axis)

Fig. A.2.5 Measured neutron flux by the PRC spectrometer at a surface of the Phase IIIA assembly (at a position of 0 mm from the position closest to the source on the surface)

Fig. A.2.6 Measured neutron flux by the PRC spectrometer at a surface of the Phase IIIA assembly (at a position of 500 mm forward from the position closest to the source on the surface)

Fig. A.2.7 Measured neutron flux by the PRC spectrometer at a surface of the Phase IIIA assembly (at a position of 500 mm backward from the position closest to the source on the surface)

Fig. A.2.8 Measured neutron flux by the PRC spectrometer inside of the Phase IIIA assembly (at a position of 0 mm from the position closest to the source on the surface)
Fig. A.2.9 Measured neutron flux by the PRC spectrometer inside of the Phase IIIA assembly (at a position of 500 mm forward from the position closest to the source on the surface)
Fig. A.2.10 Measured neutron flux by the PRC spectrometer inside of the Phase IIIA assembly (at a position of 500 mm backward from the position closest to the source on the surface)

Fig. A.3.1 Comparison of the results from $^{nat}Li_2O$ pellet and the results composed from the results of $^{7}Li_2O$ and $^{6}Li_2O$ pellets
Fig. A.3.2 The results obtained from $^{6}Li_2O$ pellets
Fig. A.3.3 The results obtained from $^{7}Li_2O$ pellets
Fig. A.3.4 Relative ratio of the T_n results of each experimental run to the first measurement in the armor blanket experiment (Phase IIIB)
Fig. A.3.5 Relative ratio of the T_7 results of each experimental run to the first measurement in the armor blanket experiment (Phase IIIB)
Fig. A.3.6 Relative ratio of the T_6 results of each experimental run to the first measurement in the armor blanket experiment (Phase IIIB)
Fig. A.4.1 Cross sectional drawing of 40 mm-diameter spherical NE213 detector
Fig. A.4.2 Detector position for gamma-ray spectrum measurement
Fig. A.4.3 Measured gamma-ray spectrum at 266 mm distance from the line source in the B drawer (Phase IIIB)
Fig. A.4.4 Measured gamma-ray spectrum at 418 mm distance from the line source in the B drawer (Phase IIIB)
Fig. A.4.5 Measured gamma-ray spectrum at 517 mm distance from the line source in the B drawer (Phase IIIB)
Fig. A.4.6 Positions of TLDs in gamma-ray exposure dose measurement without assembly. (unit in mm)
Fig. A.4.7 Positions of TLDs in gamma-ray exposure dose measurement Phase IIIA assembly. (unit in mm)
Fig. A.4.8 Positions of TLDs in gamma-ray exposure dose measurement Phase IIIB assembly. (unit in mm)
Fig. A.4.9 Neutron responses calculated for various TL detectors
Fig. A.4.10 Exposure dose distributions measured by various TLDs for the line source without assembly

Fig. A.4.11 Exposure dose distributions measured by various TLDs for the Phase IIIA assembly

Fig. A.4.12 Exposure dose distributions measured by various TLDs for the Phase IIIA assembly

1. Introduction

In a D-T fueled thermonuclear fusion system, fusion energy is shared into fast neutrons of 14.1 MeVand alpha particles of 3.5 MeV, respectively. Alpha particles are used for plasma heating and neutrons are introduced to a blanket with the essential functions for reality of fusion utilization, i.e., energy conversion, tritium recycle and radiation safety. Fast neutrons bring about a number of fundamental and technical problems, directly and indirectly, on the reactor design. Neutrons enetering into the surrounding components concern, through various nuclear processes, to heat generation, tritium production, induced activities, radiation damage and so on. They, in turn, affect the material selection, heat removal, tritium extraction, shielding arrangement, maintenance scheme and rad-waste management. Therefore, prediction of basic neutronics performance in the reactor is required as accurately as possible to reduce the ambiguity in the input data for the design of the other non-nuclear engineering elements.

At the stage to initiate an engineering design activity for the next fusion devices such as, ITER, FER or NET, it is required that the nuclear data and calculation methods to be well validated by experiments. Until now many integral neutronics experiments have been conducted at fusion neutronics source (FNS)[1] of JAERI, OKTAVIAN[2] of Osaka University, LOTUS[3] of Ecole Polytechnique Federale de Lausanne in Switzerland and others. However, experimental efforts have been limited to small-scaled and simple ones,[4-6] while the realistic blanket design such as a tokamak becomes rather complicated and the calculation tools and methods are not confined in simple one dimension which has been used in the scoping analysis. There must exists a gap of prediction accuracy of design parameters between simple experiments and realistic reactor configurations. These factors include not only neutron cross section but also approximation of system description, modeling of geometry and estimation method for nuclear parameters, and so on.[7,8]

The JAERI/USDOE collaborative program on fusion blanket neutronics was initiated to examine the current accuracy of the nuclear parameter prediction with help of large scaled blanket experiments by effective use of facility, materials and technical resources of both parties. The collaborative program started in 1984 with the objectives: 1) to establish new experimental methods for design supportive neutronics experiments, 2) to provide experimental data base, 3) to assess the current status of the accuracy of nuclear data, nuclear response data and calculation method used in the design and 4) to develop neutronics technology for nuclear performance test in a next fusion experimental reactor. The program is devided into three phases depending on the basic concept of geometrical configuration of neutron source and test blanket as shown in Fig. 1.1.[9] Simplified arrangement is required for

basic neutronics integral experiments to assure unambiguos interpreteation in the comparison between the measurements and the calculations. In an engineering sense, a mock-up experiment can directly validate the design accuracy. These stepped-up tests of neutronic design are naturally arisen in a stage up to final goal of fusion reactor design. There are many parameters to identify the fusion reactor systems from a variety of fusion blanket design studies. However, two parameters can be selected to indicate essential effects for neutronic behavior. One is geometrical configuration and another is material combination. On these parameter axes, three experimental phases are designed as shown in Fig. 1.2, where the material parameter is changed in each geometrical phase and the geometrical configuration is moved to better simulation from Phase I to Phase III of the JAERI/USDOE collaborative experiment on fusion blanket neutronics.

In the phase I, the basis was laid for engineering-oriented benchmark experiments, measuring technique development and analysis comparison using slab type test blanket assemblies embedded in a experimental port located inside of the target room wall.[10-13] Revised evaluation of $^{7}Li(n,n'\alpha)^{3}T$ was validated in this phase. Phase II experiment is characterized by a closed geometry with slab type test blanket and neutron source housed in a reflective enclosure. Including refelected source term, this arrangement gives good matching with fusion reactor blanket neutron spectra. Tritium production characteristics and other parameters in full radial dimension of fusion blanket have been measured and analyzed in the three experiment series in the phase. These provide extensive data on breeding characteristics of Li_2O and beryllium neutron multiplication effect in diffrent configurations.[14-20]

Phase III experiment is motivated by a need to examine the effect of source spread on the neutronic performance. In a tokamak reactor, a plasma region is torus shape and the reactor components surround cylindrically the source region. To simulate this configuration, a line source was planned in the Phase III. Though the Phase II concept is excellent to see the spatial distribution over the full blanket thickness, a point neutron source arrangement gives a limitation in simulating the angular distribution of neutrons incident to the surrouding reactor components as a torus blanket. The combination of the line source and annular test blanket can simulate a part of tokamak geometry as a cylindrical geometry. This provides prototypical neutronic environments such as toroidal and poloidal heterogeneities which appear in realistic designs of the experimental reactor, e.g., inbord/outbord arrangement, diverter plate and blanket test module configurations, etc. This combination also makes it possible to extend the experiment to the mock-up which includes all elements necessary to estimate their effects. The geometry of these three dimensional systems are exactly treated only by a Monte Carlo code. However, in a sense of a design calculation code, a

deterministic code is still useful, because estimations of local effects due to local arrangement are very difficult for the Monte Carlo calculation. These effects can be tested only by the experimental mock-up like the present experimental system. The features of the three phases are sumarized in Table 1.1.

This report describes a production method and performance test of a line source, experimental arrangements and results of annular test blankets using the line source. The line source part is descibed in chapter 2 and the measurement methods and results of experiments on three different configurations of annular blankets are described in chapter 3. In appendices, angle-dependent source neutron spectra from the original point source calculated by a Monte Carlo transport code are presented to use in the detailed analysis by means of neutron transport codes. Also in the appendix, seperately discussed are the experimental results by the technique which seems to be in problem. The post analyses calculated by both groups of JAERI and USA are reported seperately.

The following persons are responsoble to each technique, instrumentation, developments and measurements in the program:

Line Source Development	Y. Oyama, T. Nakamura, K. Kosako, M.Z. Youssef, Y. Watanabe, A. Kumar
Test Blanket Assmebly	Y. Oyama, H. Maekawa, A. Kumar
NE213	Y. Oyama
Proton Recoil Counter	C. Konno, E.F. Bennett
Li_2O Pellet	F. Maekawa, H. Maekawa
Activation Foil	Y. Ikeda, C. Konno
Gamma-ray Responses	F. Maekawa, Y. Oyama
Planning & Coordination	Y. Oyama, M.Z. Youssef

Table 1.1 Experimental features of JAERI/USDOE collaborative experiments on fusion blanket neutronics

	Geometry	Source Neutron Term	Material Configuration
Phase-I	Slab-like	Open (14 MeV only)	Li_2O, Be, SS, PE
Phase-II	Sphere-like	Close (refelection part)	Li_2O, Li_2CO_3, 4π- Be, Coolant channel
Phase-III	Cylinder & 3D(Opening)	Line (Volumetric)	Li_2O,Li_2CO_3, SS, Graphite

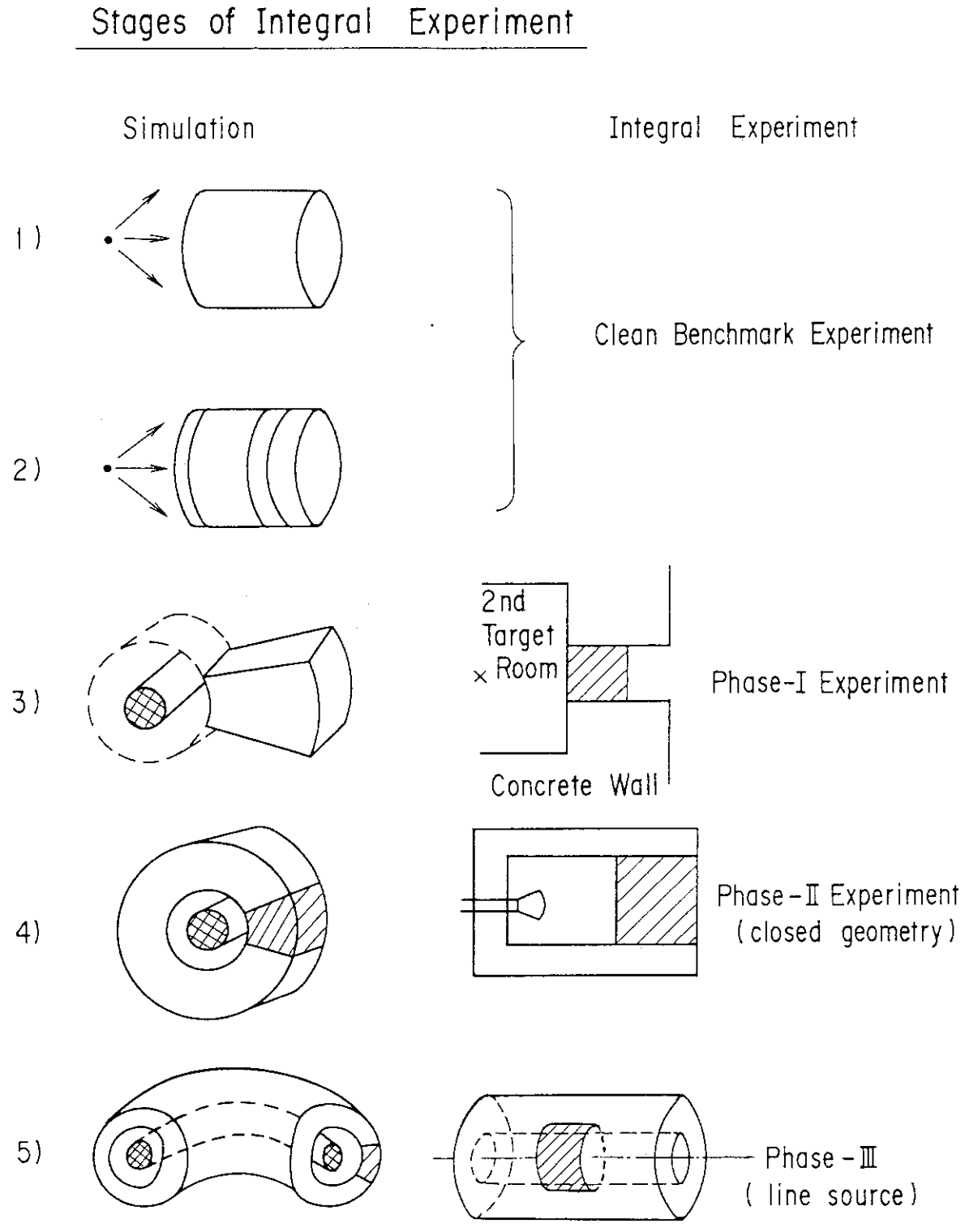

Fig. 1.1 Stages for simulation of neutron source and blanket configuration in the integral experiments at FNS

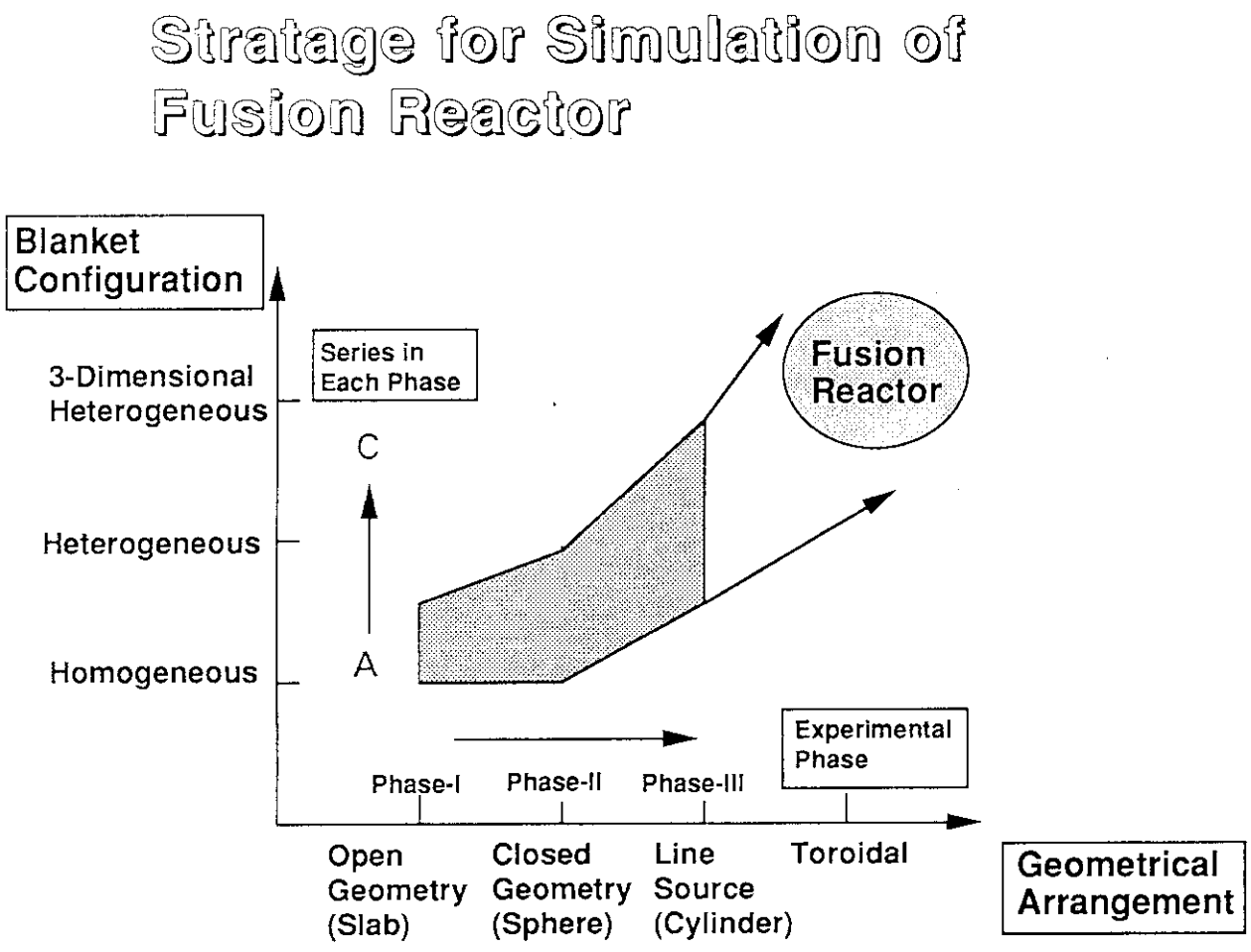

Fig. 1.2 Strategy of the JAERI/USDOE collaborative program on fusion blanket neutronics to extrapolate test data to a fusion reactor environment

2. LINE SOURCE PREPARATION

2.1 Introduction

A concept of cylindrical geometry using a line source and an annular test assembly can be easily reached with consideration of neutronic tests in fusion reactor geometry. A spherical geometry with a point neutron source is analogous to inertial fusion systems such as laser fusion, while a cylindrical geometry with a line neutron source leads us to simulation of magnetic fusion systems such as mirror and tokamak machines.

Conceptual designs of cylindrical assembly with a line source are appeared in the earlier studies for AYMAN project by Sahin[21-23] and for FRBS facility by Beller.[24] Sahin proposed experimental arrangement mainly for fusion-fission hybrid configuration in cylindrical geometry and compared various radial compositions for nuclear performances such as fissile and fusile fuel production with close examination for experimental prospect. He assumed a movable point source for simulating the line source, but technical explanation for realization was not given on the means and experimental prospect relating source characteristics. Beller reported a conceptual design of cylindrical blanket system by using a line source with a cosine-shaped intensity profile. The source design consisted of a deuteron beam, introduced through a slit on the side of the target, sweeping over an elogated target. Using blanket compositions from the works of blanket design study of BCSS,[25] he discussed the neutronic evaluation of two azimuthal effects of neutron energy and yield variations by a line source introduced from the side slit in the blanket. He pointed out, though it seems optimistic, the advantages of his proposal were flexibility for experimental configurations and separability of the flux in the radial and axial directions.

Because no line source experiment have been conducted yet, some evaluations of technique and cost were necessary to realize it. Most important problem is difficulty in producing line source uniformly with minimum distortion. The primary azimuthal neutron energy spectrum and yield distributions depend on the emission angle as far as a point neutron source using deuteron accelerator and tritium metal target system is applied. Not only technical feasibility but also development cost should be taken account for realization. Based on these considerations, a pseudo-line source system, named the FNS Line Source (FNSLS), was constructed at the FNS (Fusion Neutronics Source) facility in Japan Atomic Energy Research Institute. This chapter describes a method to produce a line source and equipments to realize it, and discusses its characteristics.

2.2 Line Source System

2.2.1 Realization of Line Source

The accelerator based D-T point neutron source FNS is utilized a pseudo-line source.

A continuous forth-and-back motion of the test blanket relatively to a fixed point source can give a line source by time-averaging when an observation is performed from the detectors moving together with the test blanket. This is the pseudo-line source, because it is effective only by time averaging or superposition, though this superposition could not be applied for time dependent response such as the activation with short decay time. To obtain an uniform distribution of source intensity requires constant moving speed and constant neutron generation rate during the shuttle motion of test blanket. A beam current of accelerated deuterons is, however, not perfectly controlled to adjust the moving speed of test blanket keeping uniform neutron yield distribution. Hence a stepwise operation mode, in addition to the continuous operation mode, is derived by superposition of a finite number of neutron source points with post-processing of collected data. In the case of stepwise mode, since the measurement is performed during staying of the source, the neutron yield can be normalized at each position. The continuous mode can be operated by using a servo-motor to drive the deck with constant speed, while the stepwise mode needs to accurately stop the test blanket at the desired positions.

A calculational study of the stepwise operation mode shows that there is a minimum number of points enough to represent the equivalent line source.[26] Considering a line source of 2m in length, the analysis pointed out that the speed of moving point source should be faster than 1.2 mm/s in the case of induced activity measurement with a half-life shorter than 10 h. This is discussed later but most of activation measurements used in practical have such half-live range. In the case of stepwise operation, when the source interval was less than 125 mm, the analysis also showed that the deviationof neutron flux around this line source from those of an ideal line source was less than 0.1 %. Based on these considerations, the specifications of equipments for a line source were determined, and a control system and measurement scheme were designed.

2.2.2 Design and Operation Control of Carriage Deck System

A basic concept of line source device was designed as shown in Fig. 2.2.1. The devices include a long tube target assembly, a large movable deck, pseudo-cylindrical annular blanket assembly, controlled servo-motor drive system, position sensor, neutron monitoring system and a managing computer. The long tube target assembly and movable deck are installed at the larger irradiation room No.1 of the FNS facility as shown in Fig. 2.2.2. The room is 15 m square and 9 m height, and the floor is made by steel grating at the 3 m height from the base floor as shown in Fig. 2.2.3. The target motion inside of the annular blanket should be accurately controlled to trace its central axis and to keep symmetry. Also the requirement for moving speed and step motion mentioned before are reflected on the

experimental system design.

The deck was designed to hold for heavy material equipments, and its rails and wheel system was installed very carefully so as to assure accurate linear motion. Two carriage-decks were combined to one large deck of 3.4 m in width and 4 m in length to place an annular test blanket assembly. Each deck has own servo-motor and is able to carry the weight more than 20 ton. Four rails are installed with adjustment so as to keep the horizontal level within 1 mm difference even if a 10 ton duty is loaded. The target position is set accurately by a laser transit and the outer rails are aligned to the target in straight and parallel to guide the wheels of the carriage-deck. The deviations in both horizontal and vertical directions during motion were confirmed to be less than 1 mm over a 2 m stroke. By splitting two decks, one can easily access the inner part of the annular test blanket whenever a change of assembly is necessary. Figure 2.2.4 shows the arrangement using the movable carriage-deck for the line source with the blanket assembly to perform the annular blanket experiment.[29]

The deck motion is controlled by the servo-motor with a feedback from the position data measured by a 2.4 m-long linear scale with optical scale reading. The motor driving system was controlled by the personal computer NEC-9801DS located in the measurement room far from the irradiation room through the RS-422 data bus line. A voltage drop type of current control was used for servo-motor power supply instead of a power supply with switching regulator elements, because the switching regulator noise influenced the detector signal for measurement. The moving speed is determined by setup of a servo-motor drive and adjusted to 6.1 mm/s for a normal speed. This speed is larger than the minimum requirement of 1.2 mm/s as described previously.

In the stepwise mode, the measurements are performed intermittently for a selected time interval (e.g., 1000s) at equi-spaced points (e.g., 100 mm) over a 2 m length. The detector signals are acquisited during stay of the source at each selected position and stopped during motion to the next position. The sequences is programmed on the personal computer in connection with a MCA (multi-channel analyser) and scaler systems. This mode is suitable for the on-line measurement techniques with higher detection efficiency such as NE213 and Li-glass scintillators, and proton recoil gas proportional counters. This scheme also can provide source position-wise data of neutron response, corresponding to importance (adjoint flux) distribution for a detector location along the line source as illustrated in Fig. 2.2.5. The measured data at each source position are normalized by the neutron emission yield calculated from the neutron monitor data taken synchronously.

In the continuous mode, the test blanket repeats forth and back motions at constant speed. For example, it takes 11 min for one cycle of motion with a speed of 6.1 mm/s. The obtained data is normalized by the total neutron emission yield which is obtained from the

integration of the data periodically sampled by a neutron monitor during the whole continuous irradiation cycles. This mode is applied to passive measurement techniques such as activation foil, thermo-luminescence dosimeter and tritium production measurement by liquid scintillation counting method with Li_2O-pellet. These passive methods require high neutron fluence and long irradiation time, so that the stepwise mode is not practical in this case.

2.2.3 Long Tube Neutron Target and Neutron Monitor

The most important requirement to the target is that the neutron emission is as close to that of the primary reaction as possible. The target structure material should be light and thin to avoid neutron spectrum deformation due to neutron scatterings. This requirement has not been assured by the other design; for example, the large size of the elongated target proposed for FRBS [24] must have disadvantage of complex and heavy structure to assure vacuum tightness, heat removal and mechanical strength. Figure 2.2.6 shows the newly developed long tube water-cooled (LTWC) target assembly with a cup-shaped tritium metal target and a drift tube of 2.3 m in length. The target assembly was made by type 304 stainless steel and set without support more than 2 m long. To sustain the whole weight of the assembly by a single side support, steel wire was used for a help as shown in Fig. 2.2.4. The azimuthal symmetry is kept by cylindrical shape and the size is very small so as to insert into the annular blanket.

The cup-shaped metal target assembly was designed to reduce the scattered neutrons by keeping the flange apart from the neutron production point, and was made of thin stainless and copper. The cup-shaped part is insulated electrically to be able to measure the beam current. The tritium is adsorbed on the about 4 micron titanium layer deposited on the bottom of 1 mm thick-copper backing with a cup shape. Total amount of tritium is 10 Ci (370 GBq). The outside of the copper backing is cooled by 1 mm-thick water layer covered by a 1 mm-thick stainless steel water jacket. The water flow line is bent backward to keep the size small so as to insert in the inner cavity of the test blanket. The deuteron beam current can be controlled from 0.1μA~2mA according to the types of measurement. The acceleration voltage was 350 kV. The position of beam spot on the target surface was monitored by temperature distribution with an infrared thermal image measurement system to keep at the center position. To keep the beam center at the cenmter is very important to achive the symmetry and the accuracy of distance between the source and the measuring positions.

Neutron production rate was monitored by detecting alpha particles emitted from the tritium layer associated with D-T reaction. A small surface-barrier silicon-lithium detector

(SSD) with a collimator of 1 mm in diameter was located inside the beam drift tube at the distance of 2.98 m form the target.[27] The low current operation is adopted for the on-line detector measurement with high sensitivity. However, the counting rate of neutron monitor is not enough because of the long distance from the target to the alpha detector. Thus the measurement time is determined by the statistics of the monitor counts. This requires longer measurement time at each source position. This is one of the reason why the stepwise mode is chosen for the on-line measurement.

The alpha counts are recorded by a computer in every 10 second for a continuous mode and in every step for a stepwise mode. For the continuous mode, the source position data was also recorded at the same time. Figure 2.2.7 shows the time dependent neutron yield and carriage-deck position. The figure indicates good stability of neutron generation and good uniformity of the carriage-deck speed. At the turning point, however, the speed does not ideally change from forward to backward; it gradually slows down and speeds up at the end. The slowing-down of the moving speed at both ends increases the staying time of the carriage-deck and makes neutron intensity higher at both end points. For the continuous mode, this end effect is considered in the correction factor for activation foil detector as described in the next section.

2.3 Characteristics of the FNS Line Source

An accelerator based D-T reaction neutron source has angular dependence of the energy spectrum and the yield as determined by reaction kinematics. In addition, since the realistic tritium-titanium metal target has usually deformed emission characteristics of energy and angular distributions due to neutron scattering on the target structure. From the previous works on neutron source characteristics of the accelerator D-T source,[12] it was proved that the Monte Carlo calculation can produce well the measured neutron spectrum and angular distribution. Thus, it can be expected that the spectrum and angular yield can be provided by the Monte Carlo calculation with good accuracy even for the present line source. However, since this line source is produced in more complicated way, the results of the Monte Carlo calculation should be checked with an experiment and optimized for the calculational modeling for this line source, e.g., geometry, reaction process, and for the output source conditions to be given.

2.3.1 Experiment of Line Source Characteristics

The continuous mode has non uniformity of neutron intensity distribution at both ends, but the stepwise mode is not practical for activation detectors with shorter life time. The stepwise mode is useful for the on-line detector to obtain a source position-wise data.

The detector responses around the line source with both operation mode are directly connected with practical source characteristics, because those responses for this line source are measured in neutronics experiments. A source model used in the calculational analysis for such experiments should be able to explain the detector response for the bare line source. Thus the measurements of source characteristics were performed for both operation modes to test the source model.[28]

2.3.1.1 Measurement for Stepwise Mode

The source characteristics for the stepwise mode was measured by using a small sphere NE213 scintillation detector. The measurement was performed along three lines of 4 m in length in parallel to the line source. The distances of lines were 200, 400 and 600 mm from the source axis. Figure 2.3.1 shows the photograph of experimental setup of the detector and the carriage-deck. The step of operation was chosen to 50 mm equi-interval. The neutron flux distributions around the line source are composed by superposition of those data obtained at every positions with numerical processing. The data at 81 measuring points in total were taken for the distribution at one distance as illustrated in Fig. 2.3.2. For example, the superposition of the first 41 data gives the neutron flux at the end point of 2 m long line source. Then the group of 41 data for superposition is shifted by one data point and that group corresponds to the flux at the next mapping position of the line source.

The flux distributions at three distance were taken at the same time by three equivalent NE213 detectors. By the NE213 detectors, only a neutron flux above 10 MeV was obtained using the spectrum weighting function method, which converted directly from the recoiled proton spectrum to the integral neutron flux, to process a large number of data in shorter time. The data of 81 points at each distance are shown in Fig. 2.3.3 and listed in Table 2.3.1. The deformed distribution is seen just beside the target. This is caused by the deformation around 90 degrees in angular neutron emission yield from the target due to scattering by target structure. The deformation is wider for the distribution at longer distance, because the same solid angle covers larger area at far position.

These measured data were summed up to be superposed in space: the 81 position data for the point source were reduced to 41 position data for the line source, i.e., the flux distribution over 4 m around the point neutron source was converted to the superposed flux distribution over 2 m around the 2 m line source. For an ideally isotropic and non disturbed line source, the neutron flux distribution is calculated analytically by the following equation:

$$\Phi = \frac{\sigma}{4\pi r} \cdot \left(\tan^{-1} \frac{L - a}{r} + \tan^{-1} \frac{L + a}{r} \right) \qquad [\,n/cm^2\,], \qquad (2.1)$$

where σ is the line density [n/cm] of the neutron source intensity, L is a half of line source length, a is the distance from the center and r is the vertical distance from the line source as illustrated in Fig. 2.3.4. Figure 2.3.5 and Table 2.3.2 shows the neutron flux distribution above 10 MeV superposed by the measured data with the NE213 detector and the distribution calculated by Eq. (2.1). The measured distributions are smaller than the calculated ones by 10-15 %, because the loss of angular neutron emission at 90 degrees also produces the anisotropy of line intensity of the source and then the total number of emitted neutrons above 10 MeV becomes smaller. In symmetrical comparison as shown in Fig. 2.3.6, the neutron flux at the forward of the target is larger in the measured distribution than the backward. This is caused by anisotropy of neutron emission due to kinematics, i.e., in reaction kinematics for 350 keV deuteron, the forward neutron emission is about 8% larger than that at the 90 degrees. Nevertheless the relative distribution agrees well within 5 % and the distribution at the mid region is very smooth and flat. This assures that the present pseudo-line source can represent a similar characteristics of an ideal line source.

In order to answer a question how many points are the number enough to simulate a line source by the stepwise mode, the number of points to be superposed was changed. This examination gives the minimum step necessary to simulate a line source. The discussion in Ref. (26) suggested that the 125 mm interval, i.e., 16 steps, is necessary for the minimum requirement. We compared four types of equi-intervals; 50, 100, 200 and 400 mm; the distributions with 50 mm spatial resolution are obtained from 41, 21, 11 and 6 data points for each position. Figure 2.3.7 shows comparison of the superposed flux distribution with different sets of point data at the 200 mm distance from the line source. The coaser step interval shows an oscillation and deformation compared to the reference distribution obtained from 50 mm spatial resolution. The range of the oscillation for the interval of 100 mm agreed well with the 50 mm interval case within 3 % . Considering the experimental acuracy for the on-line detectors, the 100 mm interval case was also considered to be enough to simulate the line source.

2.3.1.2 Measurement for Continuous Mode

Though the line source is simulated by time averaging in the continuous mode, the nuclear response which has a time dependent property can be applied approximately with a correction. As discussed in Ref (28), the time dependence of nuclear responses can be corrected by using time dependent source position and neutron yield data, if it is approximated that a only uncollided flux distribution is concerned to the response. For an activation foil detector at each positioon, the neutron flux varies by $1/r^2$ dependence with the source position moving along the pseudo-line source, i.e., with a time past from the biginning

of irradiation. This kind of time-dependent nuclear response is usually taken account in activation reaction measurement considering the irradiation history together with the decay property of activity. For the line source, this type of correction can be made by disassembling the line source to distributed sources sampled every ten second by a neutron monitor system. The real irradiation is composed by individual irradiation from each registered source. Then the correction factor of the present measurement is obtained from the following ratio, i.e., the correction PF for each point source is obtained as:

$$PF = \sum_{j=1}^{M}\left[\frac{S_j}{4\pi r_j^2}\cdot\{1-\exp(-\lambda\cdot\Delta t)\}\cdot\exp\{-\lambda\cdot(M-j)\cdot\Delta t\}\right]. \qquad (2.2)$$

where S_j is the source yield sampled by j-th monitor data at each source position r_j,

$\{1-\exp(-\lambda\cdot\Delta t)\}$ is the correction for decay time λ during irradiation time Δt,

$[\exp\{-\lambda\cdot(M-j)\cdot\Delta t\}]$ is the correction for decay for the rest time $(M-j)\cdot\Delta t$ by the end of whole irradiation time by the continuous line source mode.

On the other hand, the correction LF for an ideal line source is written as:

$$LF = \left(\sum_{j=1}^{M}\frac{S_j}{2\cdot L\cdot M}\right)\cdot\frac{1}{4\cdot\pi\cdot r}\cdot\left(\tan^{-1}\frac{L-a}{R}+\tan^{-1}\frac{L+a}{R}\right)\cdot\{1-\exp(-\lambda\cdot t_r)\}, \quad (2.3)$$

where $[\sum_{j=1}^{M}\frac{S_j}{2\cdot L\cdot M}]$ is the line source density σ (L is the half length of the line source,

M is the number of sample points),

$[\frac{1}{4\cdot\pi\cdot r}\cdot\left(\tan^{-1}\frac{L-a}{R}+\tan^{-1}\frac{L+a}{R}\right)]$ is the expected flux for ideal line source with the definition as given in Eq. (2.1),

$\{1-\exp(-\lambda\cdot t_r)\}$ is the decay correction during the whole irradiation time t_r.

Then the correction for the pseudo-line source by the continuous mode is obtained from the ratio of them :

$$F = \frac{\text{LF(line source)}}{\text{PF(point source sum)}}, \qquad (2.4)$$

Finally, the reaction rate is obtained from the photon counts measured by a germanium detector as follows:

$$RR = \frac{\lambda \cdot C \cdot F}{\varepsilon \cdot N \cdot B \cdot \{1 - \exp(-\lambda \cdot \Delta t)\} \cdot \exp(-\lambda \cdot t_c) \cdot \{1 - \exp(\lambda \cdot t_m)\}} \quad , \qquad (2.5)$$

where C is the count detected by Ge detector,

ε is the efficiency of the Ge detector,

N is the number of nuclei in the foil,

B is the branching ratio for the decay of interest,

t_c is the cooling time from end of the irradiation to the measurement

t_m is the measuring time for gamma-emission.

Assuming that the carriage-deck moves with a constant speed of 6.1 mm/s (also assumed that the constant speed is kept at the turning point), the estimated correction factor for $^{115}In(n,n')^{115m}In$ reaction ($T_{1/2}$=4.49 h) with 10 hr irradiation is 1.09 and the largest correction is due to a decrease of the source neutron yield caused by depression of the amount of tritium in the target. The correction factors in the experiment are calculated with the record of neutron and position onitors during irradiation. Figure 2.3.8 shows typical samples of three reactions with decay times of 4.5h to 10 day. The correction factors decrease by 8% at both turning points where a moving speed of the carriage-deck slows down. The factor for $^{115}In(n,n')^{115m}In$ reaction case with shorter decay time is about 8% , while the longer decay cases are less than 4%.

Table 2.3.3 summarizes the activation reactions used in the measurement of the reaction rate distribution (mapping) around the line source. Figure 2.3.9 shows the locations for each foil placed. These foils were packed and put onto nyron strings stretched by a support on the carriage-deck. The irradiation was performed for 10 hr and the neutron yield obtained was 7.8 x 10^{15} n/s in total emission. The measured results of reaction rates at the distance of 219 mm from the line source are summarized in Table 2.3.5 and shown in Fig. 2.3.10. The distribution of the threshold reactions was similar to that calculated for an ideal line source, while the $^{197}Au(n,\gamma)^{198}Au$ reaction was completely flat over the source length. Figure 2.3.11 plots the ratios of the reaction rates to their central values to see symmetry of distribution. One can see that the forward result in the $^{58}Ni(n,2n)^{57}Ni$ reaction is larger than the backward. This is because the energy of neutrons emitted forward from the target is higher and the $^{58}Ni(n,2n)^{57}Ni$ cross section for higher energy neutrons is larger. Because the reactions with lower threshold are rather symmetric, the effect of anisotropy of neutron emission yield by kinematics is not so large.

2.3.2 Calculation of Line Source Characteristics

2.3.2.1 Monte Calro Calculation of the Long Tube Target

Because the present pseudo-line source is time-superposed by point sources from each positions during motion, the line source performance is based on the neutron emission characteristics of the long tube target. In the computational analysis for the successive experiment, the line source was generated by the distributed source for the deterministic code. Thus the calculation of neutron emission characteristics was performed for the stationary long tube target.

Neutron production reaction, deuteron deceleration process in titanium-tritium layer and neutron scatterings were calculated by the external subroutine in the Monte Carlo code MORSE-DD[29] using the library based on the JENDL-3 nuclear data file.[30] The calculation mmodel simulated completely the components around the neutron emission point. The validity of this model was confirmed with a good agreement by comparison of the calculated spectrum with the mesaured one by the time-of-flight technique in the previous experiments.[12] The present calculation differs only for the target structure from the previous one, so that it is expected to have similar accuracy. Figures 2.3.12(a)-(d) show the geometrical and material model for the long tube target assembly shown in Fig. 2.2.6. Since the source neutrons come from the superposed line source with different emission angls to the detector, angular distribution is needed to calculate finely. To calculate the fine angular distribution, the point estimators with 5 degree interval on a horizontal plane and 15 degree interval on a vertical plane are placed in the Monte Calro calculation at the distance of 100 mm from the neutron emission point. When we set the detectro at the 400 mm from the line source (at the mid of the test blanket), the source step of 50 mm corresponds to 7 degrees of neutron emission angle difference. Hence the angle interval of 5 degrees was adopted in the source characteristics calaculation by the Monte Carlo code.

The result of total neutrons emitted in each angle is listed in Table 2.3.5. Figure 2.3.13 shows the calculated angular dependence of neutron emission for vertical and horizontal directions. There exists about 20% dip at 90 degrees and around 140 degrees. The former is due to the target backing whose plane is in parallel to the 90 degrees and longest path through the backing material for neutrons. The latter is caused by the flange structure of the target assembly. Because this target was specially designed as a cup shape, the dip at 90 degrees was very sharp. Nevertheless the 90 degree direction must be taken care for the annular blanket experiment using the present line source system. The figure also shows anisotropy of angular dependence due to kinematics; the forward direction is more than the backward. Figure 2.3.14 shows the calculated neutron energy spectra for three directions. By kinematic relation at the 350 keV deuteron energy, the forward energy is 14.8 MeV and the backward 13.4 MeV. These effects of the neutron emission profile were clearly observed in

the measured source characteristics of the line source. The calculated energy spectra for every 5 degree are listed in Appendix 1.

2.3.2.2 Reliability of the Line Source Model for Calculation

Using the above results for the long tube point source, the neutron flux distribution around the line source were calculated by the FNSUNCL code which was modified from the GRTUNCL code.[31] The GRTUNCL calculates the first collision source from the point source for an input source distribution to the next step calculation by using the two dimensional discrete ordinate transport code DOT3.5.[32] On the other hand, the FNSUNCL can calculate the first collision source from the distributed source by summing up the contributions from the every distributed point sources taking account of angular distributions of energy spectrum and emission yield. To calculate the neutron flux distribution around this line source, the 40 points was chosen to be distributed on the source line with 50 mm interval basing on discussion of superposition. The 37 neutron energy spectra from 0 to 180 degrees with 5 degree step calculated by the MonteCarlo code were generated at each source position.

Using the calculated neutron angular emission yield, the flux distributions along the target assembly axis corresponding to the measured distributions given in Fig. 2.3.3 are reduced and compared with the measurement. Figure 2.3.15 shows the flux distributions above 10 MeV around a long tube target for both calculation and measurement. The results show an excellent agreement with each other, except for backward distribution. Disagreement at the backward is due to insufficient model for the beam drift tube. However, the good agreement in main part of the distribution assures to be able to use the calculated neutron source as the initial source conditions for an analysis of neutronics experiment using this line source.

The calculated reaction rates around the line source were also compared to the measured results of activation reaction with the continuous mode. The calculated to the measured value ratios, C/E, are shown in Figs. 2.3.16 - 18 for various threshold recations. The reaction cross section data used in the calculation are based on Ref. (33) for (n,2n) reactions and ENDF/B-IV for the others. For all reactions, the tendency of the C/Es is very consistent with the ratios of the cross section measured at FNS reported in the Ref. (33) to the libraries. The (n,p) reactions of ^{64}Zn and ^{58}Ni show large C/Es and it is noted that those reaction cross sections of ENDF/B-IV are larger. Because an agreement is within ±5% for the calculation using the measured (n,2n) reaction cross sections, the accuracy of the calculation by the Monte Calro code and FNSUNCL is also expected to be within a few %. This approves again that the calculated neutron energy spectra and emission probability

to be used as an initial source condition of the succesive calculations for an analysis on an experiment using this line source. Also it was confirmed that the distributed source with the interval of 50 mm was equivalent to the line source with the continuous mode and the correction method for activation decay was valid.

2.4 Concluding Remarks

A pseudo-line D-T neutron source system has been successfully developed to simulate a distributed source relevant to a tokamak D-T fueled fusion reactor. The line source system consists of automatic controlled moving carriage-deck, long drift tube water cooled target assembly and synchronized data acquisition system. The operation can be performed in two ways; stepwise and continuous moving modes. Both operation condition were optimized and confirmed by the measurement of neutron flux distribution around the target. The source intensity was normalized by counting alpha particles emitted from the D-T reaction measured by the associated alpha particle counting method. The obtained neutron field around the line source was flat in the central region over 1 m.

The energy spectrum and angular emission yield of neutrons emitted from the long tube D-T target were calculated by Monte Carlo calculation and given as numerical tables. These data were confirmed by comparison with the experiment of source characteristic and validated for use as the initial source condition for a calculational analysis of experiments to be performed by using this line source system.

This line source system provides a powerful tool for engineering benchmark experiments and open a new experimental area that examine the overall performance of the design codes, specially for the engineering confirmation containing the complexity of proto-typical configurations.

Table 2.3.1 Measured flux distributions around the long tube water cooled (LTWC) target assembly

N=1 DISTANCE = 200 mm

** FLUX MAPPING DATA (En > 10 MeV) **

NO.	POS(mm)	FLUX	NO.	POS(mm)	FLUX
1	-2025.	9.7450E-07	41	-25.	1.9390E-04
2	-1975.	1.0400E-06	42	25.	1.6240E-04
3	-1925.	1.0460E-06	43	75.	1.6970E-04
4	-1875.	1.2620E-06	44	125.	1.2870E-04
5	-1825.	1.2690E-06	45	175.	1.0530E-04
6	-1775.	1.2910E-06	46	225.	8.3130E-05
7	-1725.	1.5000E-06	47	275.	6.2260E-05
8	-1675.	1.5960E-06	48	325.	5.0550E-05
9	-1625.	1.7280E-06	49	375.	4.1810E-05
10	-1575.	1.9220E-06	50	425.	3.3570E-05
11	-1525.	2.0310E-06	51	475.	2.7870E-05
12	-1475.	2.0690E-06	52	525.	2.4210E-05
13	-1425.	2.1940E-06	53	575.	2.1380E-05
14	-1375.	2.4920E-06	54	625.	1.7310E-05
15	-1325.	2.6040E-06	55	675.	1.5670E-05
16	-1275.	2.8380E-06	56	725.	1.4020E-05
17	-1225.	3.2630E-06	57	775.	1.2000E-05
18	-1175.	3.6460E-06	58	825.	1.0930E-05
19	-1125.	3.8370E-06	59	875.	9.8500E-06
20	-1075.	4.0130E-06	60	925.	8.4350E-06
21	-1025.	4.5350E-06	61	975.	7.6380E-06
22	-975.	4.8520E-06	62	1025.	6.7290E-06
23	-925.	5.4840E-06	63	1075.	6.8690E-06
24	-875.	5.7950E-06	64	1125.	5.8740E-06
25	-825.	7.2480E-06	65	1175.	5.7710E-06
26	-775.	8.6450E-06	66	1225.	5.1950E-06
27	-725.	9.8990E-06	67	1275.	4.6710E-06
28	-675.	1.2480E-05	68	1325.	4.5160E-06
29	-625.	1.4220E-05	69	1375.	4.3110E-06
30	-575.	1.6340E-05	70	1425.	3.8000E-06
31	-525.	1.7910E-05	71	1475.	3.9350E-06
32	-475.	2.0760E-05	72	1525.	3.4990E-06
33	-425.	2.3130E-05	73	1575.	3.1840E-06
34	-375.	2.7530E-05	74	1625.	3.0660E-06
35	-325.	3.3910E-05	75	1675.	2.7160E-06
36	-275.	4.8850E-05	76	1725.	2.5930E-06
37	-225.	7.0240E-05	77	1775.	2.5460E-06
38	-175.	1.0280E-04	78	1825.	2.4820E-06
39	-125.	1.3360E-04	79	1875.	2.2940E-06
40	-75.	1.7100E-04	80	1925.	2.1830E-06
41	-25.	1.9390E-04	81	1975.	2.0670E-06

Table 2.3.1 (Continued)

N=2 DISTANCE = 400 mm

** FLUX MAPPING DATA (En > 10 MeV) **

NO.	POS(mm)	FLUX	NO.	POS(mm)	FLUX
1	-2025.	1.1400E-06	41	-25.	4.9520E-05
2	-1975.	1.2030E-06	42	25.	3.8900E-05
3	-1925.	1.3930E-06	43	75.	3.9100E-05
4	-1875.	1.2730E-06	44	125.	4.2920E-05
5	-1825.	1.3890E-06	45	175.	3.8920E-05
6	-1775.	1.5350E-06	46	225.	3.4220E-05
7	-1725.	1.5440E-06	47	275.	3.1320E-05
8	-1675.	1.6890E-06	48	325.	2.8790E-05
9	-1625.	1.9340E-06	49	375.	2.6040E-05
10	-1575.	2.0480E-06	50	425.	2.3070E-05
11	-1525.	2.2290E-06	51	475.	1.9990E-05
12	-1475.	2.4960E-06	52	525.	1.7600E-05
13	-1425.	2.7310E-06	53	575.	1.4680E-05
14	-1375.	2.9010E-06	54	625.	1.4100E-05
15	-1325.	3.1630E-06	55	675.	1.2430E-05
16	-1275.	3.4930E-06	56	725.	1.1050E-05
17	-1225.	3.5580E-06	57	775.	1.0360E-05
18	-1175.	3.7840E-06	58	825.	9.4400E-06
19	-1125.	4.1430E-06	59	875.	8.3700E-06
20	-1075.	4.2230E-06	60	925.	7.3750E-06
21	-1025.	4.4780E-06	61	975.	6.9940E-06
22	-975.	4.6570E-06	62	1025.	6.3620E-06
23	-925.	5.4170E-06	63	1075.	5.8240E-06
24	-875.	5.5750E-06	64	1125.	5.0140E-06
25	-825.	6.3150E-06	65	1175.	5.0620E-06
26	-775.	6.7990E-06	66	1225.	4.5410E-06
27	-725.	7.1260E-06	67	1275.	4.0810E-06
28	-675.	8.2910E-06	68	1325.	4.1420E-06
29	-625.	9.7770E-06	69	1375.	3.8240E-06
30	-575.	1.0910E-05	70	1425.	3.4910E-06
31	-525.	1.4140E-05	71	1475.	3.1740E-06
32	-475.	1.7410E-05	72	1525.	3.1130E-06
33	-425.	2.0410E-05	73	1575.	2.7880E-06
34	-375.	2.5120E-05	74	1625.	2.7760E-06
35	-325.	2.7460E-05	75	1675.	2.4830E-06
36	-275.	3.2460E-05	76	1725.	2.5720E-06
37	-225.	3.7250E-05	77	1775.	2.4010E-06
38	-175.	4.1710E-05	78	1825.	2.2680E-06
39	-125.	4.7060E-05	79	1875.	2.1170E-06
40	-75.	4.9500E-05	80	1925.	2.1060E-06
41	-25.	4.9520E-05	81	1975.	1.9600E-06

Table 2.3.1 (Continued)

N=3 DISTANCE = 600 mm

** FLUX MAPPING DATA (En > 10 MeV) **

NO.	POS(mm)	FLUX	NO.	POS(mm)	FLUX
1	-2025.	1.4620E-06	41	-25.	2.2410E-05
2	-1975.	1.5070E-06	42	25.	1.7080E-05
3	-1925.	1.5420E-06	43	75.	1.7050E-05
4	-1875.	1.5860E-06	44	125.	1.7580E-05
5	-1825.	1.7270E-06	45	175.	1.8210E-05
6	-1775.	1.7760E-06	46	225.	1.7690E-05
7	-1725.	1.8670E-06	47	275.	1.7330E-05
8	-1675.	1.9330E-06	48	325.	1.5780E-05
9	-1625.	2.0840E-06	49	375.	1.5080E-05
10	-1575.	2.2400E-06	50	425.	1.4320E-05
11	-1525.	2.3020E-06	51	475.	1.3030E-05
12	-1475.	2.4910E-06	52	525.	1.2390E-05
13	-1425.	2.5100E-06	53	575.	1.1320E-05
14	-1375.	2.4650E-06	54	625.	9.9690E-06
15	-1325.	2.7200E-06	55	675.	9.8110E-06
16	-1275.	2.7720E-06	56	725.	8.7910E-06
17	-1225.	2.8410E-06	57	775.	8.2100E-06
18	-1175.	2.9370E-06	58	825.	7.4590E-06
19	-1125.	3.0460E-06	59	875.	6.9060E-06
20	-1075.	3.2220E-06	60	925.	6.4180E-06
21	-1025.	3.4050E-06	61	975.	5.9280E-06
22	-975.	3.7990E-06	62	1025.	5.6290E-06
23	-925.	4.0220E-06	63	1075.	5.1960E-06
24	-875.	4.3480E-06	64	1125.	4.9100E-06
25	-825.	4.8300E-06	65	1175.	4.5340E-06
26	-775.	5.4560E-06	66	1225.	4.2640E-06
27	-725.	6.2190E-06	67	1275.	3.9530E-06
28	-675.	7.5700E-06	68	1325.	3.9180E-06
29	-625.	8.5860E-06	69	1375.	3.5900E-06
30	-575.	1.0110E-05	70	1425.	3.3780E-06
31	-525.	1.2020E-05	71	1475.	3.2410E-06
32	-475.	1.2720E-05	72	1525.	2.8910E-06
33	-425.	1.3350E-05	73	1575.	2.6410E-06
34	-375.	1.4950E-05	74	1625.	2.6820E-06
35	-325.	1.6570E-05	75	1675.	2.5690E-06
36	-275.	1.7830E-05	76	1725.	2.4760E-06
37	-225.	1.8590E-05	77	1775.	2.2790E-06
38	-175.	1.9800E-05	78	1825.	2.1650E-06
39	-125.	2.1210E-05	79	1875.	2.1330E-06
40	-75.	2.1920E-05	80	1925.	2.0580E-06
41	-25.	2.2410E-05	81	1975.	1.8910E-06

Table 2.3.2 Superposed neutron flux distributions obtained from the NE213 measurement

M= 1 NO.	RPOS (mm)	50 mm step FLUX(200 mm)	ERR1	** SUPERPOSED FLUX (En > 10 MeV) ** FLUX(400 mm)	ERR2	FLUX(600 mm)	ERR3	RPOS (mm)	NO.
1	-1025.	2.3799E-05	1.6429E-02	1.1689E-05	9.9870E-03	7.1889E-06	6.8693E-03	-1025.	1
2	-975.	2.7736E-05	1.5790E-02	1.2610E-05	9.7271E-03	7.5698E-06	6.7539E-03	-975.	2
3	-925.	3.1849E-05	1.5227E-02	1.3534E-05	9.4731E-03	7.9489E-06	6.6415E-03	-925.	3
4	-875.	3.4963E-05	1.4543E-02	1.4547E-05	9.2714E-03	8.3401E-06	6.5307E-03	-875.	4
5	-825.	3.7501E-05	1.3980E-02	1.5465E-05	9.0534E-03	8.7456E-06	6.4301E-03	-825.	5
6	-775.	3.9497E-05	1.3482E-02	1.6266E-05	8.8330E-03	9.1349E-06	6.3330E-03	-775.	6
7	-725.	4.0984E-05	1.3097E-02	1.6993E-05	8.6326E-03	9.5143E-06	6.2422E-03	-725.	7
8	-675.	4.2181E-05	1.2794E-02	1.7657E-05	8.4537E-03	9.8536E-06	6.1511E-03	-675.	8
9	-625.	4.3161E-05	1.2552E-02	1.8251E-05	8.2931E-03	1.0174E-05	6.0648E-03	-625.	9
10	-575.	4.3938E-05	1.2355E-02	1.8767E-05	8.1524E-03	1.0473E-05	5.9837E-03	-575.	10
11	-525.	4.4571E-05	1.2197E-02	1.9204E-05	8.0306E-03	1.0736E-05	5.9082E-03	-525.	11
12	-475.	4.5112E-05	1.2063E-02	1.9579E-05	7.9259E-03	1.0982E-05	5.8398E-03	-475.	12
13	-425.	4.5583E-05	1.1949E-02	1.9876E-05	7.8390E-03	1.1197E-05	5.7792E-03	-425.	13
14	-375.	4.5951E-05	1.1860E-02	2.0154E-05	7.7606E-03	1.1379E-05	5.7238E-03	-375.	14
15	-325.	4.6273E-05	1.1783E-02	2.0386E-05	7.6936E-03	1.1558E-05	5.6714E-03	-325.	15
16	-275.	4.6551E-05	1.1716E-02	2.0578E-05	7.6383E-03	1.1706E-05	5.6264E-03	-275.	16
17	-225.	4.6775E-05	1.1663E-02	2.0746E-05	7.5909E-03	1.1839E-05	5.5862E-03	-225.	17
18	-175.	4.6962E-05	1.1619E-02	2.0889E-05	7.5507E-03	1.1952E-05	5.5517E-03	-175.	18
19	-125.	4.7113E-05	1.1583E-02	2.1001E-05	7.5193E-03	1.2049E-05	5.5214E-03	-125.	19
20	-75.	4.7225E-05	1.1557E-02	2.1080E-05	7.4968E-03	1.2131E-05	5.4956E-03	-75.	20
21	-25.	4.7314E-05	1.1536E-02	2.1148E-05	7.4776E-03	1.2197E-05	5.4748E-03	-25.	21
22	25.	4.7367E-05	1.1523E-02	2.1194E-05	7.4646E-03	1.2251E-05	5.4575E-03	25.	22
23	75.	4.7416E-05	1.1512E-02	2.1222E-05	7.4564E-03	1.2285E-05	5.4465E-03	75.	23
24	125.	4.7426E-05	1.1509E-02	2.1212E-05	7.4584E-03	1.2307E-05	5.4390E-03	125.	24
25	175.	4.7425E-05	1.1509E-02	2.1200E-05	7.4618E-03	1.2311E-05	5.4365E-03	175.	25
26	225.	4.7375E-05	1.1521E-02	2.1156E-05	7.4732E-03	1.2297E-05	5.4397E-03	225.	26
27	275.	4.7278E-05	1.1544E-02	2.1090E-05	7.4917E-03	1.2261E-05	5.4499E-03	275.	27
28	325.	4.7147E-05	1.1574E-02	2.1017E-05	7.5119E-03	1.2205E-05	5.4653E-03	325.	28
29	375.	4.6948E-05	1.1621E-02	2.0908E-05	7.5413E-03	1.2108E-05	5.4904E-03	375.	29
30	425.	4.6694E-05	1.1680E-02	2.0755E-05	7.5837E-03	1.1981E-05	5.5223E-03	425.	30
31	475.	4.6391E-05	1.1751E-02	2.0566E-05	7.6364E-03	1.1813E-05	5.5624E-03	475.	31
32	525.	4.6040E-05	1.1835E-02	2.0297E-05	7.7073E-03	1.1590E-05	5.6117E-03	525.	32
33	575.	4.5611E-05	1.1939E-02	1.9941E-05	7.7981E-03	1.1345E-05	5.6666E-03	575.	33
34	625.	4.5122E-05	1.2059E-02	1.9511E-05	7.9029E-03	1.1084E-05	5.7251E-03	625.	34
35	675.	4.4516E-05	1.2209E-02	1.8959E-05	8.0240E-03	1.0782E-05	5.7870E-03	675.	35
36	725.	4.3752E-05	1.2401E-02	1.8352E-05	8.1571E-03	1.0439E-05	5.8505E-03	725.	36
37	775.	4.2623E-05	1.2683E-02	1.7618E-05	8.2992E-03	1.0059E-05	5.9136E-03	775.	37
38	825.	4.0970E-05	1.3092E-02	1.6765E-05	8.4648E-03	9.6587E-06	5.9795E-03	825.	38
39	875.	3.8519E-05	1.3662E-02	1.5800E-05	8.6145E-03	9.2278E-06	6.0410E-03	875.	39
40	925.	3.5314E-05	1.4338E-02	1.4703E-05	8.7170E-03	8.7607E-06	6.0821E-03	925.	40
41	975.	3.1194E-05	1.4911E-02	1.3544E-05	8.7816E-03	8.2722E-06	6.1089E-03	975.	41

Table 2.3.2 (Continued)

M= 2 NO.	RPOS (mm)	100 mm step FLUX(200 mm)	ERR1	** SUPERPOSED FLUX (En > 10 MeV) ** FLUX(400 mm)	ERR2	FLUX(600 mm)	ERR3	RPOS (mm)	NO.
1	-1025.	2.7378E-04	2.4042E-02	1.2916E-04	1.3944E-02	7.8526E-05	9.6423E-03	-1025.	1
2	-975.	3.0917E-04	2.0777E-02	1.3623E-04	1.3520E-02	8.1189E-05	9.3813E-03	-975.	2
3	-925.	3.6020E-04	2.1940E-02	1.4861E-04	1.3218E-02	8.6510E-05	9.3174E-03	-925.	3
4	-875.	3.7456E-04	1.9170E-02	1.5760E-04	1.2951E-02	8.9422E-05	9.0803E-03	-875.	4
5	-825.	4.1360E-04	2.0179E-02	1.6783E-04	1.2613E-02	9.5048E-05	9.0266E-03	-825.	5
6	-775.	4.1649E-04	1.7871E-02	1.7447E-04	1.2325E-02	9.7670E-05	8.8121E-03	-775.	6
7	-725.	4.4484E-04	1.9031E-02	1.8316E-04	1.2045E-02	1.0304E-04	8.7654E-03	-725.	7
8	-675.	4.4172E-04	1.7057E-02	1.8843E-04	1.1820E-02	1.0484E-04	8.5603E-03	-675.	8
9	-625.	4.6548E-04	1.8312E-02	1.9571E-04	1.1590E-02	1.0981E-04	8.5176E-03	-625.	9
10	-575.	4.5810E-04	1.6524E-02	1.9939E-04	1.1416E-02	1.1119E-04	8.3325E-03	-575.	10
11	-525.	4.7887E-04	1.7845E-02	2.0495E-04	1.1244E-02	1.1541E-04	8.2993E-03	-525.	11
12	-475.	4.6951E-04	1.6161E-02	2.0735E-04	1.1116E-02	1.1639E-04	8.1417E-03	-475.	12
13	-425.	4.8878E-04	1.7510E-02	2.1133E-04	1.0993E-02	1.2003E-04	8.1229E-03	-425.	13
14	-375.	4.7732E-04	1.5918E-02	2.1329E-04	1.0890E-02	1.2022E-04	7.9878E-03	-375.	14
15	-325.	4.9569E-04	1.7280E-02	2.1630E-04	1.0801E-02	1.2377E-04	7.9769E-03	-325.	15
16	-275.	4.8322E-04	1.5736E-02	2.1747E-04	1.0728E-02	1.2346E-04	7.8562E-03	-275.	16
17	-225.	5.0050E-04	1.7122E-02	2.1998E-04	1.0661E-02	1.2658E-04	7.8625E-03	-225.	17
18	-175.	4.8737E-04	1.5609E-02	2.2051E-04	1.0614E-02	1.2586E-04	7.7588E-03	-175.	18
19	-125.	5.0387E-04	1.7011E-02	2.2245E-04	1.0568E-02	1.2867E-04	7.7747E-03	-125.	19
20	-75.	4.8982E-04	1.5533E-02	2.2235E-04	1.0543E-02	1.2764E-04	7.6846E-03	-75.	20
21	-25.	5.0582E-04	1.6948E-02	2.2391E-04	1.0512E-02	1.3014E-04	7.7128E-03	-25.	21
22	25.	4.9121E-04	1.5491E-02	2.2345E-04	1.0501E-02	1.2887E-04	7.6326E-03	25.	22
23	75.	5.0702E-04	1.6909E-02	2.2460E-04	1.0486E-02	1.3106E-04	7.6732E-03	75.	23
24	125.	4.9174E-04	1.5475E-02	2.2363E-04	1.0493E-02	1.2944E-04	7.6071E-03	125.	24
25	175.	5.0716E-04	1.6904E-02	2.2442E-04	1.0491E-02	1.3132E-04	7.6594E-03	175.	25
26	225.	4.9143E-04	1.5484E-02	2.2310E-04	1.0513E-02	1.2940E-04	7.6061E-03	225.	26
27	275.	5.0584E-04	1.6947E-02	2.2327E-04	1.0532E-02	1.3087E-04	7.6752E-03	275.	27
28	325.	4.8931E-04	1.5548E-02	2.2174E-04	1.0564E-02	1.2861E-04	7.6355E-03	325.	28
29	375.	5.0298E-04	1.7039E-02	2.2158E-04	1.0596E-02	1.2953E-04	7.7255E-03	375.	29
30	425.	4.8487E-04	1.5682E-02	2.1928E-04	1.0653E-02	1.2646E-04	7.7093E-03	425.	30
31	475.	4.9771E-04	1.7210E-02	2.1820E-04	1.0721E-02	1.2679E-04	7.8188E-03	475.	31
32	525.	4.7829E-04	1.5882E-02	2.1529E-04	1.0802E-02	1.2277E-04	7.8287E-03	525.	32
33	575.	4.9017E-04	1.7459E-02	2.1239E-04	1.0928E-02	1.2198E-04	7.9641E-03	575.	33
34	625.	4.6923E-04	1.6165E-02	2.0779E-04	1.1058E-02	1.1763E-04	7.9779E-03	625.	34
35	675.	4.7971E-04	1.7814E-02	2.0320E-04	1.1230E-02	1.1646E-04	8.1328E-03	675.	35
36	725.	4.5646E-04	1.6575E-02	1.9625E-04	1.1395E-02	1.1124E-04	8.1484E-03	725.	36
37	775.	4.6365E-04	1.8376E-02	1.9037E-04	1.1609E-02	1.0914E-04	8.3204E-03	775.	37
38	825.	4.3271E-04	1.7340E-02	1.8078E-04	1.1796E-02	1.0321E-04	8.3191E-03	825.	38
39	875.	4.2885E-04	1.9590E-02	1.7237E-04	1.2081E-02	1.0071E-04	8.5124E-03	875.	39
40	925.	3.8117E-04	1.8837E-02	1.6050E-04	1.2203E-02	9.4125E-05	8.4771E-03	925.	40
41	975.	3.6148E-04	2.1695E-02	1.4927E-04	1.2373E-02	9.0818E-05	8.6450E-03	975.	41

Table 2.3.2 (Continued)

M= 3 NO.	RPOS (mm)	200 mm step FLUX(200 mm)	ERR1	** SUPERPOSED FLUX (En > 10 MeV) ** FLUX(400 mm)	ERR2	FLUX(600 mm)	ERR3	RPOS (mm)	NO.
1	-1025.	7.8708E-06	3.5067E-02	3.3781E-06	1.9127E-02	1.9950E-06	1.3379E-02	-1025.	1
2	-975.	8.1209E-06	2.7747E-02	3.4041E-06	1.8370E-02	2.0029E-06	1.2814E-02	-975.	2
3	-925.	9.3054E-06	2.7491E-02	3.7262E-06	1.8157E-02	2.1602E-06	1.2783E-02	-925.	3
4	-875.	9.7406E-06	2.6402E-02	4.1300E-06	1.8020E-02	2.2920E-06	1.2631E-02	-875.	4
5	-825.	1.0415E-05	2.9203E-02	4.2996E-06	1.7386E-02	2.4035E-06	1.2540E-02	-825.	5
6	-775.	1.0123E-05	2.4094E-02	4.2094E-06	1.6715E-02	2.3976E-06	1.2113E-02	-775.	6
7	-725.	1.0798E-05	2.4503E-02	4.4561E-06	1.6570E-02	2.5453E-06	1.2068E-02	-725.	7
8	-675.	1.0943E-05	2.4046E-02	4.8011E-06	1.6534E-02	2.6382E-06	1.1898E-02	-675.	8
9	-625.	1.1404E-05	2.6992E-02	4.9008E-06	1.6089E-02	2.7292E-06	1.1832E-02	-625.	9
10	-575.	1.0910E-05	2.2581E-02	4.7346E-06	1.5593E-02	2.7036E-06	1.1482E-02	-575.	10
11	-525.	1.1442E-05	2.3261E-02	4.9060E-06	1.5565E-02	2.8175E-06	1.1450E-02	-525.	11
12	-475.	1.1494E-05	2.2997E-02	5.1892E-06	1.5657E-02	2.8932E-06	1.1337E-02	-475.	12
13	-425.	1.1883E-05	2.5974E-02	5.2117E-06	1.5367E-02	2.9544E-06	1.1320E-02	-425.	13
14	-375.	1.1286E-05	2.1892E-02	5.0286E-06	1.4935E-02	2.8921E-06	1.1039E-02	-375.	14
15	-325.	1.1774E-05	2.2647E-02	5.1549E-06	1.4992E-02	3.0007E-06	1.1034E-02	-325.	15
16	-275.	1.1786E-05	2.2462E-02	5.3979E-06	1.5179E-02	3.0469E-06	1.0974E-02	-275.	16
17	-225.	1.2123E-05	2.5482E-02	5.3978E-06	1.4951E-02	3.0935E-06	1.0986E-02	-225.	17
18	-175.	1.1492E-05	2.1519E-02	5.1880E-06	1.4582E-02	3.0139E-06	1.0749E-02	-175.	18
19	-125.	1.1951E-05	2.2325E-02	5.2819E-06	1.4706E-02	3.1028E-06	1.0785E-02	-125.	19
20	-75.	1.1922E-05	2.2214E-02	5.4925E-06	1.4962E-02	3.1358E-06	1.0757E-02	-75.	20
21	-25.	1.2229E-05	2.5265E-02	5.4816E-06	1.4762E-02	3.1688E-06	1.0800E-02	-25.	21
22	25.	1.1567E-05	2.1384E-02	5.2509E-06	1.4440E-02	3.0796E-06	1.0589E-02	25.	22
23	75.	1.2025E-05	2.2193E-02	5.3229E-06	1.4613E-02	3.1552E-06	1.0655E-02	75.	23
24	125.	1.1968E-05	2.2132E-02	5.5118E-06	1.4917E-02	3.1770E-06	1.0652E-02	125.	24
25	175.	1.2259E-05	2.5205E-02	5.4958E-06	1.4730E-02	3.1963E-06	1.0725E-02	175.	25
26	225.	1.1575E-05	2.1369E-02	5.2481E-06	1.4446E-02	3.0909E-06	1.0555E-02	225.	26
27	275.	1.2005E-05	2.2229E-02	5.2903E-06	1.4681E-02	3.1535E-06	1.0653E-02	275.	27
28	325.	1.1936E-05	2.2188E-02	5.4769E-06	1.4996E-02	3.1665E-06	1.0672E-02	325.	28
29	375.	1.2188E-05	2.5348E-02	5.4350E-06	1.4860E-02	3.1660E-06	1.0792E-02	375.	29
30	425.	1.1457E-05	2.1578E-02	5.1674E-06	1.4622E-02	3.0402E-06	1.0667E-02	425.	30
31	475.	1.1860E-05	2.2488E-02	5.1939E-06	1.4896E-02	3.0809E-06	1.0813E-02	475.	31
32	525.	1.1717E-05	2.2579E-02	5.3506E-06	1.5269E-02	3.0524E-06	1.0910E-02	525.	32
33	575.	1.1919E-05	2.5893E-02	5.2646E-06	1.5233E-02	3.0210E-06	1.1092E-02	575.	33
34	625.	1.1133E-05	2.2160E-02	4.9690E-06	1.5057E-02	2.8590E-06	1.1005E-02	625.	34
35	675.	1.1489E-05	2.3167E-02	4.9096E-06	1.5499E-02	2.8504E-06	1.1212E-02	675.	35
36	725.	1.1274E-05	2.3401E-02	4.9887E-06	1.6012E-02	2.8025E-06	1.1344E-02	725.	36
37	775.	1.1417E-05	2.6964E-02	4.8253E-06	1.6085E-02	2.7510E-06	1.1588E-02	775.	37
38	825.	1.0522E-05	2.3317E-02	4.4117E-06	1.5971E-02	2.5472E-06	1.1481E-02	825.	38
39	875.	1.0718E-05	2.4657E-02	4.2914E-06	1.6569E-02	2.4983E-06	1.1715E-02	875.	39
40	925.	1.0136E-05	2.5627E-02	4.2483E-06	1.7223E-02	2.4179E-06	1.1838E-02	925.	40
41	975.	9.7538E-06	3.0793E-02	3.9646E-06	1.7446E-02	2.3437E-06	1.2161E-02	975.	41

Table 2.3.2 (Continued)

M= 4 NO.	RPOS (mm)	400 mm step FLUX(200 mm)	ERR1	** SUPERPOSED FLUX (En > 10 MeV) ** FLUX(400 mm)	ERR2	FLUX(600 mm)	ERR3	RPOS (mm)	NO.
1	-1025.	3.3694E-05	4.7573E-02	1.2128E-05	2.6163E-02	6.8747E-06	1.8361E-02	-1025.	1
2	-975.	3.0027E-05	3.9823E-02	1.1393E-05	2.4325E-02	6.4639E-06	1.7244E-02	-975.	2
3	-925.	3.2257E-05	3.9242E-02	1.1920E-05	2.3715E-02	6.8384E-06	1.7095E-02	-925.	3
4	-875.	2.8884E-05	3.3279E-02	1.3414E-05	2.4085E-02	7.3579E-06	1.6852E-02	-875.	4
5	-825.	2.8940E-05	3.0142E-02	1.3836E-05	2.2924E-02	7.7602E-06	1.6716E-02	-825.	5
6	-775.	3.0864E-05	2.7338E-02	1.4039E-05	2.2696E-02	8.1424E-06	1.6477E-02	-775.	6
7	-725.	3.2687E-05	2.9313E-02	1.5021E-05	2.2723E-02	8.6589E-06	1.6480E-02	-725.	7
8	-675.	3.6957E-05	3.3890E-02	1.5579E-05	2.2475E-02	8.7034E-06	1.6314E-02	-675.	8
9	-625.	3.9670E-05	4.1038E-02	1.5772E-05	2.2268E-02	8.8676E-06	1.6259E-02	-625.	9
10	-575.	3.4787E-05	3.4891E-02	1.4593E-05	2.1102E-02	8.3390E-06	1.5531E-02	-575.	10
11	-525.	3.6182E-05	3.5308E-02	1.4641E-05	2.0889E-02	8.5196E-06	1.5394E-02	-525.	11
12	-475.	3.2242E-05	3.0178E-02	1.5803E-05	2.1478E-02	8.9390E-06	1.5286E-02	-475.	12
13	-425.	3.1883E-05	2.7694E-02	1.5781E-05	2.0804E-02	9.1640E-06	1.5273E-02	-425.	13
14	-375.	3.3208E-05	2.5631E-02	1.5878E-05	2.0737E-02	9.3414E-06	1.5157E-02	-375.	14
15	-325.	3.4760E-05	2.7710E-02	1.6614E-05	2.0999E-02	9.8214E-06	1.5238E-02	-325.	15
16	-275.	3.8775E-05	3.2380E-02	1.6949E-05	2.1007E-02	9.7070E-06	1.5188E-02	-275.	16
17	-225.	4.1173E-05	3.9581E-02	1.7005E-05	2.0959E-02	9.7640E-06	1.5243E-02	-225.	17
18	-175.	3.6106E-05	3.3662E-02	1.5675E-05	1.9973E-02	9.1027E-06	1.4693E-02	-175.	18
19	-125.	3.7327E-05	3.4258E-02	1.5540E-05	1.9932E-02	9.1933E-06	1.4635E-02	-125.	19
20	-75.	3.3174E-05	2.9365E-02	1.6517E-05	2.0700E-02	9.5137E-06	1.4649E-02	-75.	20
21	-25.	3.2680E-05	2.7049E-02	1.6405E-05	2.0147E-02	9.6642E-06	1.4713E-02	-25.	21
22	25.	3.3828E-05	2.5184E-02	1.6384E-05	2.0195E-02	9.8044E-06	1.4640E-02	25.	22
23	75.	3.5384E-05	2.7244E-02	1.7004E-05	2.0584E-02	1.0184E-05	1.4834E-02	75.	23
24	125.	3.9219E-05	3.2023E-02	1.7172E-05	2.0764E-02	1.0020E-05	1.4828E-02	125.	24
25	175.	4.1540E-05	3.9238E-02	1.7225E-05	2.0722E-02	1.0012E-05	1.4944E-02	175.	25
26	225.	3.6332E-05	3.3457E-02	1.5786E-05	1.9855E-02	9.2969E-06	1.4461E-02	225.	26
27	275.	3.7449E-05	3.4149E-02	1.5531E-05	1.9940E-02	9.3260E-06	1.4472E-02	275.	27
28	325.	3.3247E-05	2.9302E-02	1.6506E-05	2.0713E-02	9.6155E-06	1.4525E-02	325.	28
29	375.	3.2647E-05	2.7073E-02	1.6309E-05	2.0250E-02	9.6913E-06	1.4668E-02	375.	29
30	425.	3.3674E-05	2.5293E-02	1.6214E-05	2.0374E-02	9.7428E-06	1.4692E-02	425.	30
31	475.	3.5158E-05	2.7411E-02	1.6675E-05	2.0911E-02	1.0069E-05	1.4947E-02	475.	31
32	525.	3.8883E-05	3.2291E-02	1.6811E-05	2.1138E-02	9.8066E-06	1.5054E-02	525.	32
33	575.	4.0946E-05	3.9796E-02	1.6709E-05	2.1244E-02	9.6915E-06	1.5295E-02	575.	33
34	625.	3.5516E-05	3.4198E-02	1.5197E-05	2.0460E-02	8.8910E-06	1.4892E-02	625.	34
35	675.	3.6398E-05	3.5101E-02	1.4851E-05	2.0657E-02	8.7919E-06	1.5025E-02	675.	35
36	725.	3.1801E-05	3.0546E-02	1.5669E-05	2.1571E-02	8.8700E-06	1.5237E-02	725.	36
37	775.	3.0939E-05	2.8433E-02	1.5230E-05	2.1350E-02	8.7683E-06	1.5541E-02	775.	37
38	825.	3.1646E-05	2.6741E-02	1.4949E-05	2.1680E-02	8.5801E-06	1.5730E-02	825.	38
39	875.	3.2872E-05	2.9151E-02	1.4916E-05	2.2688E-02	8.6226E-06	1.6162E-02	875.	39
40	925.	3.6165E-05	3.4563E-02	1.4572E-05	2.3346E-02	8.2463E-06	1.6366E-02	925.	40
41	975.	3.7863E-05	4.2896E-02	1.4009E-05	2.3819E-02	8.0145E-06	1.6786E-02	975.	41

Table 2.3.3 Activation reactions used in the source characteristics measurement

	Reactions	Half-Life	Abundance (%)	γ-ray Energy (keV)	γ-ray Branching (%)	Threshold Energy (MeV)	Typical Foil Size [mm]
1.	$^{27}Al(n,\alpha)^{24}Na$	15.02 h	100.0	1368.6	100.0	5	15φ x 1
2.	$^{nat}Ti(n,x)^{46}Sc$	83.83 d	100.0	889.3	99.98	4	20φ x 1
3.	$^{nat}Ti(n,x)^{47}Sc$	3.341 d	100.0	159.4	68.0	1.5	20φ x 1
4.	$^{nat}Ti(n,x)^{48}Sc$	1.821 d	100.0	983.5	100.0	5	20φ x 1
5.	$Fe(n,x)^{56}Mn$	2.579 h	100.0	846.8	98.9	--------	10φ x 1
6.	$^{54}Fe(n,p)^{54}Mn$	312.2 d	5.8	834.8	99.98	2	10φ x 1
7.	$^{58}Ni(n,p)^{58}Co$	70.92 d	68.26	810.8	99.5	2	15φ x 1
8.	$^{58}Ni(n,2n)^{57}Ni$	1.503 d	68.27	1377.6	77.9	12.5	15φ x 1
9.	$^{59}Co(n,\alpha)^{56}Mn$	2.579 h	100.0	846.8	98.9	6	10φ x 1
10.	$^{64}Zn(n,p)^{64}Cu$	12.70 h	48.6	511.0	74.2	1.5	20φ x 1
11.	$^{90}Zr(n,2n)^{89}Zr$	3.268 d	51.45	909.2	99.01	12	20φ x 1
12.	$^{93}Nb(n,2n)^{92m}Nb$	10.15 d	100.0	934.5	99.0	9	20φ x 1
13.	$^{115}In(n,n')^{115m}In$	4.486 h	95.7	336.3	45.8	0.34	10 x 10 x 1
14.	$^{197}Au(n,\gamma)^{198}Au$	2.694 d	100.0	411.8	95.5	--------	10 x 10 x 0.001

Table 2.3.4 Reaction rate distributions along the line source at a distance of 219 mm from the line source without blanket (distance is measured from beam drift tube side)

DISTANCE FROM CENTER OF ASSEMBLY[mm]	Al27(n,alpha)Na24	Ti(n,x)Sc46	Ti(n,x)Sc47	Ti(n,x)Sc48	Fe54(n,p)Mn54
-1000.0*	2.943E-30(3.2)**	3.707E-30(4.2)	3.870E-31(3.6)	1.279E-30(3.3)	9.347E-30(6.6)
- 800.0	4.497E-30(3.1)	-------	-------	-------	-------
- 600.0	5.066E-30(3.1)	-------	-------	-------	-------
- 400.0	5.375E-30(3.1)	6.917E-30(4.3)	8.554E-31(3.5)	2.458E-30(3.2)	1.643E-29(6.1)
- 200.0	5.584E-30(3.1)	-------	-------	-------	-------
0.0	5.587E-30(3.1)	7.019E-30(3.9)	9.255E-31(3.5)	2.587E-30(3.2)	1.690E-29(6.1)
200.0	5.573E-30(3.1)	-------	-------	-------	-------
400.0	5.439E-30(3.1)	6.961E-30(3.8)	9.120E-31(3.5)	2.518E-30(3.2)	1.651E-29(6.2)
600.0	5.084E-30(3.1)	-------	-------	-------	-------
800.0	4.603E-30(3.1)	-------	-------	-------	-------
1000.0	2.998E-30(3.1)	3.819E-30(4.1)	5.691E-31(3.5)	1.442E-30(3.3)	8.937E-30(6.5)

* 20 mm from the front end of the assembly

** Read as 2.943×10^{-30} [reaction/total source neutron] with 3.2 % relative error

DISTANCE FROM CENTER OF ASSEMBLY[mm]	Fe(n,x)Mn56	Co59(n,alpha)Mn56	Ni58(n,2n)Ni57	Ni58(n,p)Co58	Zn64(n,p)Cu64
-1000.0	2.596E-30(3.1)	-------	3.621E-31(4.0)	9.566E-30(3.3)	4.303E-30(3.1)
- 800.0	-------	-------	-------	-------	-------
- 600.0	-------	-------	-------	-------	-------
- 400.0	4.910E-30(3.1)	1.356E-30(3.1)	1.064E-30(3.8)	1.625E-29(3.3)	7.608E-30(3.0)
- 200.0	-------	-------	-------	-------	-------
0.0	5.286E-30(3.1)	1.407E-30(3.1)	1.173E-30(3.8)	1.672E-29(3.3)	7.809E-30(3.0)
200.0	-------	-------	-------	-------	-------
400.0	5.069E-30(3.1)	1.389E-30(3.1)	1.227E-30(3.8)	1.622E-29(3.3)	7.565E-30(3.0)
600.0	-------	-------	-------	-------	-------
800.0	-------	-------	-------	-------	-------
1000.0	2.874E-30(3.1)	-------	8.837E-31(3.8)	8.694E-30(3.3)	3.806E-30(3.1)

Table 2.3.4 (Continued)

DISTANCE FROM CENTER OF ASSEMBLY [mm]	Zr90(n,2n)Zr89	Nb93(n,2n)Nb92m	In115(n,n')In115m	Au197(n,gamma)Au198
-1000.0	1.117E-29(3.1)	1.052E-29(2.8)	2.196E-30(3.5)	2.212E-29(6.5)
- 800.0	--------	1.670E-29(2.9)	3.205E-30(3.5)	2.787E-29(7.9)
- 600.0	--------	1.969E-29(2.9)	3.701E-30(3.4)	2.984E-29(8.1)
- 400.0	2.712E-29(3.0)	2.057E-29(2.9)	3.785E-30(3.4)	2.631E-29(7.9)
- 200.0	--------	2.138E-29(2.9)	3.989E-30(3.4)	2.442E-29(10.6)
0.0	2.960E-29(3.0)	2.185E-29(2.8)	4.054E-30(3.4)	2.797E-29(7.5)
200.0	--------	2.142E-29(2.9)	3.894E-30(3.4)	2.511E-29(10.0)
400.0	2.925E-29(3.0)	2.105E-29(2.9)	3.904E-30(3.5)	2.016E-29(12.1)
600.0	--------	2.044E-29(2.9)	3.597E-30(3.4)	2.517E-29(7.5)
800.0	--------	1.832E-29(2.9)	3.182E-30(3.5)	2.500E-29(12.6)
1000.0	2.020E-29(3.1)	1.292E-29(2.8)	2.074E-30(3.5)	2.644E-29(11.0)

Table 2.3.5 Calculated neutron emission intensity for each emission angle

(a) Horizontal plane

No.	Angle (deg.)	Intensity (/cm²/source)		
		Total	over 10MeV	over 1MeV
1	0	1.1312	1.0517	1.0983
2	5	1.1314	1.0518	1.0985
3	10	1.1284	1.0488	1.0956
4	15	1.1266	1.0464	1.0936
5	20	1.1314	1.0503	1.0981
6	25	1.1216	1.0396	1.0880
7	30	1.1219	1.0390	1.0880
8	35	1.1200	1.0363	1.0857
9	40	1.1204	1.0360	1.0859
10	45	1.1113	1.0262	1.0765
11	50	1.1043	1.0186	1.0692
12	55	1.1009	1.0147	1.0656
13	60	1.0872	1.0004	1.0516
14	65	1.0782	0.99101	1.0425
15	70	1.0603	0.97285	1.0247
16	75	1.0180	0.93117	0.98288
17	80	0.93854	0.85372	0.90461
18	85	0.82512	0.74455	0.79329
19	90	1.0902	1.0094	1.0577
20	95	1.0945	1.0034	1.0575
21	100	1.0840	0.98868	1.0449
22	105	1.0797	0.98087	1.0391
23	110	1.0783	0.97604	1.0362
24	115	1.0657	0.96090	1.0225
25	120	1.0532	0.94614	1.0089
26	125	1.0581	0.94863	1.0126
27	130	1.0175	0.90745	0.97166

Table 2.3.5 (Continued)

No.	Angle (deg.)	Intensity (/cm²/source)		
		Total	over 10MeV	over 1MeV
28	135	0.88820	0.78083	0.84351
29	140	0.79463	0.68890	0.75057
30	145	0.73360	0.62739	0.68923
31	150	0.74641	0.63433	0.69927
32	155	0.91711	0.78971	0.86340
33	160	0.99500	0.85129	0.93465
34	165	1.0221	0.86071	0.95440
35	170	0.97312	0.80120	0.90262
36	175	1.1785	0.97094	1.0921
37	180	1.1567	0.96016	1.0739

Table 2.3.5 (Continued)

(b) Vertical plane

No.	Angle (deg.)	Intensity (/cm²/source)		
		Total	over 10MeV	over 1MeV
38	φ 5	1.1311	1.0517	1.0983
39	φ 10	1.1283	1.0488	1.0955
40	φ 15	1.1269	1.0469	1.0939
41	φ 30	1.1224	1.0397	1.0886
42	φ 45	1.1117	1.0265	1.0773
43	φ 60	1.0885	1.0016	1.0537
44	φ 75	1.0237	0.93818	0.99020
45	φ 85	0.75078	0.67701	0.72340
46	φ 90	1.0391	0.96872	1.0109
47	φ 95	1.0594	0.97121	1.0246
48	φ 105	1.0318	0.93582	0.99470
49	φ 120	1.0030	0.89404	0.96081
50	φ 135	0.90910	0.76329	0.84815
51	φ 150	0.75261	0.63578	0.70373
52	φ 165	1.0215	0.86134	0.95471

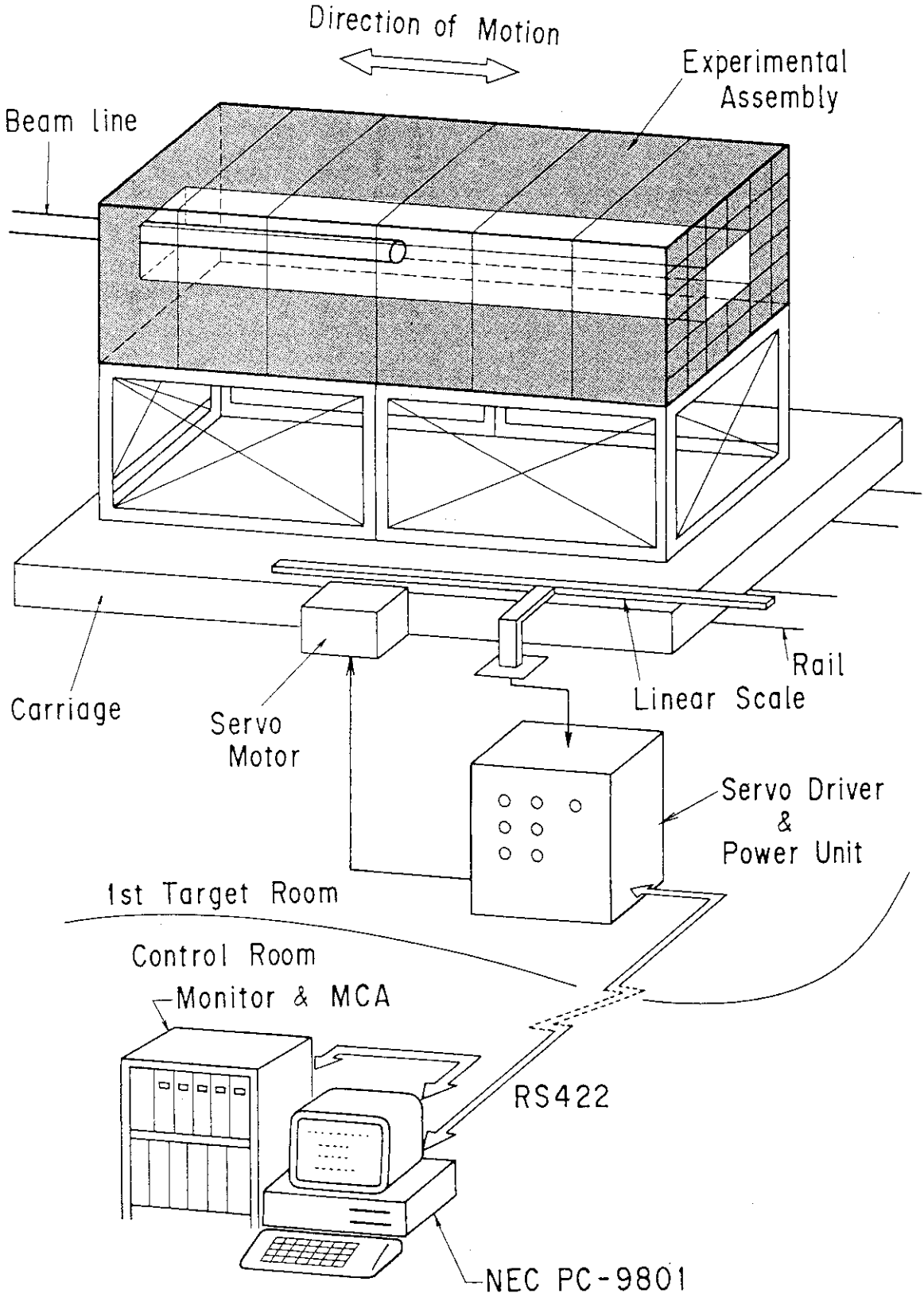

Fig. 2.2.1 Concept of the FNS line source system

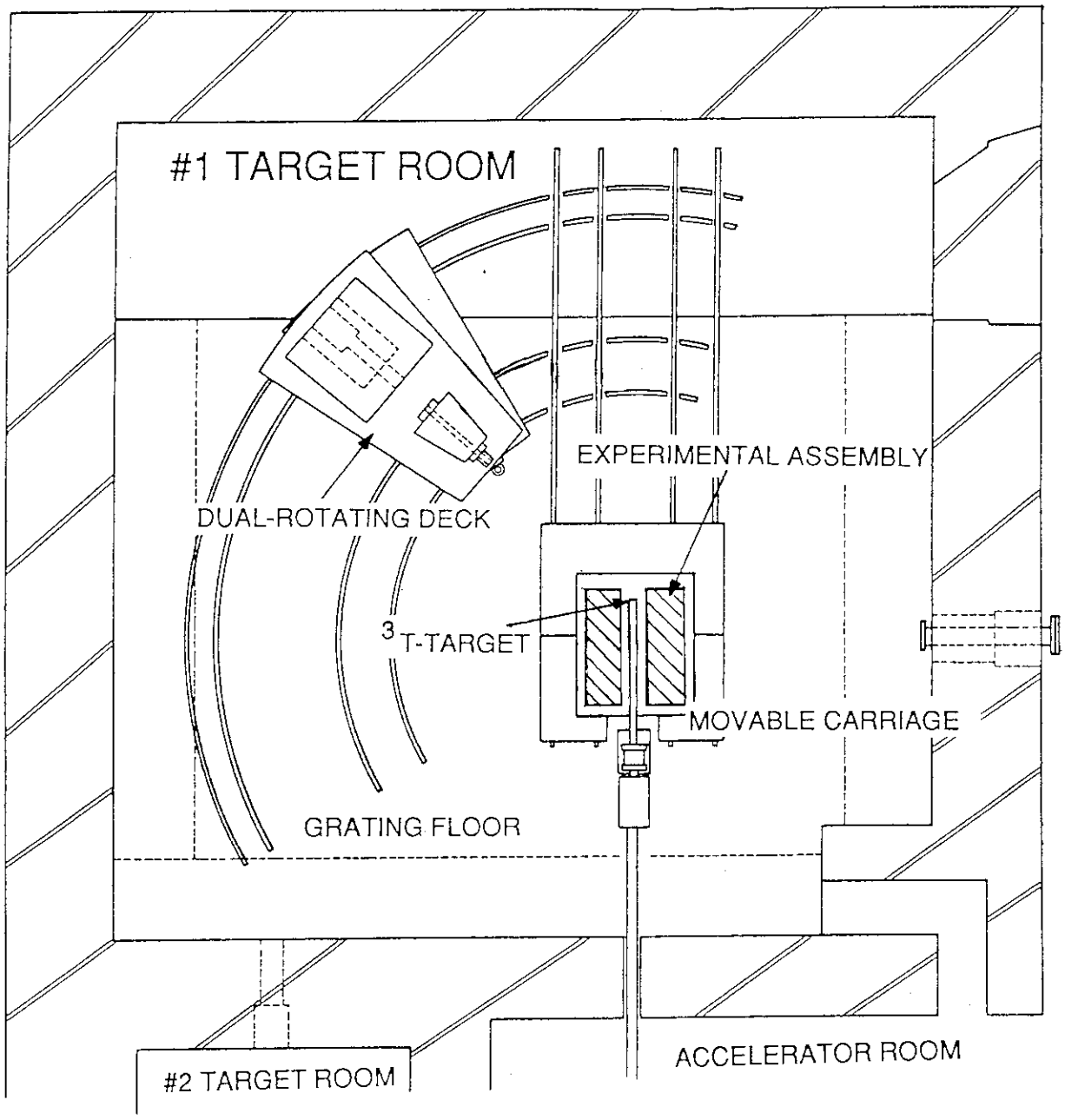

Fig. 2.2.2 Experimental room, moving deck and beam drift tube (top view)

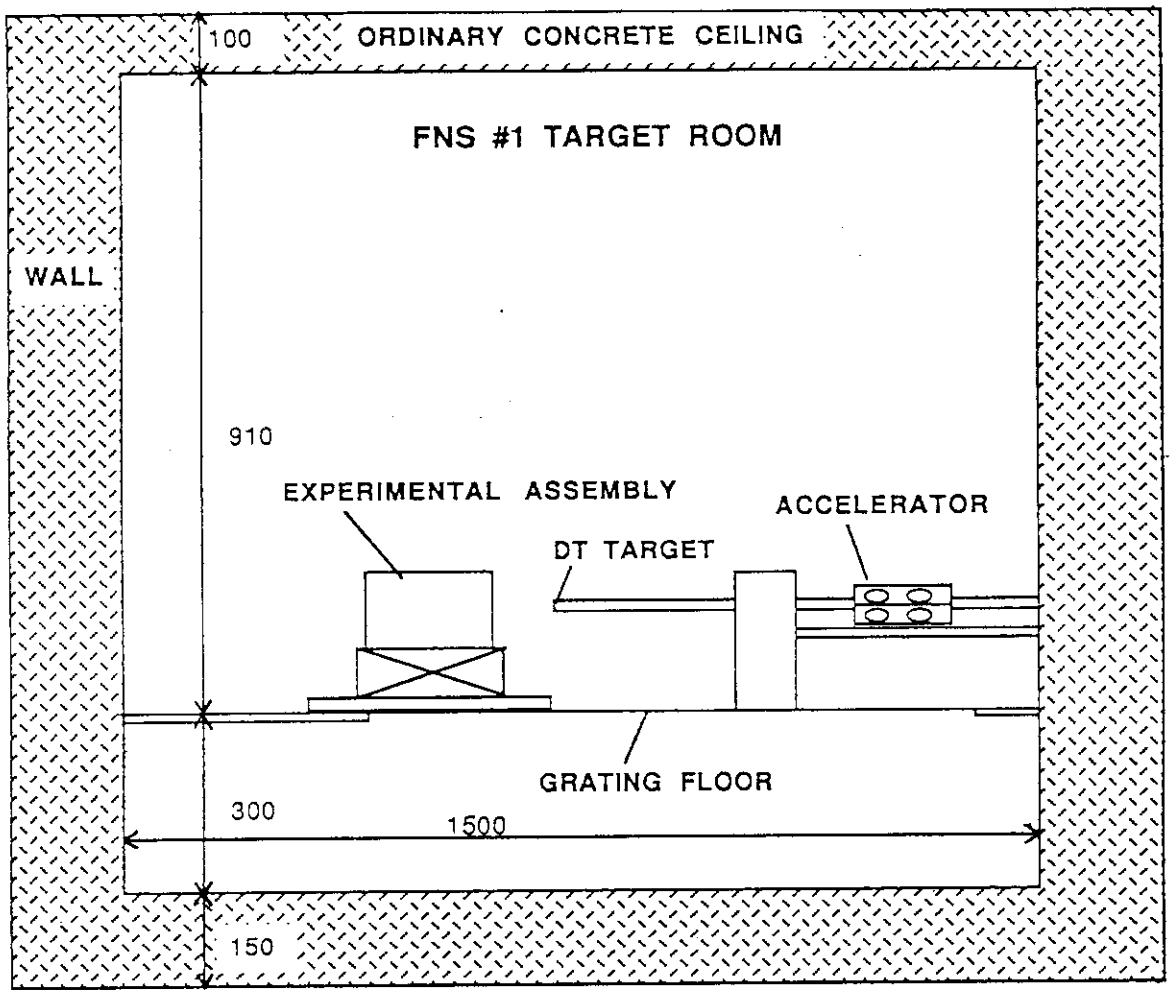

Fig. 2.2.3 Experimental room, moving deck and beam drift tube (side view)

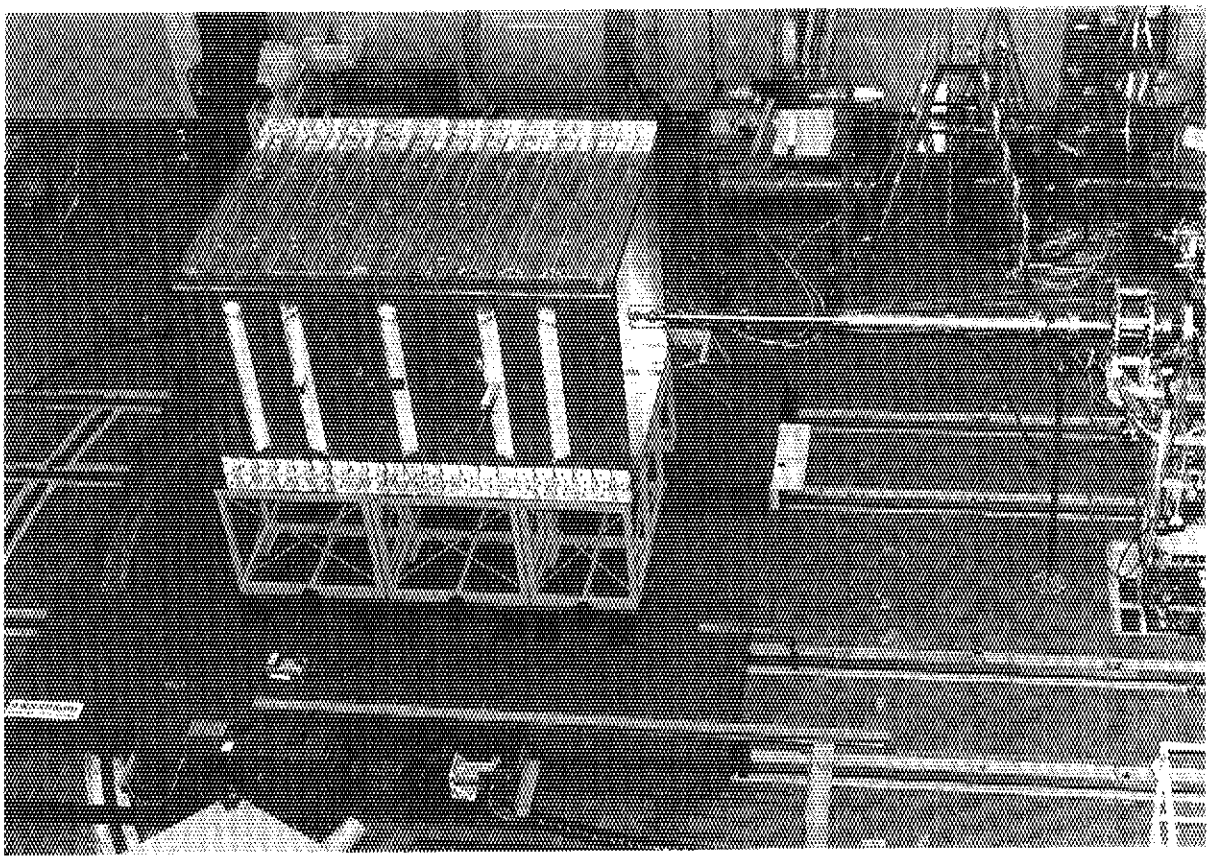

Fig. 2.2.4 Photograph of carriage-deck and annular blanket assembly

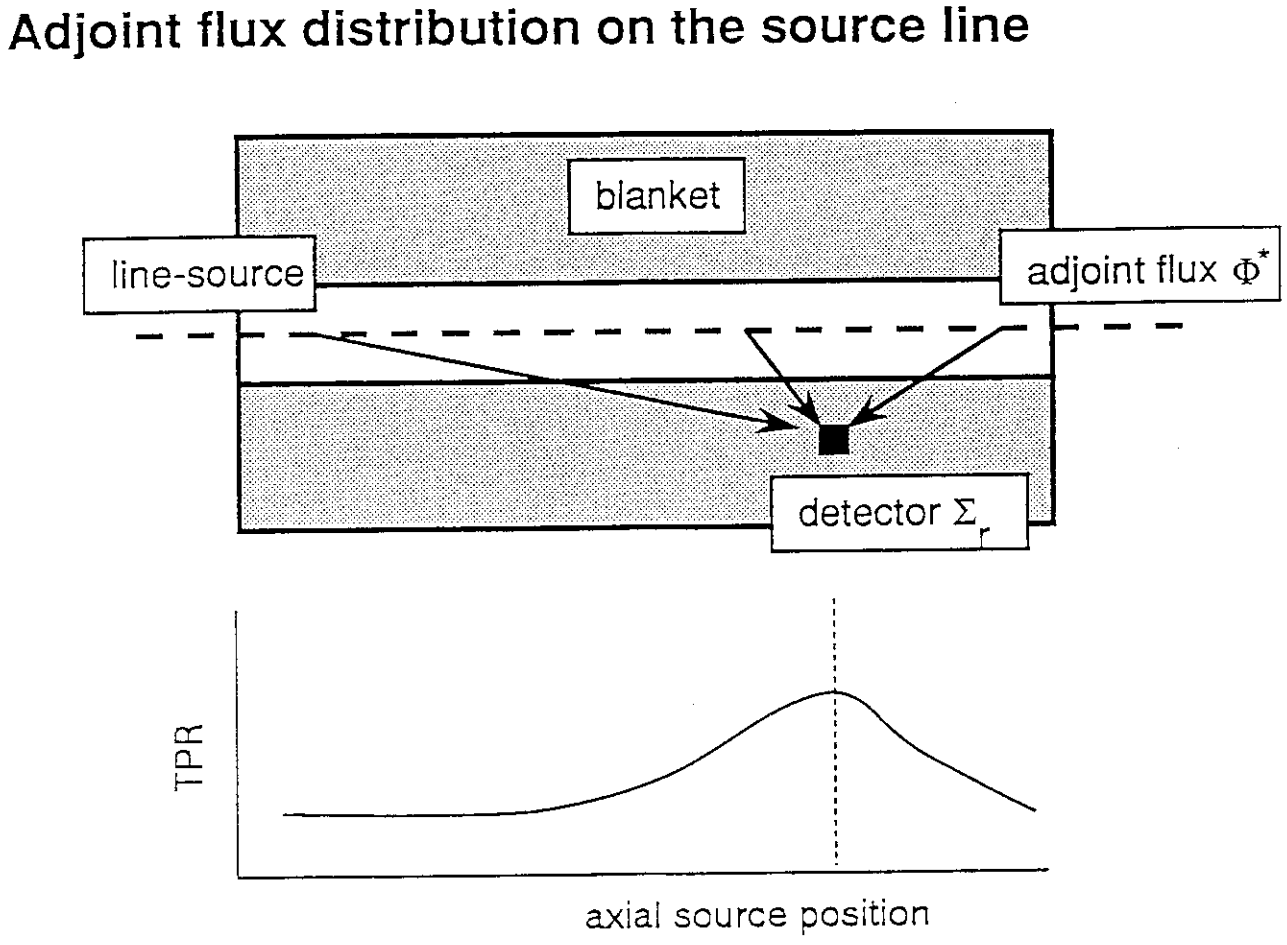

Fig. 2.2.5 Illustration of importance (adjoint flux) distribution for a detector location

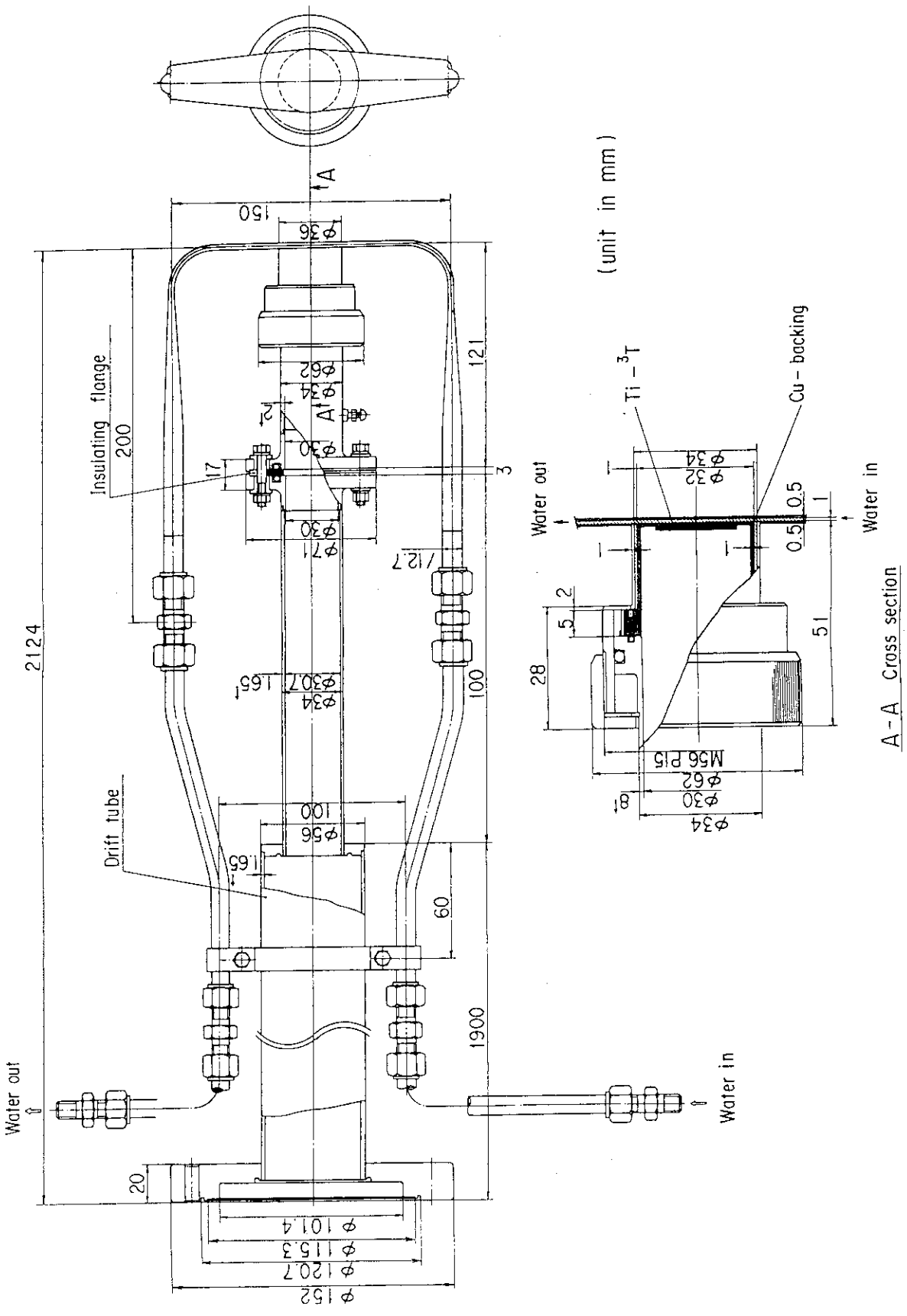

Fig. 2.2.6 Long tube water cooled target (LTWC) assembly

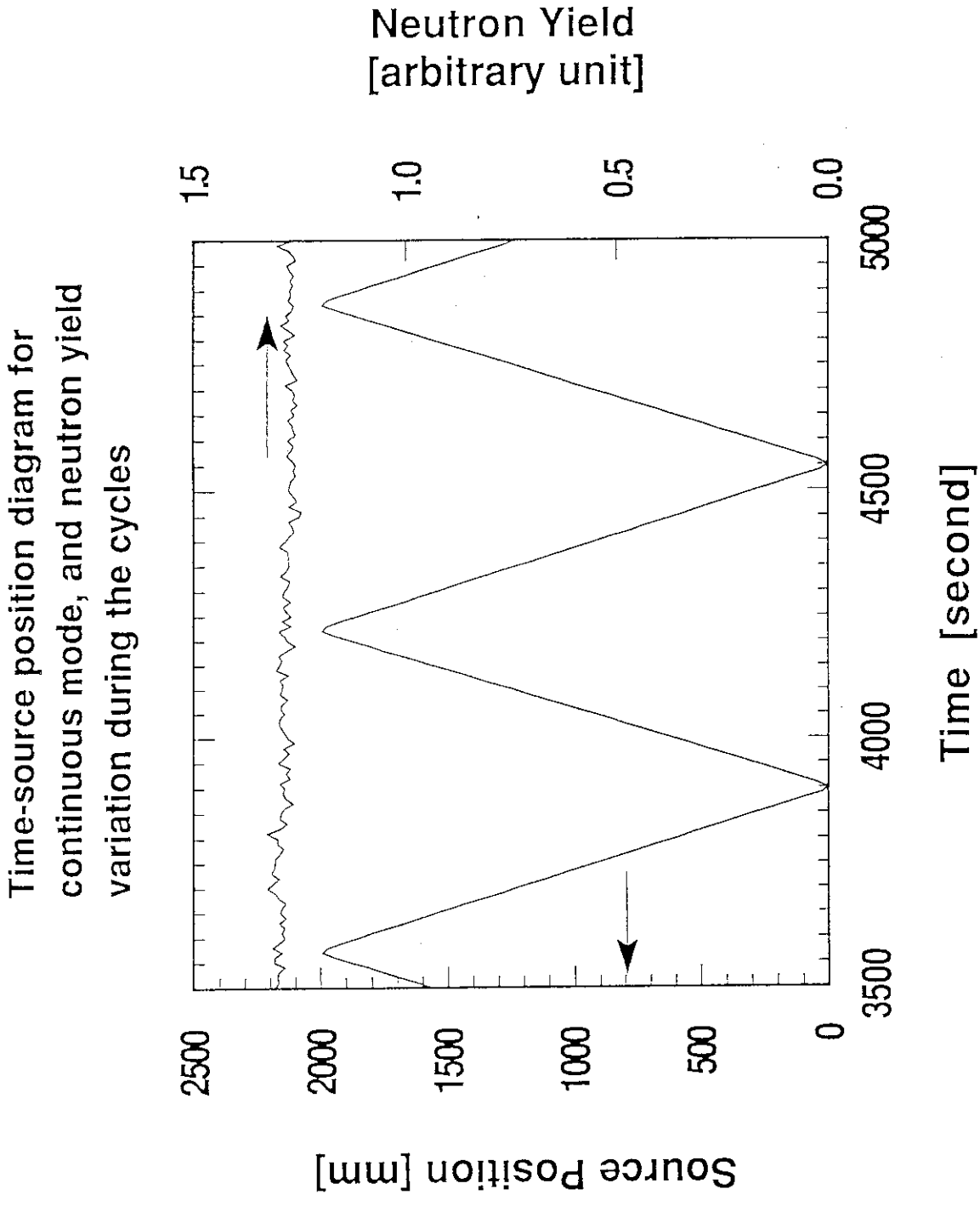

Fig. 2.2.7 Typical record of neutron emission yield and deck position as a function of irradiation time

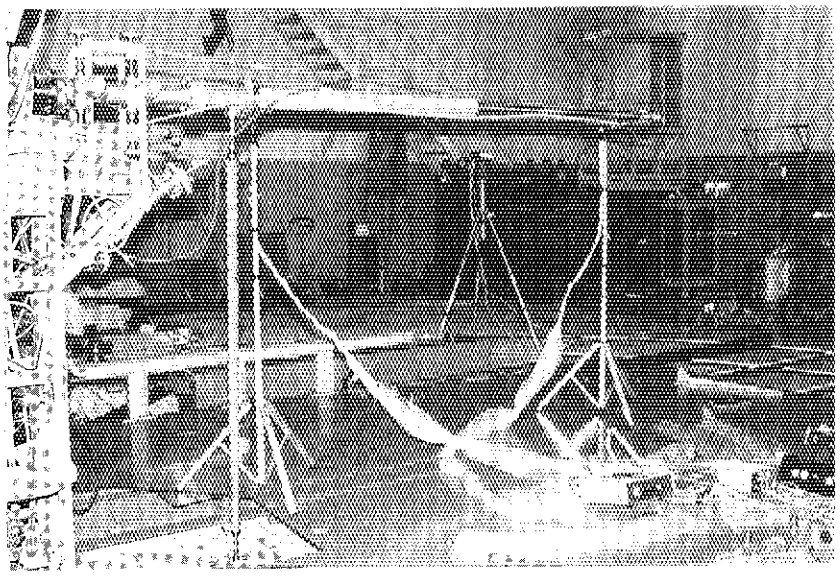

Fig. 2.3.1 Experimental setup for neutron flux distribution measurement around the target assembly using a miniature NE213 detectors

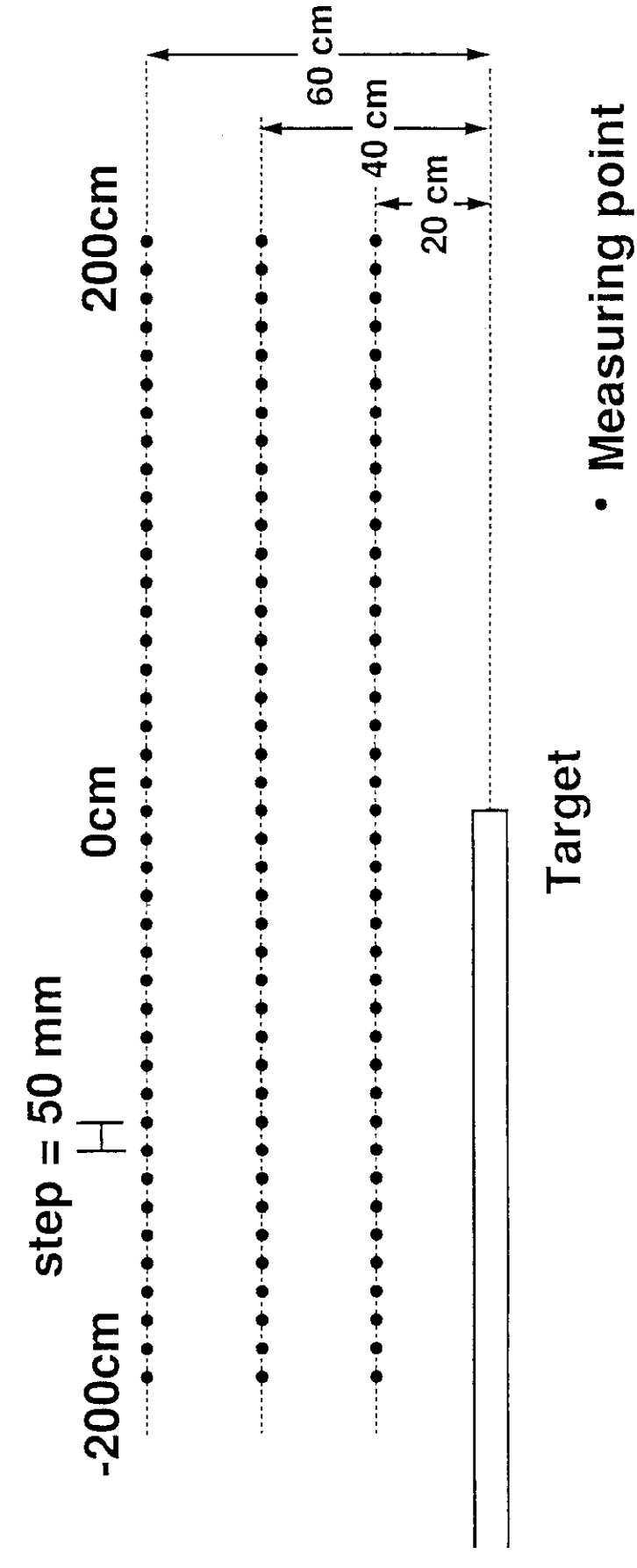

Fig. 2.3.2 Measured positions to obtain the line source characteristics.
The 81 point data along the source axis were taken for one distance.

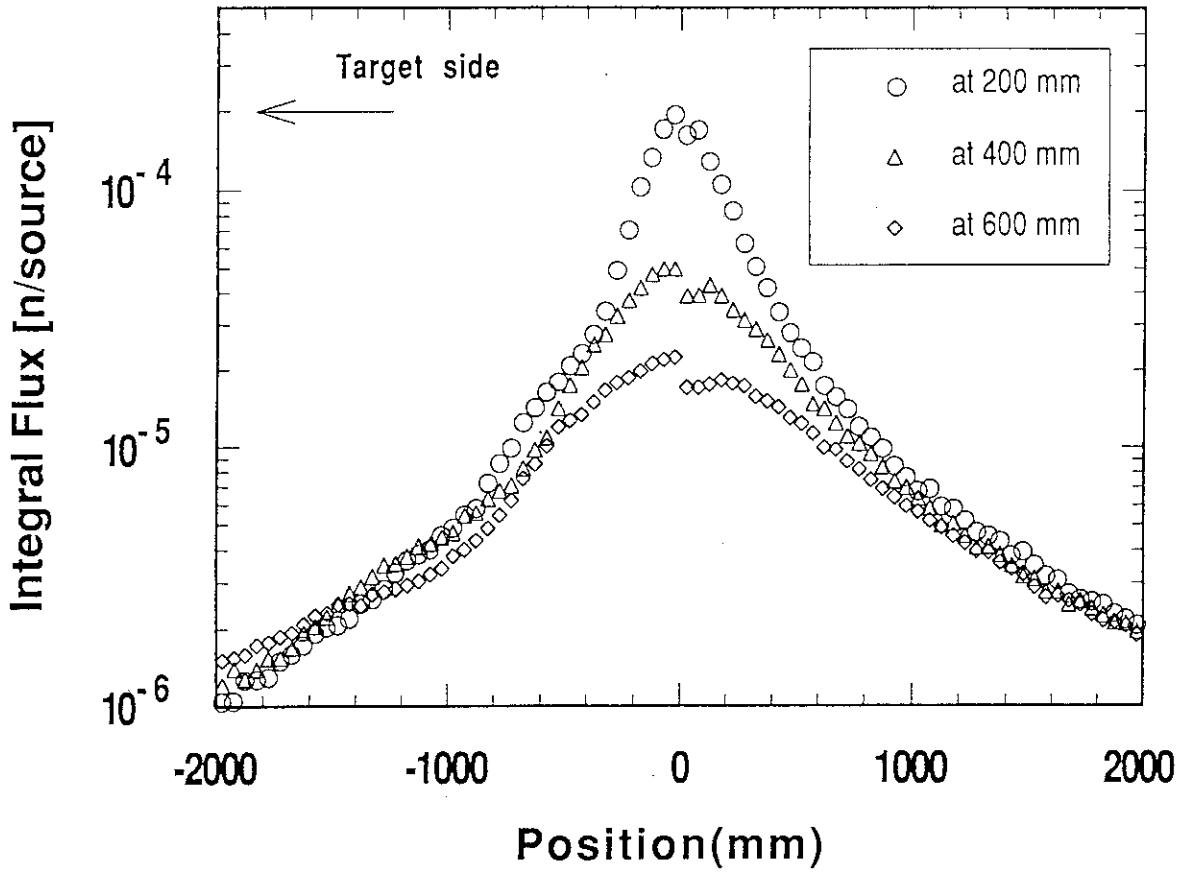

Fig. 2.3.3 Measured flux distributions at each distance from the line source axis

$$\phi = \frac{\sigma}{4 \cdot \pi \cdot r}\left[\tan^{-1}\frac{L-a}{r} + \tan^{-1}\frac{L+a}{r}\right]$$

σ : Density of line source

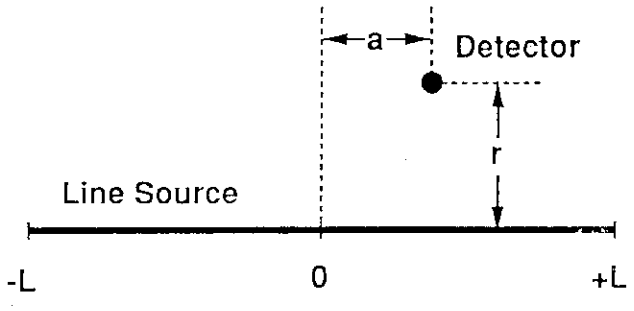

Fig. 2.3.4 Flux distribution for an ideal line source with uniform density and isotropic emission

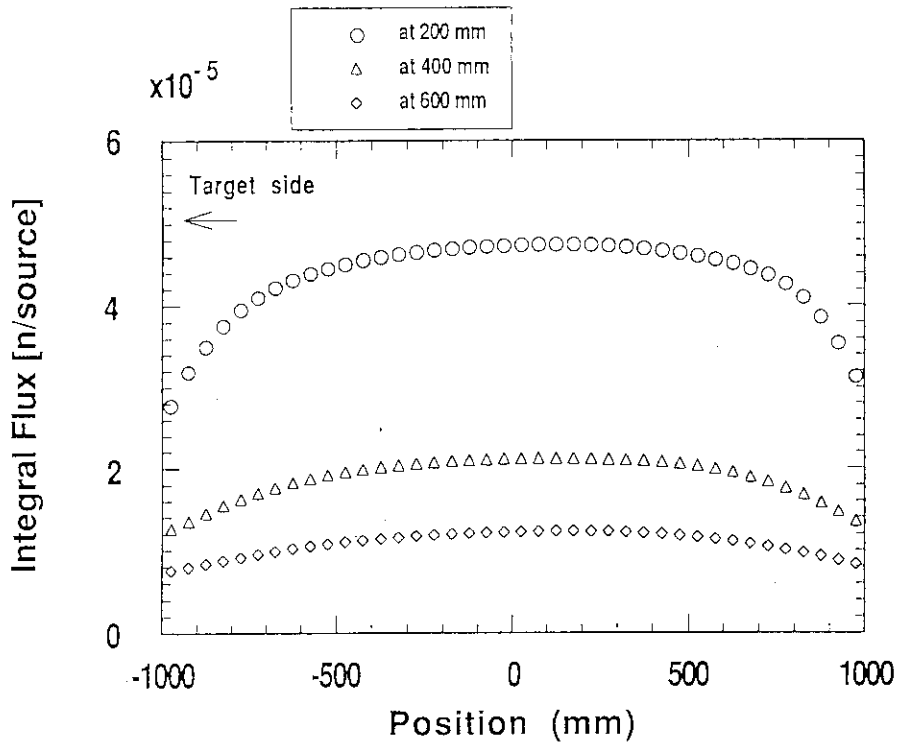

Fig. 2.3.5 Superposed neutron flux for vertical line source of 2m in length

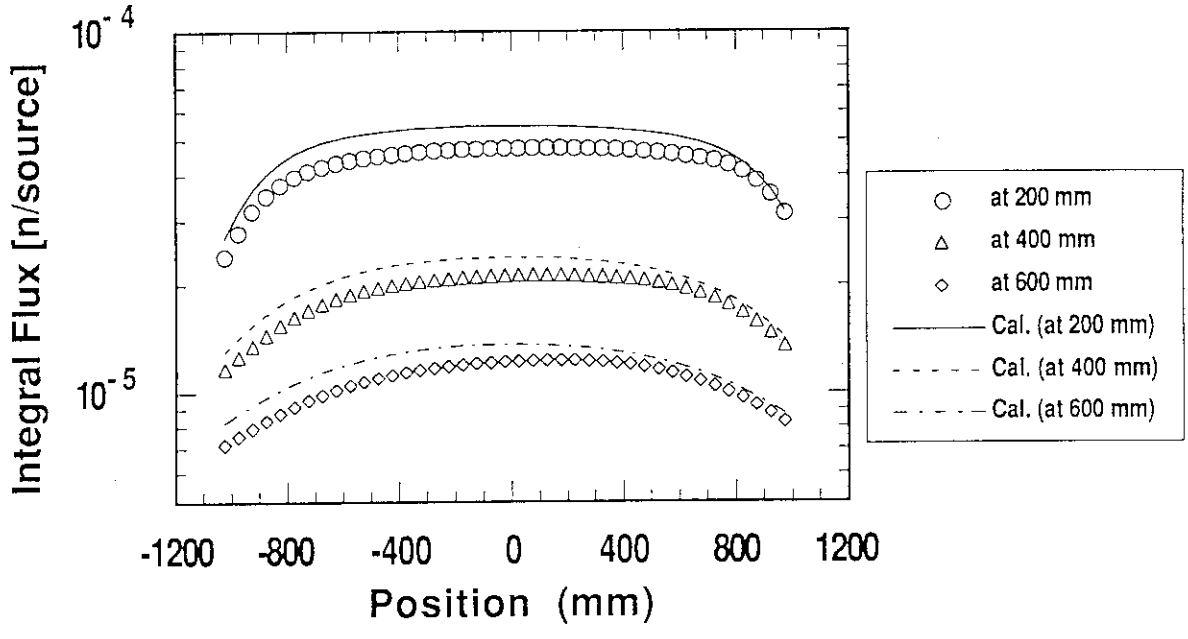

Fig. 2.3.6 Comparison of the measured superposed flux to the calculation for ideal source with uniform and isotropic emission

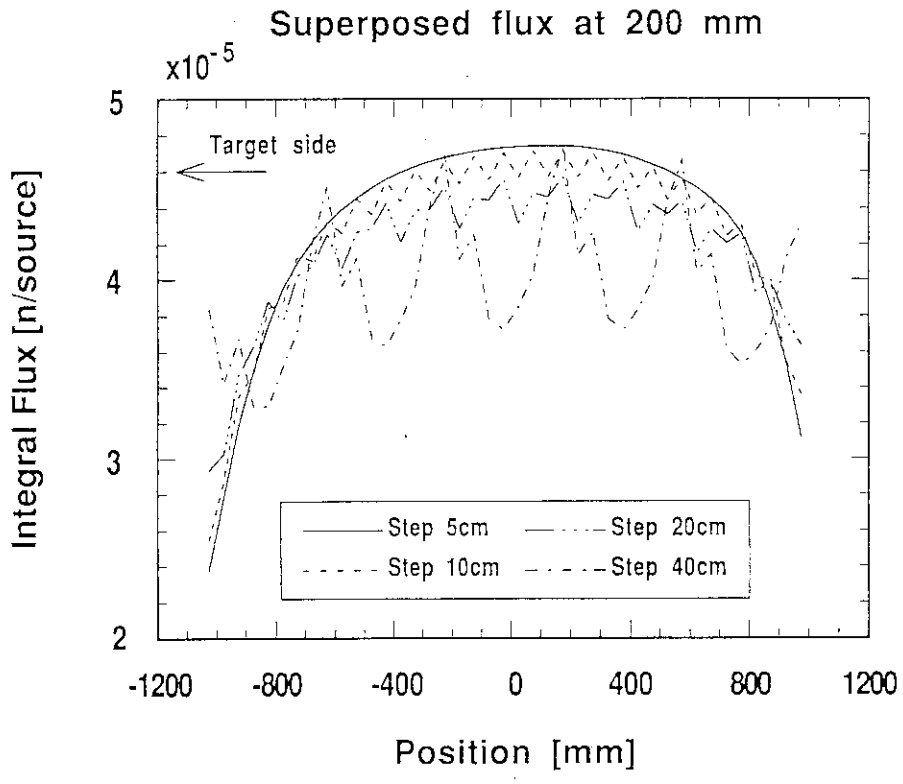

Fig. 2.3.7 Dependence of superposed flux distribution on the interval of source step (comparison in the 5 cm step distribution)

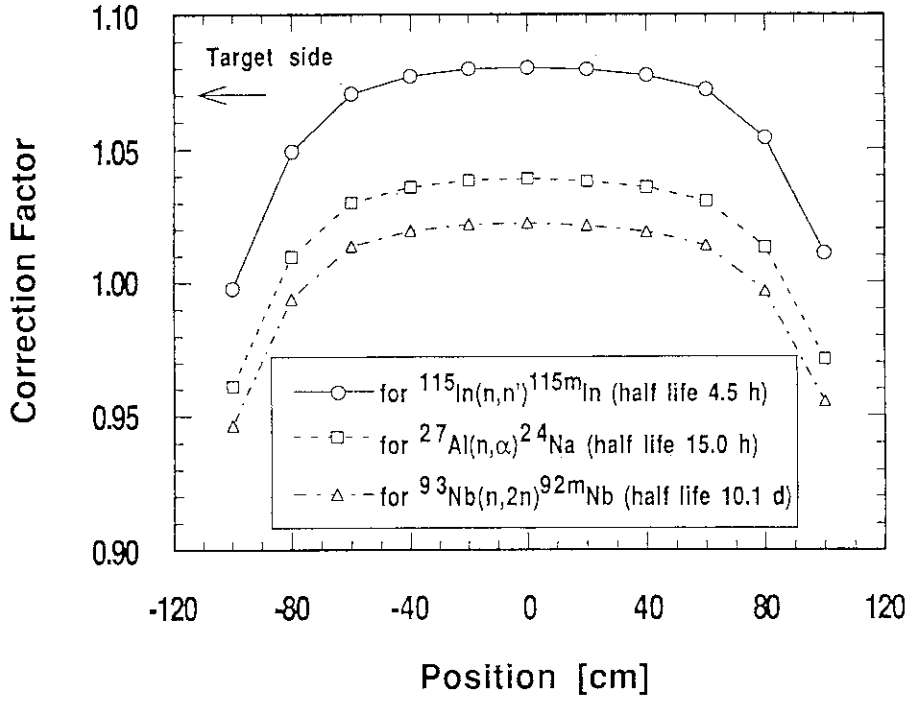

Fig. 2.3.8 Correction factor of neutron flux variance at each foil position shown for the cases of three different decay times

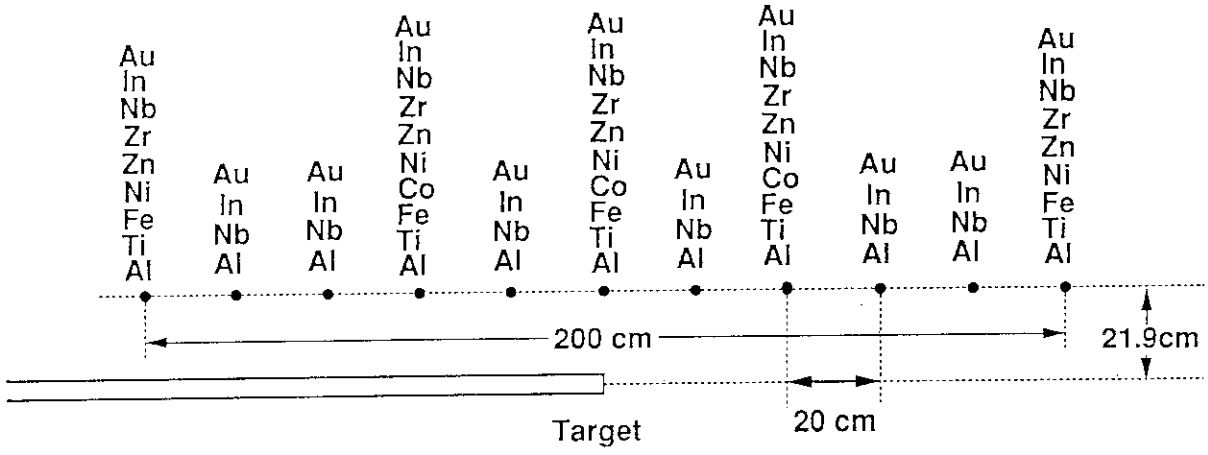

Fig. 2.3.9 Foil locations for the source characteristics measurement with the continuous mode operation

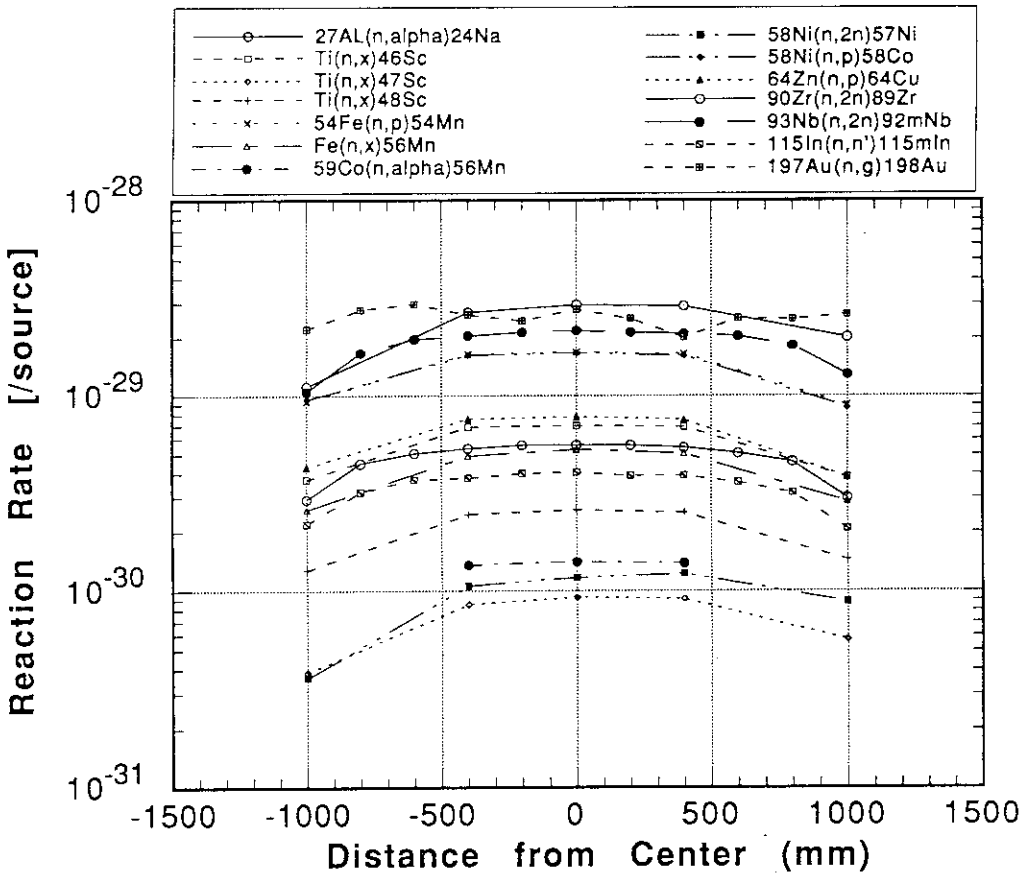

Fig. 2.3.10 Measured reaction rate distributions at 219 mm distance from the present line source

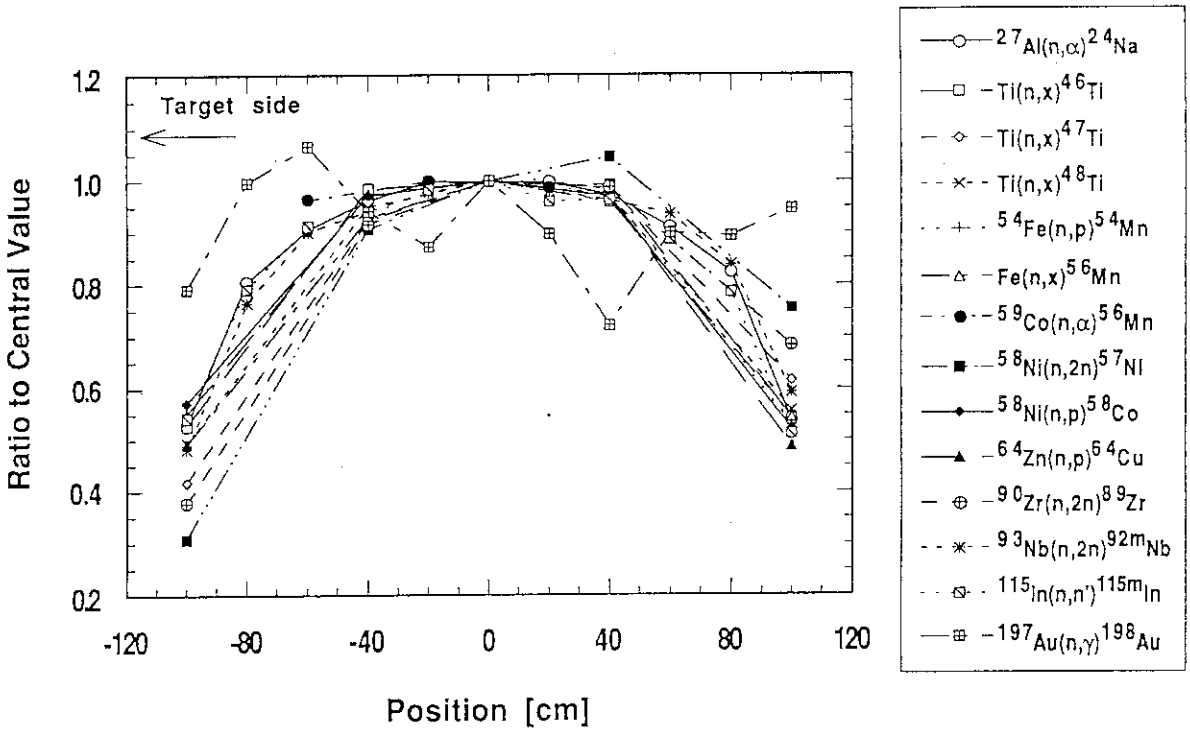

Fig. 2.3.11 Asymmetry of reaction rate distribution. Ratios to the central value are plotted

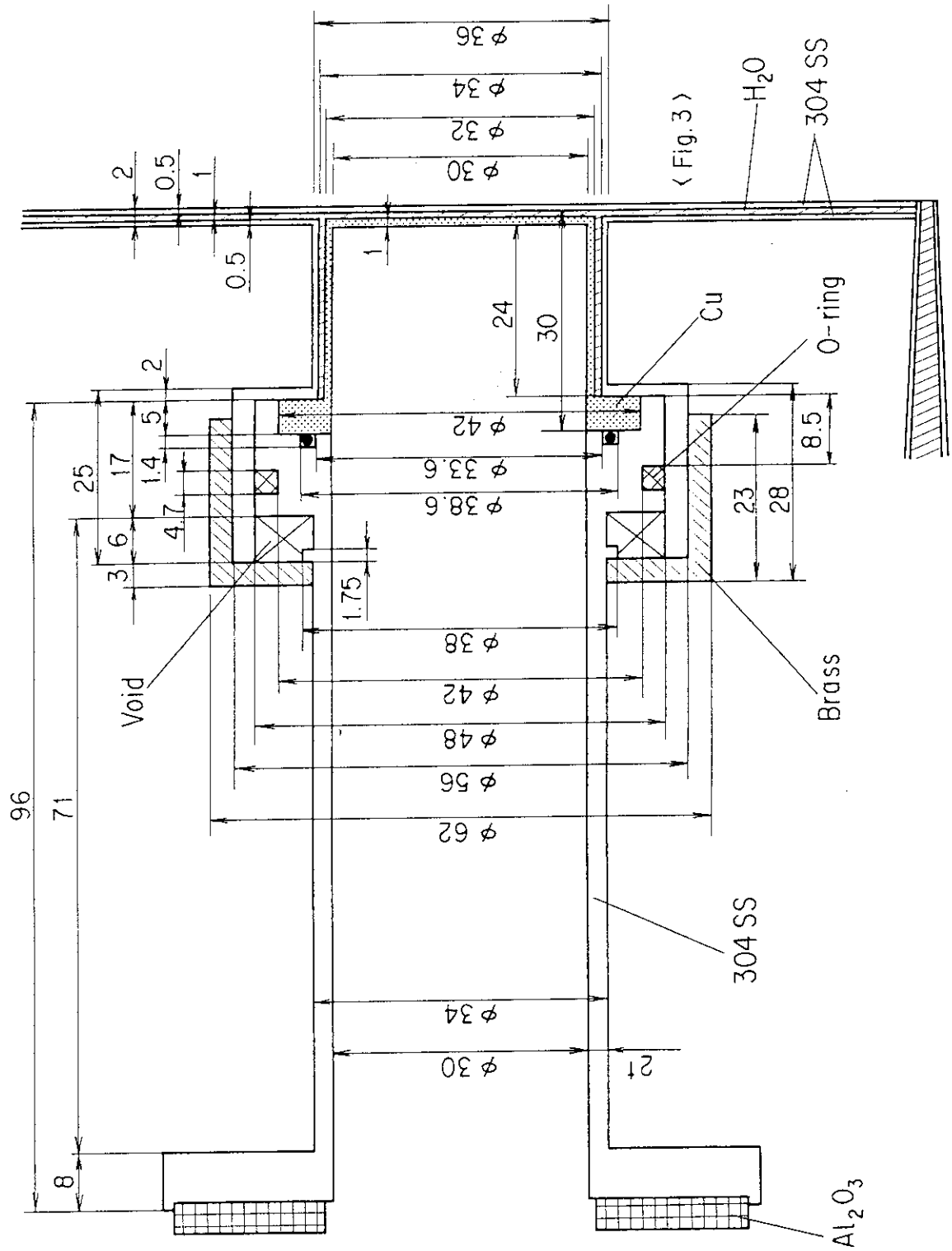

Fig. 2.3.12 Geometrical model for MORSE-DD Monte Carlo code to calculate neutron emission spectrum from the LTWC target

(a) water cooling channel and cup-shaped tritium metal target

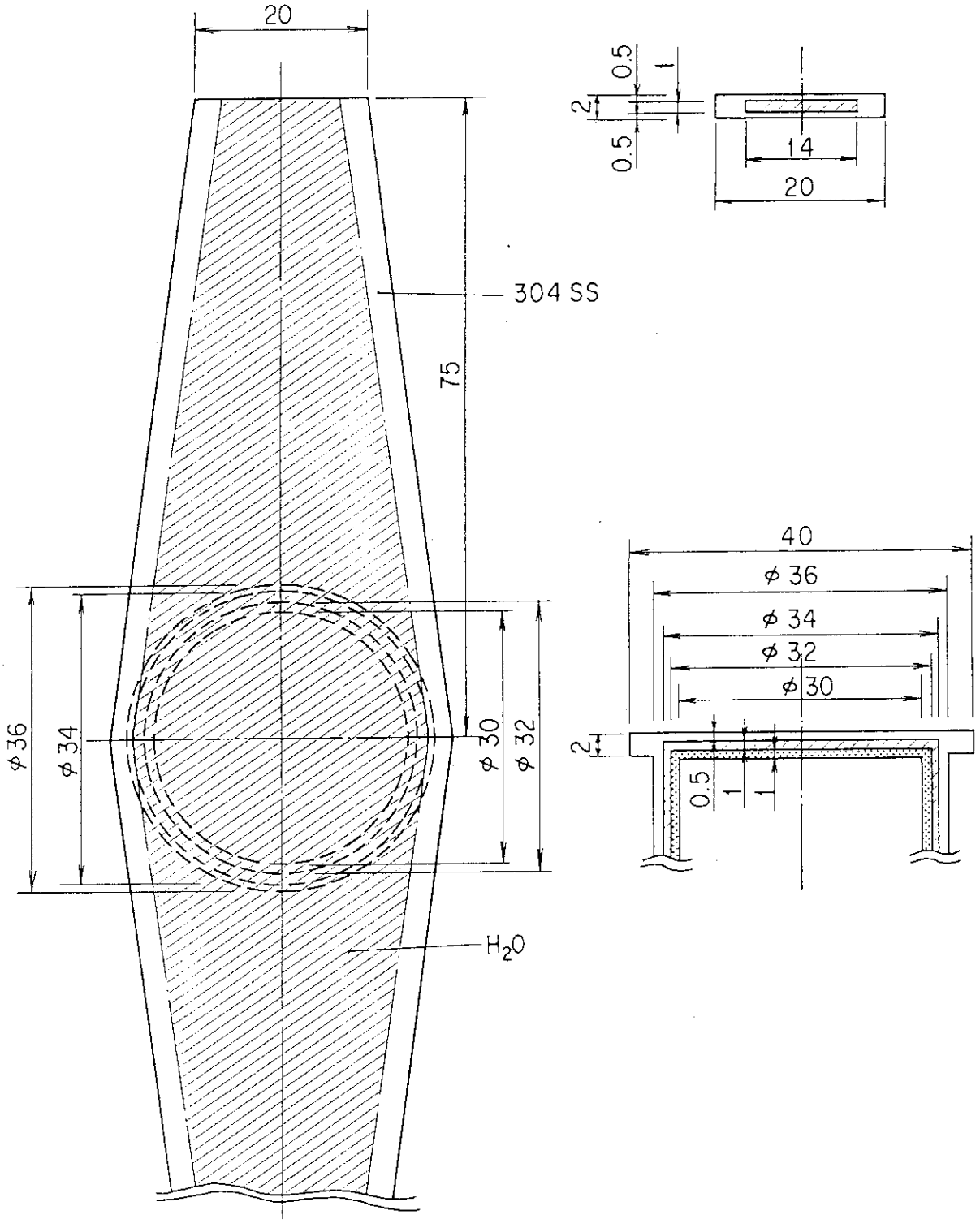

Fig. 2.3.12 (Continued) (b) water cover

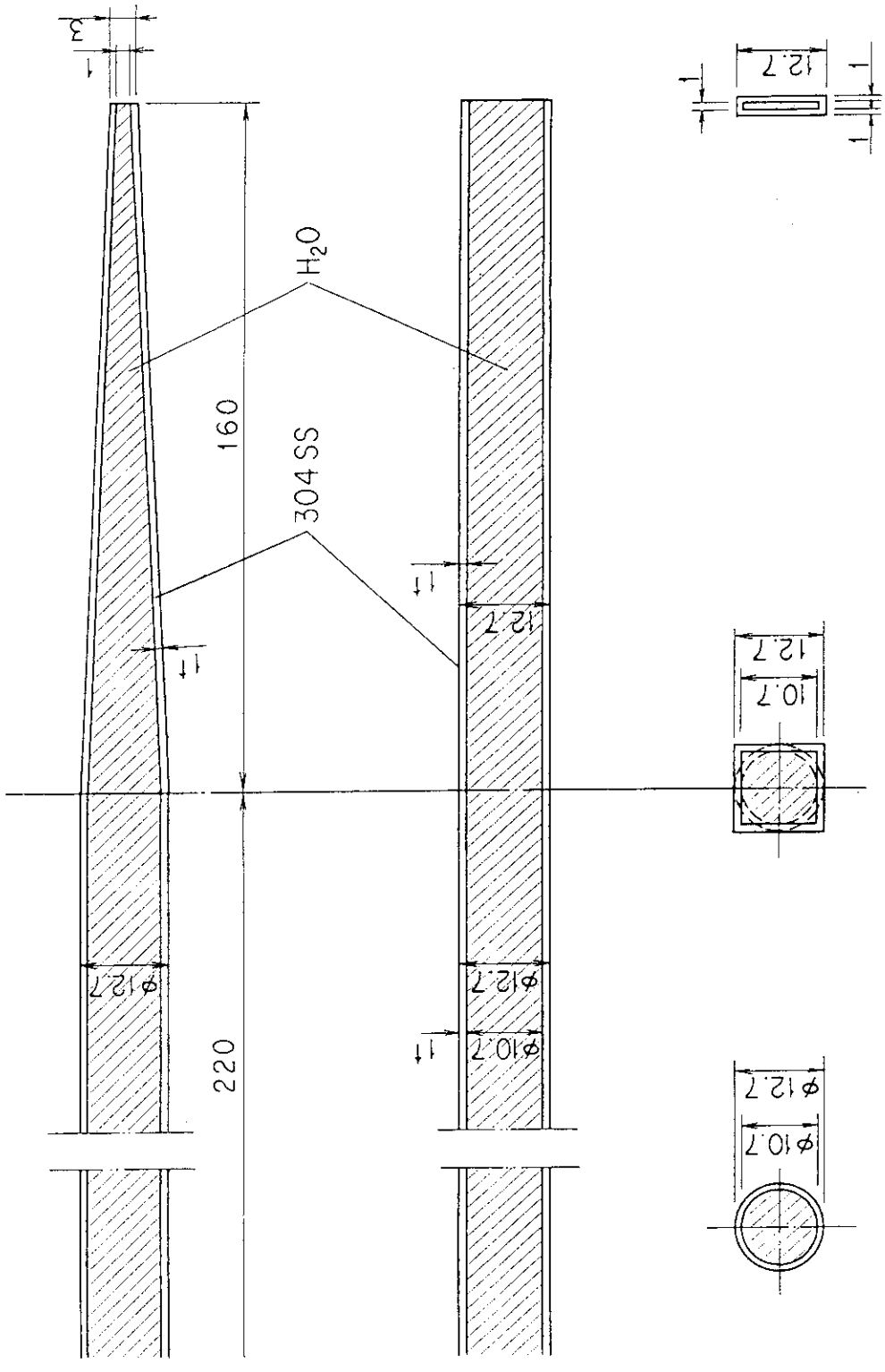

Fig. 2.3.12 (Continued) (c) water feed pipe bended in parallel to the drift tube

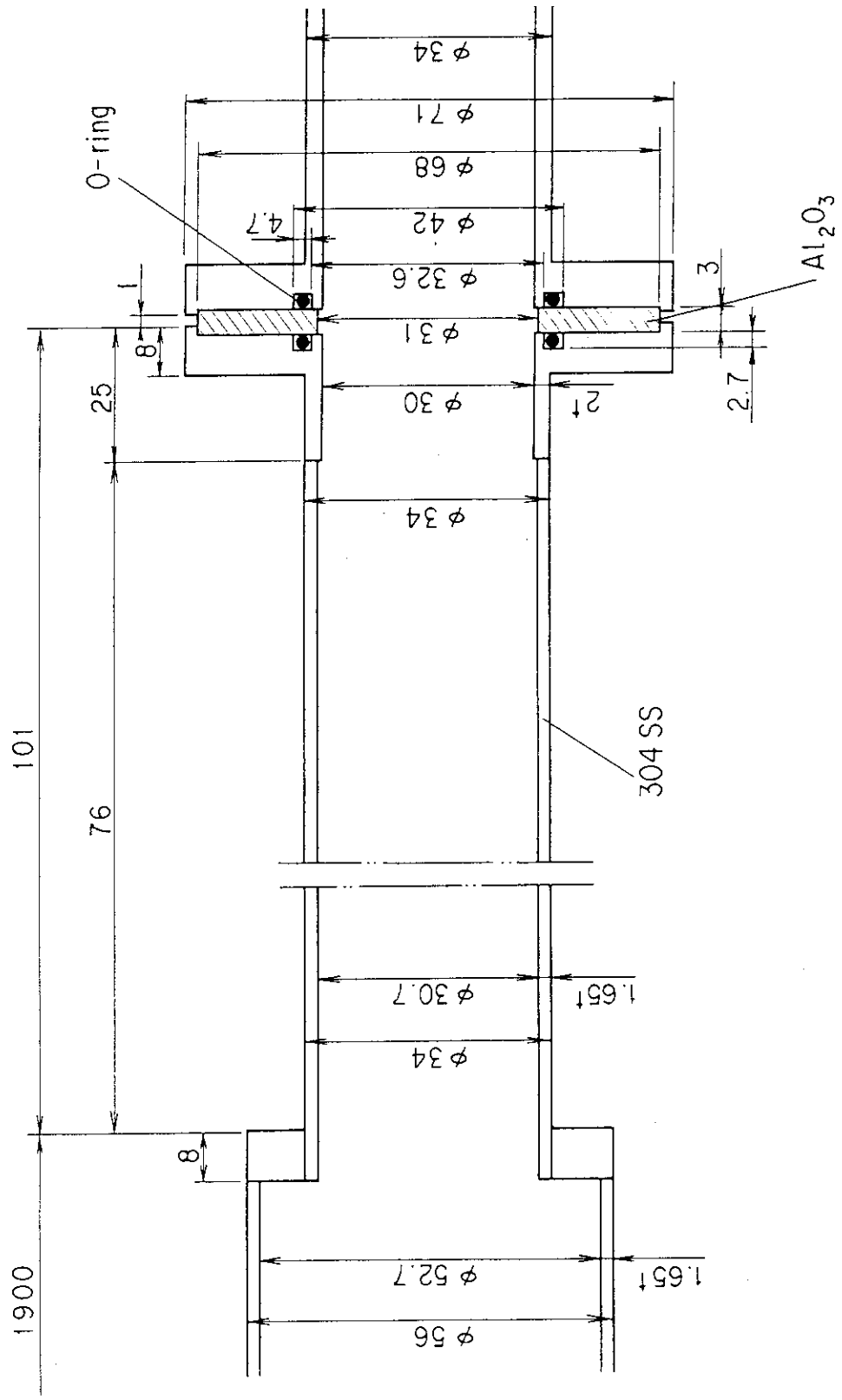

Fig. 2.3.12 (Continued) (d) drift tube (target side)

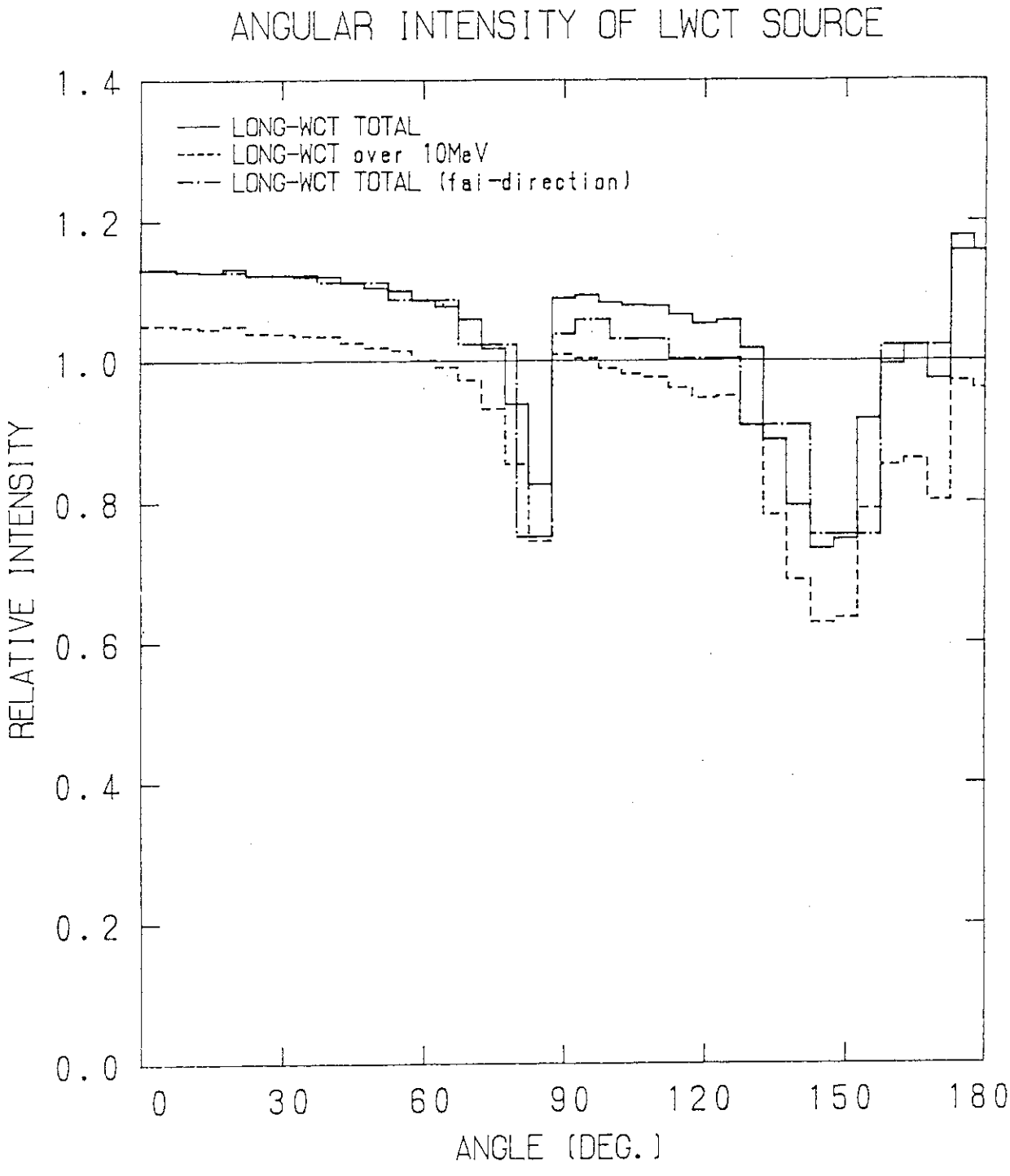

Fig. 2.3.13 Angular dependence of neutron emission yield in vertical and horizontal planes

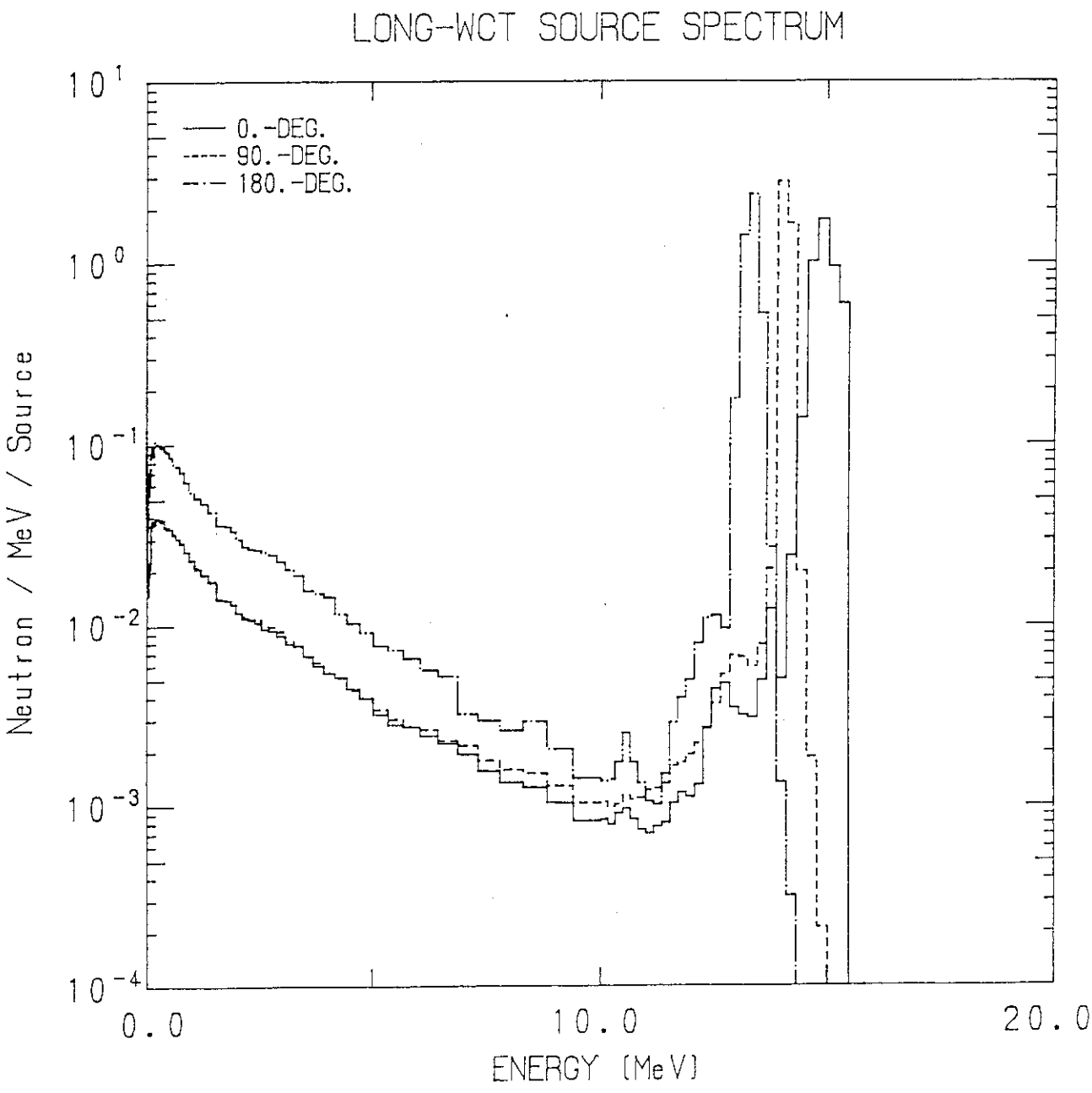

Fig. 2.3.14 Calculated neutron energy spectra for three directions emitted from the target

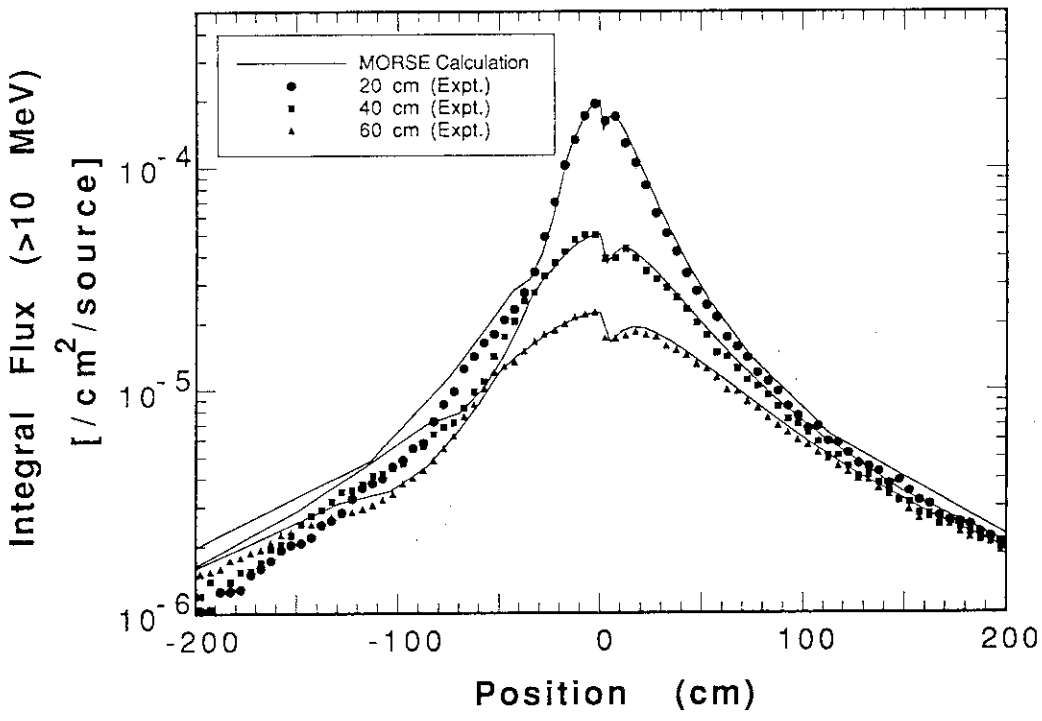

Fig. 2.3.15 Comparison of the calculated flux distribution along the target assembly with the experiment

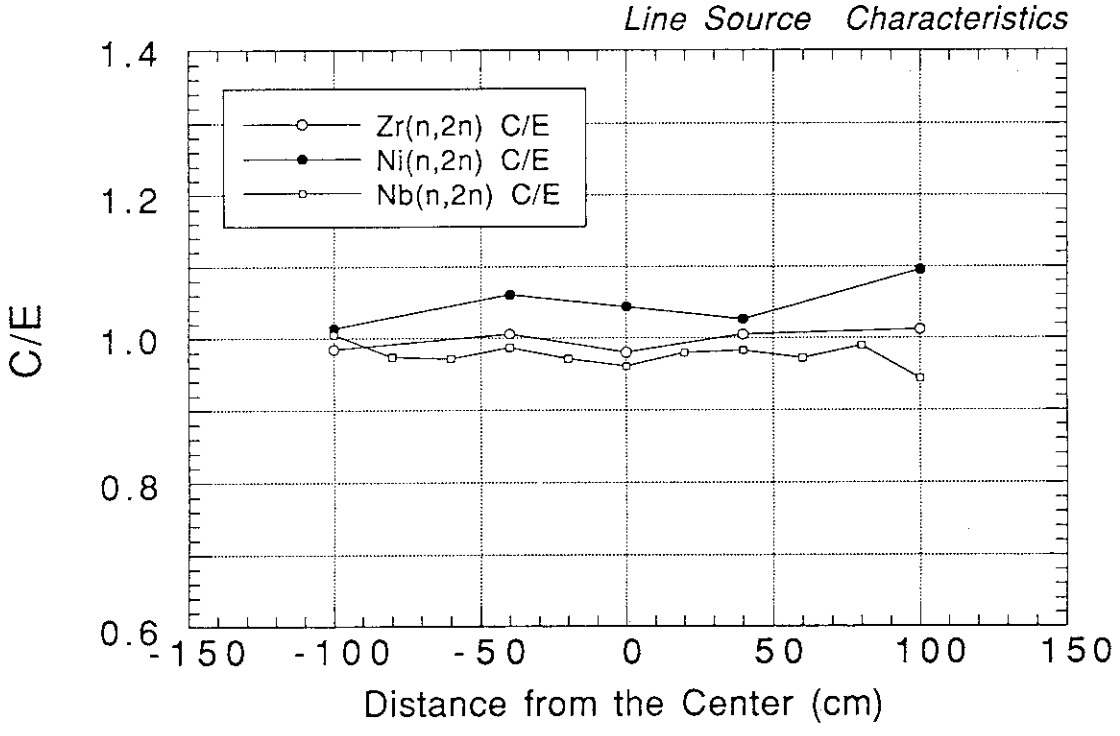

Fig. 2.3.16 Comparison of the (n,2n) reactions to the calculations

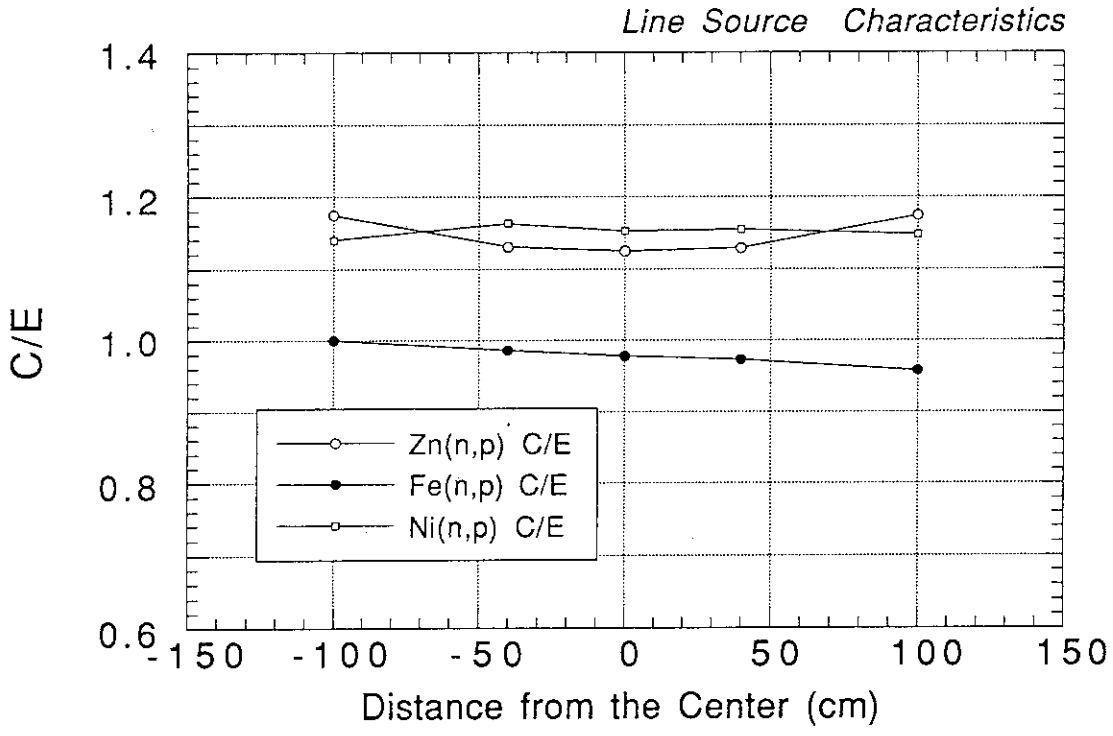

Fig. 2.3.17 Comparison of the (n,p) reactions to the calculations

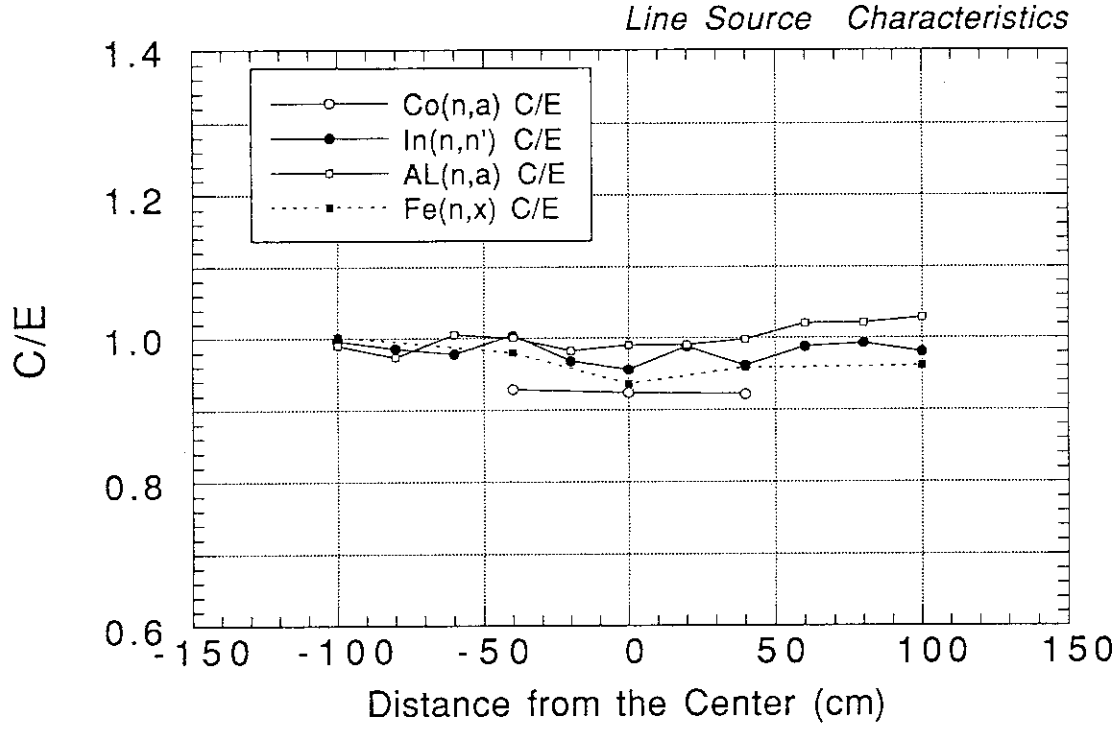

Fig. 2.3.18 Comparison of the lower threshold reactions to the calculations

3. ANNULAR BLANKET EXPERIMENT

3.1 Introduction

There aretwo primary options on the choice of the test blanket system, either clean geometry for benchmark or composite prototypical setup for design verification of a fusion reactor. To make an experimental system closer to a real reactor for appropriate dimensions of plasma cavity and blanket size, the previous PhaseII experiments[10-20] with a point neutron source were conducted simulating the material configuration and neutron spectrum inside the blanket in the JAERI/USDOE Collaborative Program. On the other hand, the present annular blanket system simulates tokamak-like geometry, i.e., the source is volumetric and the blanket is cylindrical. This feature might have an impact on neutronic characteristics in the components near the plasma cavity because of multi-angle neutron incident to the blanket and multiple scatterings of neutrons on the annular cavity.

A key problem is a design of the test blanket which has practical flexibility for configuration change. A selection of source length and test blanket size affects directly the inventory of material, i.e., cost. The conditions including material inventory have set the basic configuration and dimension of the present Phase-III experimental arrangement, along with the excellent feature of the previous experiment, i.e., a parallel-piped arrangement by assembling the unit-sized blocks. The system using blocks has large flexibility for material configuration; heterogeneity or asymmetry as well as the previous experiment. According to realistic consideration, the experimental arrangement for the annular blanket was focused on the phenomena associated with configurations near the cavity to minimize the required material inventory. Neutronics performance in the front part of the blanket influences much the tritium production and gamma-ray production by inelastic reaction. The calculation analysis for low energy response such as tritium production from ^{6}Li shows the flatter radial distribution in the finite-length annular blanket than those in the sphere and the infinite cylinder systems.[34] This feature becomes clear for the case less than two of the aspect ratio; (major radius)/(first wall radius).

Figure 3.1.1 illustrates examples of experimental configurations of the test annular blanket. These include the effects of poloidal asymmetry, axial heterogeneity and source location on the blanket neutronics performance. The poloidal geometry is very complicated in the recent design because of plasma elongation, diverter, limiter, inboard shield blanket and so on. The axial heterogeneity appears typically in the test port for the test module blanket and segment structure for maintenance. These all components impose an asymmetrical and three dimensional geometry. The design taking account of them requires three dimensional transport code such as Monte Calro code. A Monte Carlo code has the best accuracy at present in calculation schemes on integrated nuclear parameter such as

tritium breeding ratio. It is, however, not perfect to estimate local parameters in a large system because of its efficiency and modeling ambiguity. At the mean time, deterministic codes should be used together until the computer architecture is evolved. Thus, experimental confirmation is only a way to assure the calculation accuracy for such incomplete or substitutive methods.

The Phase III experiments[35-37] aims at providing experimental data to validate nuclear data files and examples to study better approaches for calculation analysis and modeling in prototypical geometry and configuratoin. The experiments are performed with the newly developed pseudo-line neutron source described in the previous section. The study includes measurement technique development suit for the pseudo-line source system and examination of three dimensional effect by three configurations; (a)FW/Li_2O, (b)Armor-FW/Li_2O and (c)FW/Li_2O with a large opening. First blanket is the reference case with poloidal symmetry and axial (toroidal) uniformity. Second and third ones simulate graphite armor plate for protection of first wall from energetic ions and opening hole for a neutral beam injector, respectively. These are very affective to neutronic feature in the front part of blanket through neutron multiple scatterings inside the cavity.

3.2 Annular Blanket Assembly

3.2.1 Reference Test Blanket (Phase IIIA)

Three annular test blankets were constructed for neutronics integral experiment. One of them is the reference test blanket for comparison to the others. The reference test blanket was made with simple configuration; consisting only of first wall and breeder zone. The basic structure of the assembly was constructed of blocks with unit size; made of Li_2O blocks with 50.6 mm unit or its multiples covered with 0.3 mm-thick stainless steel and Li_2CO_3 blocks with 101.2 mm unit painted with epoxy resin. Both 0.3 mm-thick stainless steel and epoxy resin were for protection against humidity. The Li_2CO_3 blocks were used in the outer blanket region as a buffer zone, because the cost of Li_2O blocks is more expensive than the Li_2CO_3 blocks. These were installed on the computer controlled moving carriage-deck. Figure 3.2.1 shows the cross section of the reference test blanket. Since the Li_2O is candidate material to be tested and the front part is focused on in this experiment, the Li_2O is placed inside and the Li_2CO_3 in the outer region. The Li_2O region was 203 mm-thick for the1400 mm-long central part of the 2040 mm-long whole assembly and 101.2 mm-thick at both end of 300 mm in length. Total weights of Li_2O and Li_2CO_3 used for the 2040 mm long assembly were about 2 and 3.7 tons, respectively. The inner surface was made by 15 mm-thick SS304 plates which supports the weight to make a cavity and also simulate first wall in a fusion reactor. The distance of the first wall surface from the line source was 213 mm.

Then the internal cavity was surrounded by 425.4 mm square and 2040 mm long stainless steel. The D-T point source traversed on the central axis of this cavity. The outer surface of Li_2CO_3 region was covered with 16 mm-thick polyethylene plates to shield thermal neutrons from the experimental room.

Three experimental channels for in-situ measurement were installed horizontally in each side of the assembly with 509 mm interval. The channels, named the drawer A, B and C from the target side, are made of thin SS304 sheath of 0.3 mm in thickness so as to insert the special blocks and a detector for measurement. The special blocks are smaller than the blocks used in the assembly construction and have 20 mm square hole. On the inner surface of the first wall of 304SS, the detector voids of 30 mm in diameter and 5 mm in depth with 50 mm pitch were machined to be able to emplace the irradiation samples such as TLDs and activation foils. These voids are usually plugged as seen in Fig.3.2.2.

Figure 3.2.3 shows a photograph of annular blanket assembly and long tube target assembly. The carriage-deck is moving on four rails and the photograph shows the carriage-deck staying at the end point, so the tritium target head can be seen. The test blanket was aligned exactly for the target assembly so as to set at the center by using a laser transit. The blocks piled up for the annular test blanket is bundled by aluminum frames. Table 3.2.1 summarizes homogenized atomic densities of materials used in the test blanket.

3.2.2 Armor Test Blanket (Phase IIIB)

In a promary design of the ITER reactor, carbon fiber composite (CFC) tiles of 20 mm in thickness are attached on few mm-thick stainless steel plate in front of the first wall.[38] To simulate this kind of graphite armor located as plasma facing components, 25 mm-thick graphite layer was placed on the cavity surface in addition to the first wall of the reference blanket. The graphite armor would play a role of moderator or reflector to increase lower energy neutrons inside of the cavity. Figure 3.2.4 shows a view from the assembly end including the target head with cooling cap. The graphite blocks of 25 mm-thick and 50.8 mm and 203.2 mm square was piled up inside of the cavity with aluminum spacers. The ceiling part the graphite blocks was supported by 1 mm-thick aluminum plates. The atomic density of the graphite used is 1.652 g/cm^3 (8.2894 x 10^{22} atom/cm^3). The other parts are completely the same as the reference test blanket including the experimental channel structure. The dimensions and cross sections of this test assembly are shown in Fig. 3.2.5.

3.2.3 Large Opening Test Blanket (Phase IIIC)

In a realistic reactor, there are many ports and penetrations for neutral beam injector (NBI), plasma diagnostics, vacuum pumping and so on. These openings and holes, especially

large openings for NBI, should influence nuclear parameters around the ports due to leakage of neutrons and reduction of reflected neutrons. For example, a coverage factor for estimating tritium breeding ratio should take account of the opening effect. A simple area fraction factor has been used so far to obtain tritium breeding ratio in a whole reactor from local breeding ratio estimated by one-dimensional calculations. Since the opening structure can not be treated by such a simple calculation, the present experiment provides a good example for three dimensional benchmark for precise calculations by sophisticated transport codes.

A square opening of 425.4 mm x 376 mm was made in the middle of the armor test blanket (Phase-IIIB) and lined by the same as the cavity of 15 mm-thick SS304 as shown in Fig. 3.2.6. The inner surface of the opening was not covered with the graphite. The experimental channels were changed for the opening side; one channel was placed beside the opening, and named as drawer-D. Figure 3.2.7 shows the photograph of opening at the assembly side.

3.3 Measurements

The parameters measured in the experiments were tritium production rate, neutron spectrum and reaction rate. Most of measurements were performed using experimental channels, except for reaction rate on the cavity surface. The techniques applied for those measurements are summarized in Table 3.3.1. Most of the techniques were the same as applied in the previous experiments in the JAERI/USDOE collaboration program using a point neutron source, i.e., Phase-I and -II experiments.[13,14,19] For tritium production, a pair of Li-glass scintillators method using response difference of both ^{7}Li-enriched and ^{6}Li-enriched Li glass scintillators[39] and an indirect NE213 scintillation detector method using evaluated value of $^{7}Li(n,n'\alpha)^{3}T$ cross section are applied for on-line detectors. The stepwise operation mode of the line source was used for the on-line detectors. For passive measurements, only Li_2O pellet irradiation method was applied with the continuous operation mode of the line source. However, because the measured results were scattered by about ±10% for repetition of measurement, the data were finally decided to be treated as second class data which are described in the appendix. The neutron spectrum was measured by both recoil proton detectors with NE213 scintillator[40] and gas proportional counter (PRC)[41] with the stepwise operation mode. Two kinds of PRC counter filled with gases of hydrogen and hydrogen/argon were applied as well as the previous experiments, so that the measurement energy is covered from 10 keV to 1 MeV. In the latter case, argon gas is used to increase stopping power for recoil protons. The reaction rates were obtained by activation foil method with the continuous operation mode of the line source.

The techniques mentioned above are almost the same as in the previous experiments of the JAERI/USDOE Collaborative Program, but the following modifications or new techniques were introduced for application to the present line source experiment.

1) Ramp high voltage applying and data acquisition system for proton recoil gas proportional counter (PRC),
2) Multi-detector data acquisition system for the Li-glass,
3) Spectrum weighting function method for the NE213 detector ,
4) Flux variation and gamma-ray decay correction technique for activation foil detector.

The last techniques was explained in Chap. 2 of the source characteristics experiment .

Besides the above techniques, gamma-ray response measurements were attempted on trial but not applied to all of the test blankets. One is an 40 mm diameter spherical NE213 scintillation detector and the other is an extrapolation method using several TLDs. These results are presented in the appendix 4.

3.3.1 Proton Recoil Gas Proportional Counter (PRC)

The new technique for proton recoil gas proportional counter (PRC) was developed to reduce the measurement time and data processing.[42] In the conventional technique, several high voltage runs were separately performed for one measurement, but new technique can take data by single measurement run using high voltage sweep with a ramp shape. This significantly reduces the measurement time and allows us to applly the PRC technique to the experiment with the stepwise mode of line source where a large number of measurements are needed corresponding to the number of steps. The PRC measurement for several sweep cycles of voltage is repeated at each source position.

The voltage is scanned from 300 to 4200 V for hydrogen counter and from 2400 to 3000 V for hydrogen/argon counter in 165 seconds for one cycle, and six cycles are performed for measurement at each source position. The data for measurement are collected in three dimension, i.e., applied voltage, rise time and pulse height. The pulse height signals are separated from gamma-ray signals by two dimensional analysis of fast and slow amplifier outputs and converted the recoil proton energy with gas multiplication factor corresponding to the supplied voltage recorded at the same time. The neutron spectrum is finally obtained by differentiation of recoil proton spectrum. By this innovative technique, the recoil proton spectrum in the whole energy range can be taken without any connection of several measurement runs with different applied voltages.

3.3.2 Li-glass Detector with Multi-Detector Data Acquisition System

For a Li-glass detector, a background subtraction measured by ^{7}Li-glass scintillator is necessary to obtain tritium production of ^{6}Li. Utilizing a symmetric geometry of annular blanket, a pair of detectors of ^{7}Li and ^{6}Li-glass scintillators, 10 mm in diameter and 0.3 mm in thickness, are placed in a symmetrical position in experimental drawers in both sides. As illustrated in Fig. 3.3.1, two pairs of Li-glass detectors are set to obtain the data in two positions at the same time. The measurement time is 1000 second for one source position. When the source is moved from the one end to the other of the assembly, the background fraction due to gamma-ray from the materials around the detector becomes higher after the source passes the detector position, because gamma-ray flux increases by produced short-lived activities and neutron flux decreases by increasing a distance from the source. Hence the beam current was kept lower even in the source position far from the detector.

Four pulse height spectra are taken at one source position to obtain the tritium production rates at two positions and repeated for 20 source positions with 100 mm source interval. The 20 pulse height spectra for one measurement position are collected for each detector, i.e., the 20 subtractions and summation are performed to get one tritium production data at one position. These data are acquired into a floppy disk with neutron monitor and source position data by using a personal computer. The data subtraction to deduce the tritium production rate is made by a least square fitting program on the personal computer. The data processing time for one subtraction takes about one minute and then 20 minutes for 20 data of one position. Finally two radial distributions at the center and front experimental channels, and three positions for each drawer were obtained.

3.3.3 NE213 Detector with Spectrum Weighting Function Method

The spectrum weighting function method was used to obtain the tritium production and integrated neutron flux from the pulse height spectrum measured by a small sphere NE213 liquid scintillation detector.[43] This method can deduce the nuclear parameter more simply than a spectrum unfolding technique along with its neutron response. Hence when it is necessary to process a large number of data at the same time, this method reduces the measurement and processing time. Since the spectrum weighting method works well even in low counting statistics, the position-wise data processing became practical in spite of short acqusition time at each source position.

Using the spectrum weighting function method, nuclear response R is given by,

$$R = \int F(E_n) \cdot \phi(E_n) dE, \qquad (3.1)$$

where $F(E_n)$ is nuclear response, $\Phi(E_\nu)$ is neutron flux with energy E_ν.
Here, assuming that the function W exists which satisfy the following relation,

$$F(E_n) = \int Res(E_n, H_p) \cdot W(H_p) dH_p \quad . \tag{3.2}$$

The nuclear response R is rewritten as:

$$\begin{aligned} R &= \int F(E_n) \cdot \phi(E_n) dE_n \\ &= \int [\int Res(E_n, H_p) \cdot W(H_p) dH_p] \cdot \phi(E_n) dE_n \end{aligned} \tag{3.3}$$

Exchanging a turn of integration,

$$\begin{aligned} R &= \int [\int Res(E_n, H_p) \cdot \phi(E_n) dE_n] \cdot W(H_p) dH_p \\ &= \int C(H_p) \cdot W(H_p) dH_p \end{aligned} \tag{3.4}$$

In the last equation, $C(H_p)$ is a recoil proton energy spectrum measured by the NE213 scintillator. The spectrum weighting function $W(H_p)$ is determined by solving the equation (3.2) with both neutron response matrices and nuclear parameter .

The result can be obtained simply by multiplication from the measured pulse height spectrum. This simple way reduces significantly the data processing time and also makes it free from the instability of unfolding due to counting statistics by shorter measurement time in one source position. The spectrum function method almost follows to statistics of total counts. In addition, by utilizing the above multi-detector data acquisition system, three NE213 scintillation detectors were applied at the same time for three experimental channels. Figure 3.3.2 shows a virtual response of the detector operated with the spectrum weight which gives an integrated flux above 10 MeV. The integrated flux are obtained by multiplying the pulse height spectrum with the prepared weighting function. The weighting function can be calculated for many kinds of nuclear responses $F(E_n)$ sensitive to high energy neutrons such as tritium production cross section, DPA cross section, gamma-heating and so on. However, the accuracy of the results depends on the original response data; cross section, neutron and gamma-ray kerma, etc.

To obtain the energy spectrum, a conventional unfolding technique is applied to the measured recoil proton spectrum. The pulse height spectra are summed up for all source position data normalized alpha counts and the summed spectrum is converted to neutron spectrum by using the FORIST code.[44]

3.3.4 Activation Foil Detector

For activation foil detector, as discussed in Chap.2, the neutron flux at the foil position varies with the source position depending on the distance between them. This causes time variation of neutron flux during the irradiation by the continuous mode of the line

source. For the foils with shorter decay time, because the concept of the time averaged line sourceis not valid exactly, the correction is necessary to deduce the reaction rates for the line source from the observed response. This correction was performed in the same way as the source characteristics experiment, though the neutron attenuation in the blanket assembly had to be neglected. Because the error due to neglection of the attenuation is also small if the correction is small, this approximation is reasonable for most of foils. The activation reactions used were $^{27}Al(n,\alpha)^{24}Na$, $^{58}Ni(n,2n)^{57}Ni$, $^{58}Ni(n,p)^{58}Co$, $^{90}Zr(n,2n)^{89}Zr$, $^{115}In(n,n')^{115m}In$, $^{197}Au(n,\gamma)^{198}Au$, $Ti(n,x)^{46}Sc$, $Ti(n,x)^{47}Sc$, $Ti(n,x)^{48}Sc$, $Fe(n,x)^{56}Mn$, $^{59}Co(n,\alpha)^{56}Mn$ and $^{64}Zn(n,p)^{64}Cu$, and Table 3.3.2 summarizes the parameters for these reactions. The sizes of foil were 10-20 mm in diameter and 1 mm in thickness, and, especially for gold, a thin foil of 1 μm in thickness was used to avoid a self-shielding effect.

3.4 Experimental Results and Discussions

Experiments were performed for three assemblies: the reference, the armor and the opening test blankets. Each experiment was performed in the separated period; one experiment for one period and some measurements, e.g., Li-glass, Li_2O pellet and foil measurements were retried to assure the reproducibility when curious data were obtained. Each experimental period is about 6 weeks. Of these measurements, the Li_2O pellet data could not determined within ±10%, because the reproducibility was more than 10% for three same measurements. The reason of instability of the measurement could not be solved, so the data were decided to be the second reference with error larger than expected. Hence the Li_2O pellet results were reported in Appendix.

3.4.1 Neutron Spectrum

Neutron spectrum were measured by the NE213 and the proton recoil gas proportional counter (PRC) spectrometer with the stepwise line source mode. The data were taken every 100 mm step of the source position. The raw pulse height spectra were summed up and then they were unfolded to obtain neutron spectra. This stepwise measurement is applied only to the selected positions, i.e., the surface of the test blanket and the position of 79.4 mm from the surface of the first wall, where both the NE213 and the PRC measurements were performed.

The measured spectra of the annular test blanket surfaces with the line source are compared in Fig. 3.4.1 with the experiments of a closed geometry using a point source (Phase-IIA). Since the spectrum of the point source experiment was obtained at the forward direction, the mean energy is almost 14.8 MeV due to D-T reaction kinematics. On the other

hand, the dominant energy of the line source is 14.1 MeV for the test blanket because of 90 degree direction of neutron emission angle, and the peak is broader due to contribution of neutrons from various emission angles. These mean energy and broadness of the peak spectrum are more similar to plasma neutron source which is produced by isotopic reaction.

The spectra at the front surface and the inside of the test blanket, at the 79.4 mm depth from the first wall, in the reference (IIIA) are compared by Fig. 3.4.2. The difference of spectra at two positions is seen in the range above 200 keV, where the flux at the inside is decreased by less than a half. Below 200 keV the flux is almost the same but the different resonances are clearly seen for iron at the surface and for Li at the inside, respectively. The spectra between the reference (IIIA) and the armor (IIIB) experiments are compared at a depth of 79.4 mm from the FW surface (292.4 mm from the line source) in Fig. 3.4.3. Both the spectra are very similar, though a dip due to the resonance of ^{6}Li cross section at 250 keV is a little sharper for the armor blanket. Figure 3.4.4 shows the comparisons the lower energy spectra measured by PRC at the surfaces of both opening and normal sides for the opening test blanket (IIIC). The higher energy part by the NE213 was not measured because the same spectra as the armor experiment (IIIB) were expected. In the figure, the spectrum at the side with the opening hole is lower than the other side by about 10%. This is because there is no neutron reflected from the graphite armor at the opening side.

The flux values obtained by the NE213 and the PRC detectors at two positions in the IIIA and IIIB blankets are listed in Tables 3.4.1 and 2. In the NE213 data, the window denotes the energy resolution and connected to the true flux by the following relation:

$$\phi_{obs}(E_n) = \int_0^{\infty} \frac{1}{\sqrt{2\pi}\sigma(E_n)} \cdot \exp\left\{\frac{(E_n - E_n')^2}{2\sigma^2(E_n)}\right\} \cdot \phi_{true}(E_n')dE_n' ,$$

where ϕ_{true} is true neutron spectrum without any deformation, and

$$\sigma(E_n) = \frac{W(E_n) \cdot E_n}{235} \quad ; \ W(E_n) \text{ is window function in \%.}$$

The source position-wise spectra were also obtained from the pulse height data of the PRC measurements at each position. Those spectra represent the quantity how much one neutron at each source position does contribute to the spectrum at the measuring position. For all phases, Figures 3.4.5 - 7 show the energy integrated spectra for each source position measured by the detectors at the surface and the depth of 79.4 mm from the FW surface, respectively.

3.4.2 Tritium Production Rate

The tritium production rates (TPR) from ^{7}Li and ^{6}Li (i.e., T_7 and T_6) were measured separately by the NE213 scintillator and Li-glass scintillators. The data obtained from the irradiated Li_2O pellet gave the inconsistent results between the test blankets compared with the other measurements such as the Li-glass, the NE213 and the foils; even in comparison among the repeated measurements, reproducibility was not obtained within 10%. Thus the experimental results are not presented here but discussed in the appendix.

Since both the on-line methods utilized the stepwise mode line source operation, and the source position-wise tritium production rates (named as the source profile) were obtained at the same time and the TPRs for the line source were deduced by superposition of them. Figures 3.4.8(a)-(c) shows the source profiles of ^{7}Li (T_7) by the NE213 in the central drawer (drawer B) at the distances of 227 mm and 393 mm from the source traveling line. Though the source profiles inside the blanket are similar to each other, there are some differences between the blankets with and without graphite armor, corresponding to IIIB and IIIC, and IIIA, respectively. By the graphite layer, the T_7 decreases at both end, because the effective thickness of graphite increases due to the oblique incident. In comparison of the opening blanket (IIIC) with the non-opening blanket (IIIB), the T_7 decreases at the center due to decrease of reflected neutrons. At the forward region, there is a structure in the profile of the reference (IIIA). This can be compared to the source profile of the integrated flux above 10 MeV without the blanket as shown in Fig. 3.4.9. This structure is seen only for the reference experiment. Thus this could be explained as follows: parasitic neutrons by $D(d,n)^{3}He$ reaction with a beam flare on the step of drift tube create second neutron source at a distance of about 200 mm from the target. This parasitic source is also differed by about 200 mm from the target. A peak appears only at one side and there is no flare in the other experiments (IIIB and IIIC) because a beam tuning might be fine. Consequently, the contribution is not so large that the effect on the superposed TPR can be neglected.

Figures 3.4.10(a)-(c) show the source profile of T_6 measured by the Li-glass detector in the drawer B at the distance of 279 mm and 380 mm from the source traveling line. The T_6 profiles are broader than those of T_7, because the T_6 profile is not dominated by an inverse square law of the distance from the target. The width of T_6 profile is two times larger than the T_7 profile. The effect of armor layer, a 10% increase of TPR, spreads to the whole blanket region, and especially at front region and at the center. However, the effect of opening is only in the region comparable with the opening size as seen in Fig. 3.4.11. This means that the opening effect on the T_6 is caused by chaneg of amount of reflected neutrons, and is contrarye to the $^{197}Au(n,\gamma)$ reaction on which the effect spreads over the cavity along the whole line source as discussed later.

Figures 3.4.12(a)-(c) show the ^{7}Li tritium production rates (T_7) superposed by the source profile data to obtain for the line source. The distributions are measured along the radial axis of each drawer channel. The results of three drawers are almost the same as each other, though the armor and opening blankets are about 10% smaller than the reference due to existence of graphite layer of 25 mm in thick but there is no effect of the opening. Figures 3.4.13(a) and (b) are the ^{6}Li tritium production rates (T_6) superposed by source profile data along the radial axis for drawers B (center) and C (forward). In the central drawer, the T_6 increases by graphite layer but decreases by opening, while in the forward drawer at a distance of 500mm far from the center, there is no difference between the T_6 obtained by the armor and opening blankets. This indicates that the opening influences T_6 only at the opposite side blanket of the opening and this is consistent with the results of the source profile of T_6 as shown in Fig. 3.4.10.

The numerical results of the figures obtained by the NE213 and the Li-glass detectors are listed in Table 3.4.3.and 4.

3.4.3 Activation Reaction Rate

Measurements of reaction rates with activation foil method were performed in two directions: along the line source axis on the cavity surface and along the radial axis using experimental drawers. To obtain a distribution along the source axis, the distances of mapping position from the line source were changed by every test blankets because the armor layer was added to the inner surface. Two experimental drawers (B and C channels) were used in the radial distribution measurements. For the opening test blanket experiments, both mapping measurement was performed on the surfaces at normal and opening sides, and the distributions around the opening hole was measured precisely. To perform the mapping measurement on the cavity surface, a thin stainless steel tape was stretched on the surface and the foils were put on the tape. This method is introduced to easily remove the foils for measurement. Inside the opening hole, the scotch tapes with foils were stretched in a similar way as seen in Fig. 3.2.7.

Figures 3.4.14 shows reaction rate distributions along the line source at the first wall surface of the reference test blanket in the Phase IIIA experiment. The distance from the source is adjusted to 219 mm by setting foils at 50 mm lower from the horizontal plane of the line source so that the obtained distribution could be directly compared to the results of the source characteristic measurement described in Chap.2. The reaction rates for higher threshold reaction such as ^{58}Ni(n,2n)^{57}Ni and ^{93}Nb(n,2n)^{92m}Nb are similar to those in the experiment without the test blanket, but for the other reactions the results in the experiment with the blankets are larger. However, for the higher threshold reactions, the distributions are

not symmetry between the forward and the backward. This is due to angular dependence of neutron energy from the source.

The relative ratios of reaction rates on the first wall surface at the central position in the reference blanket is plotted as a function of threshold energy in Fig. 3.4.15. This indicates clearly that the energy of reflected neutron ranges mainly below 5 MeV. The radial distributions in the experimental drawers are shown in Fig.3.4.16(a) and (b) for the center (B) and the forward (C) drawers. Reaction rates for most reactions decrease monotonously with the depth, and for the higher threshold reactions with steeper gradient . In contrast, the gold capture reaction distributes almost in flat. The values of the reaction rates for most reactoins are very close between the results in the two drawers except $^{197}Au(n,\gamma)^{198}Au$ reaction; in the front region of the blanket the gold reaction at the center is about 30% larger than the forward. This seems to be a leakage effect of low energy neutrons from the cavity made by the first wall of 213 mm square and 2 m long.

Figures 3.4.17 shows reaction rate distributions along the line source on the graphite surface of the armor test blanket in the Phase IIIB experiment. The distance of 187 mm from the line source to the foils is closer than the reference case by the armor layer thickness. The measured reaction rates were increased by shorter distance, but the gold reaction increased more than expected by such effect. The armor increases neutrons reflected on the graphite. The radial distributions of reaction rates inside of the armor test blanket are also shown in Figs. 3.4.18(a) and (b) for the two drawers. Results of both drawers are almost the same. The reaction rates in the armor test blanket decrease by 10% for most reactions and by about 30% especially for higher threshold reactions such as $^{98}Nb(n,2n)^{92m}Nb$ of 9 MeV and $^{90}Zr(n,2n)^{89}Zr$ of 12 MeV, while the gold capture reaction rate increases by a factor of 2 at the font region but there is no effect in deep position.

In the Phase-IIIC experiment of the opening test blanket, the measurements were performed in various positions more than the previous experiments; the distributions were obtained along the line source for both surfaces with and without opening, at the inside of the opening, in radial directions of the center drawer-B and at the position just beside the opening (drawer-D). The foil arrangement for measurement in the drawer-D is shown in Fig. 3.4.19. Figures 3.4.20(a)-(c) shows the measured distributions along the line source on both surfaces for three reactions; $^{93}Nb(n,2n)^{92m}Nb$, $^{115}In(n,n')^{115m}In$ and $^{197}Au(n,\gamma)^{198}Au$. For the high threshold reactions, there is not a significant difference between both sides, but for the others a decrease of the reaction rate is clearly seen in the region corresponding to the width of opening hole. This is caused by a decrease of reflected neutron component due to the opening.

The radial distribution in the central drawer (B) is shown in Fig. 3.4.21. There is also

no difference from the armor test blanket case, but at the front region of 200 mm depth, the gold reaction is lower than the armor blanket. This is also influenced by a decrease of the reflected component from the opening side. The distributions along the line source at the inside of the opening are shown in Figs 3.4.22(a)-(c) and the radial distribution around the opening in Figs. 3.4.23. The distributions at the inside of the opening are also different from each other by the threshold energy. The high threshold shows a spatial dependence of direct neutron component, while the distributions of non-threshold reactions are formed by neutron flow from the wall of opening hole. As a result, the reaction with intermediate threshold energy such as ^{115}In(n,n') shows accidentaly flat distribution, i.e., neither convex nor concave. The reaction rates in the drawer-D are increased by the direct incident neutrons from the wall of opening hole but the gold reaction is the same as that without opening, i.e., the result of drawer-B. This suggests that the low energy neutrons sensitive to the ^{197}Au(n,γ)^{198}Au reaction spread uniformly throughout the test blanket. In Figs 3.4.24(a) and (b), the reaction rates of ^{197}Au(n,γ)^{198}Au are compared among the three test blankets. It is clearly seen that the armor graphite increases the reaction rate in front region within 200 mm but the opening at the opposite side decreases those. This is also seen in the distributions on the cavity surface along the source in which the armor increases uniformly neutrons over the cavity and the opening decreases them just at the opposite side of opening.

The numerical results of the activation reaction rates measured for all test blankets (Phase-IIIA-IIIC) are listed in Table 3.4.5 - 3.4.15.

3.5 Concluding Remarks

Neutron spectra, tritium production rates and activation reaction rates were measured in three annular test blankets with the pseudo-line D-T neutron source system. The experiments were performed for the reference (FW/Li_2O/Li_2CO_3/PE), the armor (C/FW/Li_2O/Li_2CO_3/PE) and the large opening (the armor configuration with a opening at the center) configurations of the test blankets.

The results obtained from the annular blanket experiments were different from those of the point source experiment like the Phase-II experiment in the following points:

1) Neutron spectrum incident to the blanket is broader for the line source than the point source.
2) Gradients for high threshold reactions are higher than the Phase-II point source geometry because the distance from the source is shorter even though the space dependence should be followed by a 1/r law for a line source.
3) Gradients of the reaction rate distributions for low energy response in the blanket

are more modest by contribution of the line source.
The first point is better simulation for neutron spectrum from DT plasma of 14 MeV mean energy. The last two points are three dimensional effects by superposition of contribution from distributed source and will give good sample problems for three dimensional benchmark for neutron transport codes.

The effects of the armor layer and the large opening are directly observed in comparison to the results of the reference blanket. The graphite armor increases significantly low energy neutrons inside the source cavity and increases ^{6}Li tritium production in the front region of blanket. The opening decreases low energy neutrons contained in the cavity and especially decreases ^{6}Li tritium production in the blanket at the opposite side. This situation is frequently appeared in the environment of fusion reactor core, and the present result suggests that the nuclear parameters on the components around the plasma core are very sensitive to the configuration of them. Hence the present data can play a role as a higher step of benchmark, i.e., proto-typical test to check an ability of neutronic calculation for a realistic reactor design.

Table 3.2.1 Homogenized atomic densities of material used in the Phase III test blanket

Material	Element	Atomic density [atoms/cm^3]
304SS	Fe	6.0210×10^{22}
	Cr	1.5302×10^{22}
	Ni	8.2258×10^{21}
	^{55}Mn	1.2607×10^{21}
Li_2O block*	^{6}Li	4.1921×10^{21}
	^{7}Li	5.2411×10^{22}
	^{16}O	2.8302×10^{22}
	Cr	3.0188×10^{20}
	^{55}Mn	1.5440×10^{19}
	Fe	1.0976×10^{21}
	Ni	1.3358×10^{20}
Li_2CO_3 block	^{6}Li	2.2798×10^{21}
	^{7}Li	2.8030×10^{22}
	^{12}C	1.5155×10^{22}
	^{16}O	4.5464×10^{22}
polyethylene	H	8.2560×10^{22}
	^{12}C	4.1280×10^{22}

* including stainless steel can

Table 3.3.1 Techniques applied to nuclear parameter measurements in the annular blanket experiments Phase III

Parameter	Technique	Principle
Tritium Production	**NE213**	indirect method using recoil-proton spectrum
	Li-glass	on-line counting of $^{6}Li(n,\alpha)$ reaction
	Li_2O Pellet	tritium extraction and liquid scintillation counting
Neutron Spectrum	**NE213**	liquid scintillator with recoil-proton spectrum unfolding
	PRC	proton-recoil gas proportional counter with spectrum unfolding
Reaction Rate	**Activation Foil**	counting gamma-rays from induced activation with Ge detector

Table 3.3.2 Nuclear parameters of activation reactions used in the experiment

	Reactions	Half-Life	Abundance (%)	γ-ray Energy (keV)	γ-ray Branching (%)	Threshold Energy (MeV)	Typical Foil Size [mm]
1.	$^{27}Al(n,\alpha)^{24}Na$	15.02 h	100.0	1368.6	100.0	5	15φ x 1
2.	$^{nat}Ti(n,x)^{46}Sc$	83.83 d	100.0	889.3	99.98	4	20φ x 1
3.	$^{nat}Ti(n,x)^{47}Sc$	3.341 d	100.0	159.4	68.0	1.5	20φ x 1
4.	$^{nat}Ti(n,x)^{48}Sc$	1.821 d	100.0	983.5	100.0	5	20φ x 1
5.	$^{55}Mn(n,\gamma)^{56}Mn$	2.579 h	100.0	846.8	98.9	--------	12.7φ x 0.05
6.	$^{54}Fe(n,p)^{54}Mn$	312.2 d	5.8	834.8	99.98	2	10φ x 1
7.	$^{58}Ni(n,p)^{58}Co$	70.92 d	68.26	810.8	99.5	2	15φ x 1
8.	$^{58}Ni(n,2n)^{57}Ni$	1.503 d	68.27	1377.6	77.9	12.5	15φ x 1
9.	$^{59}Co(n,\alpha)^{56}Mn$	2.579 h	100.0	846.8	98.9	6	10φ x 1
10.	$^{64}Zn(n,p)^{64}Cu$	12.70 h	48.6	511.0	74.2	1.5	20φ x 1
11.	$^{90}Zr(n,2n)^{89}Zr$	3.268 d	51.45	909.2	99.01	12	20φ x 1
12.	$^{93}Nb(n,2n)^{92m}Nb$	10.15 d	100.0	934.5	99.0	9	20φ x 1
13.	$^{115}In(n,n')^{115m}In$	4.486 h	95.7	336.3	45.8	0.34	10 x 10 x 1
14.	$^{197}Au(n,\gamma)^{198}Au$	2.694 d	100.0	411.8	95.5	--------	10 x 10 x 0.001

Table 3.4.1(a) Measured neutron flux by the NE213 spectrometer at the surface of Phase IIIA assembly

Energy(eV)	Flux	Error	Window(%)
2.10200E+05	0.00000E+00	0.00000E+00	0.00000E+00
2.21000E+05	0.00000E+00	0.00000E+00	0.00000E+00
2.32300E+05	0.00000E+00	0.00000E+00	0.00000E+00
2.44200E+05	0.00000E+00	0.00000E+00	0.00000E+00
2.56800E+05	0.00000E+00	0.00000E+00	0.00000E+00
2.69900E+05	0.00000E+00	0.00000E+00	0.00000E+00
2.83800E+05	0.00000E+00	0.00000E+00	0.00000E+00
2.98300E+05	0.00000E+00	0.00000E+00	0.00000E+00
3.13600E+05	0.00000E+00	0.00000E+00	1.40000E+01
3.29700E+05	0.00000E+00	0.00000E+00	2.77600E+01
3.46600E+05	4.32283E-13	1.07859E-12	4.12900E+01
3.64400E+05	6.22268E-13	1.55200E-12	5.45800E+01
3.83000E+05	9.06402E-13	2.26093E-12	6.76800E+01
4.02700E+05	1.33740E-12	3.33601E-12	6.66000E+01
4.23300E+05	1.99965E-12	4.98712E-12	6.56300E+01
4.45000E+05	3.02724E-12	7.55176E-12	6.46900E+01
4.67800E+05	4.89696E-12	1.12669E-11	6.38300E+01
4.91800E+05	7.62579E-12	1.75263E-11	6.29600E+01
5.17000E+05	1.20286E-11	2.76188E-11	6.21000E+01
5.43600E+05	1.92454E-11	4.41375E-11	6.12000E+01
5.71400E+05	3.11862E-11	7.14476E-11	6.03000E+01
6.00700E+05	5.12341E-11	1.17218E-10	5.93600E+01
6.31500E+05	8.59284E-11	1.95118E-10	5.84300E+01
6.63900E+05	1.44980E-10	3.28394E-10	5.74900E+01
6.97900E+05	2.47468E-10	5.59352E-10	5.65600E+01
7.33700E+05	4.27472E-10	9.63735E-10	5.56200E+01
7.71300E+05	7.46716E-10	1.67824E-09	5.47200E+01
8.10900E+05	1.31817E-09	2.95072E-09	5.38600E+01
8.52500E+05	2.34618E-09	5.23103E-09	5.29900E+01
8.96200E+05	4.20475E-09	9.33329E-09	5.21600E+01
9.42100E+05	7.58723E-09	1.67465E-08	5.13400E+01
9.90400E+05	1.37521E-08	3.01418E-08	5.04700E+01
1.04100E+06	2.49410E-08	5.42666E-08	4.95700E+01
1.09500E+06	4.52458E-08	9.75591E-08	4.86400E+01
1.15100E+06	8.16521E-08	1.74221E-07	4.75900E+01
1.21000E+06	1.46450E-07	3.08454E-07	4.65100E+01
1.27200E+06	2.59619E-07	5.38397E-07	4.54000E+01
1.33700E+06	4.53187E-07	9.22416E-07	4.42100E+01
1.40600E+06	7.75800E-07	1.54283E-06	4.29500E+01
1.47800E+06	1.29435E-06	2.49991E-06	4.17200E+01
1.55300E+06	2.09288E-06	3.89632E-06	4.05700E+01
1.63300E+06	3.25955E-06	5.79156E-06	3.95300E+01
1.71700E+06	4.86269E-06	8.12798E-06	3.85600E+01
1.80500E+06	6.90046E-06	1.06453E-05	3.76900E+01
1.89700E+06	9.25506E-06	1.28275E-05	3.68600E+01
1.99500E+06	1.17065E-05	1.40208E-05	3.60000E+01
2.09700E+06	1.39101E-05	1.36299E-05	3.51400E+01
2.20400E+06	1.55660E-05	1.15349E-05	3.43100E+01
2.31700E+06	1.65026E-05	8.28514E-06	3.35500E+01
2.43600E+06	1.67396E-05	4.90739E-06	3.28000E+01
2.56100E+06	1.64469E-05	2.36573E-06	3.20400E+01
2.69200E+06	1.58358E-05	1.07622E-06	3.12500E+01
2.83000E+06	1.50877E-05	7.75792E-07	3.04900E+01
2.97500E+06	1.43195E-05	8.11343E-07	2.97400E+01
3.12800E+06	1.35883E-05	8.91000E-07	2.90200E+01
3.28800E+06	1.29220E-05	9.27189E-07	2.83000E+01
3.45700E+06	1.23794E-05	8.93408E-07	2.75800E+01
3.63400E+06	1.20066E-05	8.40569E-07	2.68200E+01
3.82100E+06	1.17814E-05	8.31981E-07	2.60600E+01
4.01600E+06	1.15972E-05	8.68714E-07	2.52700E+01
4.22200E+06	1.13421E-05	9.25333E-07	2.45500E+01
4.43900E+06	1.09680E-05	9.66555E-07	2.39400E+01
4.66600E+06	1.04363E-05	1.00931E-06	2.33300E+01
4.90600E+06	9.72966E-06	1.06472E-06	2.27200E+01
5.15700E+06	8.87640E-06	1.11550E-06	2.21800E+01
5.42200E+06	7.92306E-06	1.18870E-06	2.16700E+01
5.70000E+06	6.88275E-06	1.27207E-06	2.11000E+01
5.99200E+06	5.80833E-06	1.32610E-06	2.05600E+01
6.29900E+06	4.90295E-06	1.47451E-06	2.00200E+01
6.62200E+06	4.46747E-06	1.66029E-06	1.94800E+01
6.96100E+06	4.64695E-06	1.71895E-06	1.89700E+01
7.31800E+06	5.22064E-06	1.97215E-06	1.84900E+01
7.69400E+06	5.74979E-06	2.30584E-06	1.80400E+01
8.08800E+06	5.97038E-06	2.48977E-06	1.76200E+01
8.50300E+06	5.95739E-06	2.84573E-06	1.72200E+01
8.93900E+06	5.67326E-06	3.58011E-06	1.67800E+01
9.39700E+06	5.04416E-06	3.94398E-06	1.63600E+01
9.87900E+06	4.51059E-06	4.15020E-06	1.59300E+01
1.03900E+07	5.89742E-06	4.74212E-06	1.54700E+01
1.09200E+07	1.16212E-05	4.65639E-06	1.50700E+01
1.14800E+07	2.61360E-05	4.67966E-06	1.47600E+01
1.20700E+07	6.39116E-05	5.23046E-06	1.41900E+01
1.26800E+07	1.41414E-04	5.59436E-06	1.40700E+01
1.33400E+07	2.32090E-04	5.99977E-06	1.40500E+01
1.40200E+07	2.43213E-04	7.80689E-06	1.40500E+01
1.47400E+07	1.57287E-04	1.10175E-05	1.40500E+01
1.54900E+07	6.47797E-05	4.02522E-06	1.44000E+01
1.62900E+07	2.24352E-05	5.59286E-06	1.44000E+01
1.71200E+07	1.50919E-05	3.95997E-06	1.44000E+01
1.80000E+07	1.07261E-05	1.06786E-06	1.44000E+01

Table 3.4.1(b) Measured neutron flux by the NE213 spectrometer inside of Phase IIIA assembly

Energy(eV)	Flux	Error	Window(%)
2.10200E+05	0.00000E+00	0.00000E+00	0.00000E+00
2.21000E+05	0.00000E+00	0.00000E+00	0.00000E+00
2.32300E+05	0.00000E+00	0.00000E+00	0.00000E+00
2.44200E+05	0.00000E+00	0.00000E+00	0.00000E+00
2.56800E+05	0.00000E+00	0.00000E+00	0.00000E+00
2.69900E+05	0.00000E+00	0.00000E+00	0.00000E+00
2.83800E+05	0.00000E+00	0.00000E+00	0.00000E+00
2.98300E+05	0.00000E+00	0.00000E+00	0.00000E+00
3.13600E+05	0.00000E+00	0.00000E+00	1.40000E+01
3.29700E+05	0.00000E+00	0.00000E+00	2.77600E+01
3.46600E+05	3.74357E-13	6.33225E-13	4.12900E+01
3.64400E+05	5.38784E-13	9.11245E-13	5.45800E+01
3.83000E+05	7.84924E-13	1.32754E-12	6.76800E+01
4.02700E+05	1.15801E-12	1.95901E-12	6.66000E+01
4.23300E+05	1.73093E-12	2.92753E-12	6.56300E+01
4.45000E+05	2.62003E-12	4.43283E-12	6.46900E+01
4.67800E+05	4.20261E-12	6.61786E-12	6.38300E+01
4.91800E+05	6.54022E-12	1.02910E-11	6.29600E+01
5.17000E+05	1.03172E-11	1.62207E-11	6.21000E+01
5.43600E+05	1.65055E-11	2.59202E-11	6.12000E+01
5.71400E+05	2.67471E-11	4.19636E-11	6.03000E+01
6.00700E+05	4.39394E-11	6.88486E-11	5.93600E+01
6.31500E+05	7.35850E-11	1.14594E-10	5.84300E+01
6.63900E+05	1.24041E-10	1.92846E-10	5.74900E+01
6.97900E+05	2.11744E-10	3.28521E-10	5.65600E+01
7.33700E+05	3.65705E-10	5.66001E-10	5.56200E+01
7.71300E+05	6.38630E-10	9.85726E-10	5.47200E+01
8.10900E+05	1.12603E-09	1.73262E-09	5.38600E+01
8.52500E+05	2.00379E-09	3.07181E-09	5.29900E+01
8.96200E+05	3.59180E-09	5.48288E-09	5.21600E+01
9.42100E+05	6.47754E-09	9.83874E-09	5.13400E+01
9.90400E+05	1.17145E-08	1.76994E-08	5.04700E+01
1.04100E+06	2.12372E-08	3.18686E-08	4.95700E+01
1.09500E+06	3.84837E-08	5.72907E-08	4.86400E+01
1.15100E+06	6.93930E-08	1.02341E-07	4.75900E+01
1.21000E+06	1.24158E-07	1.81122E-07	4.65100E+01
1.27200E+06	2.19754E-07	3.16204E-07	4.54000E+01
1.33700E+06	3.82781E-07	5.41750E-07	4.42100E+01
1.40600E+06	6.53737E-07	9.06471E-07	4.29500E+01
1.47800E+06	1.08681E-06	1.46882E-06	4.17200E+01
1.55300E+06	1.74892E-06	2.28882E-06	4.05700E+01
1.63300E+06	2.71027E-06	3.40328E-06	3.95300E+01
1.71700E+06	4.01314E-06	4.77564E-06	3.85600E+01
1.80500E+06	5.64413E-06	6.25482E-06	3.76900E+01
1.89700E+06	7.48586E-06	7.53826E-06	3.68600E+01

Energy(eV)	Flux	Error	Window(%)
1.99500E+06	9.32902E-06	8.24032E-06	3.60000E+01
2.09700E+06	1.08828E-05	8.01319E-06	3.51400E+01
2.20400E+06	1.19015E-05	6.78148E-06	3.43100E+01
2.31700E+06	1.22819E-05	4.87136E-06	3.35500E+01
2.43600E+06	1.20953E-05	2.88169E-06	3.28000E+01
2.56100E+06	1.15276E-05	1.38400E-06	3.20400E+01
2.69200E+06	1.07815E-05	6.22676E-07	3.12500E+01
2.83000E+06	1.00068E-05	4.38418E-07	3.04900E+01
2.97500E+06	9.29832E-06	4.37514E-07	2.97400E+01
3.12800E+06	8.70678E-06	4.62252E-07	2.90200E+01
3.28800E+06	8.26259E-06	4.74157E-07	2.83000E+01
3.45700E+06	7.99873E-06	4.71381E-07	2.75800E+01
3.63400E+06	7.92563E-06	4.64378E-07	2.68200E+01
3.82100E+06	7.99530E-06	4.71915E-07	2.60600E+01
4.01600E+06	8.09939E-06	4.84530E-07	2.52700E+01
4.22200E+06	8.16821E-06	5.06372E-07	2.45500E+01
4.43900E+06	8.21733E-06	5.29229E-07	2.39400E+01
4.66600E+06	8.24445E-06	5.49633E-07	2.33300E+01
4.90600E+06	8.19562E-06	5.74390E-07	2.27200E+01
5.15700E+06	7.93348E-06	5.93107E-07	2.21800E+01
5.42200E+06	7.44003E-06	6.18936E-07	2.16700E+01
5.70000E+06	6.86034E-06	6.53927E-07	2.11000E+01
5.99200E+06	6.40629E-06	6.70739E-07	2.05600E+01
6.29900E+06	6.23410E-06	7.14553E-07	2.00200E+01
6.62200E+06	6.34804E-06	7.81951E-07	1.94800E+01
6.96100E+06	6.61247E-06	8.06060E-07	1.89700E+01
7.31800E+06	6.89974E-06	8.93862E-07	1.84900E+01
7.69400E+06	7.14233E-06	1.01235E-06	1.80400E+01
8.08800E+06	7.33937E-06	1.07338E-06	1.76200E+01
8.50300E+06	7.70389E-06	1.19040E-06	1.72200E+01
8.93900E+06	8.23546E-06	1.45306E-06	1.67800E+01
9.39700E+06	8.20719E-06	1.57652E-06	1.63600E+01
9.87900E+06	7.70860E-06	1.63761E-06	1.59300E+01
1.03900E+07	9.09157E-06	1.83732E-06	1.54700E+01
1.09200E+07	1.40231E-05	1.77126E-06	1.50700E+01
1.14800E+07	2.27678E-05	1.73751E-06	1.47600E+01
1.20700E+07	3.80440E-05	1.95607E-06	1.43700E+01
1.26800E+07	6.14558E-05	2.07296E-06	1.42500E+01
1.33400E+07	8.12737E-05	2.32378E-06	1.42300E+01
1.40200E+07	7.14433E-05	2.98261E-06	1.42300E+01
1.47400E+07	3.72515E-05	4.01981E-06	1.42300E+01
1.54900E+07	1.21698E-05	1.59351E-06	1.44000E+01
1.62900E+07	3.41418E-06	2.00747E-06	1.44000E+01
1.71200E+07	1.34343E-06	1.45050E-06	1.44000E+01
1.80000E+07	7.37349E-07	3.75488E-07	1.44000E+01

Table 3.4.1(c) Measured neutron flux by the NE213 spectrometer at the surface of Phase IIIB assembly

Energy(eV)	Flux	Error	Window(%)
2.10200E+05	0.00000E+00	0.00000E+00	0.00000E+00
2.21000E+05	0.00000E+00	0.00000E+00	0.00000E+00
2.32300E+05	0.00000E+00	0.00000E+00	0.00000E+00
2.44200E+05	0.00000E+00	0.00000E+00	0.00000E+00
2.56800E+05	0.00000E+00	0.00000E+00	0.00000E+00
2.69900E+05	0.00000E+00	0.00000E+00	0.00000E+00
2.83800E+05	0.00000E+00	0.00000E+00	0.00000E+00
2.98300E+05	0.00000E+00	0.00000E+00	0.00000E+00
3.13600E+05	0.00000E+00	0.00000E+00	1.40000E+01
3.29700E+05	0.00000E+00	0.00000E+00	2.77600E+01
3.46600E+05	3.58324E-13	1.02445E-12	4.12900E+01
3.64400E+05	5.15915E-13	1.47438E-12	5.45800E+01
3.83000E+05	7.51100E-13	2.14792E-12	6.76800E+01
4.02700E+05	1.10916E-12	3.16954E-12	6.66000E+01
4.23300E+05	1.65716E-12	4.73731E-12	6.56300E+01
4.45000E+05	2.50997E-12	7.17424E-12	6.46900E+01
4.67800E+05	4.12357E-12	1.07056E-11	6.38300E+01
4.91800E+05	6.42303E-12	1.66523E-11	6.29600E+01
5.17000E+05	1.01313E-11	2.62470E-11	6.21000E+01
5.43600E+05	1.62057E-11	4.19338E-11	6.12000E+01
5.71400E+05	2.62749E-11	6.78864E-11	6.03000E+01
6.00700E+05	4.31909E-11	1.11376E-10	5.93600E+01
6.31500E+05	7.26513E-11	1.85384E-10	5.84300E+01
6.63900E+05	1.22530E-10	3.11975E-10	5.74900E+01
6.97900E+05	2.09281E-10	5.31428E-10	5.65600E+01
7.33700E+05	3.61866E-10	9.15738E-10	5.56200E+01
7.71300E+05	6.32351E-10	1.59454E-09	5.47200E+01
8.10900E+05	1.11733E-09	2.80371E-09	5.38600E+01
8.52500E+05	1.98999E-09	4.96939E-09	5.29900E+01
8.96200E+05	3.57154E-09	8.87062E-09	5.21600E+01
9.42100E+05	6.45113E-09	1.59123E-08	5.13400E+01
9.90400E+05	1.16928E-08	2.86310E-08	5.04700E+01
1.04100E+06	2.12454E-08	5.15477E-08	4.95700E+01
1.09500E+06	3.86219E-08	9.26925E-08	4.86400E+01
1.15100E+06	6.98736E-08	1.65551E-07	4.75900E+01
1.21000E+06	1.25589E-07	2.93037E-07	4.65100E+01
1.27200E+06	2.23351E-07	5.11586E-07	4.54000E+01
1.33700E+06	3.91136E-07	8.76380E-07	4.42100E+01
1.40600E+06	6.72861E-07	1.46630E-06	4.29500E+01
1.47800E+06	1.12848E-06	2.37522E-06	4.17200E+01
1.55300E+06	1.83553E-06	3.70097E-06	4.05700E+01
1.63300E+06	2.88463E-06	5.50387E-06	3.95300E+01
1.71700E+06	4.34427E-06	7.72237E-06	3.85600E+01
1.80500E+06	6.24360E-06	1.01134E-05	3.76900E+01
1.89700E+06	8.50969E-06	1.21901E-05	3.68600E+01

Energy(eV)	Flux	Error	Window(%)
1.99500E+06	1.09678E-05	1.33237E-05	3.60000E+01
2.09700E+06	1.33232E-05	1.29532E-05	3.51400E+01
2.20400E+06	1.52699E-05	1.09606E-05	3.43100E+01
2.31700E+06	1.65716E-05	7.87033E-06	3.35500E+01
2.43600E+06	1.71160E-05	4.65948E-06	3.28000E+01
2.56100E+06	1.69447E-05	2.24501E-06	3.20400E+01
2.69200E+06	1.62121E-05	1.01251E-06	3.12500E+01
2.83000E+06	1.51628E-05	7.33075E-07	3.04900E+01
2.97500E+06	1.40763E-05	7.79361E-07	2.97400E+01
3.12800E+06	1.31660E-05	8.78947E-07	2.90200E+01
3.28800E+06	1.25159E-05	9.19079E-07	2.83000E+01
3.45700E+06	1.21322E-05	8.80309E-07	2.75800E+01
3.63400E+06	1.19399E-05	8.03087E-07	2.68200E+01
3.82100E+06	1.18456E-05	7.70023E-07	2.60600E+01
4.01600E+06	1.17268E-05	8.15796E-07	2.52700E+01
4.22200E+06	1.15310E-05	8.76156E-07	2.45500E+01
4.43900E+06	1.12605E-05	9.06267E-07	2.39400E+01
4.66600E+06	1.09060E-05	9.21189E-07	2.33300E+01
4.90600E+06	1.04289E-05	9.61401E-07	2.27200E+01
5.15700E+06	9.76626E-06	1.00231E-06	2.21800E+01
5.42200E+06	8.89606E-06	1.06094E-06	2.16700E+01
5.70000E+06	7.89239E-06	1.12703E-06	2.11000E+01
5.99200E+06	7.00931E-06	1.16193E-06	2.05600E+01
6.29900E+06	6.54977E-06	1.27124E-06	2.00200E+01
6.62200E+06	6.58343E-06	1.41590E-06	1.94800E+01
6.96100E+06	6.85622E-06	1.46497E-06	1.89700E+01
7.31800E+06	7.13166E-06	1.66111E-06	1.84900E+01
7.69400E+06	7.46329E-06	1.93001E-06	1.80400E+01
8.08800E+06	7.87980E-06	2.07735E-06	1.76200E+01
8.50300E+06	8.31768E-06	2.34700E-06	1.72200E+01
8.93900E+06	8.94318E-06	2.93569E-06	1.67800E+01
9.39700E+06	9.96383E-06	3.21951E-06	1.63600E+01
9.87900E+06	1.10588E-05	3.30360E-06	1.59300E+01
1.03900E+07	1.23060E-05	3.72393E-06	1.54700E+01
1.09200E+07	1.45750E-05	3.68530E-06	1.50700E+01
1.14800E+07	1.89214E-05	3.70291E-06	1.47600E+01
1.20700E+07	3.34411E-05	4.50284E-06	1.45400E+01
1.26800E+07	7.97961E-05	5.15890E-06	1.44200E+01
1.33400E+07	1.60851E-04	6.07164E-06	1.44000E+01
1.40200E+07	2.08406E-04	8.18681E-06	1.44000E+01
1.47400E+07	1.62654E-04	1.27708E-05	1.44000E+01
1.54900E+07	7.17732E-05	5.03274E-06	1.44000E+01
1.62900E+07	1.60684E-05	6.35586E-06	1.44000E+01
1.71200E+07	4.63492E-06	4.70583E-06	1.44000E+01
1.80000E+07	4.17772E-06	1.25419E-06	1.44000E+01

Table 3.4.1(d) Measured neutron flux by the NE213 spectrometer inside of Phase IIIB assembly

Energy(eV)	FLux	Error	Window(%)
2.10200E+05	0.00000E+00	0.00000E+00	0.00000E+00
2.21000E+05	0.00000E+00	0.00000E+00	0.00000E+00
2.32300E+05	0.00000E+00	0.00000E+00	0.00000E+00
2.44200E+05	0.00000E+00	0.00000E+00	0.00000E+00
2.56800E+05	0.00000E+00	0.00000E+00	0.00000E+00
2.69900E+05	0.00000E+00	0.00000E+00	0.00000E+00
2.83800E+05	0.00000E+00	0.00000E+00	0.00000E+00
2.98300E+05	0.00000E+00	0.00000E+00	0.00000E+00
3.13600E+05	0.00000E+00	0.00000E+00	1.40000E+01
3.29700E+05	0.00000E+00	0.00000E+00	2.77600E+01
3.46600E+05	2.50177E-13	6.37427E-13	4.12900E+01
3.64400E+05	3.59759E-13	9.16953E-13	5.45800E+01
3.83000E+05	5.24578E-13	1.33631E-12	6.76800E+01
4.02700E+05	7.73813E-13	1.97137E-12	6.66000E+01
4.23300E+05	1.15661E-12	2.94692E-12	6.56300E+01
4.45000E+05	1.75190E-12	4.46385E-12	6.46900E+01
4.67800E+05	2.87953E-12	6.66007E-12	6.38300E+01
4.91800E+05	4.48271E-12	1.03591E-11	6.29600E+01
5.17000E+05	7.07077E-12	1.63243E-11	6.21000E+01
5.43600E+05	1.13184E-11	2.60890E-11	6.12000E+01
5.71400E+05	1.83474E-11	4.22301E-11	6.03000E+01
6.00700E+05	3.01540E-11	6.92940E-11	5.93600E+01
6.31500E+05	5.06841E-11	1.15321E-10	5.84300E+01
6.63900E+05	8.55213E-11	1.94108E-10	5.74900E+01
6.97900E+05	1.46099E-10	3.30680E-10	5.65600E+01
7.33700E+05	2.52443E-10	5.69637E-10	5.56200E+01
7.71300E+05	4.41129E-10	9.91968E-10	5.47200E+01
8.10900E+05	7.79228E-10	1.74383E-09	5.38600E+01
8.52500E+05	1.38787E-09	3.09120E-09	5.29900E+01
8.96200E+05	2.49203E-09	5.51909E-09	5.21600E+01
9.42100E+05	4.50028E-09	9.89971E-09	5.13400E+01
9.90400E+05	8.16196E-09	1.78151E-08	5.04700E+01
1.04100E+06	1.48221E-08	3.20705E-08	4.95700E+01
1.09500E+06	2.69452E-08	5.76680E-08	4.86400E+01
1.15100E+06	4.87318E-08	1.03004E-07	4.75900E+01
1.21000E+06	8.75849E-08	1.82325E-07	4.65100E+01
1.27200E+06	1.55702E-07	3.18255E-07	4.54000E+01
1.33700E+06	2.72727E-07	5.45181E-07	4.42100E+01
1.40600E+06	4.69141E-07	9.12338E-07	4.29500E+01
1.47800E+06	7.86282E-07	1.47805E-06	4.17200E+01
1.55300E+06	1.27913E-06	2.30321E-06	4.05700E+01
1.63300E+06	2.00682E-06	3.42303E-06	3.95300E+01
1.71700E+06	3.02331E-06	4.80645E-06	3.85600E+01
1.80500E+06	4.34017E-06	6.29498E-06	3.76900E+01
1.89700E+06	5.90553E-06	7.58743E-06	3.68600E+01
1.99500E+06	7.59237E-06	8.29087E-06	3.60000E+01
2.09700E+06	9.19812E-06	8.06197E-06	3.51400E+01
2.20400E+06	1.05039E-05	6.82405E-06	3.43100E+01
2.31700E+06	1.13422E-05	4.90061E-06	3.35500E+01
2.43600E+06	1.16472E-05	2.90550E-06	3.28000E+01
2.56100E+06	1.14464E-05	1.40172E-06	3.20400E+01
2.69200E+06	1.08618E-05	6.34299E-07	3.12500E+01
2.83000E+06	1.00645E-05	4.55591E-07	3.04900E+01
2.97500E+06	9.25637E-06	4.96345E-07	2.97400E+01
3.12800E+06	8.60453E-06	5.60327E-07	2.90200E+01
3.28800E+06	8.17455E-06	5.90905E-07	2.83000E+01
3.45700E+06	7.94976E-06	5.62095E-07	2.75800E+01
3.63400E+06	7.85843E-06	5.04181E-07	2.68200E+01
3.82100E+06	7.82272E-06	4.76998E-07	2.60600E+01
4.01600E+06	7.76945E-06	5.14283E-07	2.52700E+01
4.22200E+06	7.67784E-06	5.64743E-07	2.45500E+01
4.43900E+06	7.57890E-06	5.89889E-07	2.39400E+01
4.66600E+06	7.50280E-06	6.02985E-07	2.33300E+01
4.90600E+06	7.40328E-06	6.39740E-07	2.27200E+01
5.15700E+06	7.18288E-06	6.78516E-07	2.21800E+01
5.42200E+06	6.84100E-06	7.24462E-07	2.16700E+01
5.70000E+06	6.49767E-06	7.74977E-07	2.11000E+01
5.99200E+06	6.29804E-06	8.03253E-07	2.05600E+01
6.29900E+06	6.30917E-06	8.73946E-07	2.00200E+01
6.62200E+06	6.44674E-06	9.69138E-07	1.94800E+01
6.96100E+06	6.56060E-06	1.00449E-06	1.89700E+01
7.31800E+06	6.70665E-06	1.13316E-06	1.84900E+01
7.69400E+06	7.04677E-06	1.31070E-06	1.80400E+01
8.08800E+06	7.45597E-06	1.40269E-06	1.76200E+01
8.50300E+06	7.82243E-06	1.46092E-06	1.72200E+01
8.93900E+06	8.30187E-06	1.72156E-06	1.67800E+01
9.39700E+06	8.67653E-06	1.96246E-06	1.63600E+01
9.87900E+06	8.62999E-06	1.96194E-06	1.59300E+01
1.03900E+07	8.96074E-06	2.10900E-06	1.54700E+01
1.09200E+07	1.04392E-05	2.28858E-06	1.50700E+01
1.14800E+07	1.29385E-05	2.45470E-06	1.47600E+01
1.20700E+07	1.89805E-05	2.98354E-06	1.45400E+01
1.26800E+07	3.53114E-05	3.47196E-06	1.44200E+01
1.33400E+07	6.41132E-05	4.06074E-06	1.44000E+01
1.40200E+07	8.49447E-05	5.53984E-06	1.44000E+01
1.47400E+07	7.15332E-05	8.97384E-06	1.44000E+01
1.54900E+07	3.46236E-05	3.49352E-06	1.44000E+01
1.62900E+07	9.22535E-06	4.48776E-06	1.44000E+01
1.71200E+07	3.21415E-06	3.32022E-06	1.44000E+01
1.80000E+07	2.45017E-06	8.91715E-07	1.44000E+01

Table 3.4.2(a) Measured neutron flux by the PRC spectrometer at the surface of Phase IIIA assembly

J	Energy [keV]	Flux	Flux Error[%]	J	Energy [keV]	Flux	Flux Error[%]	J	Energy [keV]	Flux	Flux Error[%]	J	Energy [keV]	Flux	Flux Error[%]
1	2.85	1.275E-06	104.3	34	12.27	8.321E-06	11.2	66	53.95	1.380E-05	8.3	98	241.56	1.514E-05	7.3
2	2.97	1.526E-06	84.5	35	12.85	8.150E-06	11.4	67	56.52	1.552E-05	7.4	99	253.14	1.521E-05	7.2
3	3.10	3.195E-06	39.4	36	13.45	8.480E-06	11.1	68	59.22	1.423E-05	8.2	100	265.27	1.695E-05	6.5
4	3.23	4.219E-06	28.9	37	14.08	7.659E-06	12.3	69	62.05	1.599E-05	7.3	101	277.99	1.662E-05	6.6
5	3.37	4.460E-06	26.5	38	14.74	7.733E-06	12.2	70	65.01	1.726E-05	6.8	102	291.31	1.773E-05	6.1
6	3.52	2.808E-06	41.0	39	15.43	8.247E-06	11.5	71	68.12	1.734E-05	6.8	103	305.28	2.210E-05	4.9
7	3.68	3.937E-06	28.4	40	16.16	7.800E-06	12.2	72	71.37	1.892E-05	6.3	104	319.92	2.498E-05	4.4
8	3.84	5.186E-06	21.2	41	16.92	6.478E-06	14.8	73	74.78	1.742E-05	6.8	105	335.25	2.255E-05	4.8
9	4.01	1.569E-06	68.8	42	17.72	8.863E-06	10.9	74	78.36	1.812E-05	6.6	106	351.33	2.378E-05	4.5
10	4.19	1.703E-06	62.8	43	18.55	9.760E-06	9.9	75	82.10	1.844E-05	6.5	107	368.17	2.529E-05	4.2
11	4.37	6.018E-06	17.4	44	19.43	9.449E-06	10.3	76	86.03	1.676E-05	7.2	108	385.83	2.413E-05	4.4
12	4.57	4.862E-06	21.4	45	20.35	8.473E-06	11.5	77	90.14	1.630E-05	7.5	109	404.33	2.325E-05	4.6
13	4.77	4.761E-06	21.4	46	21.31	1.186E-05	8.3	78	94.45	1.711E-05	7.1	110	423.72	2.140E-05	5.0
14	4.99	5.549E-06	18.0	47	22.32	1.334E-05	7.3	79	98.97	1.866E-05	6.6	111	444.04	2.286E-05	4.7
15	5.21	4.896E-06	20.2	48	23.37	1.257E-05	7.8	80	103.71	1.863E-05	6.7	112	465.34	2.570E-05	4.2
16	5.45	5.913E-06	16.4	49	24.48	1.090E-05	9.0	81	108.67	1.762E-05	7.1	113	487.66	2.882E-05	3.7
17	5.70	5.087E-06	18.8	50	25.64	1.016E-05	9.7	82	113.87	2.387E-05	5.3	114	511.04	3.333E-05	3.3
18	5.95	6.454E-06	14.6	51	26.86	4.827E-06	20.5	83	119.32	2.648E-05	4.8	115	535.56	3.539E-05	3.2
19	6.23	4.783E-06	19.6	52	28.13	5.683E-06	17.6	84	125.03	2.338E-05	5.6	116	561.24	3.757E-05	3.0
20	6.51	5.213E-06	17.7	53	29.47	7.183E-06	14.2	85	131.02	1.942E-05	6.8	117	588.16	3.860E-05	3.0
21	6.81	5.224E-06	17.6	54	30.87	6.857E-06	15.0	86	137.29	2.175E-05	6.3	118	616.38	3.884E-05	3.1
22	7.12	4.659E-06	19.6	55	32.33	8.157E-06	12.9	87	143.87	2.395E-05	5.8	119	645.94	3.783E-05	3.2
23	7.45	3.488E-06	26.2	56	33.87	1.027E-05	10.3	88	150.76	2.216E-05	6.4	120	676.93	3.773E-05	3.3
24	7.79	6.222E-06	14.7	57	35.48	1.137E-05	9.4	89	158.52	2.417E-05	5.9	121	709.40	3.739E-05	3.4
25	8.15	6.075E-06	15.2	58	37.17	1.246E-05	8.7	90	166.11	2.762E-05	4.9	122	743.43	3.724E-05	3.5
26	8.53	7.075E-06	13.0	59	38.94	1.085E-05	10.0	91	174.07	2.801E-05	4.6	123	779.09	3.121E-05	4.2
27	8.92	9.149E-06	10.1	60	40.79	1.240E-05	8.8	92	182.41	2.508E-05	5.0	124	816.47	2.467E-05	5.6
28	9.34	8.897E-06	10.4	61	42.74	1.318E-05	8.3	93	191.15	2.051E-05	5.9	125	855.64	2.629E-05	5.4
29	9.77	7.068E-06	13.1	62	44.78	1.343E-05	8.3	94	200.31	2.085E-05	5.7	126	896.68	3.176E-05	4.6
30	10.22	9.315E-06	10.0	63	46.91	1.277E-05	8.8	95	209.91	1.954E-05	5.9	127	939.70	3.780E-05	4.0
31	10.70	1.011E-05	9.2	64	49.15	1.164E-05	9.6	96	219.97	1.745E-05	6.5	128	984.79	4.230E-05	3.6
32	11.20	9.049E-06	10.2	65	51.49	1.303E-05	8.7	97	230.51	1.726E-05	6.5	129	1032.03	4.235E-05	3.7
33	11.72	9.694E-06	9.6												

* Flux Unit: [n/cm^2/Lethargy/Source]

Table 3.4.2(b) Measured neutron flux by the PRC spectrometer inside of Phase IIIA assembly

J	Energy [keV]	Flux	Flux Error[%]	J	Energy [keV]	Flux	Flux Error[%]	J	Energy [keV]	Flux	Flux Error[%]	J	Energy [keV]	Flux	Flux Error[%]
1	2.81	5.880E-07	188.8	34	12.09	8.911E-06	9.1	66	53.12	1.327E-05	7.2	98	241.56	9.259E-06	7.3
2	2.93	-4.666E-07	-233.6	35	12.65	9.376E-06	8.7	67	55.65	1.239E-05	7.7	99	253.14	7.538E-06	8.9
3	3.06	2.077E-06	50.6	36	13.24	8.809E-06	9.3	68	58.31	1.591E-05	6.1	100	265.27	7.683E-06	8.7
4	3.19	3.276E-06	31.7	37	13.86	9.026E-06	9.0	69	61.09	1.543E-05	6.3	101	277.99	9.447E-06	7.1
5	3.33	7.135E-07	143.0	38	14.52	8.963E-06	9.1	70	64.01	1.478E-05	6.5	102	291.31	9.956E-06	6.7
6	3.47	2.684E-06	37.0	39	15.20	8.273E-06	9.9	71	67.07	1.529E-05	6.4	103	305.28	1.086E-05	6.1
7	3.62	3.882E-06	25.2	40	15.91	9.521E-06	8.7	72	70.27	1.677E-05	5.8	104	319.92	1.298E-05	5.1
8	3.78	2.810E-06	33.9	41	16.66	7.824E-06	10.6	73	73.63	1.759E-05	5.5	105	335.25	1.505E-05	4.4
9	3.95	2.256E-06	41.7	42	17.45	9.624E-06	8.6	74	77.15	1.632E-05	6.0	106	351.33	1.522E-05	4.3
10	4.13	3.502E-06	26.4	43	18.27	1.044E-05	8.0	75	80.83	1.685E-05	5.8	107	368.17	1.468E-05	4.4
11	4.31	2.740E-06	33.4	44	19.13	8.559E-06	9.8	76	84.70	1.806E-05	5.4	108	385.83	1.501E-05	4.3
12	4.50	4.194E-06	21.5	45	20.04	8.678E-06	9.7	77	88.75	1.659E-05	5.9	109	404.33	1.528E-05	4.2
13	4.70	5.926E-06	15.0	46	20.98	8.446E-06	10.0	78	93.00	1.813E-05	5.4	110	423.72	1.322E-05	4.9
14	4.91	4.617E-06	18.9	47	21.98	1.020E-05	8.3	79	97.44	1.792E-05	5.5	111	444.04	1.170E-05	5.5
15	5.14	3.596E-06	24.0	48	23.02	1.093E-05	7.8	80	102.11	1.691E-05	5.8	112	465.34	1.369E-05	4.7
16	5.37	5.046E-06	16.9	49	24.11	1.067E-05	8.0	81	106.99	1.918E-05	5.1	113	487.66	1.707E-05	3.8
17	5.61	4.174E-06	20.3	50	25.25	9.434E-06	9.1	82	112.11	2.016E-05	4.9	114	511.04	2.106E-05	3.2
18	5.87	4.502E-06	18.6	51	26.45	9.421E-06	9.1	83	117.48	1.961E-05	5.1	115	535.56	2.300E-05	2.9
19	6.13	5.774E-06	14.4	52	27.70	8.511E-06	10.2	84	123.10	2.055E-05	4.9	116	561.24	2.248E-05	3.0
20	6.41	6.094E-06	13.5	53	29.01	9.007E-06	9.7	85	128.99	1.965E-05	5.2	117	588.16	2.329E-05	3.0
21	6.71	7.190E-06	11.3	54	30.39	1.040E-05	8.5	86	135.17	1.922E-05	5.4	118	616.38	2.349E-05	3.0
22	7.01	6.370E-06	12.6	55	31.84	1.061E-05	8.4	87	141.64	2.104E-05	4.9	119	645.94	2.212E-05	3.2
23	7.34	5.331E-06	15.0	56	33.35	9.877E-06	9.1	88	148.43	2.082E-05	5.0	120	676.93	2.184E-05	3.3
24	7.68	5.920E-06	13.5	57	34.94	1.039E-05	8.7	89	155.53	2.023E-05	5.1	121	709.40	2.199E-05	3.3
25	8.03	7.839E-06	10.2	58	36.60	1.108E-05	8.2	90	166.11	2.114E-05	4.2	122	743.43	2.073E-05	3.6
26	8.40	8.650E-06	9.3	59	38.34	1.291E-05	7.1	91	174.07	2.196E-05	3.8	123	779.09	1.931E-05	3.9
27	8.79	8.065E-06	10.0	60	40.17	1.148E-05	8.0	92	182.41	2.085E-05	3.9	124	816.47	1.720E-05	4.5
28	9.20	8.381E-06	9.6	61	42.08	1.237E-05	7.5	93	191.15	1.966E-05	3.9	125	855.64	1.663E-05	4.8
29	9.62	9.162E-06	8.8	62	44.09	1.335E-05	6.9	94	200.31	1.664E-05	4.4	126	896.68	1.871E-05	4.4
30	10.07	8.485E-06	9.6	63	46.19	1.308E-05	7.2	95	209.91	1.415E-05	5.0	127	939.70	1.866E-05	4.5
31	10.54	8.774E-06	9.2	64	48.39	1.265E-05	7.4	96	219.97	1.416E-05	4.9	128	984.79	2.113E-05	4.1
32	11.03	9.570E-06	8.5	65	50.70	1.345E-05	7.0	97	230.51	1.074E-05	6.4	129	1032.03	1.988E-05	4.4
33	11.55	8.157E-06	9.9												

* Flux Unit: [n/cm^2/Lethargy/Source]

Table 3.4.2(c) Measured neutron flux by the PRC spectrometer at the surface of Phase IIIB assembly

J	Energy [keV]	Flux	Flux Error[%]	J	Energy [keV]	Flux	Flux Error[%]	J	Energy [keV]	Flux	Flux Error[%]	J	Energy [keV]	Flux	Flux Error[%]
1	2.85	4.087E-06	43.3	34	12.27	1.240E-05	9.2	66	53.95	1.790E-05	7.0	98	241.56	1.945E-05	6.2
2	2.97	7.079E-06	24.3	35	12.85	1.123E-05	10.1	67	56.52	1.665E-05	7.6	99	253.14	1.868E-05	6.4
3	3.10	3.680E-06	44.8	36	13.45	1.190E-05	9.5	68	59.22	1.623E-05	7.8	100	265.27	1.809E-05	6.6
4	3.23	2.544E-06	63.3	37	14.08	1.072E-05	10.6	69	62.05	1.837E-05	6.9	101	277.99	2.123E-05	5.6
5	3.37	4.986E-06	31.5	38	14.74	1.203E-05	9.5	70	65.01	1.723E-05	7.4	102	291.31	2.398E-05	4.9
6	3.52	6.167E-06	24.6	39	15.43	1.161E-05	9.8	71	68.12	1.738E-05	7.4	103	305.28	2.395E-05	4.9
7	3.68	4.954E-06	30.1	40	16.16	1.105E-05	10.4	72	71.37	2.065E-05	6.2	104	319.92	2.342E-05	5.0
8	3.84	6.961E-06	20.8	41	16.92	1.253E-05	9.2	73	74.78	1.678E-05	7.6	105	335.25	2.466E-05	4.7
9	4.01	8.429E-06	16.8	42	17.72	1.264E-05	9.0	74	78.36	1.465E-05	8.8	106	351.33	2.535E-05	4.6
10	4.19	9.824E-06	13.9	43	18.55	1.192E-05	9.6	75	82.10	1.716E-05	7.6	107	368.17	2.811E-05	4.1
11	4.37	1.170E-05	11.5	44	19.43	1.207E-05	9.5	76	86.03	1.609E-05	8.1	108	385.83	2.583E-05	4.5
12	4.57	4.009E-06	32.4	45	20.35	1.161E-05	9.9	77	90.14	1.923E-05	6.8	109	404.33	2.476E-05	4.6
13	4.77	3.328E-06	38.8	46	21.31	1.217E-05	9.5	78	94.45	1.809E-05	7.3	110	423.72	2.300E-05	5.0
14	4.99	4.898E-06	26.3	47	22.32	1.342E-05	8.6	79	98.97	1.858E-05	7.1	111	444.04	1.763E-05	6.6
15	5.21	5.943E-06	21.2	48	23.37	1.466E-05	7.8	80	103.71	1.701E-05	7.8	112	465.34	1.666E-05	7.0
16	5.45	8.994E-06	14.0	49	24.48	1.216E-05	9.5	81	108.67	1.902E-05	7.0	113	487.66	2.209E-05	5.4
17	5.70	7.303E-06	16.8	50	25.64	1.151E-05	10.1	82	113.87	2.035E-05	6.7	114	511.04	3.318E-05	3.7
18	5.95	8.733E-06	14.0	51	26.86	1.246E-05	9.4	83	119.32	1.836E-05	7.5	115	535.56	3.473E-05	3.6
19	6.23	9.316E-06	12.9	52	28.13	1.222E-05	9.6	84	125.03	1.847E-05	7.6	116	561.24	3.907E-05	3.3
20	6.51	9.243E-06	12.8	53	29.47	1.261E-05	9.4	85	131.02	1.798E-05	8.1	117	588.16	4.688E-05	2.8
21	6.81	1.069E-05	10.9	54	30.87	1.313E-05	9.1	86	137.29	1.779E-05	8.3	118	616.38	4.973E-05	2.7
22	7.12	8.902E-06	12.9	55	32.33	1.224E-05	9.7	87	143.87	1.806E-05	8.5	119	645.94	5.043E-05	2.7
23	7.45	8.055E-06	14.2	56	33.87	1.114E-05	10.8	88	150.76	1.646E-05	9.5	120	676.93	4.500E-05	3.0
24	7.79	1.003E-05	11.4	57	35.48	1.268E-05	9.5	89	157.98	1.806E-05	9.0	121	709.40	3.546E-05	3.9
25	8.15	1.108E-05	10.3	58	37.17	1.259E-05	9.6	90	166.11	2.107E-05	6.9	122	743.43	3.465E-05	4.2
26	8.53	9.977E-06	11.4	59	38.94	1.473E-05	8.3	91	174.07	2.310E-05	6.1	123	779.09	3.621E-05	4.1
27	8.92	1.275E-05	8.9	60	40.79	1.352E-05	9.0	92	182.41	2.314E-05	5.9	124	816.47	3.890E-05	3.9
28	9.34	1.142E-05	10.0	61	42.74	1.495E-05	8.2	93	191.15	2.368E-05	5.6	125	855.64	3.871E-05	4.1
29	9.77	1.233E-05	9.2	62	44.78	1.670E-05	7.4	94	200.31	2.390E-05	5.4	126	896.68	3.840E-05	4.2
30	10.22	1.215E-05	9.4	63	46.91	1.414E-05	8.8	95	209.91	2.021E-05	6.2	127	939.70	4.337E-05	3.8
31	10.70	1.324E-05	8.5	64	49.15	1.285E-05	9.7	96	219.97	1.994E-05	6.2	128	984.79	4.370E-05	3.9
32	11.20	9.252E-06	12.3	65	51.49	1.479E-05	8.5	97	230.51	2.102E-05	5.9	129	1032.03	4.512E-05	3.8
33	11.72	1.316E-05	8.6												

* Flux Unit: [n/cm^2/Lethargy/Source]

Table 3.4.2(d) Measured neutron flux by the PRC spectrometer inside of Phase IIIB assembly

J	Energy [keV]	Flux	Flux Error[%]	J	Energy [keV]	Flux	Flux Error[%]	J	Energy [keV]	Flux	Flux Error[%]	J	Energy [keV]	Flux	Flux Error[%]
1	2.85	2.435E-06	53.4	34	12.27	9.272E-06	9.1	66	53.95	1.421E-05	6.8	98	234.14	9.240E-06	7.6
2	2.97	3.586E-06	34.6	35	12.85	1.008E-05	8.4	67	56.52	1.520E-05	6.4	99	245.36	8.547E-06	8.2
3	3.10	4.637E-06	26.1	36	13.45	1.114E-05	7.6	68	59.22	1.415E-05	6.8	100	257.12	5.486E-06	12.7
4	3.23	3.142E-06	36.9	37	14.08	8.727E-06	9.7	69	62.05	1.383E-05	7.0	101	269.44	5.015E-06	14.0
5	3.37	4.877E-06	23.2	38	14.74	8.900E-06	9.5	70	65.01	1.740E-05	5.6	102	282.36	7.161E-06	9.8
6	3.52	5.211E-06	20.9	39	15.43	9.586E-06	8.9	71	68.12	1.552E-05	6.3	103	295.90	1.054E-05	6.7
7	3.68	3.287E-06	32.6	40	16.16	1.059E-05	8.1	72	71.37	1.566E-05	6.2	104	310.08	1.235E-05	5.7
8	3.84	5.674E-06	18.3	41	16.92	9.684E-06	8.8	73	74.78	1.632E-05	6.0	105	324.95	1.376E-05	5.0
9	4.01	6.385E-06	15.8	42	17.72	7.782E-06	11.1	74	78.36	1.642E-05	6.0	106	340.53	1.413E-05	4.9
10	4.19	3.892E-06	25.6	43	18.55	9.985E-06	8.7	75	82.10	1.568E-05	6.3	107	356.86	1.502E-05	4.6
11	4.37	4.515E-06	21.6	44	19.43	1.027E-05	8.5	76	86.03	1.675E-05	5.9	108	373.97	1.484E-05	4.6
12	4.57	3.547E-06	27.2	45	20.35	9.846E-06	8.9	77	90.14	1.795E-05	5.5	109	391.90	1.361E-05	5.0
13	4.77	3.767E-06	25.3	46	21.31	9.807E-06	8.9	78	94.45	1.794E-05	5.5	110	410.70	1.410E-05	4.8
14	4.99	5.713E-06	16.4	47	22.32	1.110E-05	7.9	79	98.97	1.722E-05	5.7	111	430.39	1.131E-05	6.0
15	5.21	4.244E-06	22.0	48	23.37	1.235E-05	7.1	80	103.71	1.661E-05	5.9	112	451.03	8.827E-06	7.7
16	5.45	5.821E-06	15.8	49	24.48	1.075E-05	8.2	81	108.67	1.784E-05	5.5	113	472.66	1.102E-05	6.3
17	5.70	7.247E-06	12.5	50	25.64	1.001E-05	8.8	82	113.87	2.157E-05	4.6	114	495.33	1.395E-05	5.1
18	5.95	6.235E-06	14.3	51	26.86	7.974E-06	11.1	83	119.32	2.076E-05	4.8	115	519.09	2.054E-05	3.5
19	6.23	8.076E-06	10.9	52	28.13	9.404E-06	9.5	84	125.03	1.925E-05	5.2	116	543.98	2.236E-05	3.3
20	6.51	7.037E-06	12.4	53	29.47	1.023E-05	8.8	85	131.02	1.976E-05	5.1	117	570.08	2.287E-05	3.3
21	6.81	6.899E-06	12.4	54	30.87	9.660E-06	9.5	86	137.29	2.004E-05	5.0	118	597.42	2.466E-05	3.1
22	7.12	8.780E-06	9.7	55	32.33	1.041E-05	8.8	87	143.87	1.801E-05	5.7	119	626.08	2.630E-05	2.9
23	7.45	7.690E-06	10.9	56	33.87	1.216E-05	7.6	88	150.76	1.783E-05	5.8	120	656.11	2.658E-05	2.9
24	7.79	8.010E-06	10.5	57	35.48	1.186E-05	7.8	89	157.98	1.816E-05	5.7	121	687.58	2.414E-05	3.2
25	8.15	8.446E-06	10.0	58	37.17	1.228E-05	7.6	90	161.01	2.308E-05	4.3	122	720.57	2.137E-05	3.7
26	8.53	8.058E-06	10.5	59	38.94	1.230E-05	7.6	91	168.73	2.253E-05	4.1	123	755.13	2.090E-05	3.9
27	8.92	9.434E-06	9.0	60	40.79	1.174E-05	8.0	92	176.81	2.168E-05	4.0	124	791.36	2.170E-05	3.8
28	9.34	1.011E-05	8.4	61	42.74	1.311E-05	7.2	93	185.28	2.245E-05	3.7	125	829.32	2.253E-05	3.7
29	9.77	9.875E-06	8.5	62	44.78	1.397E-05	6.8	94	194.16	2.034E-05	3.9	126	869.11	2.000E-05	4.2
30	10.22	1.057E-05	8.0	63	46.91	1.298E-05	7.3	95	203.46	1.699E-05	4.4	127	910.80	1.952E-05	4.4
31	10.70	8.558E-06	9.8	64	49.15	1.251E-05	7.7	96	213.21	1.434E-05	5.1	128	954.50	1.990E-05	4.4
32	11.20	8.870E-06	9.6	65	51.49	1.401E-05	6.8	97	223.43	1.192E-05	6.0	129	1000.29	1.993E-05	4.5
33	11.72	1.052E-05	8.0												

* Flux Unit: [n/cm^2/Lethargy/Source]

Table 3.4.2(e) Measured neutron flux by the PRC spectrometer at the surface of Phase IIIC assembly (hole side)

J	Energy [keV]	Flux	Flux Error[%]	J	Energy [keV]	Flux	Flux Error[%]	J	Energy [keV]	Flux	Flux Error[%]	J	Energy [keV]	Flux	Flux Error[%]
1	2.89	4.380E-06	27.2	34	12.46	8.088E-06	9.3	66	54.79	1.264E-05	6.8	98	241.06	1.722E-05	5.3
2	3.01	2.144E-06	52.7	35	13.04	9.006E-06	8.4	67	57.41	1.164E-05	7.4	99	252.61	1.608E-05	5.8
3	3.14	3.962E-06	27.8	36	13.65	8.607E-06	8.8	68	60.15	1.346E-05	6.4	100	264.72	1.334E-05	7.0
4	3.28	5.939E-06	17.7	37	14.30	7.379E-06	10.2	69	63.02	1.235E-05	7.0	101	277.41	1.708E-05	5.6
5	3.42	5.456E-06	18.5	38	14.97	8.157E-06	9.3	70	66.03	1.382E-05	6.3	102	290.71	1.737E-05	5.5
6	3.57	3.259E-06	30.4	39	15.67	8.039E-06	9.5	71	69.18	1.500E-05	5.8	103	304.64	1.752E-05	5.6
7	3.73	4.049E-06	23.5	40	16.41	7.791E-06	9.8	72	72.49	1.431E-05	6.1	104	319.25	1.726E-05	5.7
8	3.89	5.141E-06	18.3	41	17.18	8.914E-06	8.6	73	75.96	1.239E-05	7.1	105	334.56	2.179E-05	4.6
9	4.07	3.929E-06	23.1	42	17.99	8.282E-06	9.3	74	79.59	1.096E-05	8.1	106	350.60	2.229E-05	4.6
10	4.25	3.718E-06	24.3	43	18.84	9.173E-06	8.4	75	83.39	1.182E-05	7.5	107	367.41	1.994E-05	5.3
11	4.44	3.781E-06	23.2	44	19.73	8.076E-06	9.6	76	87.38	1.332E-05	6.7	108	385.03	2.000E-05	5.4
12	4.64	6.661E-06	13.0	45	20.66	8.742E-06	8.8	77	91.56	1.423E-05	6.3	109	403.49	1.967E-05	5.7
13	4.84	6.261E-06	13.5	46	21.64	1.017E-05	7.6	78	95.94	1.363E-05	6.6	110	422.84	2.084E-05	5.6
14	5.06	5.166E-06	16.1	47	22.66	1.017E-05	7.6	79	100.53	1.503E-05	6.0	111	443.12	2.439E-05	4.9
15	5.29	4.256E-06	19.3	48	23.74	1.060E-05	7.3	80	105.34	1.345E-05	6.8	112	464.37	2.534E-05	4.9
16	5.53	5.581E-06	14.4	49	24.86	9.427E-06	8.2	81	110.38	1.586E-05	5.8	113	486.64	2.589E-05	4.9
17	5.78	6.523E-06	12.2	50	26.04	7.311E-06	10.6	82	115.66	1.554E-05	6.0	114	509.98	2.939E-05	4.4
18	6.04	5.428E-06	14.4	51	27.28	7.377E-06	10.6	83	121.20	1.464E-05	6.5	115	534.44	2.725E-05	4.9
19	6.32	7.130E-06	10.8	52	28.57	8.590E-06	9.2	84	127.00	1.466E-05	6.6	116	560.08	2.820E-05	4.8
20	6.61	7.029E-06	10.9	53	29.93	8.003E-06	9.9	85	131.20	1.592E-05	6.2	117	586.94	2.795E-05	5.0
21	6.91	3.929E-06	19.1	54	31.35	7.232E-06	11.1	86	137.48	1.766E-05	5.5	118	615.09	2.339E-05	6.2
22	7.23	5.582E-06	13.4	55	32.84	9.328E-06	8.7	87	144.06	1.696E-05	5.6	119	644.60	2.344E-05	6.4
23	7.56	5.756E-06	12.9	56	34.40	8.327E-06	9.8	88	150.96	1.544E-05	6.1	120	675.52	2.558E-05	6.1
24	7.91	7.727E-06	9.6	57	36.04	1.031E-05	7.9	89	158.19	1.431E-05	6.6	121	707.92	2.349E-05	6.9
25	8.27	6.703E-06	11.1	58	37.75	1.184E-05	6.9	90	165.77	1.539E-05	6.0	122	741.88	2.479E-05	6.7
26	8.66	6.528E-06	11.4	59	39.55	1.005E-05	8.2	91	173.71	1.657E-05	5.6	123	777.47	2.073E-05	8.4
27	9.06	7.262E-06	10.3	60	41.43	9.572E-06	8.7	92	182.03	1.606E-05	5.7	124	814.77	2.133E-05	8.5
28	9.48	8.453E-06	8.9	61	43.41	9.748E-06	8.6	93	190.75	1.664E-05	5.5	125	853.85	2.465E-05	7.8
29	9.92	7.825E-06	9.6	62	45.48	1.007E-05	8.4	94	199.89	1.437E-05	6.3	126	894.82	2.876E-05	7.0
30	10.38	7.105E-06	10.6	63	47.64	1.153E-05	7.3	95	209.47	1.415E-05	6.4	127	937.75	3.038E-05	6.9
31	10.86	6.984E-06	10.8	64	49.92	1.141E-05	7.4	96	219.51	1.453E-05	6.2	128	982.73	3.589E-05	6.1
32	11.37	7.745E-06	9.8	65	52.30	1.155E-05	7.4	97	230.03	1.377E-05	6.6	129	1029.88	3.515E-05	6.5
33	11.90	8.795E-06	8.6												

* Flux Unit: [n/cm^2/Lethargy/Source]

Table 3.4.2(f) Measured neutron flux by the PRC spectrometer at the surface of Phase IIIC assembly (normal side)

J	Energy [keV]	Flux	Flux Error[%]	J	Energy [keV]	Flux	Flux Error[%]	J	Energy [keV]	Flux	Flux Error[%]	J	Energy [keV]	Flux	Flux Error[%]
1	2.93	3.808E-06	36.2	33	12.09	1.085E-05	8.2	65	53.12	1.381E-05	7.3	97	237.32	2.129E-05	5.0
2	3.06	5.188E-06	25.4	34	12.65	1.038E-05	8.6	66	55.65	1.456E-05	7.0	98	248.70	1.945E-05	5.6
3	3.19	6.038E-06	21.0	35	13.24	1.071E-05	8.3	67	58.31	1.688E-05	6.0	99	260.62	1.767E-05	6.2
4	3.33	5.210E-06	23.8	36	13.86	9.558E-06	9.4	68	61.09	1.510E-05	6.8	100	273.11	1.972E-05	5.6
5	3.47	4.801E-06	25.0	37	14.52	9.991E-06	9.0	69	64.01	1.595E-05	6.4	101	286.20	2.113E-05	5.3
6	3.62	4.945E-06	23.5	38	15.20	1.006E-05	8.9	70	67.07	1.632E-05	6.3	102	299.93	1.971E-05	5.7
7	3.78	4.906E-06	23.2	39	15.91	1.020E-05	8.8	71	70.27	1.664E-05	6.2	103	314.30	2.312E-05	5.0
8	3.95	5.995E-06	18.3	40	16.66	8.997E-06	10.0	72	73.63	1.511E-05	6.8	104	329.38	2.420E-05	4.8
9	4.13	5.644E-06	19.3	41	17.45	1.035E-05	8.7	73	77.15	1.545E-05	6.7	105	345.17	2.524E-05	4.7
10	4.31	4.557E-06	23.3	42	18.27	1.107E-05	8.2	74	80.83	1.569E-05	6.6	106	361.72	2.319E-05	5.2
11	4.50	6.065E-06	17.1	43	19.13	9.169E-06	9.9	75	84.70	1.603E-05	6.5	107	379.06	2.309E-05	5.4
12	4.70	7.436E-06	13.9	44	20.04	1.192E-05	7.7	76	88.75	1.812E-05	5.8	108	397.24	2.185E-05	5.9
13	4.91	5.680E-06	17.6	45	20.98	1.055E-05	8.7	77	93.00	1.639E-05	6.4	109	416.29	2.551E-05	5.2
14	5.14	6.022E-06	16.3	46	21.98	1.080E-05	8.5	78	97.44	1.538E-05	6.8	110	436.25	2.596E-05	5.3
15	5.37	6.649E-06	14.6	47	23.02	1.155E-05	7.9	79	102.11	1.546E-05	6.9	111	457.17	2.553E-05	5.5
16	5.61	6.419E-06	14.9	48	24.11	1.288E-05	7.1	80	106.99	1.610E-05	6.6	112	479.10	2.881E-05	5.0
17	5.87	6.820E-06	13.9	49	25.25	1.052E-05	8.8	81	112.11	1.820E-05	5.9	113	502.08	2.815E-05	5.3
18	6.13	7.225E-06	12.9	50	26.45	7.087E-06	13.1	82	117.48	1.904E-05	5.8	114	526.16	3.238E-05	4.7
19	6.41	7.245E-06	12.7	51	27.70	1.091E-05	8.6	83	123.10	1.610E-05	7.0	115	551.40	3.160E-05	5.0
20	6.71	8.178E-06	11.1	52	29.01	1.193E-05	7.9	84	128.99	1.474E-05	7.9	116	577.84	2.873E-05	5.6
21	7.01	8.101E-06	11.0	53	30.39	1.015E-05	9.3	85	135.17	1.690E-05	7.0	117	605.56	3.066E-05	5.4
22	7.34	6.392E-06	13.9	54	31.84	9.978E-06	9.5	86	141.83	2.017E-05	5.7	118	634.61	3.071E-05	5.5
23	7.68	8.343E-06	10.6	55	33.35	1.206E-05	7.9	87	148.63	1.801E-05	6.2	119	665.05	2.606E-05	6.8
24	8.03	8.734E-06	10.2	56	34.94	1.236E-05	7.8	88	155.74	1.833E-05	6.1	120	696.95	2.550E-05	7.2
25	8.40	9.333E-06	9.5	57	36.60	1.067E-05	9.0	89	163.20	1.728E-05	6.4	121	730.38	2.696E-05	7.1
26	8.79	9.388E-06	9.5	58	38.34	1.138E-05	8.6	90	171.02	1.933E-05	5.6	122	765.42	2.905E-05	6.9
27	9.20	1.016E-05	8.7	59	40.17	1.275E-05	7.7	91	179.21	1.742E-05	6.2	123	802.14	2.232E-05	9.3
28	9.62	9.714E-06	9.1	60	42.08	1.351E-05	7.3	92	187.80	1.870E-05	5.7	124	840.62	2.772E-05	7.9
29	10.07	7.767E-06	11.5	61	44.09	1.245E-05	8.0	93	196.80	1.884E-05	5.7	125	880.95	3.490E-05	6.5
30	10.54	7.332E-06	12.2	62	46.19	1.285E-05	7.7	94	206.23	1.677E-05	6.3	126	923.21	3.896E-05	6.1
31	11.03	1.051E-05	8.5	63	48.39	1.441E-05	6.9	95	216.11	1.721E-05	6.2	127	967.50	3.946E-05	6.2
32	11.55	9.543E-06	9.4	64	50.70	1.309E-05	7.6	96	226.47	1.712E-05	6.3	128	1013.92	3.684E-05	6.9

* Flux Unit: [n/cm^2/Lethargy/Source]

Table 3.4.3 Tritium production rate of ^{7}Li for the line source measured by the detector ($^{7}Li(n,n'\alpha)^{3}T$ cross section from JENDL-3 was used)

	Position (mm)	IIIA TPR-7/Li	Error(%)	IIIB TPR-7/Li	Error(%)	IIIC TPR-7/Li	Error(%)
A-drawer							
	216.80	1.4710e-29	6.1318	----------	--------	----------	--------
	226.70	----------	--------	1.2372e-29	6.1866	1.2460e-29	5.8996
	292.40	6.9970e-30	6.0227	6.2062e-30	6.1774	6.2830e-30	6.1139
	343.40	----------	--------	3.9639e-30	6.1989	4.0306e-30	6.3474
	393.40	2.6490e-30	6.0285	2.3176e-30	6.0915	2.5119e-30	6.3296
	545.80	6.4650e-31	6.0209	5.9840e-31	6.0012	6.0412e-31	6.0441
B-drawer							
	216.80	1.6590e-29	6.1027	----------	--------	----------	--------
	226.70	----------	--------	1.3551e-29	6.1653	1.2558e-29	5.9146
	292.40	7.2574e-30	6.0086	6.5405e-30	6.1509	6.3344e-30	6.4955
	343.40	----------	--------	4.2838e-30	6.1609	3.9450e-30	6.2769
	393.40	2.7468e-30	6.0121	2.5497e-30	6.0722	2.5389e-30	6.0985
	545.80	7.0628e-31	5.9994	6.4683e-31	5.9812	6.3342e-31	6.0178
C-drawer							
	216.80	1.4860e-29	6.1252	----------	--------	----------	--------
	226.70	----------	--------	1.2885e-29	6.1959	1.2274e-29	5.9286
	292.40	7.2670e-30	6.0090	6.1945e-30	6.1442	6.3396e-30	6.4668
	343.40	----------	--------	4.1836e-30	6.1818	3.9667e-30	6.2612
	393.40	2.6640e-30	6.0178	2.5120e-30	6.0740	2.5731e-30	6.1022
	545.80	6.9270e-31	6.0055	6.1696e-31	6.0099	6.1048e-31	6.0240

Experimental error includes both statistical and systematical errors of detector and neutron yield monitor.

Table 3.4.4 Tritium production rate of ^{6}Li for the line source measured by the Li-glass detector

	Drawer	Position (mm)	TPR-6/Li	Error(%)
Phase-IIIA				
	B-drawer	254.00	1.2435e-28	4.9110
		279.40	1.1875e-28	4.4990
		329.80	1.0737e-28	4.3070
		380.40	9.6718e-29	4.3260
		512.20	7.4942e-29	4.2560
	C-drawer	279.40	1.0550e-28	4.5290
		329.80	9.5338e-29	4.3260
		380.40	8.7267e-29	4.3056
Phase-IIIB				
	B-drawer	279.40	1.4363e-28	5.0330
		329.80	1.2134e-28	4.7210
		380.40	1.0625e-28	4.5640
		512.20	8.0615e-29	4.5150
	C-drawer	279.40	1.2439e-28	5.1410
		329.80	1.0503e-28	4.8200
		380.40	9.5212e-29	4.6200
Phase-IIIC				
	B-drawer	279.40	1.3185e-28	4.9360
		329.80	1.0942e-28	4.7300
		380.40	9.4882e-29	4.7570
	C-drawer	279.40	1.2284e-28	4.9360
		329.80	1.0631e-28	4.7530
		380.40	9.1434e-29	4.7790

Experimental error includes both statistical and systematical errors of detector and neutron yield monitor.

Table 3.4.5 Reaction rate distributions along the line source at a distance of 219 mm from the line source for the reference test blanket (Phase IIIA)

DISTANCE FROM FRONT OF ASSEMBLY[mm]	Al27(n,alpha)Na24	Ti(n,x)Sc46	Ti(n,x)Sc47	Ti(n,x)Sc48	Fe54(n,p)Mn54
20.0	3.291E-30(3.6)*	4.133E-30(3.7)	4.380E-31(3.7)	1.390E-30(3.8)	1.174E-29(6.1)
220.0	4.815E-30(3.6)	----------	----------	----------	----------
420.0	5.458E-30(3.6)	----------	----------	----------	----------
620.0	5.912E-30(3.4)	7.814E-30(3.6)	1.001E-30(3.7)	2.752E-30(3.8)	2.160E-29(6.1)
820.0	6.089E-30(3.5)	----------	----------	----------	----------
1020.0	6.291E-30(3.5)	8.083E-30(3.5)	1.056E-30(3.6)	2.860E-30(3.8)	2.268E-29(6.0)
1220.0	6.222E-30(3.5)	----------	----------	----------	----------
1420.0	6.064E-30(3.4)	7.624E-30(3.5)	1.045E-30(3.6)	2.793E-30(3.7)	2.067E-29(6.4)
1620.0	5.722E-30(3.3)	----------	----------	----------	----------
1820.0	5.234E-30(3.5)	----------	----------	----------	----------
2020.0	3.377E-30(3.6)	4.388E-30(3.3)	6.744E-31(3.6)	1.625E-30(3.8)	1.182E-29(6.5)

* Read as 3.291×10^{-30}[reaction/total source neutron] with 3.6 % relative error

DISTANCE FROM FRONT OF ASSEMBLY[mm]	Fe(n,x)Mn56	Co59(n,alpha)Mn56	Ni58(n,2n)Ni57	Ni58(n,p)Co58	Zn64(n,p)Cu64
20.0	2.811E-30(3.3)	----------	3.617E-31(4.5)	1.225E-29(3.2)	5.728E-30(3.4)
220.0	----------	----------	7.335E-31(3.9)	1.841E-29(3.2)	----------
420.0	----------	----------	9.658E-31(4.4)	2.123E-29(3.3)	----------
620.0	5.302E-30(3.3)	1.430E-30(3.7)	1.047E-30(4.4)	2.277E-29(3.2)	9.948E-30(3.3)
820.0	----------	----------	1.120E-30(4.4)	2.324E-29(3.2)	----------
1020.0	5.604E-30(3.3)	1.528E-30(3.7)	1.182E-30(4.2)	2.338E-29(3.3)	1.015E-29(3.3)
1220.0	----------	----------	1.215E-30(4.3)	2.299E-29(3.2)	----------
1420.0	5.305E-30(3.2)	1.457E-30(3.7)	1.204E-30(4.5)	2.245E-29(3.2)	9.817E-30(3.4)
1620.0	----------	----------	1.199E-30(4.2)	2.115E-29(3.2)	----------
1820.0	----------	----------	1.164E-30(4.4)	1.817E-29(3.2)	----------
2020.0	3.200E-30(3.3)	----------	9.105E-31(4.4)	1.106E-29(3.2)	4.618E-30(3.3)

Table 3.4.5 (Continued)

DISTANCE FROM FRONT OF ASSEMBLY[mm]	Zr90(n,2n)Zr89	Nb93(n,2n)Nb92m	In115(n,n')In115m	Au197(n,gamma)Au198
20.0	1.079E-29(3.0)	1.038E-29(3.0)	6.071E-30(3.5)	5.234E-29(5.9)
220.0	----------	1.654E-29(2.9)	9.609E-30(3.5)	8.962E-29(5.5)
420.0	----------	1.970E-29(2.9)	1.188E-29(3.3)	1.255E-28(5.4)
620.0	2.682E-29(3.1)	2.099E-29(3.0)	1.279E-29(3.3)	1.368E-28(5.8)
820.0	----------	2.172E-29(2.9)	1.317E-29(3.3)	1.505E-28(5.3)
1020.0	2.926E-29(3.1)	2.178E-29(2.9)	1.344E-29(3.3)	1.622E-28(5.2)
1220.0	----------	2.214E-29(2.9)	1.318E-29(3.3)	1.517E-28(5.1)
1420.0	2.931E-29(3.1)	2.130E-29(2.9)	1.305E-29(3.4)	1.325E-28(5.1)
1620.0	----------	2.078E-29(2.9)	1.173E-29(3.4)	1.158E-28(5.3)
1820.0	----------	1.902E-29(2.9)	1.008E-29(3.4)	8.428E-29(5.5)
2020.0	2.086E-29(3.1)	1.308E-29(2.9)	5.452E-30(3.5)	4.738E-29(5.8)

Table 3.4.6 Reaction rate distribution along radial direction at central drawer (drawer B) for the reference (Phase IIIA) test blanket

DISTANCE FROM THE CENTRAL AXIS [mm]	Al27(n,alpha)Na24	Ti(n,x)Sc46	Ti(n,x)Sc47	Ti(n,x)Sc48	Ni58(n,2n)Ni57
213.00	----------	----------	----------	----------	----------
231.00	4.497E-30(3.5)*	5.866E-30(4.4)	8.488E-31(3.4)	2.119E-30(3.3)	8.815E-31(4.1)
256.00	3.403E-30(3.4)	----------	----------	----------	----------
281.70	2.574E-30(3.5)	3.555E-30(5.3)	4.682E-31(3.6)	1.215E-30(3.6)	4.002E-31(4.1)
332.20	1.533E-30(3.6)	1.925E-30(5.4)	2.684E-31(3.6)	6.612E-31(3.6)	1.933E-31(4.9)
382.80	8.844E-31(3.8)	1.277E-30(5.5)	1.622E-31(3.6)	3.768E-31(3.6)	9.750E-32(7.1)
433.30	5.351E-31(4.0)	8.100E-31(5.3)	1.011E-31(3.3)	2.291E-31(3.3)	5.227E-32(4.5)
484.00	----------	----------	----------	----------	----------
535.00	----------	----------	----------	----------	----------
585.50	1.150E-31(4.2)	----------	----------	----------	----------

* Read as 4.497×10^{-30} [reaction/total source neutron] with 3.5 % relative error

DISTANCE FROM THE CENTRAL AXIS [mm]	Ni58(n,p)Co58	Zn64(n,p)Cu64	Zr90(n,2n)Zr89	Nb93(n,2n)Nb92m	In115(n,n')In115m
213.00	----------	----------	----------	----------	----------
231.00	1.986E-29(3.0)	8.836E-30(3.5)	2.105E-29(3.3)	1.701E-29(2.9)	1.248E-29(3.1)
256.00	----------	----------	----------	----------	1.089E-29(3.0)
281.70	1.365E-29(3.0)	5.689E-30(3.6)	9.866E-30(3.3)	9.051E-30(3.0)	8.995E-30(3.2)
332.20	8.840E-30(3.0)	3.687E-30(3.5)	4.733E-30(3.3)	4.967E-30(3.0)	6.602E-30(3.3)
382.80	5.888E-30(3.1)	2.334E-30(3.4)	2.465E-30(3.3)	2.871E-30(3.1)	4.571E-30(3.2)
433.30	3.888E-30(3.1)	1.559E-30(3.8)	1.323E-30(3.2)	1.722E-30(3.1)	3.277E-30(3.3)
484.00	----------	----------	----------	----------	2.164E-30(3.4)
535.00	----------	----------	----------	----------	1.458E-30(3.5)
585.50	----------	----------	----------	----------	9.137E-31(3.6)

Table 3.4.6 (Continued)

DISTANCE FROM THE CENTRAL AXIS[mm]	Au197(n,gamma)Au198
213.00	1.541E-28(6.0)
231.00	1.590E-28(6.2)
256.00	1.447E-28(5.8)
281.70	1.362E-28(6.0)
332.20	1.201E-28(5.5)
382.80	1.045E-28(7.5)
433.30	1.313E-28(3.8)
484.00	1.457E-28(5.2)
535.00	1.287E-28(6.7)
585.50	1.310E-28(6.4)

Table 3.4.7 Reaction rate distribution along radial direction at off-central drawer (drawer C) for the reference (Phase IIIA) test blanket

DISTANCE FROM THE CENTRAL AXIS [mm]	Al27(n,alpha)Na24	Ti(n,x)Sc46	Ti(n,x)Sc47	Ti(n,x)Sc48	Ni58(n,2n)Ni57
230.50	4.274E-30(3.5)*	5.614E-30(5.0)	8.204E-31(3.7)	1.971E-30(3.8)	9.374E-31(4.3)
256.10	3.345E-30(3.5)	----------	----------	----------	----------
281.70	2.572E-30(3.6)	3.538E-30(5.3)	4.616E-31(3.5)	1.158E-30(3.6)	4.148E-31(4.2)
332.50	1.454E-30(3.5)	1.968E-30(5.3)	2.627E-31(3.7)	6.561E-31(4.0)	2.016E-31(7.0)
383.20	8.780E-31(4.0)	1.283E-30(5.3)	1.550E-31(3.5)	3.640E-31(3.6)	9.985E-32(6.0)
433.50	5.290E-31(4.0)	7.610E-31(5.9)	9.705E-32(3.3)	2.191E-31(3.3)	5.325E-32(5.3)
483.00	----------	----------	----------	----------	----------
532.20	----------	----------	----------	----------	----------
581.00	----------	----------	----------	----------	----------

* Read as 4.274×10^{-30} [reaction/total source neutron] with 3.5 % relative error

DISTANCE FROM THE CENTRAL AXIS [mm]	Ni58(n,p)Co58	Zn64(n,p)Cu64	Zr90(n,2n)Zr89	Nb93(n,2n)Nb92m	In115(n,n')In115m
230.50	1.846E-29(3.0)	8.351E-30(3.5)	2.101E-29(3.3)	1.618E-29(3.0)	1.216E-29(3.3)
256.10	----------	----------	----------	----------	1.040E-29(3.3)
281.70	1.312E-29(3.0)	5.625E-30(3.6)	9.518E-30(3.2)	8.532E-30(3.0)	8.807E-30(3.3)
332.50	8.560E-30(3.0)	3.516E-30(3.8)	4.903E-30(3.3)	4.843E-30(3.0)	6.357E-30(3.3)
383.20	5.645E-30(3.0)	----------	2.443E-30(3.4)	2.761E-30(3.1)	4.396E-30(3.3)
433.50	3.698E-30(3.0)	----------	1.320E-30(3.5)	1.673E-30(3.0)	3.082E-30(3.5)
483.00	----------	----------	----------	----------	2.169E-30(3.6)
532.20	----------	----------	----------	----------	1.429E-30(3.6)
581.00	----------	----------	----------	----------	9.140E-31(3.9)

Table 3.4.7 (Continued)

DISTANCE FROM THE CENTRAL AXIS[mm]	Au197(n,gamma)Au198
230.50	1.166E-28(4.3)
256.10	1.055E-28(4.7)
281.70	1.039E-28(5.3)
332.50	9.874E-29(5.1)
383.20	9.911E-29(5.5)
433.50	1.136E-28(4.3)
483.00	1.283E-28(5.0)
532.20	1.201E-28(4.8)
581.00	1.140E-28(4.4)

Table 3.4.8 Reaction rate distributions along the line source at a distance of 187 mm from the line source for the armor test blanket (Phase IIIB)

DISTANCE FROM FRONT OF ASSEMBLY[mm]	Al27(n,alpha)Na24	Ni58(n,2n)Ni57	Ni58(n,p)Co58	Nb93(n,2n)Nb92m	In115(n,n')In115m
20.0	3.739E-30(3.0)*	4.703E-31(4.4)	1.500E-29(3.0)	1.302E-29(3.0)	5.204E-30(3.1)
220.0	6.018E-30(3.0)	1.003E-30(4.6)	2.437E-29(3.0)	2.123E-29(3.1)	1.064E-29(3.1)
420.0	6.986E-30(3.0)	1.276E-30(4.3)	2.809E-29(3.0)	2.475E-29(3.1)	1.305E-29(3.1)
620.0	7.405E-30(3.0)	1.378E-30(4.3)	3.001E-29(3.0)	2.591E-29(3.1)	1.426E-29(3.0)
820.0	7.628E-30(3.0)	1.407E-30(4.3)	3.120E-29(3.0)	2.659E-29(3.1)	1.462E-29(3.0)
1020.0	7.697E-30(3.0)	1.459E-30(4.1)	3.125E-29(3.0)	2.758E-29(3.1)	1.505E-29(3.0)
1220.0	7.680E-30(3.0)	1.457E-30(4.2)	3.053E-29(3.0)	2.798E-29(3.1)	1.485E-29(3.0)
1420.0	7.596E-30(3.0)	1.520E-30(4.2)	3.066E-29(3.0)	2.668E-29(3.1)	1.429E-29(3.1)
1620.0	7.117E-30(3.0)	1.447E-30(4.2)	2.860E-29(3.0)	2.573E-29(3.0)	1.331E-29(3.1)
1820.0	6.355E-30(3.0)	1.297E-30(4.2)	2.469E-29(3.0)	2.280E-29(3.1)	1.112E-29(3.1)
2020.0	4.215E-30(3.0)	1.016E-30(4.3)	1.465E-29(3.0)	1.540E-29(3.0)	6.211E-30(3.1)

* Read as 3.739×10^{-30} [reaction/total source neutron] with 3.0 % relative error

DISTANCE FROM FRONT OF ASSEMBLY[mm]	Au197(n,gamma)Au198
20.0	1.536E-28(3.6)
220.0	3.619E-28(3.4)
420.0	5.258E-28(3.5)
620.0	5.817E-28(3.4)
820.0	6.241E-28(3.4)
1020.0	6.630E-28(3.2)
1220.0	5.944E-28(3.3)
1420.0	5.454E-28(3.5)
1620.0	4.590E-28(3.5)
1820.0	2.912E-28(3.4)
2020.0	8.946E-29(3.3)

Table 3.4.9 Reaction rate distribution along radial direction at central drawer (drawer B) for the armor (Phase IIIB) test blanket

DISTANCE FROM THE CENTRAL AXIS [mm]	Al27(n,alpha)Na24	Ti(n,x)Sc46	Ti(n,x)Sc47	Ti(n,x)Sc48	Ni58(n,2n)Ni57
231.00	3.902E-30(3.0)*	5.409E-30(4.3)	6.736E-31(4.4)	1.634E-30(3.9)	6.423E-31(4.0)
253.50	----------	----------	----------	----------	----------
281.00	2.247E-30(3.1)	3.191E-30(4.8)	3.769E-31(4.6)	8.700E-31(4.1)	2.796E-31(4.2)
332.20	1.299E-30(3.1)	1.876E-30(5.2)	2.212E-31(4.6)	4.997E-31(4.2)	1.367E-31(4.5)
383.00	7.671E-31(3.1)	1.146E-30(6.2)	1.317E-31(4.8)	2.876E-31(4.4)	6.997E-32(4.1)
429.10	4.623E-31(3.3)	7.343E-31(6.6)	8.417E-32(5.2)	1.742E-31(4.9)	3.721E-32(4.3)
480.60	----------	----------	----------	----------	----------
530.70	----------	----------	----------	----------	----------
580.60	----------	----------	----------	----------	----------

* Read as 3.902×10^{-30} [reaction/total source neutron] with 3.0 % relative error

DISTANCE FROM THE CENTRAL AXIS [mm]	Ni58(n,p)Co58	Zn64(n,p)Cu64	Zr90(n,2n)Zr89	Nb93(n,2n)Nb92m	In115(n,n')In115m
231.00	1.932E-29(3.0)	7.719E-30(3.3)	1.544E-29(3.1)	1.340E-29(3.1)	1.221E-29(3.0)
253.50	----------	----------	----------	----------	1.159E-29(3.0)
281.00	1.266E-29(3.0)	4.914E-30(3.5)	7.466E-30(3.1)	7.242E-30(3.1)	8.707E-30(3.1)
332.20	8.260E-30(3.0)	3.113E-30(3.5)	3.672E-30(3.2)	3.998E-30(3.1)	6.094E-30(3.1)
383.00	5.333E-30(3.0)	2.000E-30(3.7)	1.867E-30(3.4)	2.296E-30(3.1)	4.181E-30(3.0)
429.10	3.525E-30(3.0)	1.334E-30(3.2)	1.045E-30(3.6)	1.424E-30(3.0)	2.936E-30(3.1)
480.60	----------	----------	----------	----------	2.028E-30(3.2)
530.70	----------	----------	----------	----------	1.303E-30(3.2)
580.60	----------	----------	----------	----------	8.423E-31(3.4)

Table 3.4.9 (Continued)

DISTANCE FROM THE CENTRAL AXIS [mm]	Au197(n,gamma)Au198
231.00	3.309E-28(3.4)
253.50	2.027E-28(3.5)
281.00	1.661E-28(3.9)
332.20	1.296E-28(4.5)
383.00	1.125E-28(3.2)
429.10	1.185E-28(4.7)
480.60	1.365E-28(4.3)
530.70	1.148E-28(4.3)
580.60	1.144E-28(4.2)

Table 3.4.10 Reaction rate distribution along radial direction at off-central drawer (drawer C) for the armor (Phase IIIB) test blanket

DISTANCE FROM THE CENTRAL AXIS [mm]	Al27(n,alpha)Na24	Nb93(n,2n)Nb92m	In115(n,n')In115m	Au197(n,gamma)Au198
230.20	3.888E-30(3.0)*	1.316E-29(3.1)	1.185E-29(3.0)	2.659E-28(4.1)
255.30	0.000E+00(0.0)	0.000E+00(0.0)	9.990E-30(3.0)	1.712E-28(4.7)
280.50	2.185E-30(3.1)	6.927E-30(3.1)	8.430E-30(3.0)	1.481E-28(4.5)
331.50	1.244E-30(3.2)	3.975E-30(3.1)	5.882E-30(3.1)	1.173E-28(5.2)
382.20	7.689E-31(3.2)	2.286E-30(3.0)	3.995E-30(3.1)	1.018E-28(4.3)
428.00	4.771E-31(3.3)	1.387E-30(3.0)	2.795E-30(3.1)	1.115E-28(3.4)

* Read as 3.888×10^{-30} [reaction/total source neutron] with 3.0 % relative error

Table 3.4.11 Reaction rate distributions along the line source at a distance of 187 mm from the source axis for the opening (Phase IIIC) test blanket (normal side)

Distance From Front of Assembly [cm]	$^{93}Nb(n,2n)^{92m}Nb$	$^{115}In(n,n')^{115m}In$	$^{197}Au(n,g)^{198}Au$
2.00	1.442E-29(3.2)*	6.191E-30(3.1)	1.339E-28(3.2)
22.00	2.277E-29(3.2)	1.121E-29(3.1)	2.962E-28(3.3)
42.00	2.667E-29(3.2)	1.355E-29(3.1)	3.946E-28(3.2)
52.00	2.806E-29(3.2)	1.435E-29(3.1)	4.380E-28(3.3)
62.00	2.823E-29(3.1)	1.466E-29(3.1)	4.671E-28(3.2)
72.00	2.883E-29(3.1)	1.492E-29(3.1)	4.553E-28(3.1)
82.00	2.934E-29(3.1)	1.500E-29(3.1)	4.430E-28(3.2)
92.00	2.950E-29(3.2)	1.520E-29(3.1)	4.287E-28(3.2)
102.00	2.994E-29(3.1)	1.514E-29(3.1)	4.373E-28(3.1)
112.00	2.941E-29(3.1)	1.510E-29(3.1)	4.295E-28(3.3)
122.00	2.883E-29(3.1)	1.492E-29(3.1)	4.089E-28(3.2)
132.00	2.889E-29(3.1)	1.491E-29(3.1)	4.210E-28(3.2)
142.00	2.843E-29(3.1)	1.467E-29(3.1)	4.196E-28(3.1)
152.00	2.802E-29(3.1)	1.437E-29(3.1)	4.094E-28(3.2)
162.00	2.760E-29(3.1)	1.376E-29(3.1)	3.557E-28(3.1)
182.00	2.455E-29(3.0)	1.166E-29(3.1)	2.627E-28(3.2)
202.00	1.604E-29(3.2)	6.558E-30(3.1)	1.328E-28(3.3)

* Read as 1.442×10^{-29} [reaction/total source neutron] with 3.2 % relative error

Table 3.4.12 Reaction rate distributions along the line source at a distance of 187 mm from the source axis for the opening (Phase IIIC) test blanket (opening side)

Distance From Front of Assembly [cm]	$^{93}Nb(n,2n)^{92m}Nb$	$^{115}In(n,n')^{115m}In$	$^{197}Au(n,g)^{198}Au$
2.00	1.514E-29(3.0)*	6.313E-30(3.4)	1.438E-28(3.0)
22.00	2.381E-29(3.0)	1.114E-29(3.3)	2.987E-28(3.3)
42.00	2.824E-29(3.0)	1.343E-29(3.3)	4.136E-28(3.1)
62.00	2.927E-29(3.0)	1.457E-29(3.3)	4.580E-28(3.3)
72.00	2.912E-29(3.0)	1.466E-29(3.3)	4.761E-28(3.2)
84.50	2.875E-29(3.0)	1.248E-29(3.3)	3.540E-28(3.2)
92.00	2.870E-29(3.0)	1.188E-29(3.3)	3.154E-28(3.1)
102.00	2.889E-29(3.0)	1.148E-29(3.3)	3.081E-28(3.2)
112.00	2.898E-29(3.0)	1.192E-29(3.4)	3.117E-28(3.3)
119.50	2.922E-29(3.0)	1.257E-29(3.3)	3.500E-28(3.3)
132.00	2.919E-29(3.1)	1.509E-29(3.4)	4.507E-28(3.3)
142.00	2.850E-29(3.1)	1.478E-29(3.3)	3.708E-28(3.1)
162.00	2.697E-29(3.1)	1.384E-29(3.3)	3.887E-28(3.3)
182.00	2.441E-29(3.1)	1.160E-29(3.4)	2.569E-28(3.1)
202.00	1.596E-29(3.1)	6.346E-30(3.4)	1.244E-28(3.3)

* Read as 1.514×10^{-29} [reaction/total source neutron] with 3.0 % relative error

Table 3.4.13 Reaction rate distributions along the line source for the opening (Phase IIIC) test blanket (inside of opening)

(at a distance of 451 mm from the source axis)

Distance From Front of Assembly [cm]	$^{93}Nb(n,2n)^{92m}Nb$	$^{115}In(n,n')^{115m}In$	$^{197}Au(n,g)^{198}Au$
87.00	6.055E-30(3.1)*	4.861E-30(3.3)	1.801E-28(3.7)
92.00	6.642E-30(3.1)	4.945E-30(3.4)	1.750E-28(3.5)
97.00	7.193E-30(3.1)	5.024E-30(3.4)	1.754E-28(3.3)
102.00	7.298E-30(3.0)	5.027E-30(3.4)	1.819E-28(3.8)
107.00	7.283E-30(3.1)	5.029E-30(3.4)	1.788E-28(3.9)
112.00	6.935E-30(3.1)	4.647E-30(3.4)	1.778E-28(3.3)
117.00	6.284E-30(3.1)	4.875E-30(3.4)	1.829E-28(3.7)

* Read as 6.055×10^{-30} [reaction/total source neutron] with 3.1 % relative error

(at a distance of 651 mm from the source axis)

Distance From Front of Assembly [cm]	$^{93}Nb(n,2n)^{92m}Nb$	$^{115}In(n,n')^{115m}In$	$^{197}Au(n,g)^{198}Au$
87.00	2.916E-30(3.1)	2.258E-30(3.5)	1.150E-28(3.9)
92.00	3.058E-30(3.2)	2.348E-30(3.5)	1.079E-28(3.7)
97.00	3.217E-30(3.0)	2.393E-30(3.4)	1.099E-28(3.8)
102.00	3.187E-30(3.1)	2.394E-30(3.4)	1.082E-28(3.9)
107.00	3.212E-30(3.1)	2.360E-30(3.5)	1.090E-28(3.8)
112.00	3.075E-30(3.2)	2.295E-30(3.6)	1.089E-28(3.8)
117.00	2.921E-30(3.2)	2.188E-30(3.6)	1.144E-28(3.8)

Table 3.4.14 Reaction rate distribution along radial direction at central drawer (drawer B) for the opening (Phase IIIC) test blanket

Distance from Central Axis [mm]	$^{27}Al(n,a)^{24}Na$	$Ti(n,x)^{46}Sc$	$Ti(n,x)^{47}Sc$	$Ti(n,x)^{48}Sc$	$^{55}Mn(n,g)^{56}Mn$
230.0	4.185E-30(3.4)*	5.125E-30(5.1)	6.837E-31(4.1)	1.790E-30(4.0)	————
280.5	2.384E-30(3.5)	2.905E-30(5.8)	3.875E-31(4.2)	1.015E-30(4.2)	————
331.2	1.391E-30(3.7)	1.833E-30(5.5)	2.251E-31(4.2)	5.639E-31(4.1)	1.144E-29(3.3)
382.0	7.843E-31(3.8)	1.156E-30(5.6)	1.321E-31(4.3)	3.385E-31(4.4)	————
428.5	4.992E-31(3.8)	6.897E-31(6.7)	8.597E-32(4.1)	2.775E-31(3.7)	————

* Read as 4.185×10^{-30} [reaction/total source neutron] with 3.4 % relative error

Distance from Central Axis [cm]	$Fe(n,x)^{56}Mn$	$^{59}Co(n,a)^{56}Mn$	$^{58}Ni(n,2n)^{57}Ni$	$^{58}Ni(n,p)^{58}Co$	$^{64}Zn(n,p)^{64}Cu$
230.0	3.519E-30(3.0)	9.564E-31(3.2)	6.742E-31(3.7)	1.819E-29(2.9)	8.061E-30(3.3)
280.5	————	————	3.164E-31(3.8)	1.232E-29(3.0)	5.396E-30(3.3)
331.2	1.204E-30(3.7)	3.070E-31(4.1)	1.564E-31(4.0)	8.084E-30(3.0)	3.313E-30(3.4)
382.0	————	————	7.415E-32(3.6)	5.242E-30(2.9)	2.152E-30(3.4)
428.5	————	————	4.062E-32(4.2)	3.475E-30(3.0)	1.464E-30(3.5)

Distance from Central Axis [mm]	$^{90}Zr(n,2n)^{89}Zr$	$93Nb(n,2n)^{92m}Nb$	$^{115}In(n,n')^{115m}In$	$^{197}Au(n,g)^{198}Au$
230.0	1.683E-29(3.1)	1.547E-29(3.1)	1.247E-29(3.1)	2.501E-28(3.1)
255.0	————	————	1.028E-29(3.1)	1.661E-28(3.2)
280.5	8.165E-30(3.2)	8.451E-30(3.1)	8.620E-30(3.1)	1.383E-28(3.5)
331.2	4.100E-30(3.2)	4.679E-30(3.1)	5.963E-30(3.3)	1.139E-28(3.0)
382.0	2.141E-30(3.2)	2.708E-30(3.2)	4.060E-30(3.3)	1.066E-28(3.1)
428.5	1.160E-30(3.2)	1.651E-30(3.2)	2.874E-30(3.4)	1.183E-28(3.2)
479.2	————	————	2.035E-30(3.3)	1.298E-28(3.2)
530.0	————	————	1.332E-30(3.5)	1.184E-28(3.4)
579.0	————	————	8.631E-31(3.8)	1.178E-28(3.0)

JAERI—M 94—015

Table 3.4.15 Reaction rate distribution along radial direction in drawer D for the opening (Phase IIIC) test blanket

(a) at a distance of 1211 mm from the front end of assembly

Distance From Central Axis [cm]	$^{93}Nb(n,2n)^{92m}Nb$	$^{115}In(n,n')^{115m}In$	$^{197}Au(n,g)^{198}Au$
21.30	2.381E-29(3.1)*	1.235E-29(3.1)	3.032E-28(4.0)
26.30	1.484E-29(3.1)	9.979E-30(3.1)	2.471E-28(4.4)
31.30	1.038E-29(3.2)	8.002E-30(3.1)	2.084E-28(4.4)
36.30	8.073E-30(3.3)	6.533E-30(3.1)	1.936E-28(4.3)
41.30	6.287E-30(3.1)	5.376E-30(3.1)	1.811E-28(4.3)
46.30	5.052E-30(3.0)	4.503E-30(3.2)	1.753E-28(4.7)
51.30	4.009E-30(3.3)	3.728E-30(3.2)	1.548E-28(4.1)
56.30	3.403E-30(3.4)	3.075E-30(3.2)	1.460E-28(4.5)
61.30	2.803E-30(3.3)	2.430E-30(3.2)	1.942E-28(3.8)
64.80	2.524E-30(3.3)	1.960E-30(3.2)	1.490E-28(3.9)

* Read as 2.381×10^{-29} [reaction/total source neutron] with 3.1 % relative error

(b) at a distance of 1275 mm from the front end of assembly

Distance From Central Axis [cm]	$^{93}Nb(n,2n)^{92m}Nb$	$^{115}In(n,n')^{115m}In$	$^{197}Au(n,g)^{198}Au$
25.50	1.257E-29(3.0)*	1.138E-29(3.3)	1.769E-28(3.7)
30.10	8.465E-30(2.9)	8.822E-30(3.3)	1.321E-28(3.6)
40.20	3.921E-30(3.1)	5.078E-30(3.3)	1.137E-28(3.8)

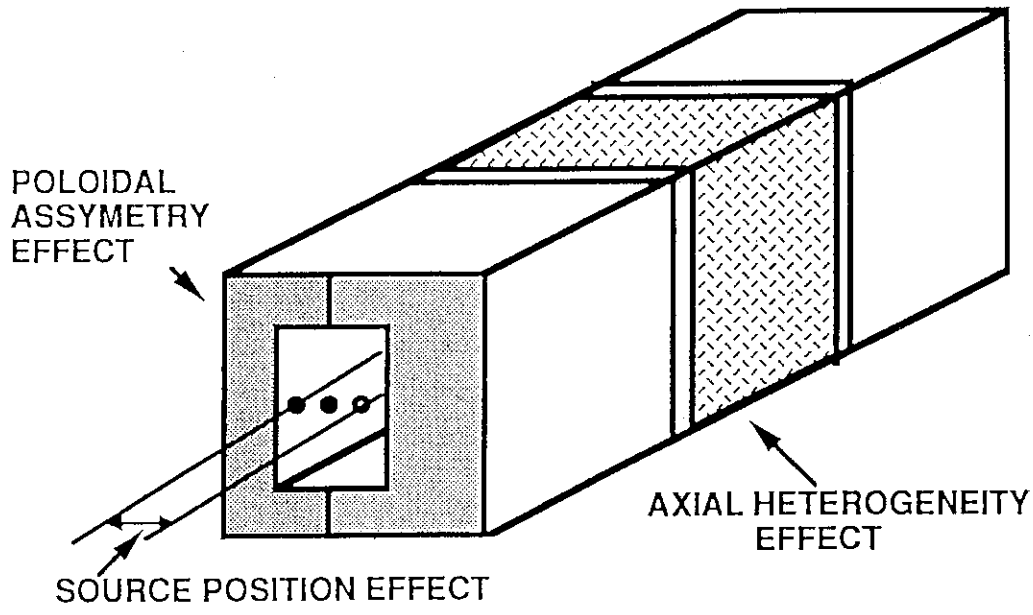

Fig. 3.1.1 Illustration of candidate blanket configurations with variations of asymmetry, heterogeneity and source condition

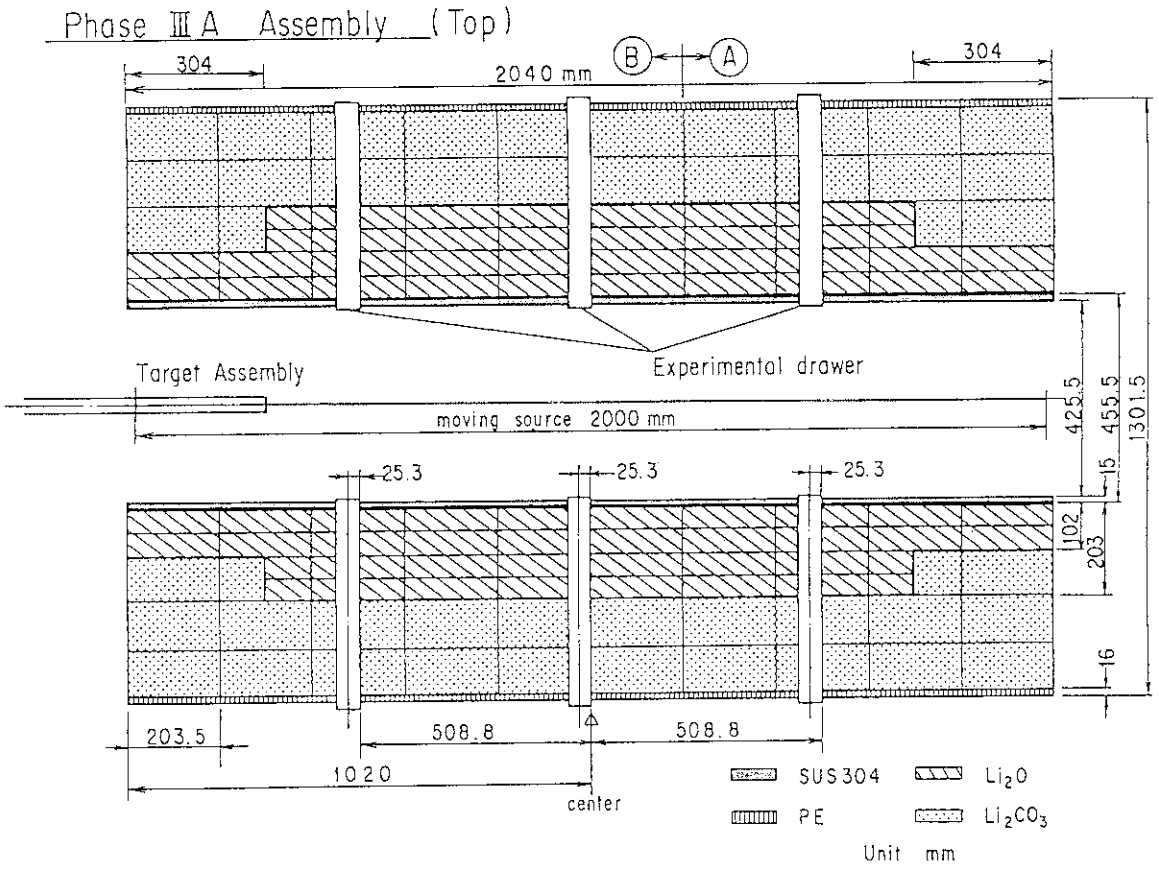

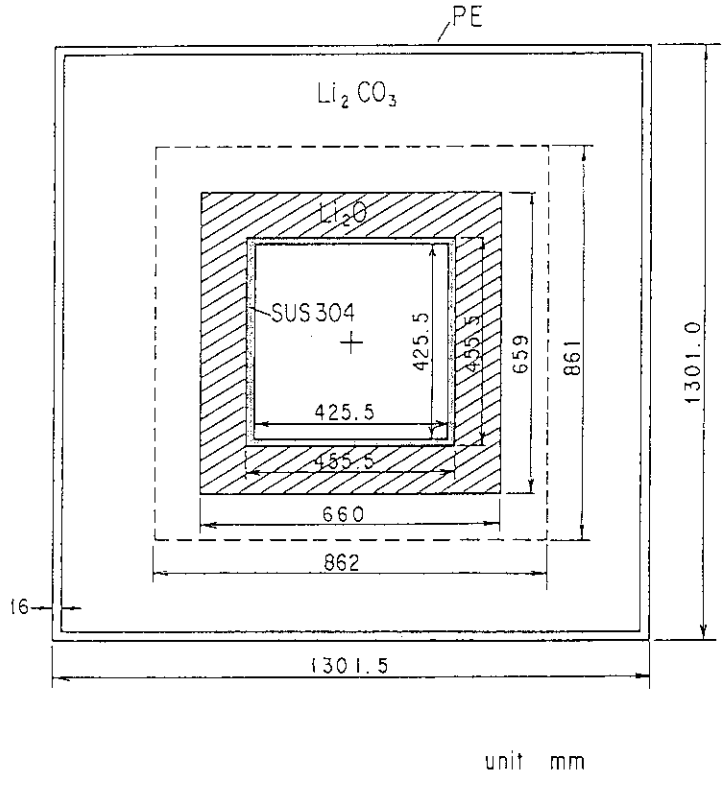

Fig. 3.2.1 Cross section of the reference configuration of annular test blanket assembly

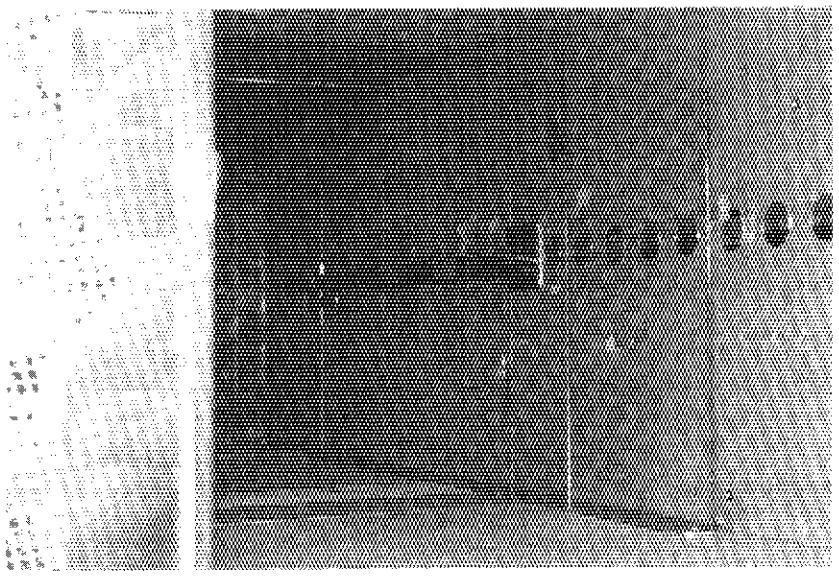

Fig. 3.2.2 First wall surface with detector holes plugged by disks

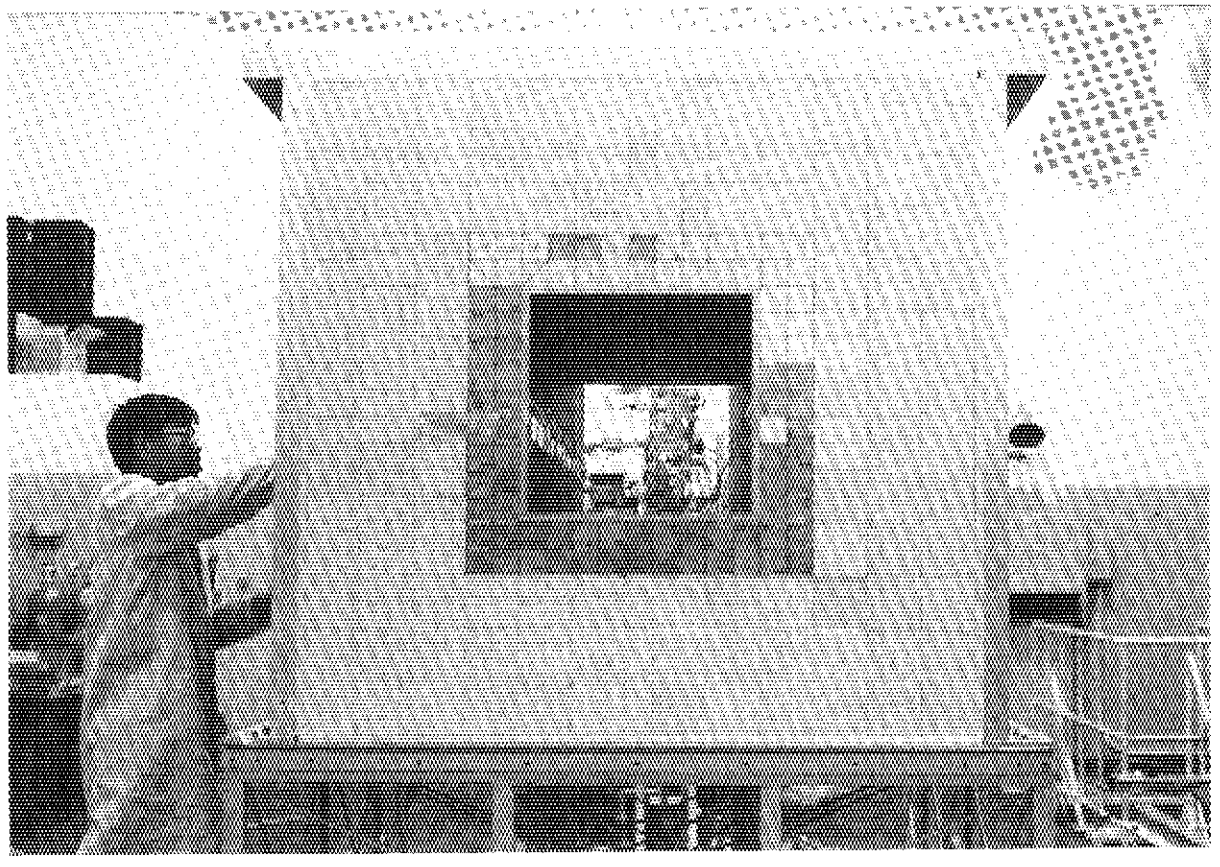

Fig. 3.2.3 Photograph of the annular test blanket and the drift tube of long tube water cooled target assembly

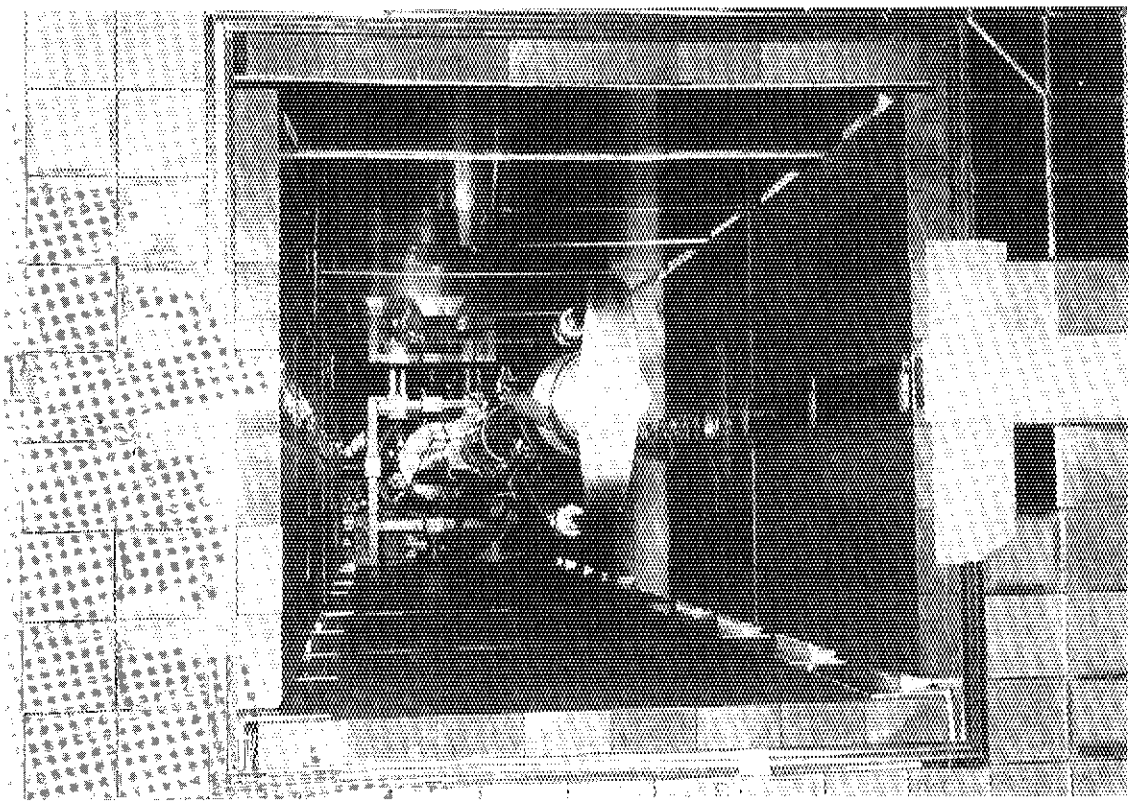

Fig. 3.2.4 Armor test blanket, the 25 mm thick graphite layer is attached to the reference blanket

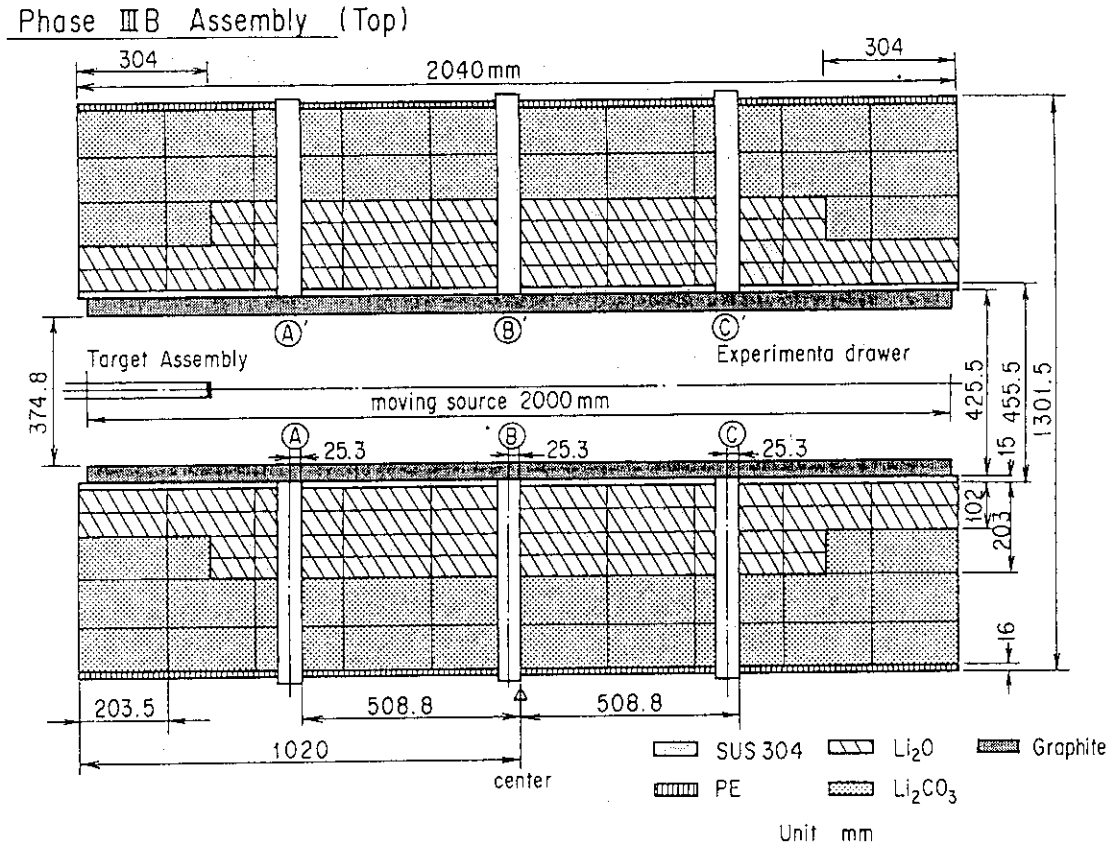

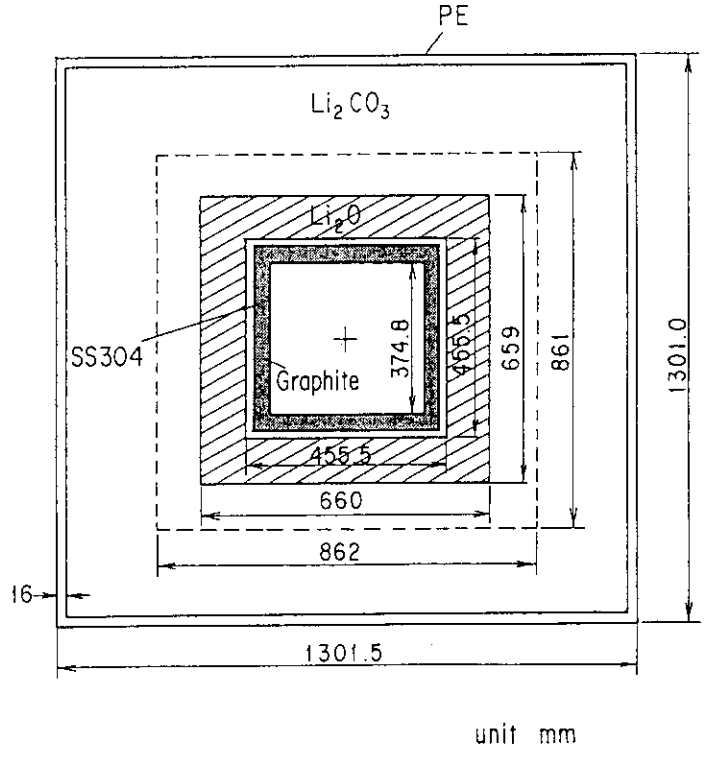

Fig. 3.2.5 Cross section of the armor test blanket and its dimensions

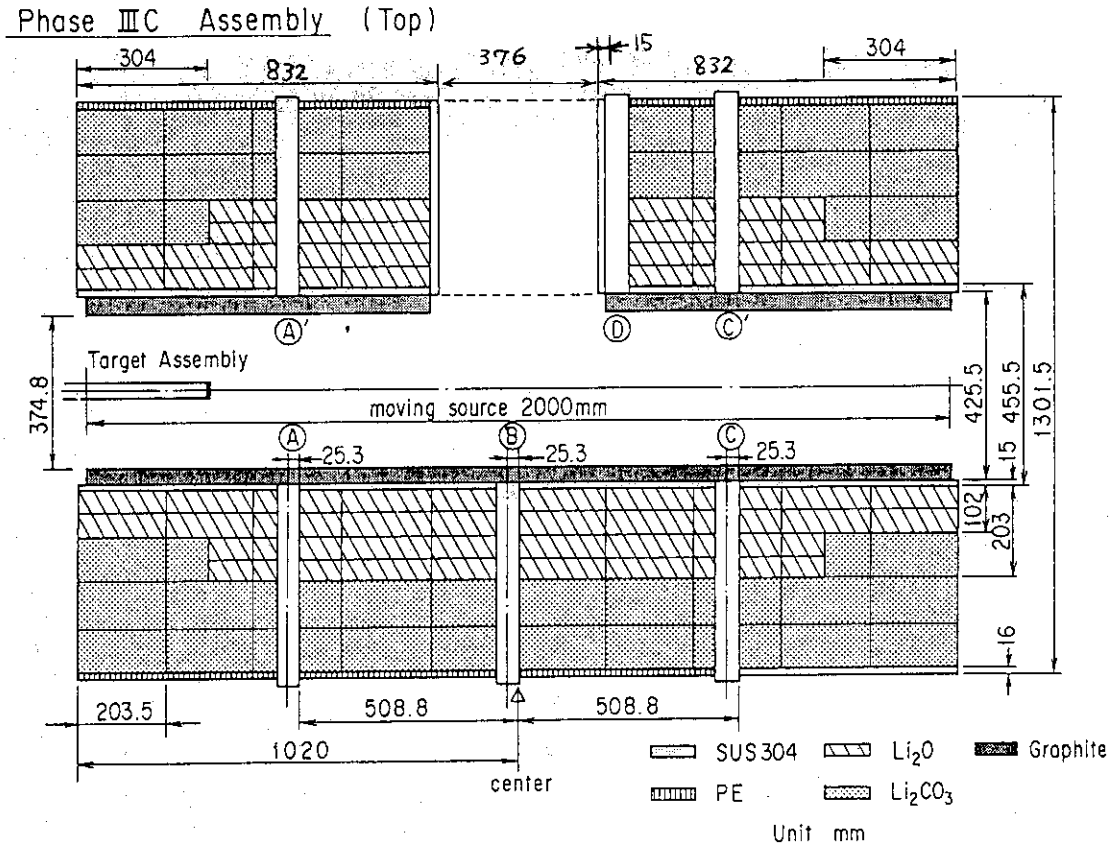

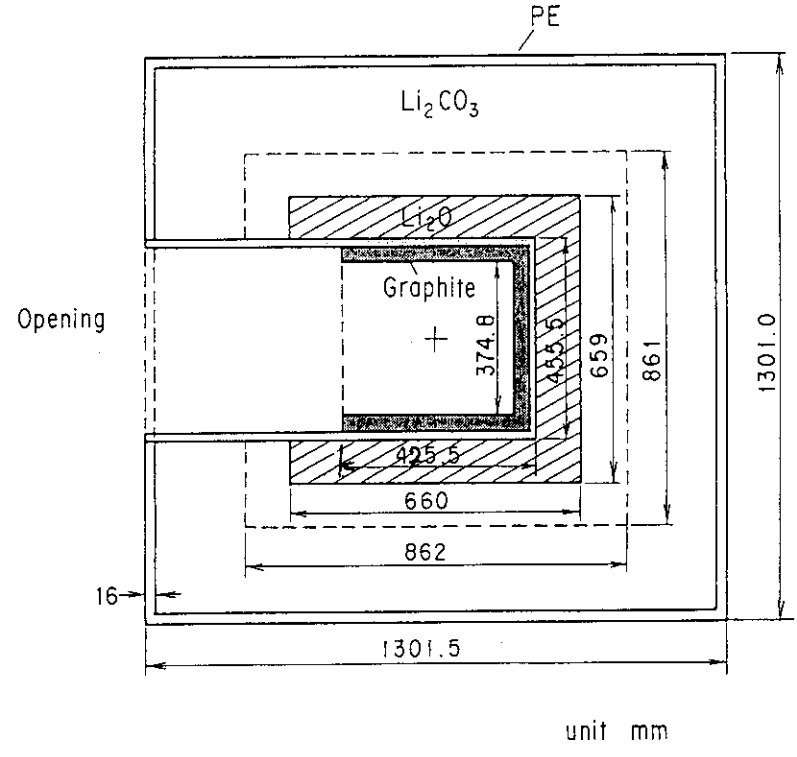

Fig. 3.2.6 Large opening test blanket assembly and dimensions

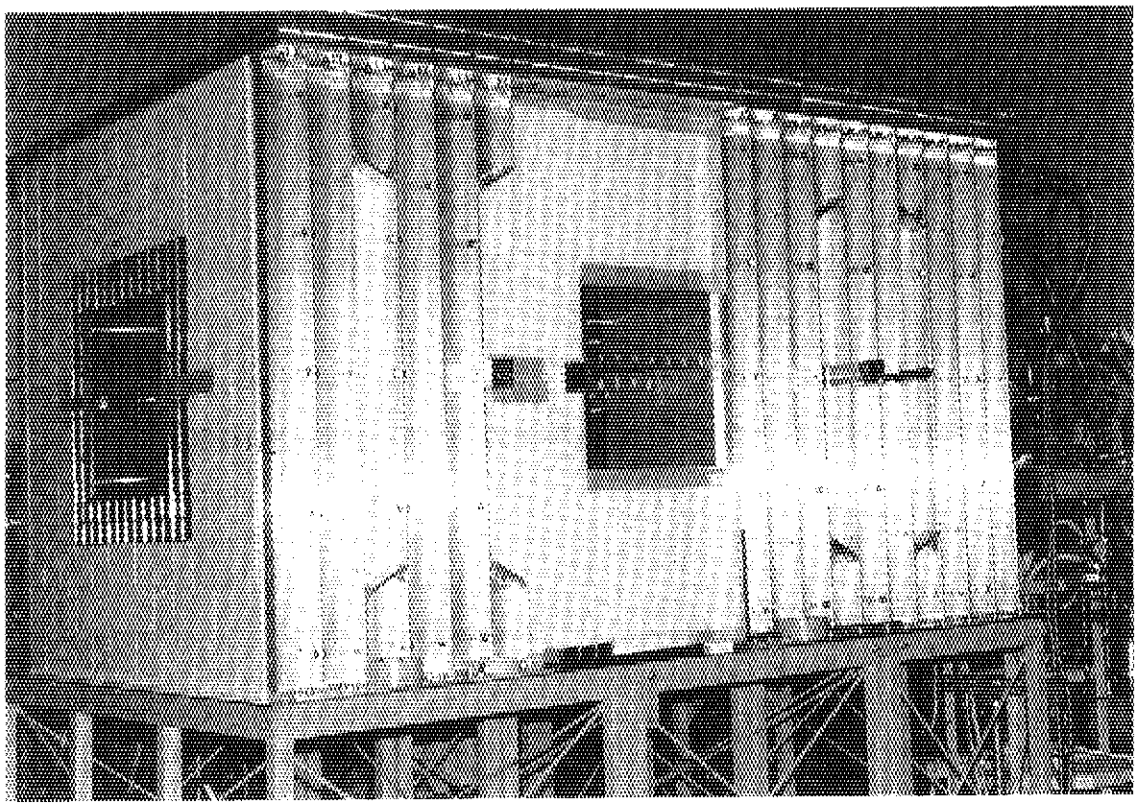

Fig. 3.2.7 Photograph of the opening in the Phase IIIC test blanket

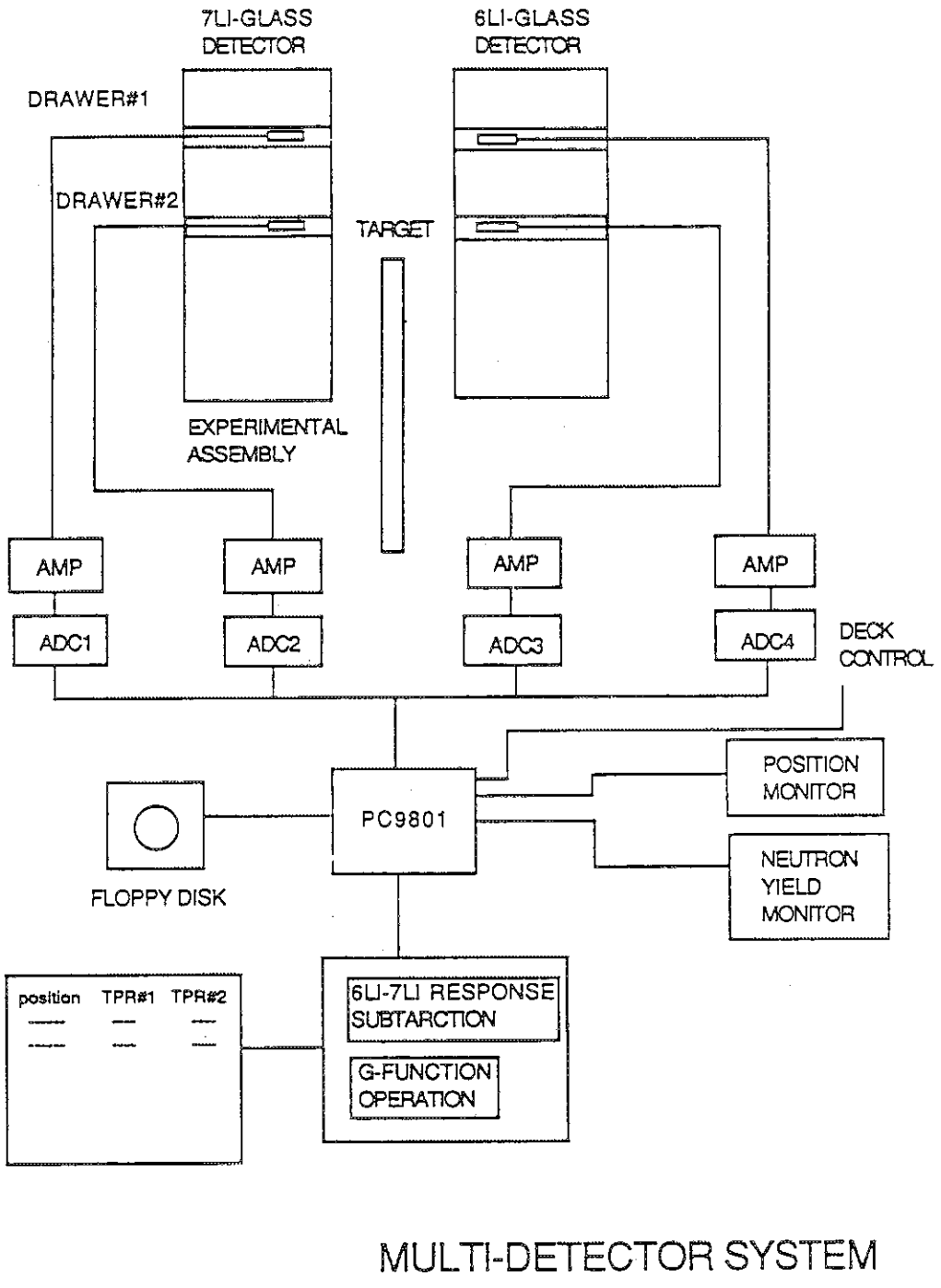

Fig. 3.3.1 Multi-detector data acquisition system for simultaneous measurement of ^{7}Li and ^{6}Li glass detectors

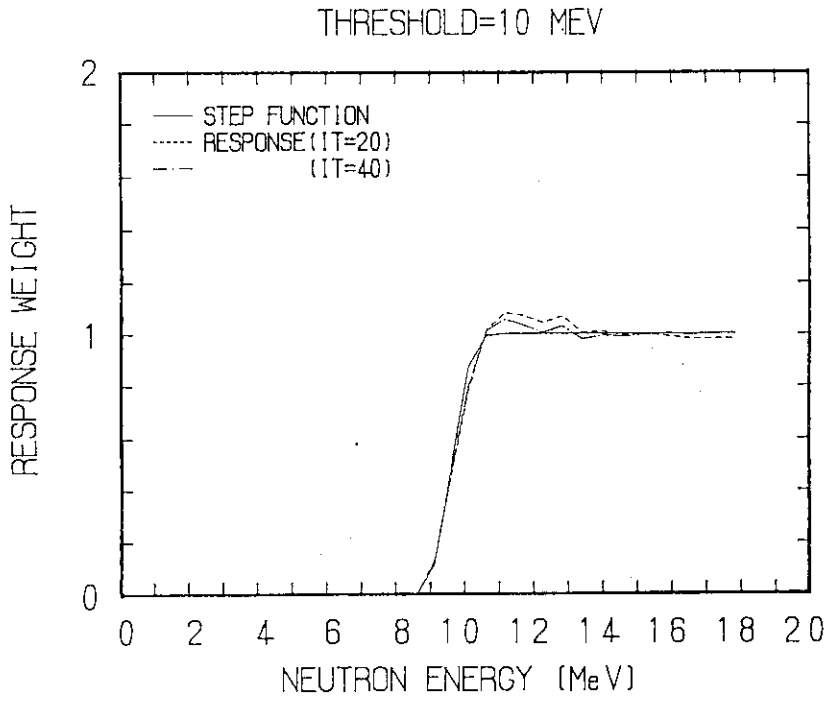

Fig. 3.3.2 Virtual step response of the NE213 detector to act as an integral flux detector

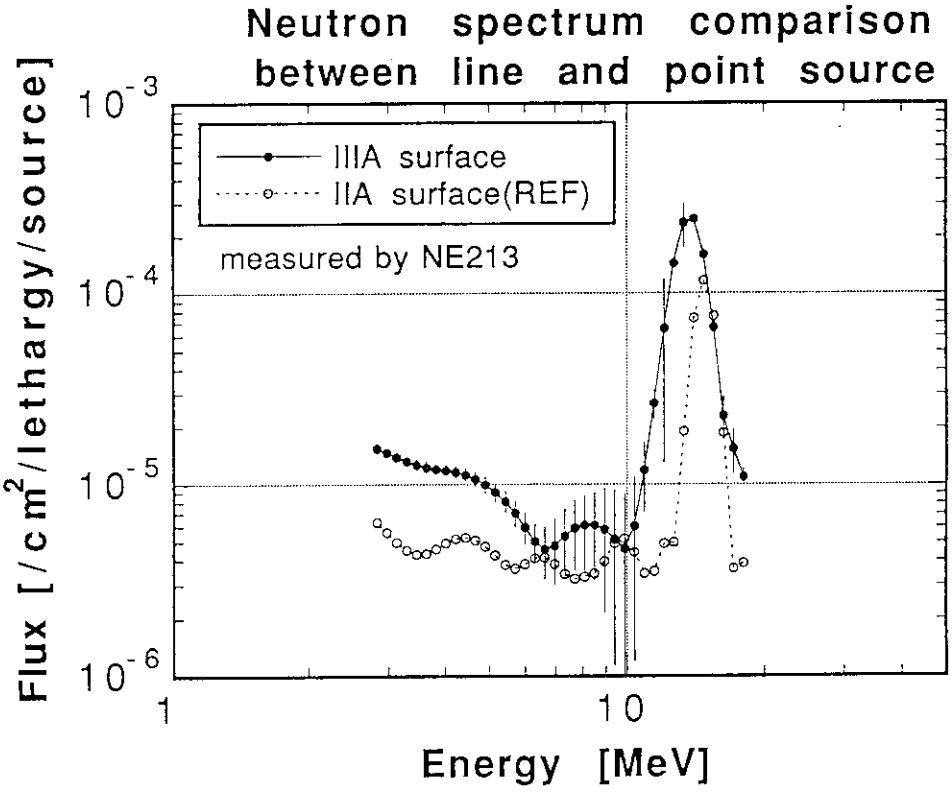

Fig. 3.4.1 Comparison of source neutron spectra measured at the surface of test blanket between the point source experiment Phase II and the line source experiment Phase III

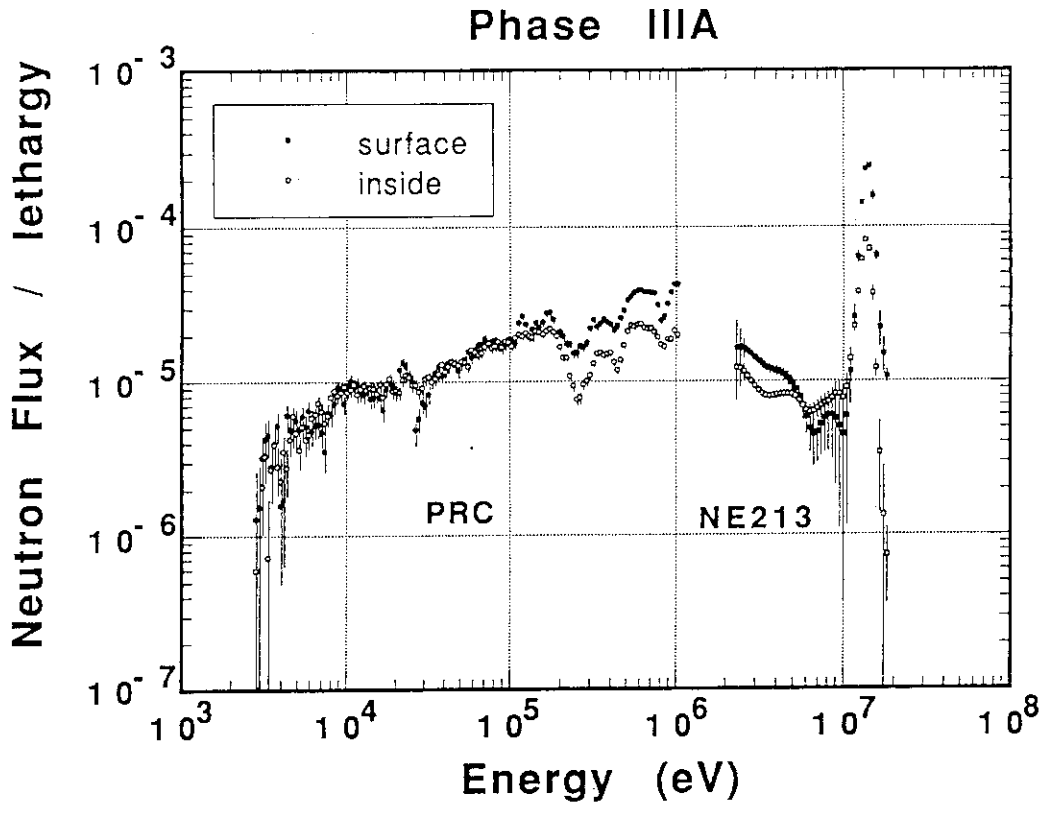

Fig. 3.4.2 Measured spectra at the surface and inside of the reference blanket by the NE213 and the PRC spectrometers

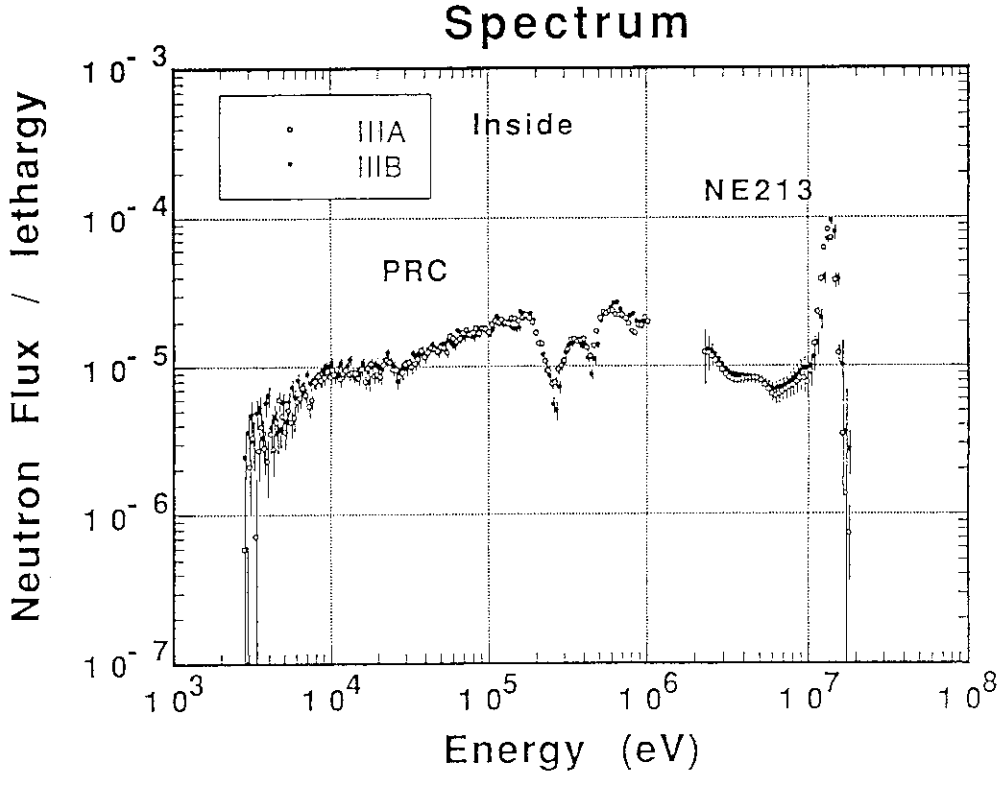

Fig. 3.4.3 Measured spectra inside the blanket for the reference (IIIA) and the armor (IIIB) test blankets

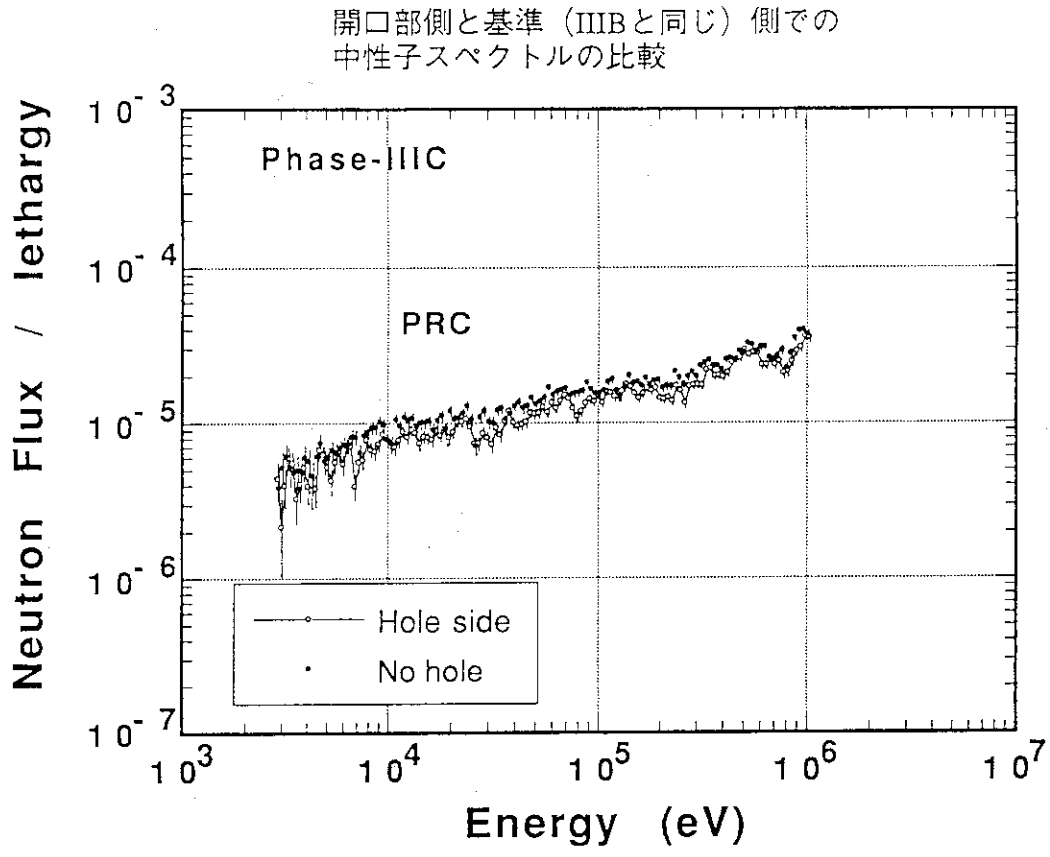

Fig. 3.4.4 Comparison of low energy spectra measured at both sides of the surface of the opening test blanket

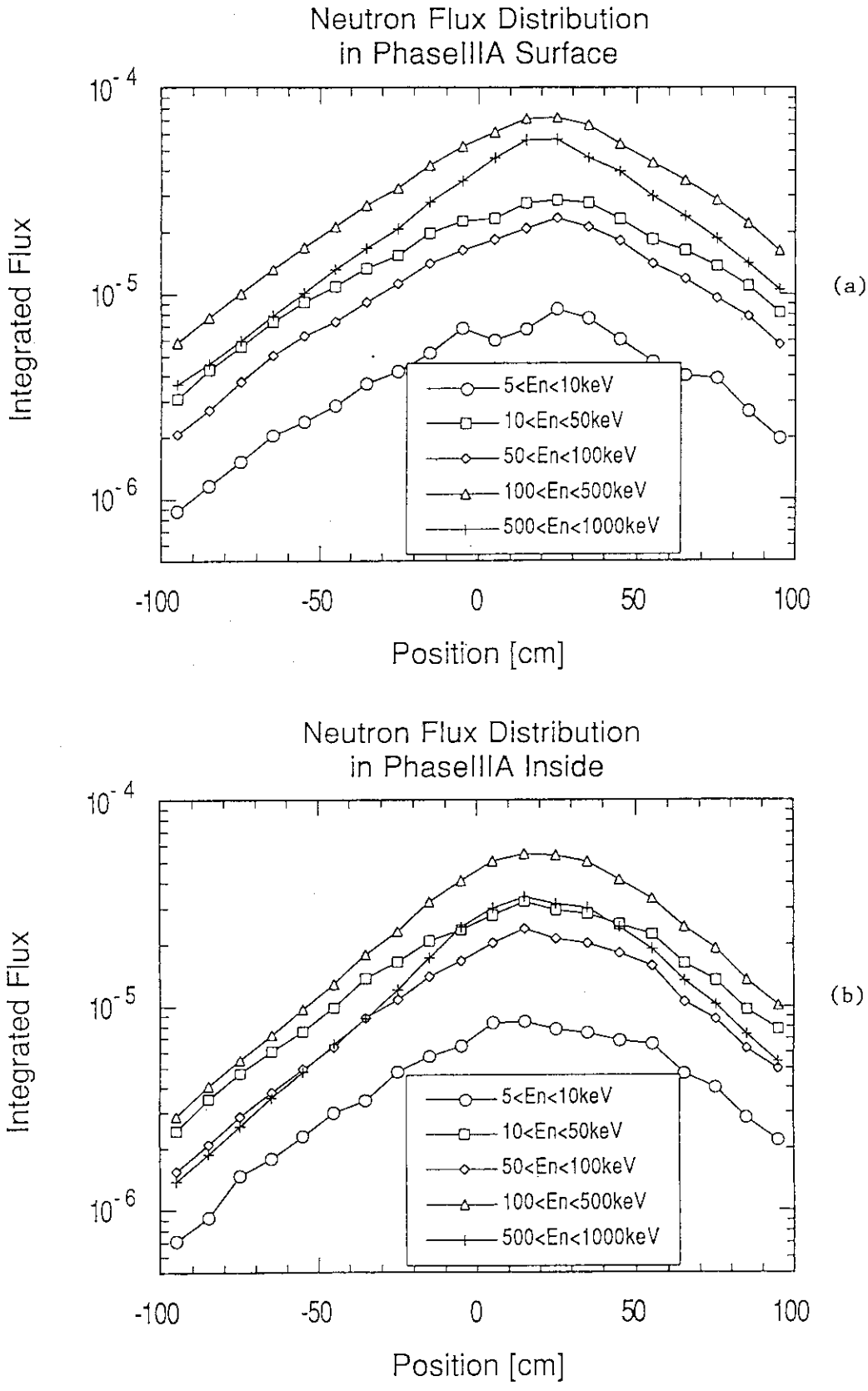

Fig. 3.4.5 Source position-wise profile of the energy integrated neutron flux measured by the PRC spectrometer (a) at the FW surface and (b) inside of the reference blanket (Phase IIIA)

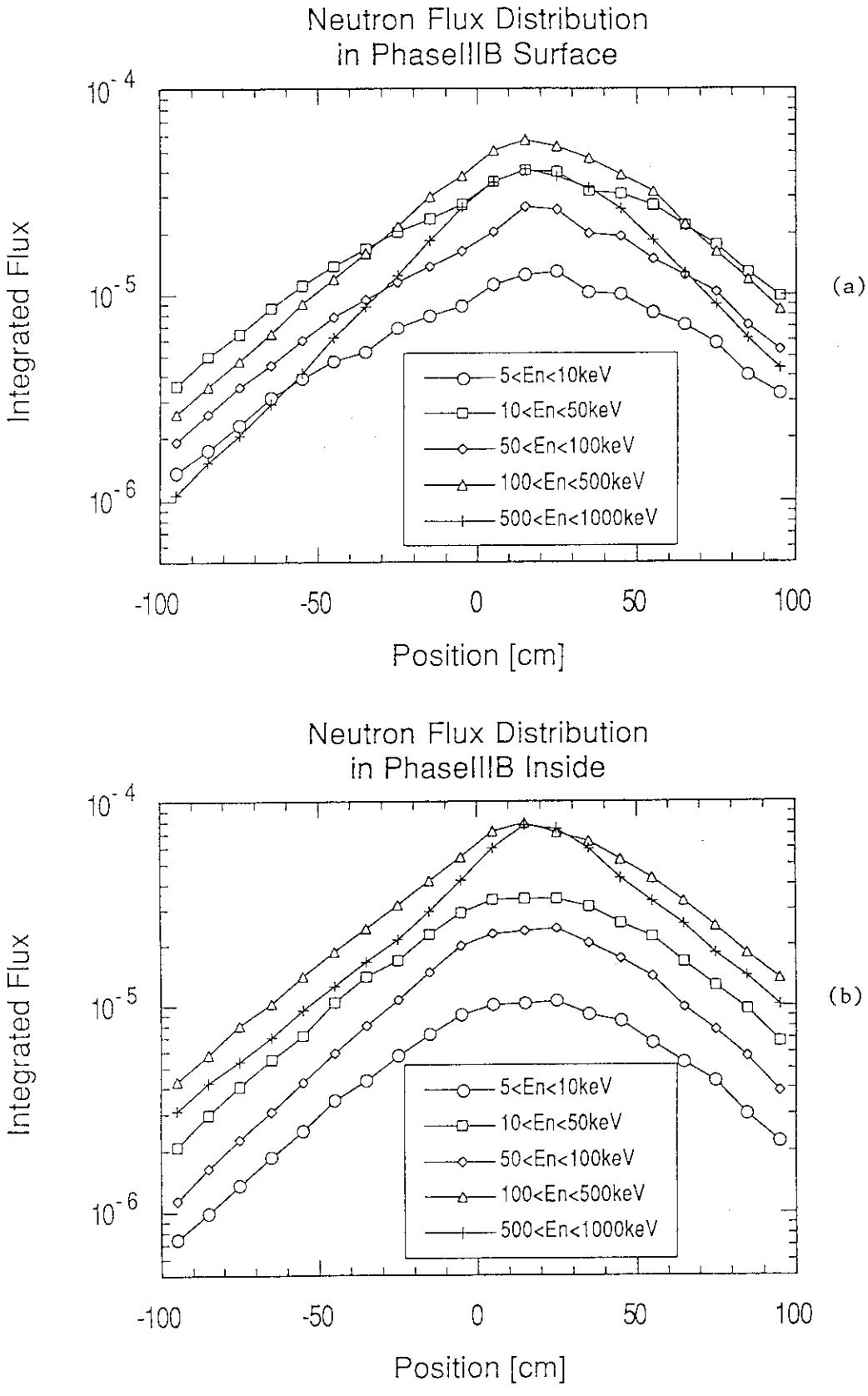

Fig. 3.4.6 Source position-wise profile of the energy integrated neutron flux measured by the PRC spectrometer (a) at the Graphite surface and (b) inside of the armor blanket (Phase IIIB)

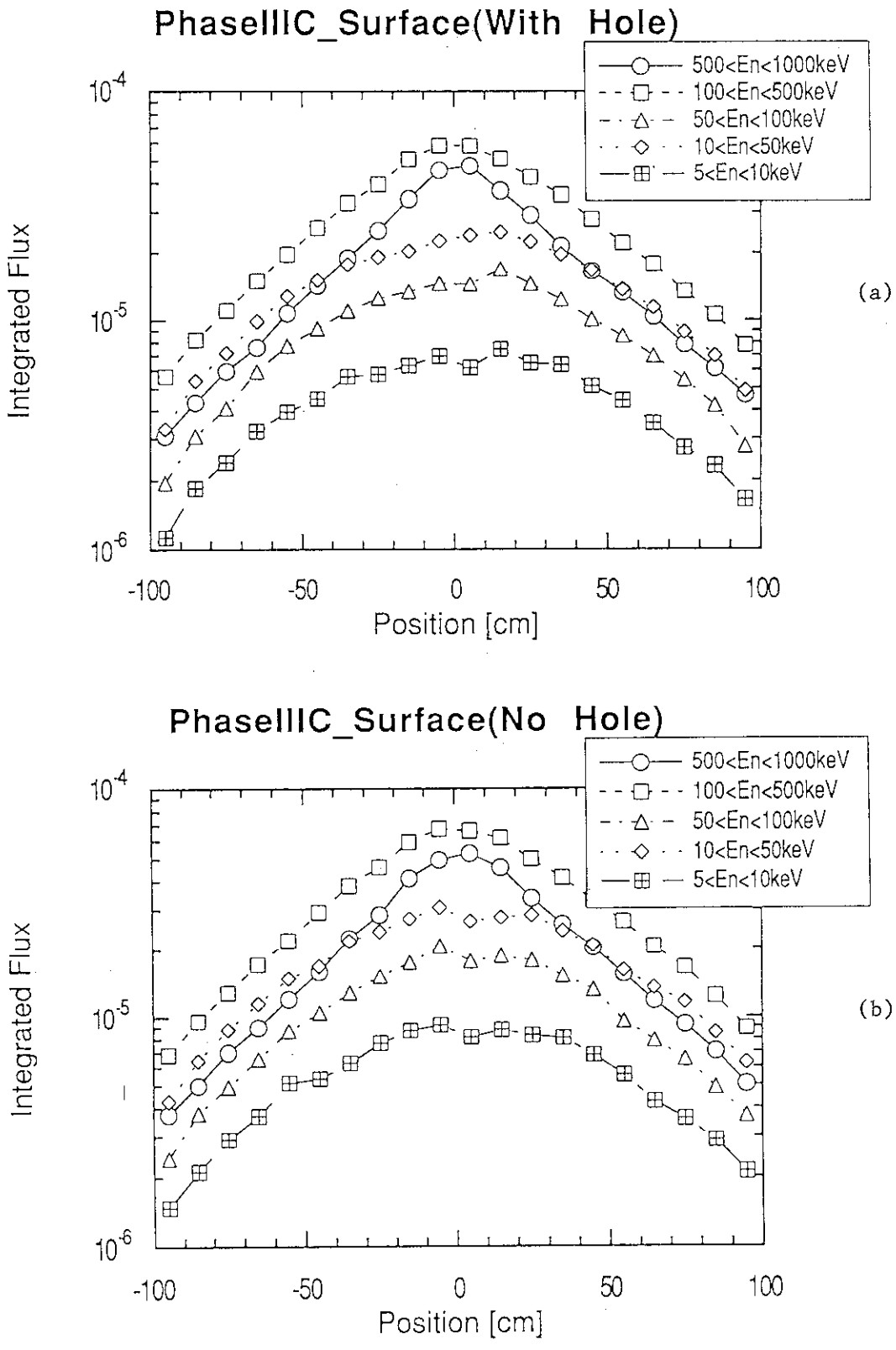

Fig. 3.4.7 Source position-wise profile of the energy integrated neutron flux measured by the PRC spectrometer (a) at the opening side and (b) no-opening side of the Graphite surfaces of the large opening test blanket (Phase IIIC)

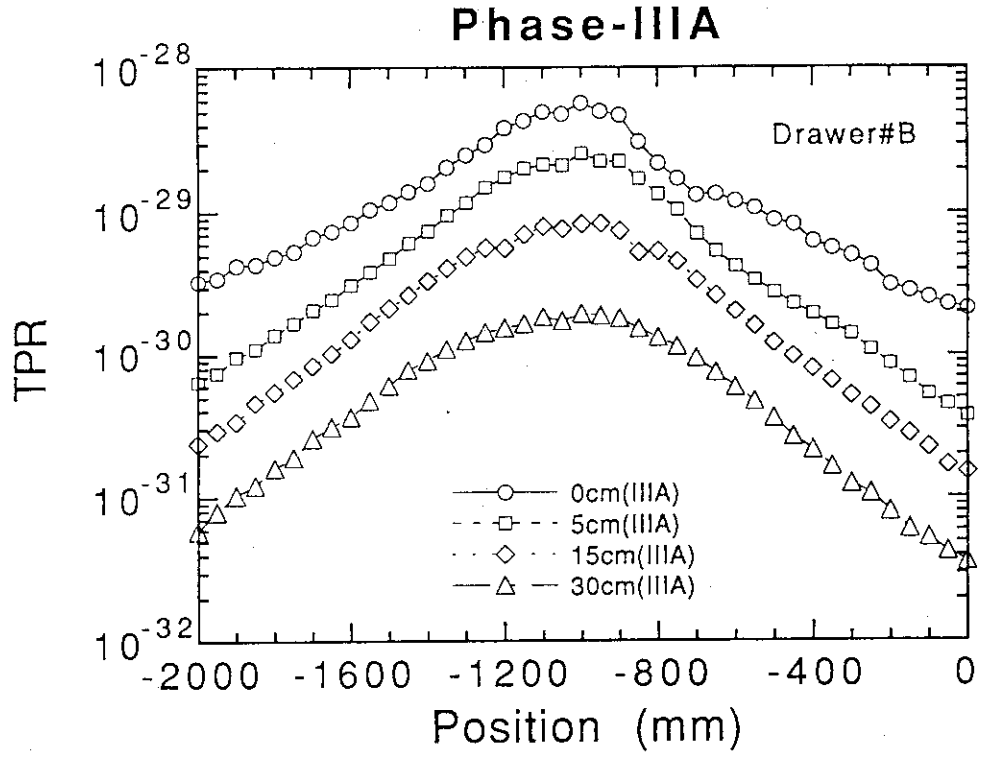

(a)

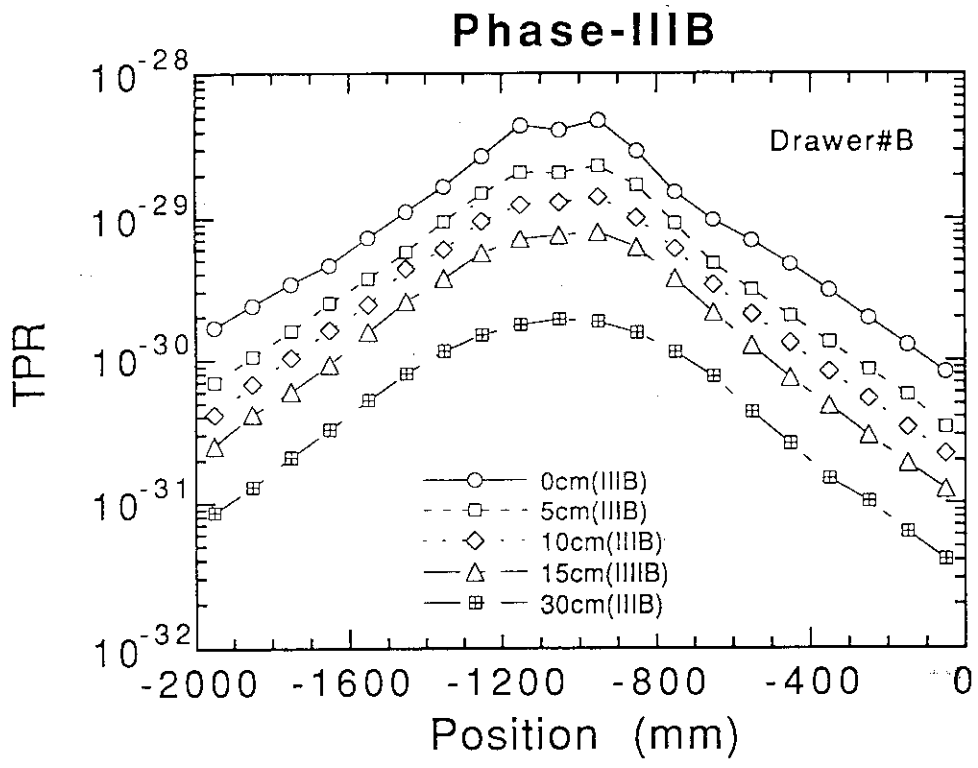

(b)

Fig. 3.4.8 Source position-wise ^{7}Li tritium production rate (TPR) profile measured by the NE213 detector in the central drawer for three blankets of (a) Phase IIIA, (b) IIIB and (c) IIIC (reference, armor and opening)

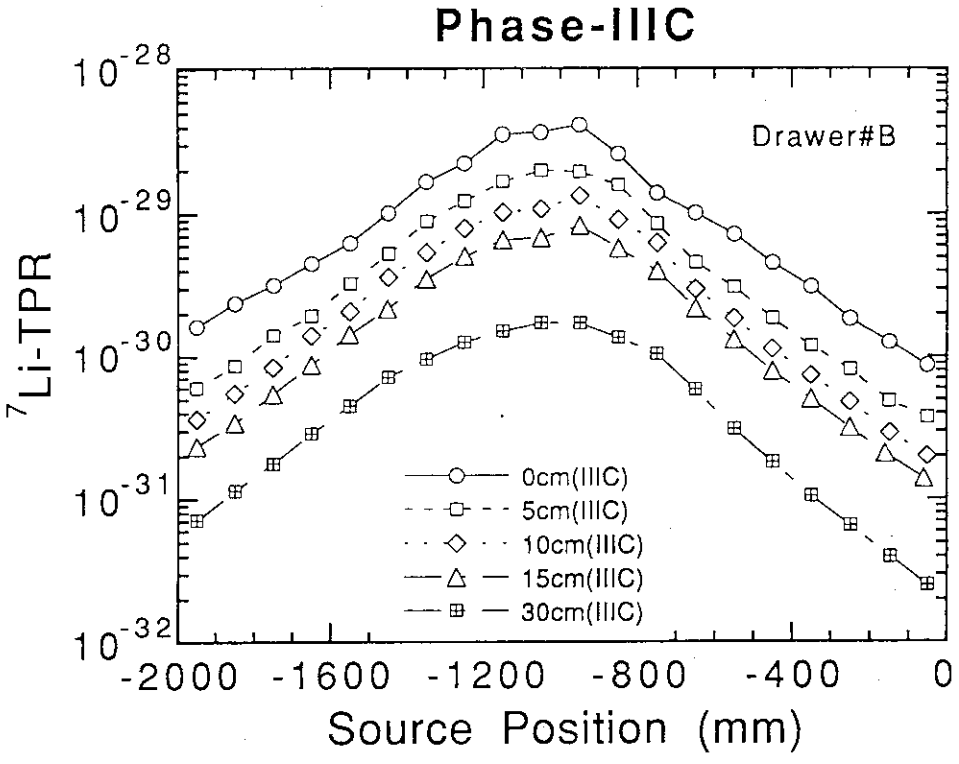

(c)

Fig. 3.4.8 (Continued)

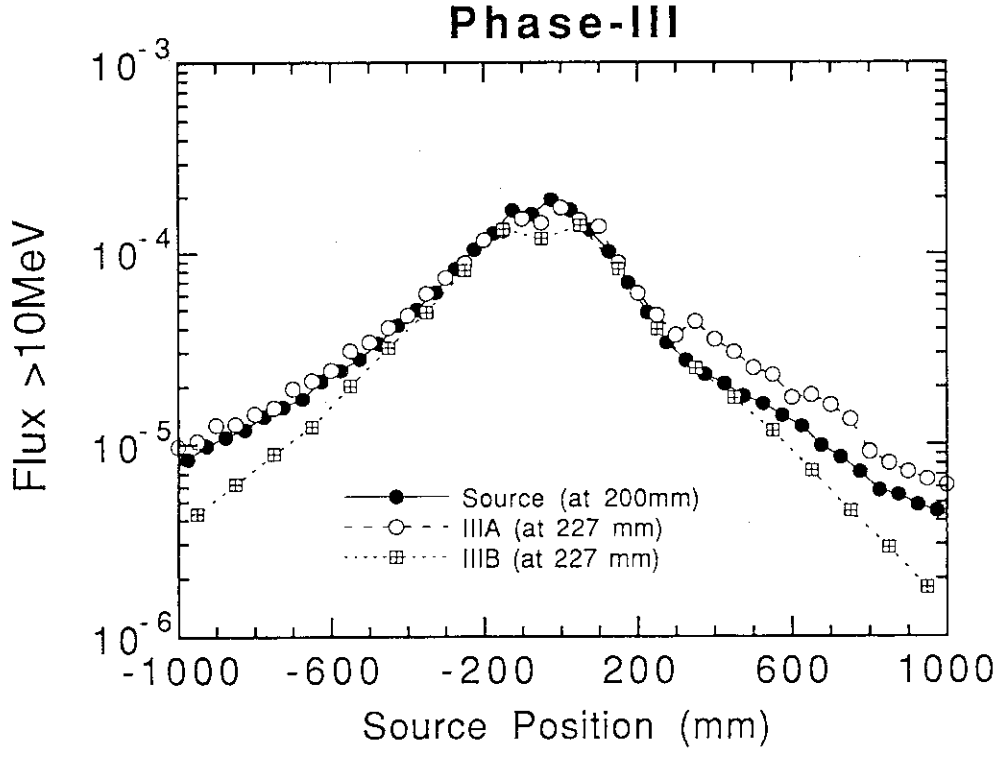

Fig. 3.4.9 Source profile comparison of integrated fast neutron flux between the measurements at the positions with and without assembly

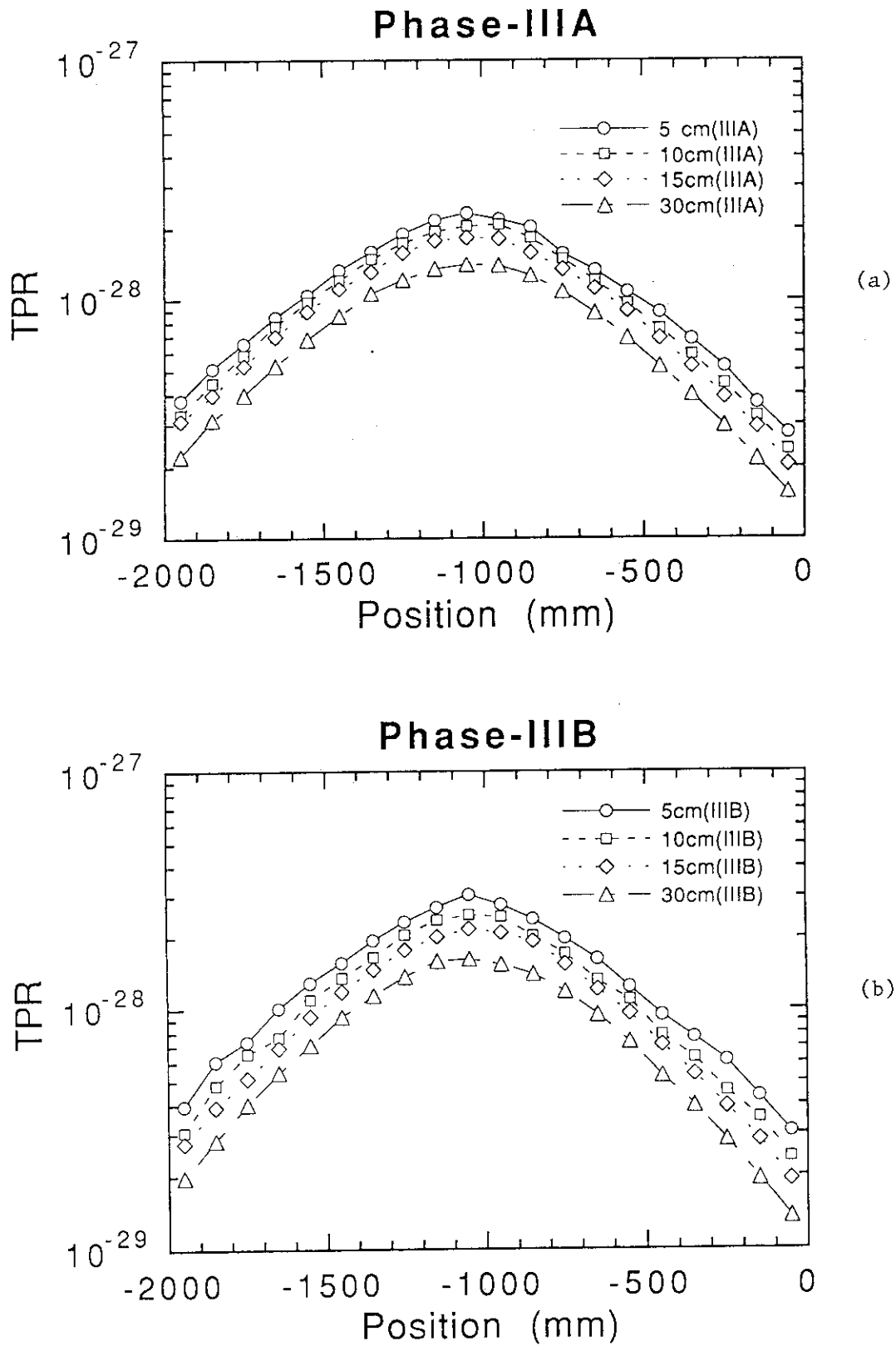

Fig. 3.4.10 Source position-wise ^{6}Li tritium production rate (TPR) profile measured by the Li-glass detector in the central drawer for three blankets of (a) Phase IIIA, (b) IIIB and (c) IIIC (reference, armor and opening)

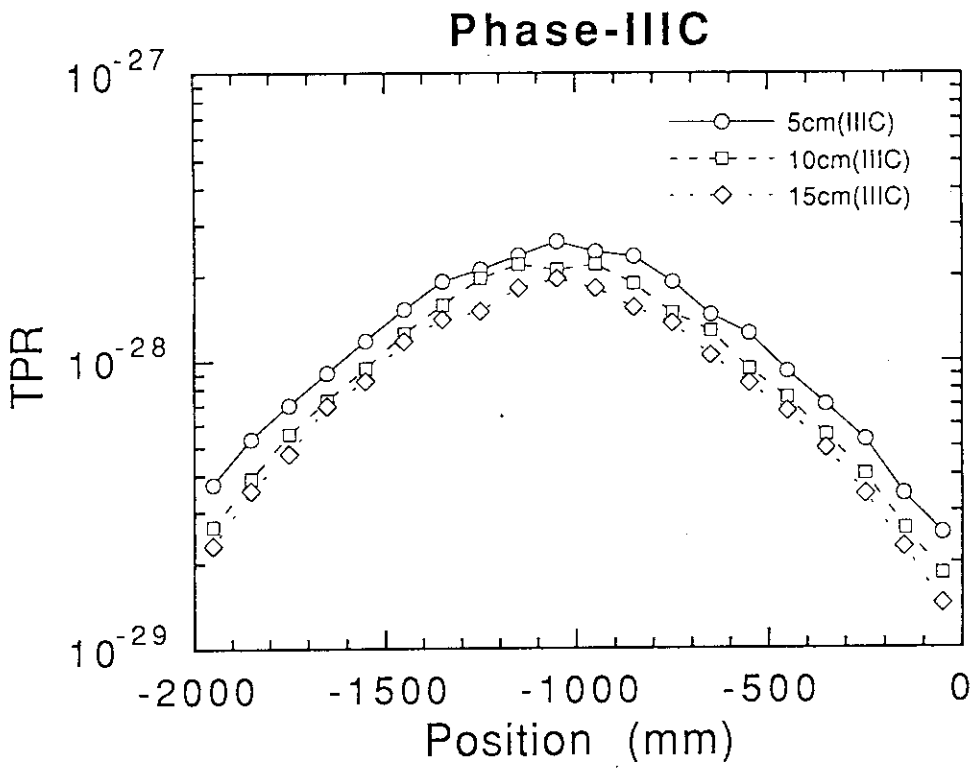

(c)

Fig. 3.4.10 (Continued)

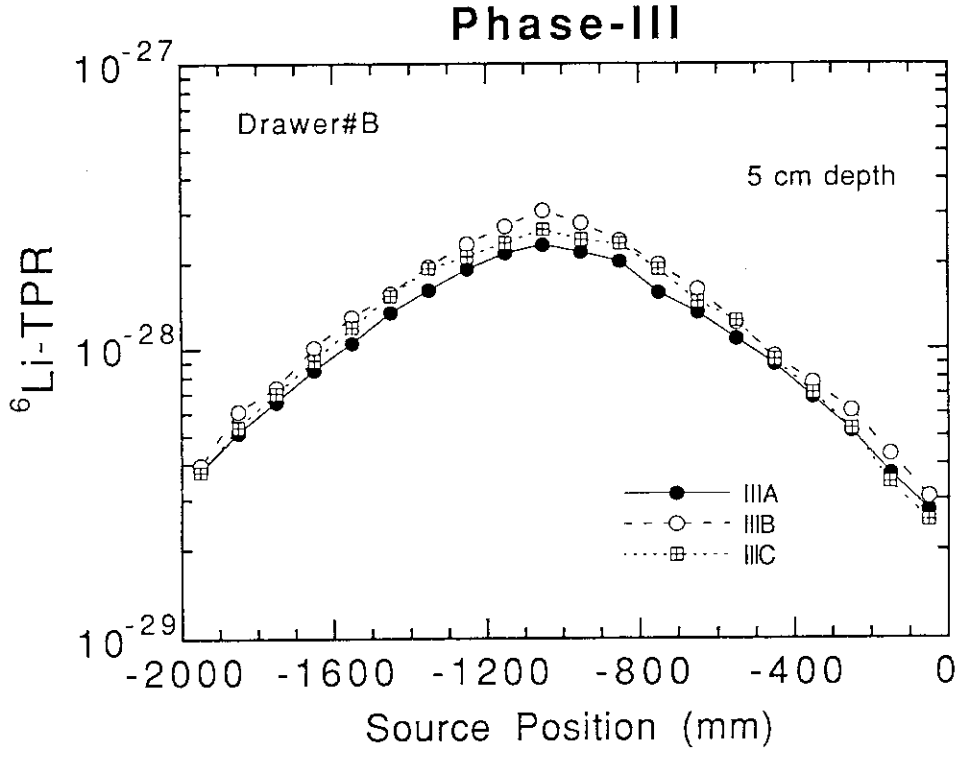

Fig. 3.4.11 Effect of opening on the source position-wise ^{6}Li-TPR profile

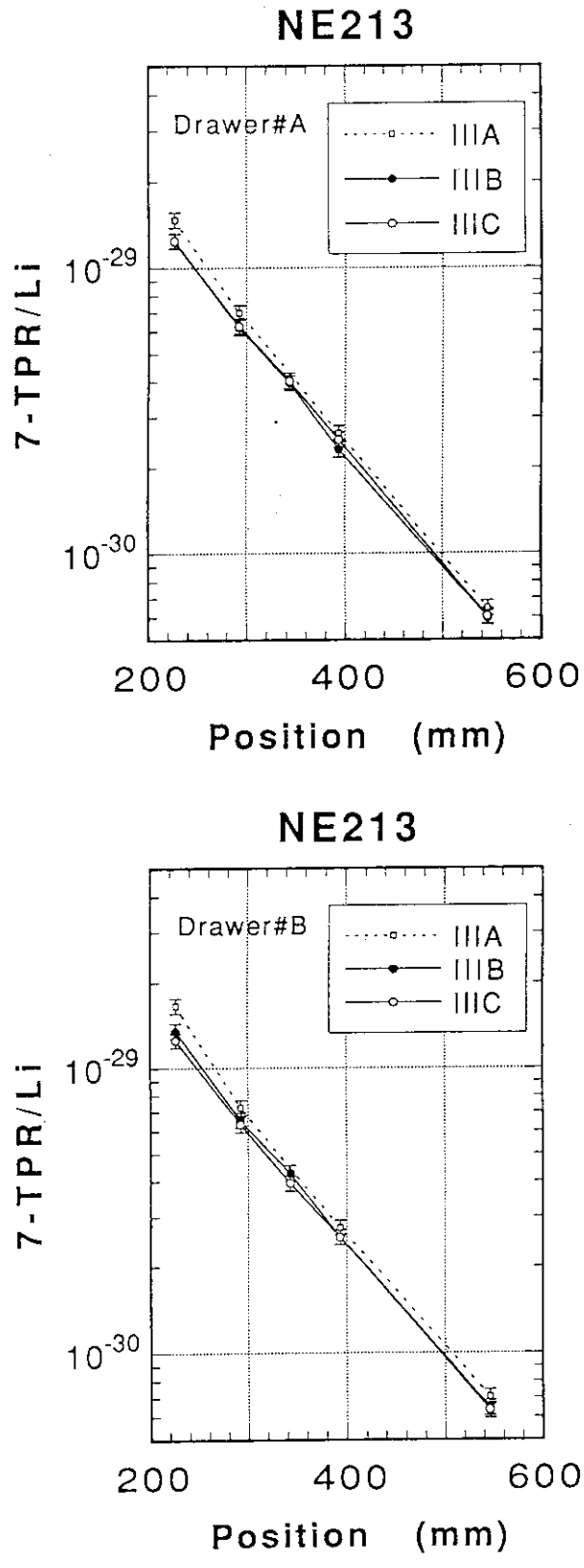

Fig. 3.4.12 Superposed results of the source position-wise ^{7}Li tritium production rate (TPR) corresponding to the line source; (a) drawer A at a distance of -500 mm from the center (backward), (b) drawer B at the center and (c) drawer C at a distance of +500 mm from the center (forward).

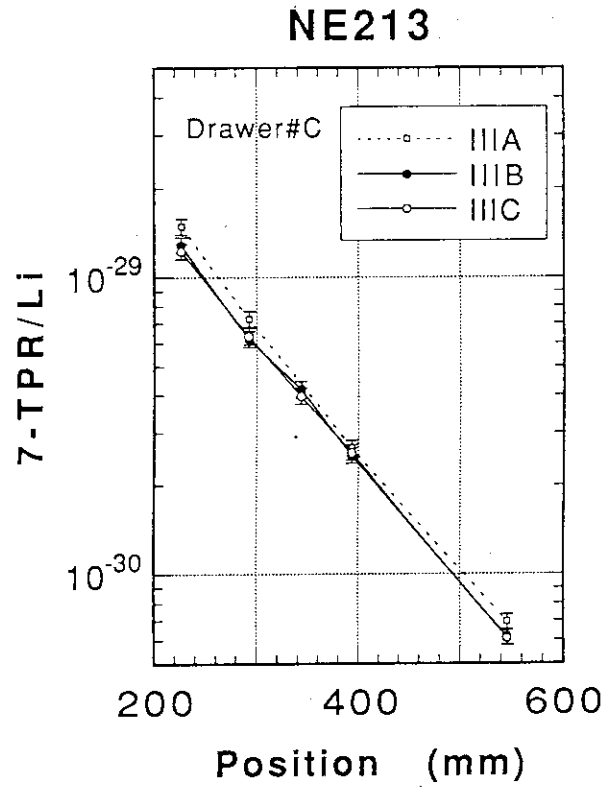

(c)

Fig. 3.4.12 (Continued)

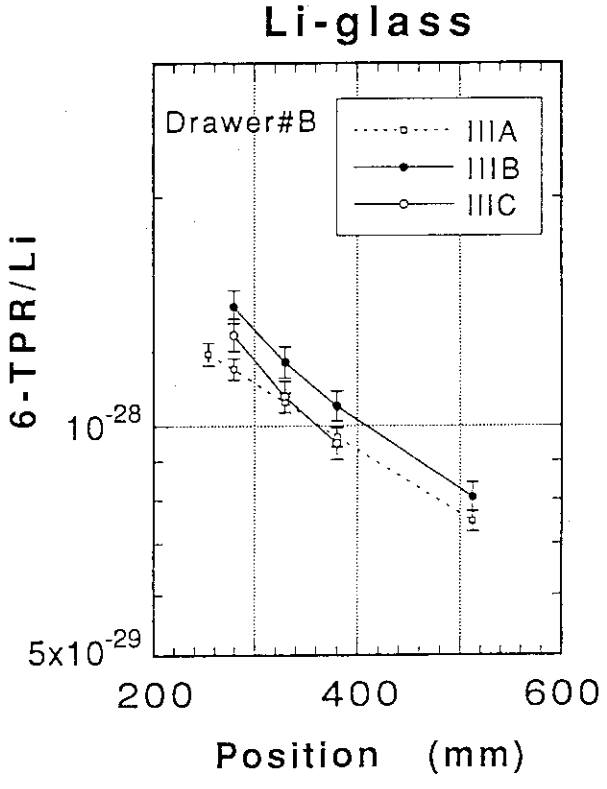

(a)

Fig. 3.4.13 Superposed results of the source position-wise ^{6}Li tritium production rate (TPR) corresponding to the line source; (a) drawer B at the center and (b) drawer C at a distance of +500 mm from the center (forward).

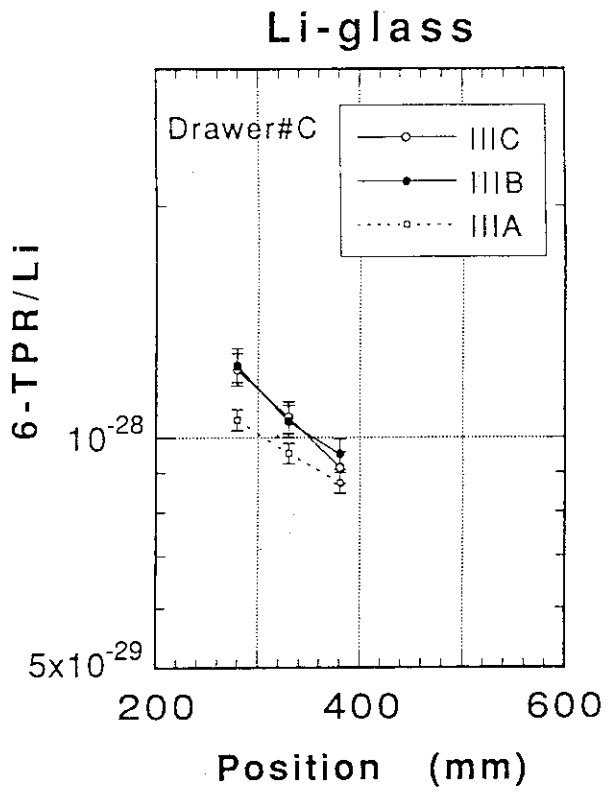

(b)

Fig. 3.4.13 (Continued)

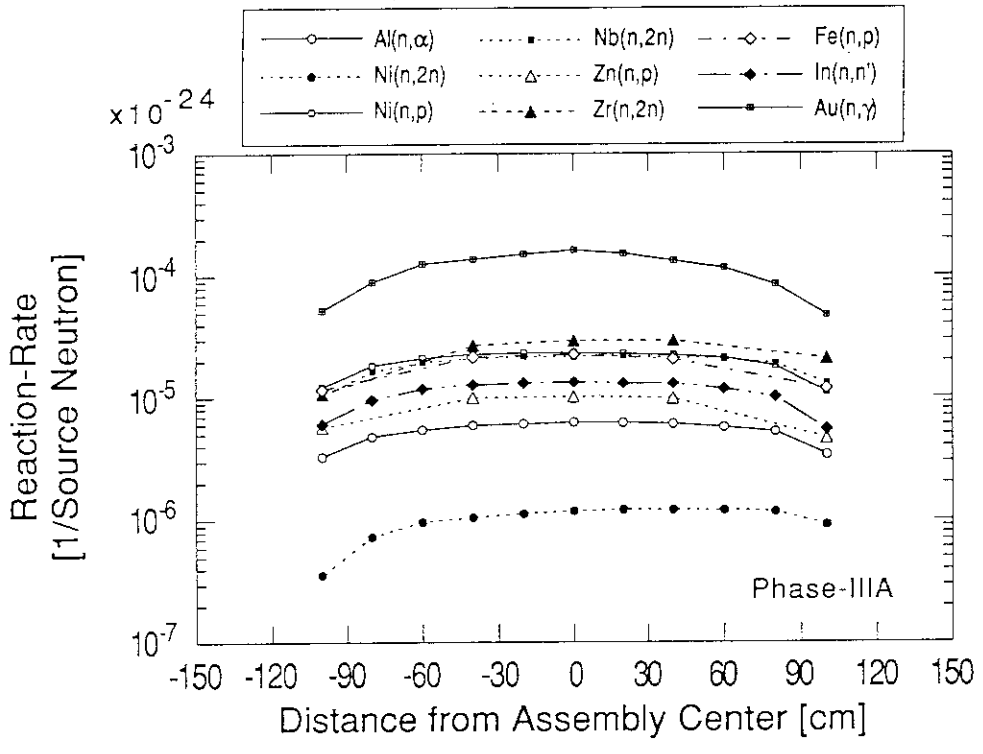

Fig. 3.4.14 Activation reaction rate distribution along the line source at the first wall surface of the reference (IIIA) blanket

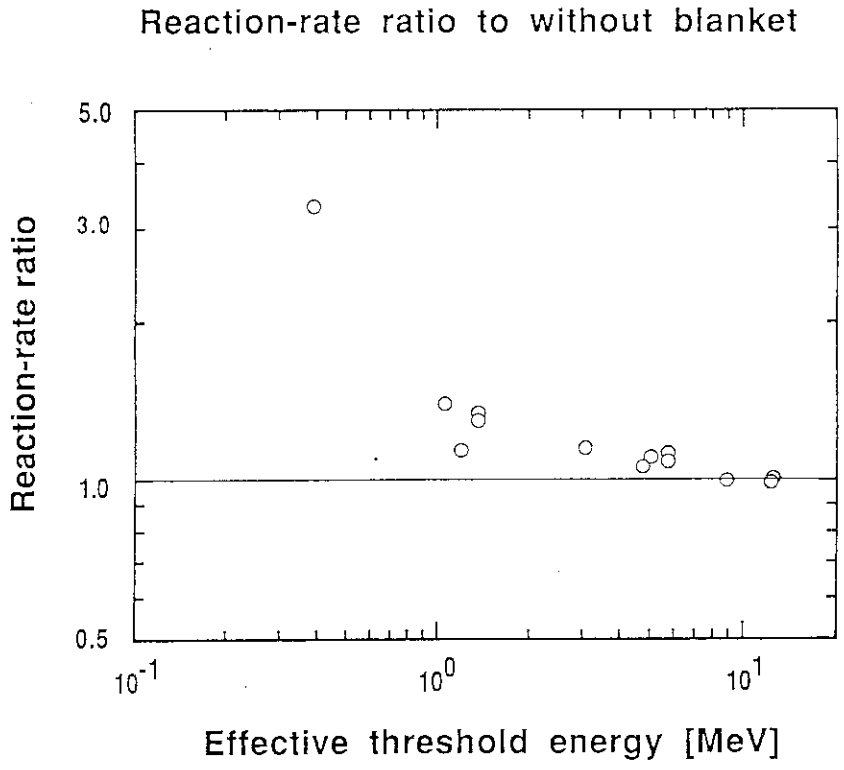

Fig. 3.4.15 Relative ratios of the reaction rates in the reference (IIIA) to in the source itself (source characteristics experiment)

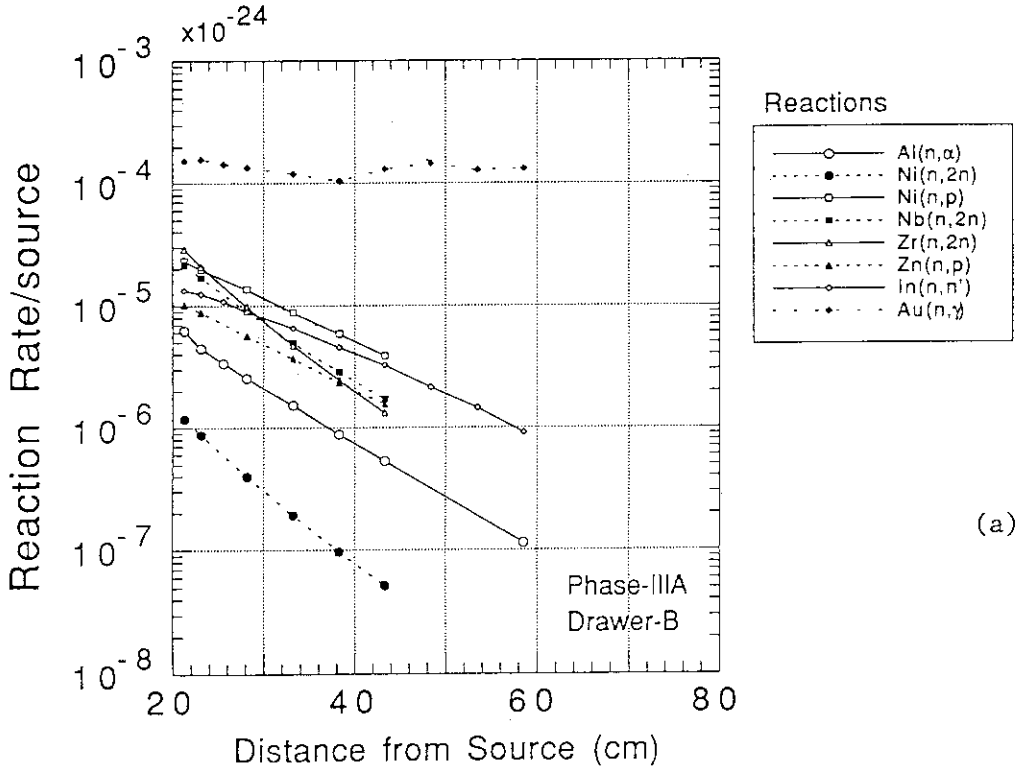

(a)

Fig. 3.4.16 Radial distributions of activation reaction rates in the reference blanket; (a) drawer B at the center and (b) drawer C at the forward

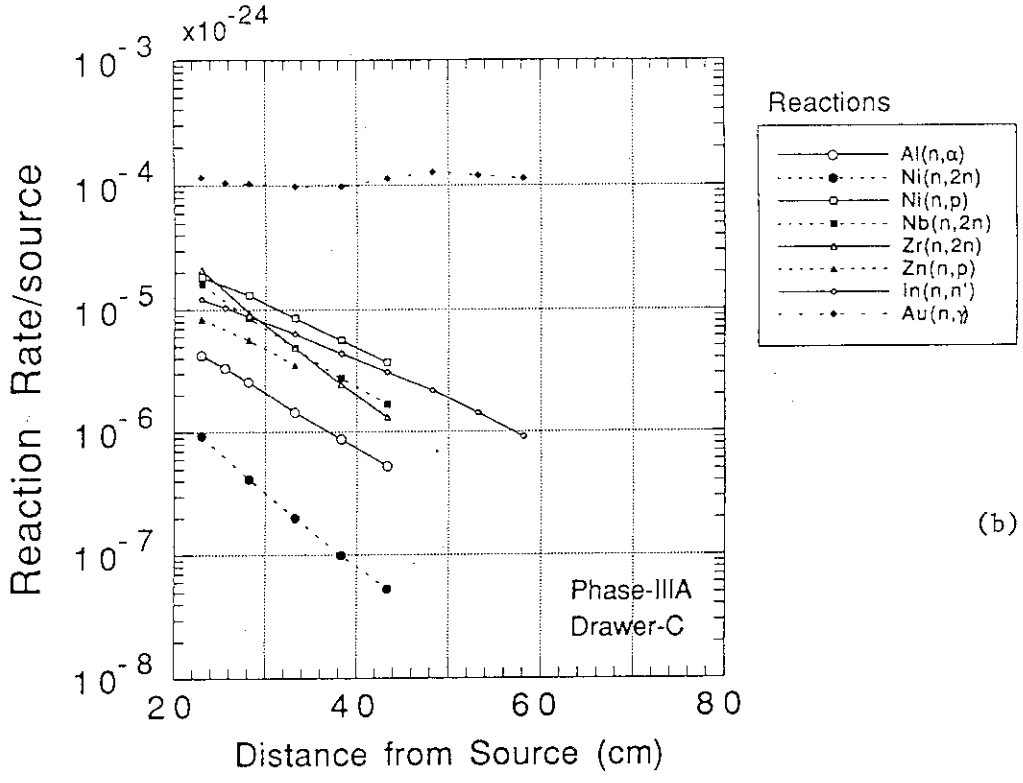

Fig. 3.4.16 (Continued)

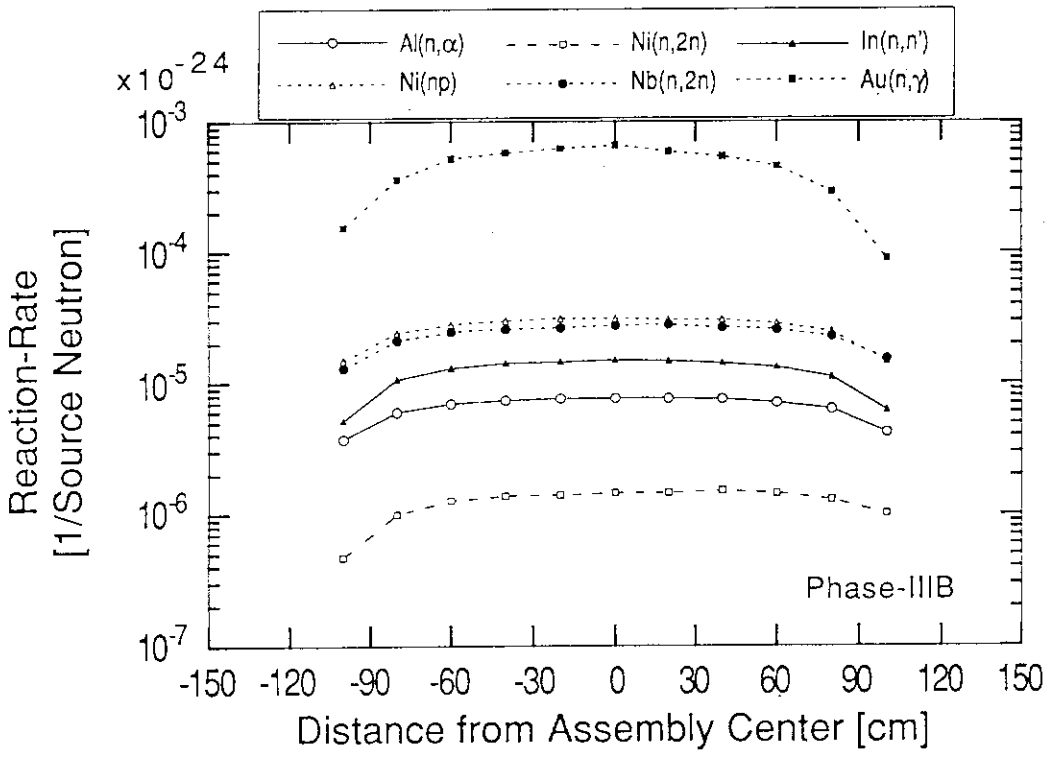

Fig. 3.4.17 Activation reaction rate distribution along the line source at the graphite surface of the armor (IIIB) blanket

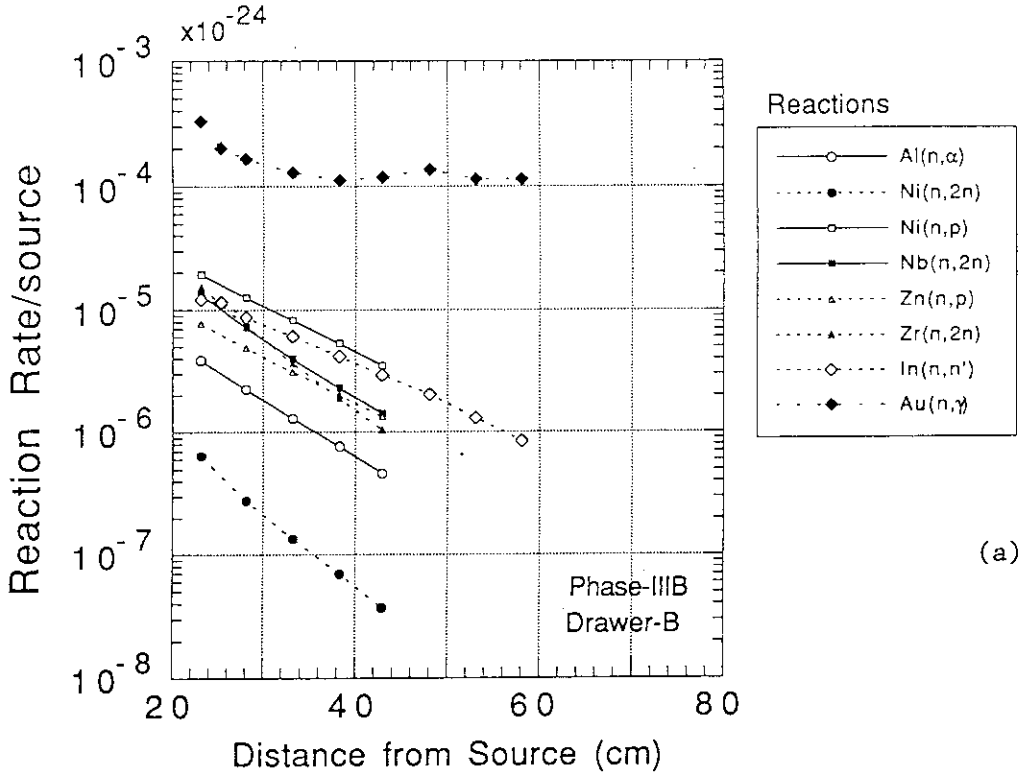

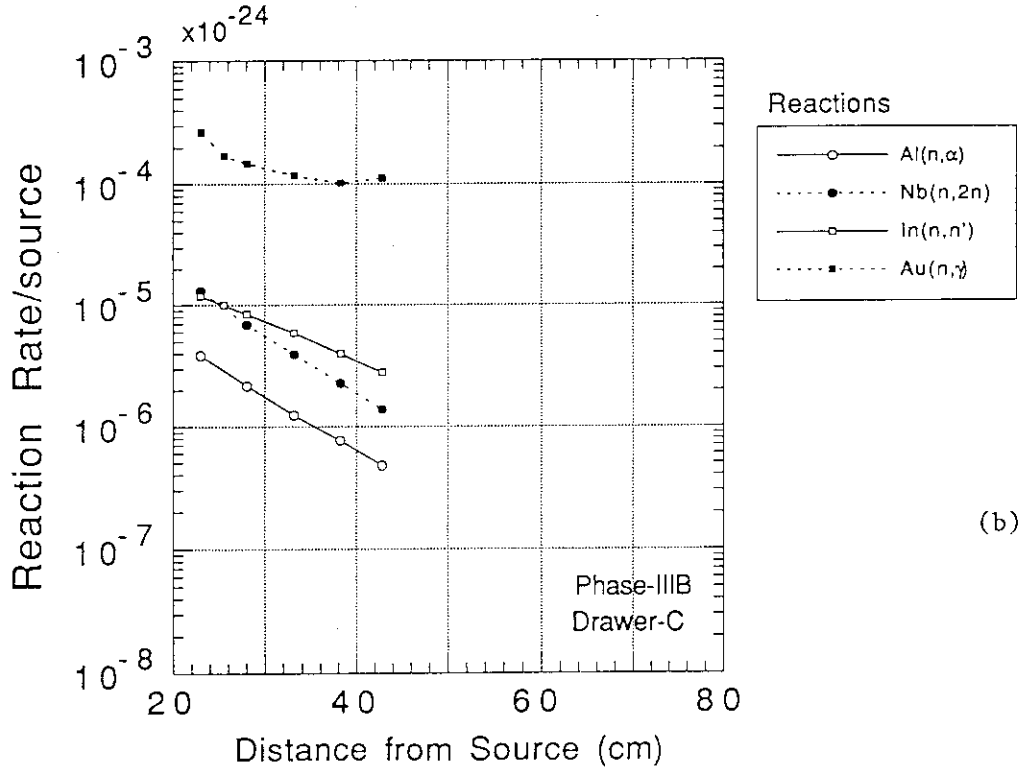

Fig. 3.4.18 Radial distributions of activation reaction rates in the armor blanket; (a) drawer B at the center and (b) drawer C at the forward

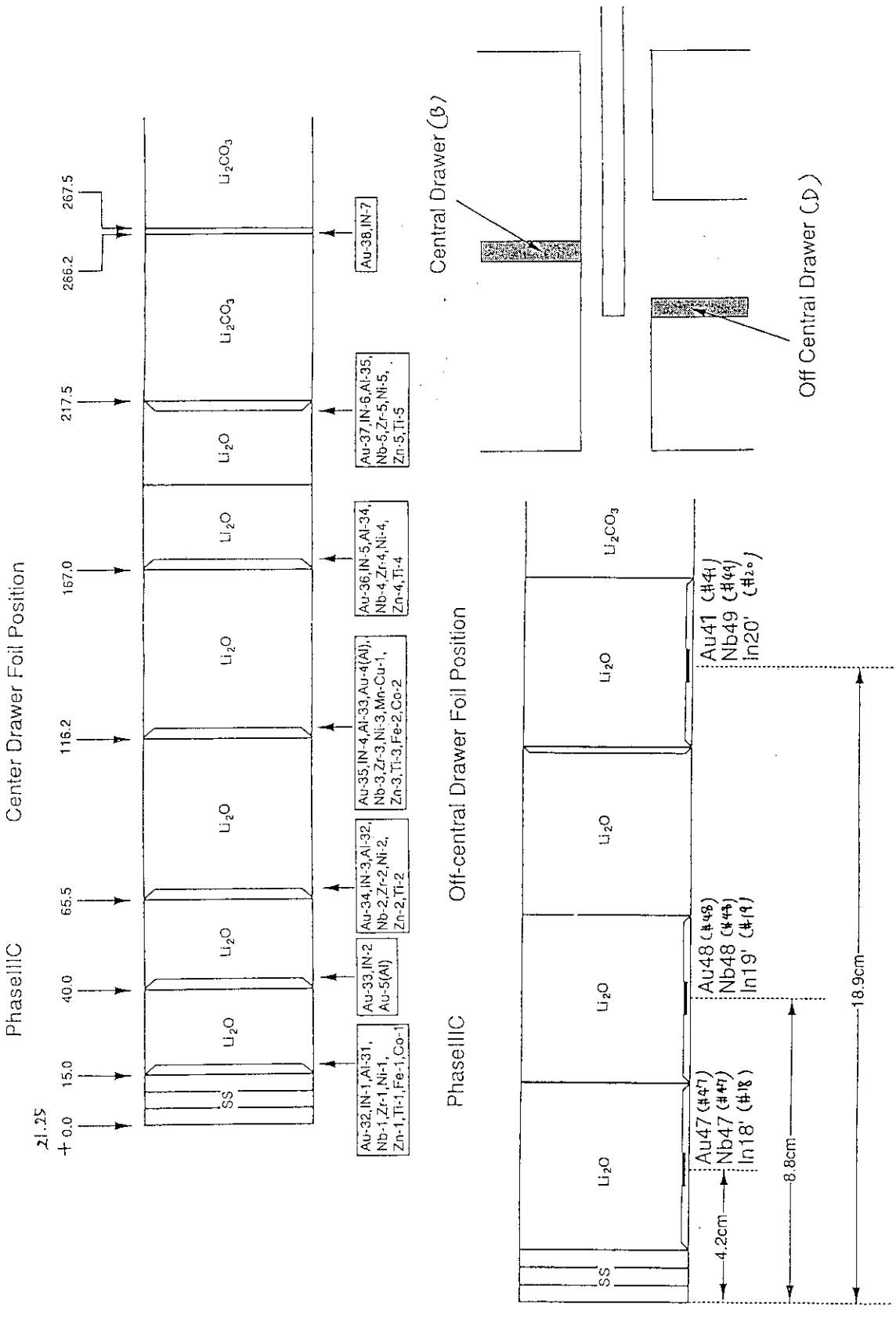

Fig. 3.4.19 Two foil arrangements in the drawer D to measure the distributions near the opening in the test blanket (IIIC)

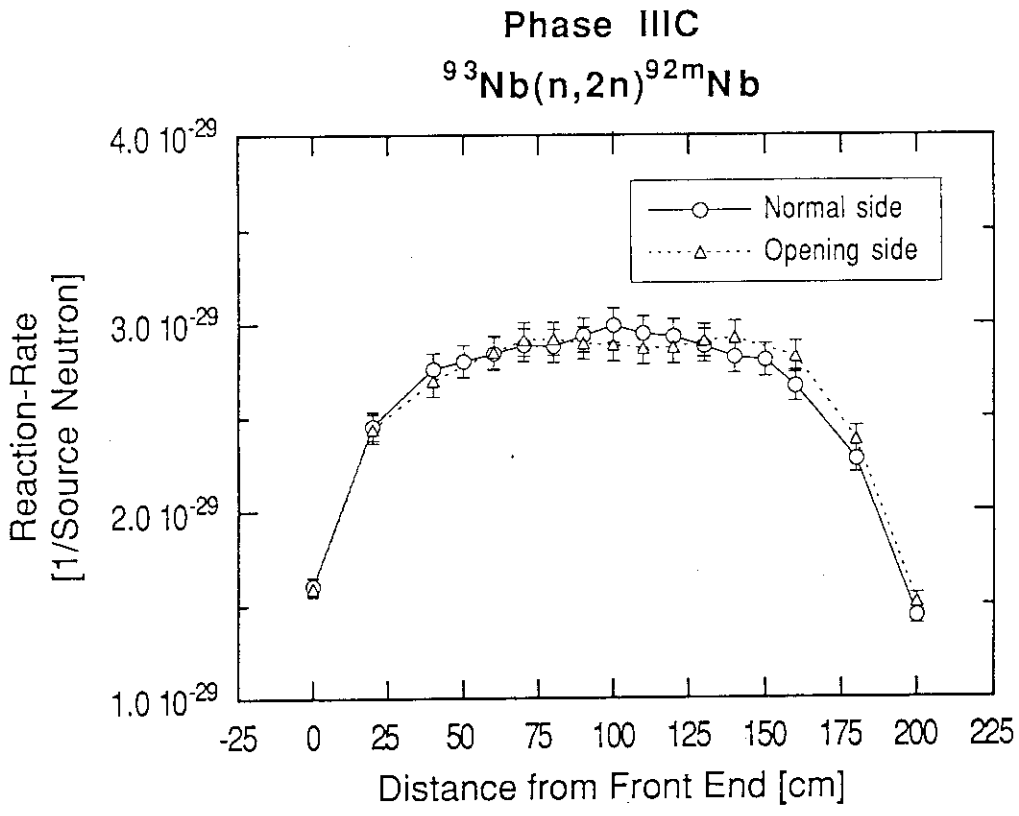

(a)

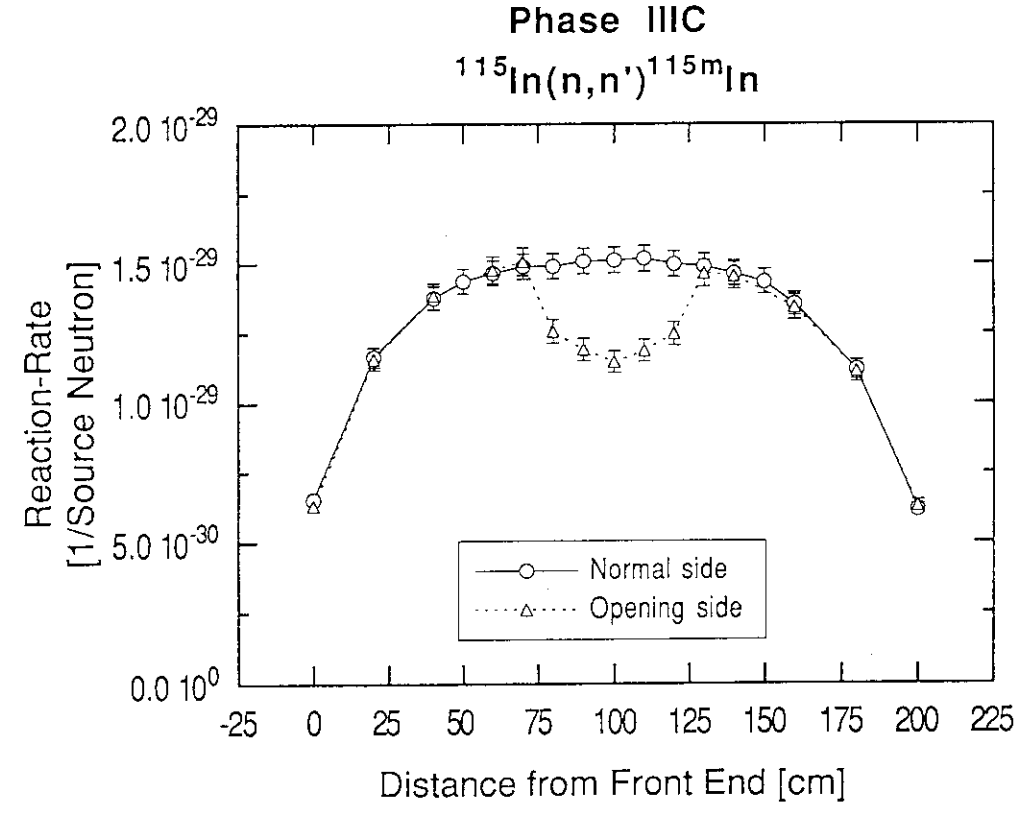

(b)

Fig. 3.4.20 Distributions of reaction rates on the graphite surface of both sides with and without an opening; (a) $^{93}Nb(n,2n)^{92m}Nb$ reaction, (b) $^{115}In(n,n')^{115m}In$ reaction and (c) $^{197}Au(n,\gamma)^{198}Au$ reaction

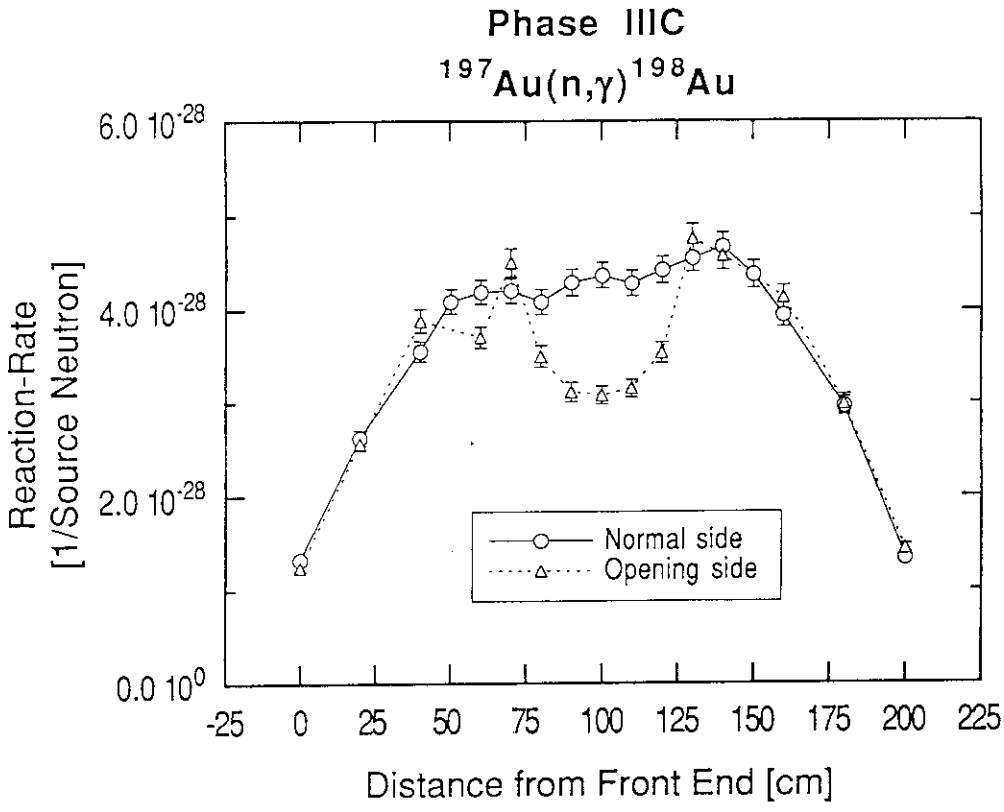

(c)

Fig. 3.4.20 (Continued)

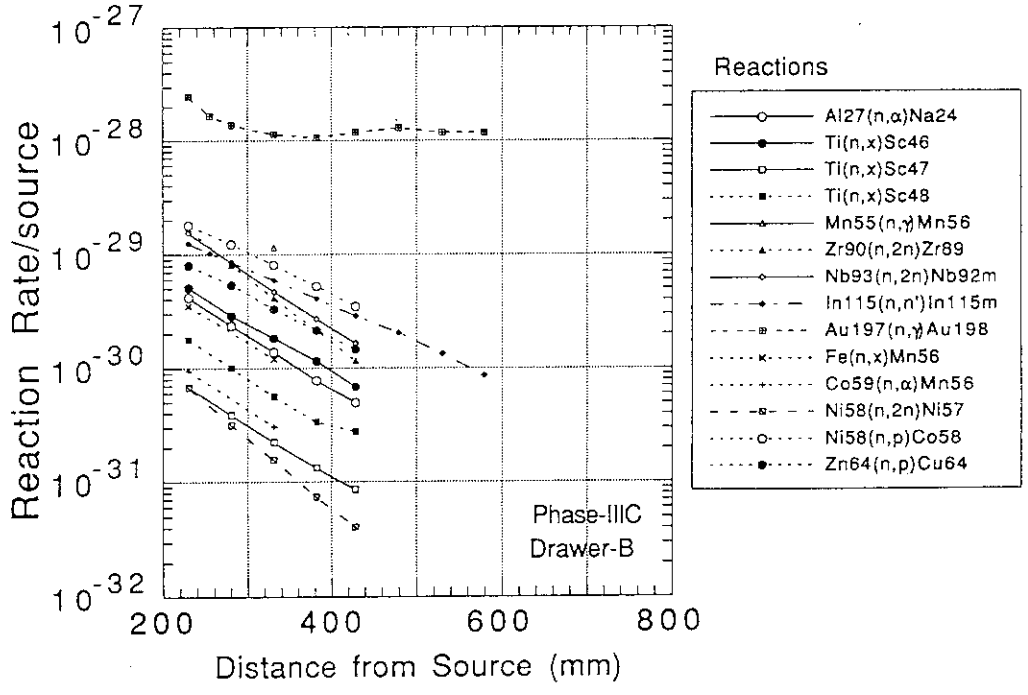

Fig. 3.4.21 Radial distributions of activation reaction rates in the opening test blanket (drawer B at the center)

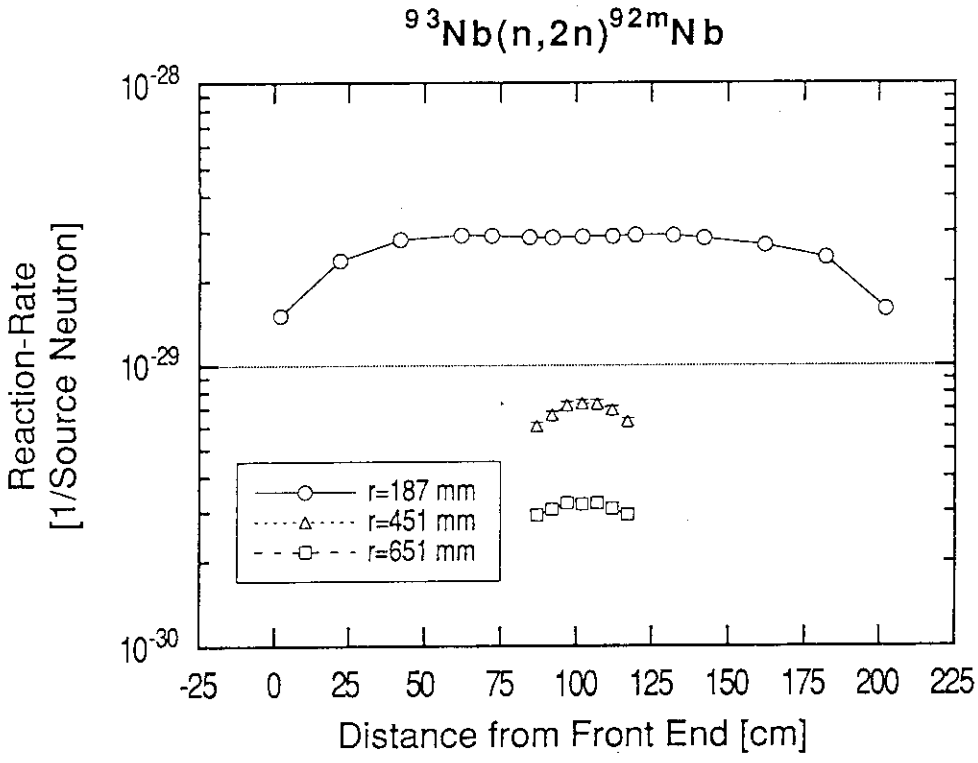

(a)

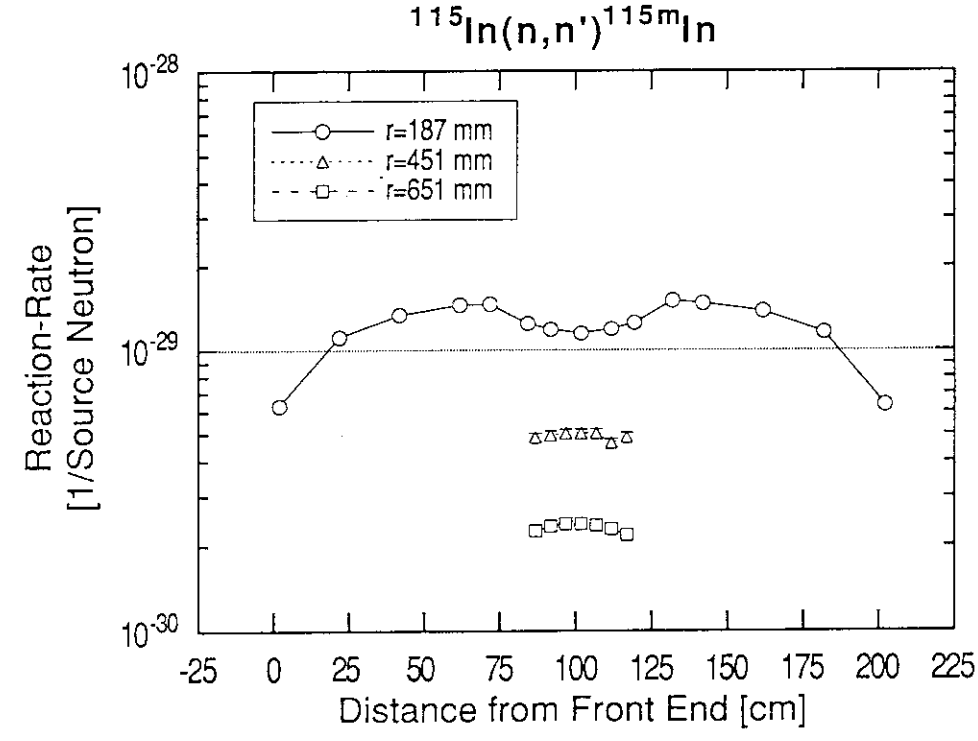

(b)

Fig. 3.4.22 Distributions of reaction rates inside of the opening; (a) ^{93}Nb(n,2n)^{92m}Nb reaction, (b) ^{115}In(n,n')^{115m}In reaction and (c) ^{197}Au(n,γ)^{198}Au reaction

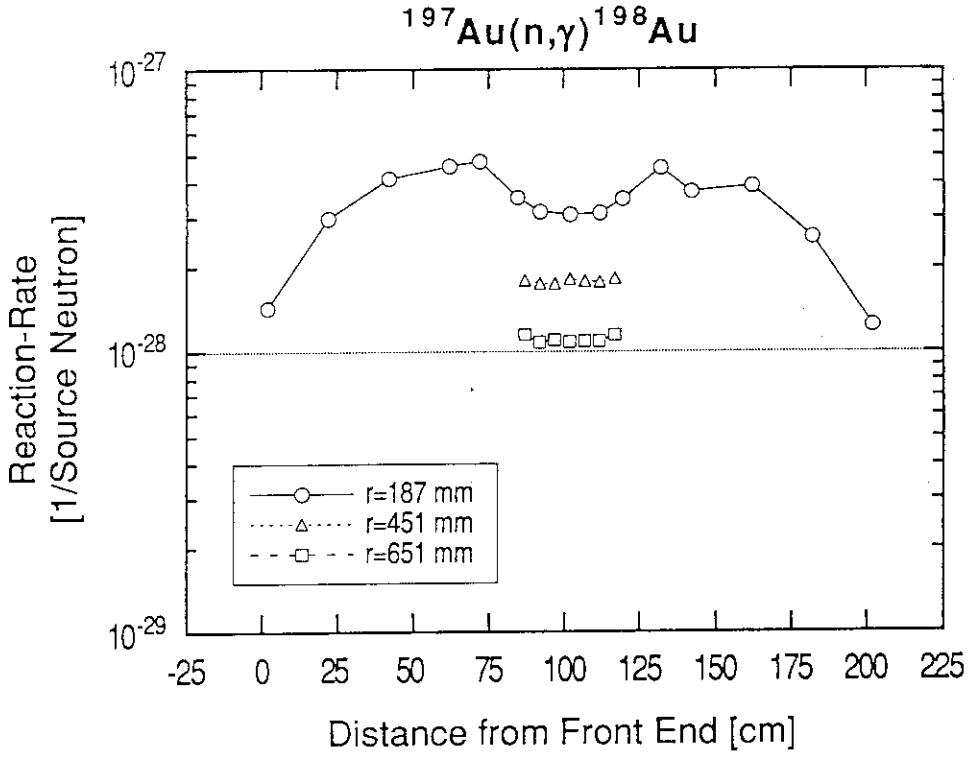

(c)

Fig. 3.4.22 (Continued)

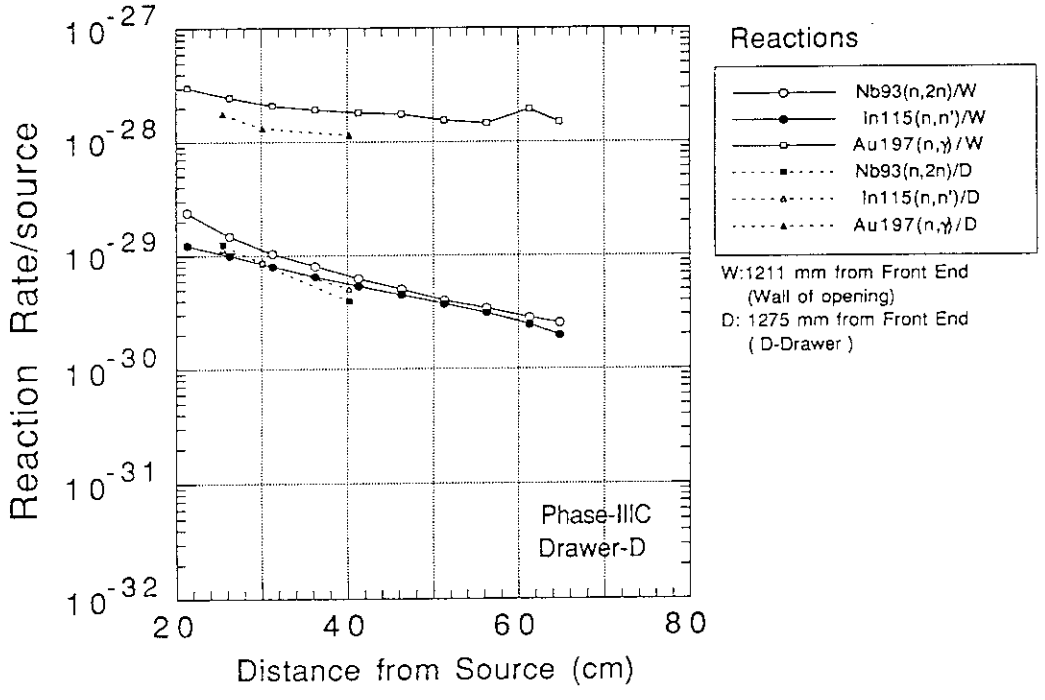

Fig. 3.4.23 Radial distributions of activation reaction rates near the opening in the opening test blanket (drawer D)

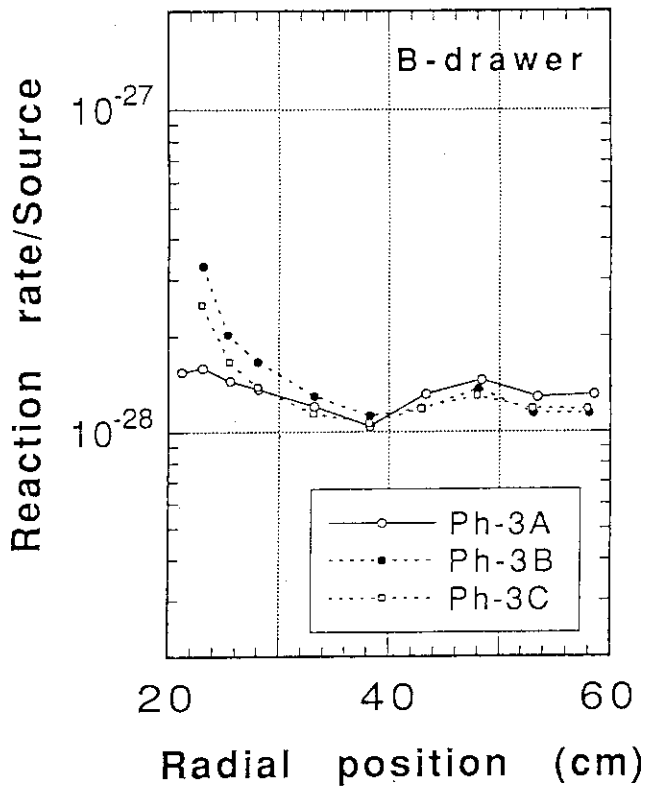

(a)

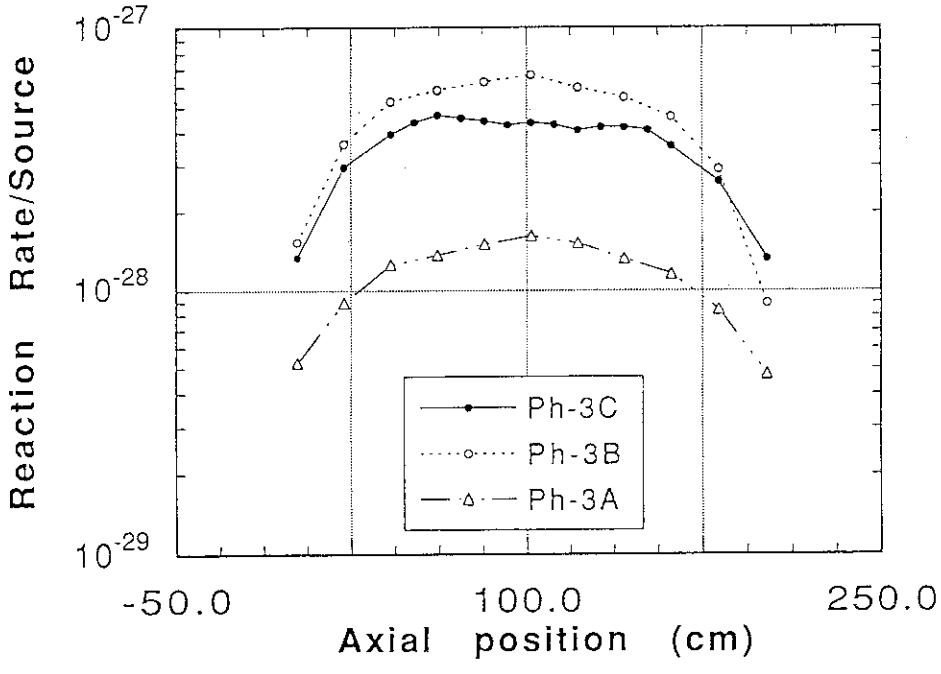

(b)

Fig. 3.4.24 Comparisons of (a) radial distributions and (b) distributions along the line source of $^{197}Au(n,\gamma)^{198}Au$ activation reaction rates among the three test blankets

4. Summary

Neutronics experiments were planned and performed for blankets in an annular geometry with a line distributed source. The annular system simulates the geometry of the blanket to the neutron source. This is very similar to a mirror or a tokamak fusion reactor configuration which has cylindrical or toroidal plasma neutron source surrounded by a blanket. To set up the experimental system for this geometry, firstly the line source system was prepared. The line source was designed and successfully realized by relative motion of the annular blanket to a fixed point neutron source. The FNS deuteron accelerator neutron source was utilized for this purpose.

Three annular blanket configurations were selected for neutronic experiments which focus rather on the effect of components relevant to the fusion reactor core, because it was expected for the geometrical effects to appear in them. One of the test blankets is the reference and the others are selected to examine the configurations of the armor lining on the first wall and of the large opening like a neutral beam injector (NBI) port. The measurements were carried out for tritium production rate, neutron spectrum and activation reaction rate. The applied techniques were modified or developed to be adapted for the present line source system.

The experimental features of the annular and line source, i.e., differences from the point neutron system, were a better simulation of incident neutron spectrum, an increase of the nuclear response at the deep position and additional information of neutron importance at each source position with dependence of blanket configuration. For example, the effects of the armor liner and the opening were directly observed from both results of the source position-wise data and the superposed data. The results of the opening experiment showed that a change of local configuration affected the neutron field in the neighborhood especially for low energy response. This situation impacts on an estimation of a coverage factor for accumulating local breeding rate to obtain an overall tritium breeding ratio from the whole of breeder blanket. Hence the present experimental data could give a good example to check such an estimation.

In conclusions, by this experiment, three series of neutronics integral experiments on simulated fusion blankets have been completed for Phase I to Phase III. Simulations of neutronic environments were stepped up to the systems more complicated but closer to fusion reactors. A plenty of experimental data of nuclear parameters were taken for various geometries and configurations through the series. These results can be a set of benchmark data to test various situations of reactor blanket designs and to grasp the design accuracy. On the other hand, these experimental data are very useful as sample problems to confirm and train the calculation techniques such as input preparation or model selection for application of the calculation codes. Pre-test and skill making for code applications are practically

necessary to make the design calculations reliable, because the calculation will become sophisticated and complicated for a realistic structure of reactors. In this sense, this series of experiments are very unique in an area of fusion integral experiments and has made the experimental basis for the technology test using a next D-T fueled fusion reactor such as ITER.

Acknowledgment

The authors thank the FNS operation group for their excellent operation and assistance through the experiment. The US contributions to the Joint collaborative Program are supported by the United States Department of Energy, Office of Fusion Energy.

necessary to make the design calculations reliable, because the calculation will become sophisticated and complicated for a realistic structure of reactors. In this sense, this series of experiments are very unique in an area of fusion integral experiments and has made the experimental basis for the technology test using a next D-T fueled fusion reactor such as ITER.

Acknowledgment

The authors thank the FNS operation group for their excellent operation and assistance through the experiment. The US contributions to the Joint collaborative Program are supported by the United States Department of Energy, Office of Fusion Energy.

References

1) T. Nakamura, H. Maekawa, Y. Ikeda and Y. Oyama: " A D-T Neutron Source for Fusion Neutronics Experiments at the JAERI," Proc. Int. Ion Engineering Congress-ISIAT '83 & IPAT '83, Kyoto, 567 (1983).

2) K. Sumita, et al.: "Status of OKTAVIAN and Proposal of OKTAVIAN-II," Nucl Sci. Eng., 106, 249 (1990).

3) P.-A. Haldy, et al.:" Experimental Program at the LOTUS Facility," Fusion Technol., 10, 931 (1986).

4) H. Maekawa, et al:" Fusion Blanket Benchmark Experiments on a 60 cm-Thick Lithium Oxide Cylindrical Assembly," JAERI-M 86-182, Japan Atomic Energy Research Institute (1986).

5) Y. Oyama and H. Maekawa:" Measurement and Analysis of an Angualr Neutron Flux Spectra on a Beryllium Slab Irradiated with Deuterium Tritium Neutrons," Nucl. Sci. Eng., 97, 220 (1987).

6) A. Takahashi, M. Kawata and A. Masago:" Tritium Breeding Experiment for a Thermal Blanket Model of Pb-Li-C," Fusion Eng. Des., 9, 333 (1989)

7) Y. Oyama, M.Z. Youssef and M.A. Abdou: " Operating and Geometrical Arrangement Requirements for Fusion Neutronics Testing," Fusion Technol., 8, 1484 (1985).

8) M.A. Abdou, et al.:" A Study of Issues and Experiments for Fusion Nuclear Technology," Fusion Technol., 8, 2595 (1985); FINESSE Interrim Report, UCLA-ENG-84-30, University of California (1984).

9) T. Nakamura, et al.: " A Line D-T Neutron Source Facility for Annular Blanket Experiment: Phase III of the JAERI/USDOE Collaborative Program on Fusion Neutronics," Fusion Technol, 19, 1873 (1973).

10) T. Nakamura and M.A. Abdou: "Summary and Results from the JAERI/U.S. Fusion Neutronics Phase I Experiments," Fusion Technol., 10, 541 (1986).

11) M.Z. Youssef, G. Gung, M. Nakagawa, T. Mori, K. Kosako and T. Nakamura: "Analyses and Intercomparison for Phase I Fusion Integral Experiments at the FNS Facility," Fusion Technol., 10, 549 (1986).

12) Y. Oyama, Y. Ikeda, T. Mori, M. Nakagawa, T. Nakamura and H. Maekawa:" Neutron Field Characteristics in a Concrete Cavity Having a DT Neutron Source," Fusion Technol., 10, 585 (1986).

13) H. Maekawa, T. Nakamura, Y. Oyama, Y. Ikeda, S. Yamaguchi, K. Tsuda, and K. Oishi: " Measured Parameters for Phase I Experiments at the FNS Facility," Fusion Technol., 10, 564 (1986).

14) Y. Oyama, et al.: Fusion Eng. Des., 9, 309 (1989); Fusion Technol., 15, 1293 (1989); see also " Phase IIA and IIB Experiments of JAERI/USDOE Collaborative Program on Fusion Blanket Neutronics - Experimental RTesults- ," JAERI-M 89-215, Japan Atomic Energy Research Institute (1989).

15) M. Nakagawa, T. Mori, K. Kosako, Y. Oyama and T. Nakamura: " JAERI/USDOE Collaborative Program on Fusion Blanket Neutronics - Analysis of Phase IIA and IIB Experiments-," JAERI-M 89-154, Japan Atomic Energy Research Institute (1989).

16) M.Z. Youssef, M.A. Abdou, Y. Watanabe and P.M. Song: " U.S./JAERI Collaborative Program on Fusion Neutronics - Phsae IIA and IIB Fusion Integral Experiments, The U.S. Analysis- ," UCLA-ENG-90-14, FNT-31, University of California(1990).

17) M. Nakagawa, et al.: "Analysis of Neutronics Parameters Measured in Phase II Experiments of the JAERI/US Collaborative Program on Fusion Blanket Neutronics, Part I," Fusion Eng. Des., 9, 315 (1989).

18) M.Z. Youssef, et al.: "Analysis of Neutronics Parameters Measured in Phase II Experiments of the JAERI/US Collaborative Program on Fusion Blanket Neutronics, Part II," Fusion Eng. Des., 9, 323 (1989).

19) Y. Oyama, et al.:" Measured Characteristics of Be Multi-Layered and Coolant Channel Blankets: Phase IIC Experiments of the JAERI/USDOE Collaborative Program on Fusion Neutronics," Fusion Technol. 19, 1955 (1991); see also " Phase IIC Experiments of the JAERI/USDOE Collaborative Program on Fusion Blanket Neutronics, Volume 1: Experimental Results," JAERI-M 92-182, Japan Atomic Energy Research Institute , UCL-ENG-93-18 , University of California (1992).

20) M.Z. Youssef, et al.: " Analysis for Heterogeneous Blankets and Comparison to Measurements: Phase IIC Experiments of the USDOE/JAERI Collaborative Program on Fusion Neutronics," Fusion Technol. 19, 1891 (1991); see also "Phase IIC Experiments of the U.S./JAERI Collaborative Program on Fusion Blanket Neutronics, Volume 2: Analysis," UCLA-ENG-93-19, University of California, JAERI-M 92-183, Japan Atomic Energy Research Institute (1992).

21) S. Sahin and A. Kumar:Neutronics Analysis of Deuterium-Tritium-Driven Experiemntal Hybrid Blankets," Fusion Technol., 6, 97 (1984).

22) S. Sahin and T.A. Al-Kusayer:" Conceptual design Studies of a Cylindrical Experimental ThO_2 Hybrid Blanket with (D,D) Driver," Atomkernenergie, 47, 259 (1985).

23) S. Sahin, T. A. Al-kusayer and M.A. Raoof: " Preliminary Design Studies of a Cylindrical Experimental Hybrid Blanket with Deuterium-Tritium Driver," Fusion Technol., 10, 84 (1986).

24) D.E. Beller, K.O. Ott and W.K. Terry:" Conceptual Design and Neutronics Analyses of a Fusion Reactor Blanket Simulation Facility," Nucl. Sci. Eng., 97, 175 (1987).

25) D.L. Smith, et al. : " Blanket Comparison and Selection Study, Fianl Report" ANL/FPP-84-1, Argonne National Laboratory (1984).

26) M.Z. Youssef, et al. :" Analysis for the Simulation of a Line Source by a 14 MeV Moving Point Source and Impact on Blanket Characteristics: The USDOE/JAERI Collaborative Program on Fusion Neutronics," Fusion Technol., 19, 1843 (1991).

27) H. Maekawa, et al.: " Neutron Yield Monitors forthe Fusion Nutronics Source (FNS)," JAERI-M 84-193, Japan Atomic Energy Research Institute (1984).

28) C. Konno, et al.: " Measurements of the Source Term for Annular Blanket Experiment with a Line Source: Phase IIIA of the JAERI/USDOE Collaborative Program on Fusion Neutronics," Fusion Technol., 19, 1885 (1991).

29) M. Nakagawa and T. Mori: " MORSE-DD, A Monte Carlo Code Using Multigroup Double Differential Form Cross Sections," JAERI-M 84-126, Japan Atomic Energy Research Institute (1984).

30) K. Shibata, et al.:" Japanese Evaluated Nuclear Data Library, Version-3 -JENDL-3-," JAERI 1319, Japan Atomic Energy Research Institute (1990).

31) E. F. Bennett:" A Continuous Mode Data Acquisition Technique for Proton Recoil Proportional Counter Neutron Spectrometers," ANL/FPP/TM-239, Argonne National Laboratory (1989).

32) K. Kosako:"FNSUNCL," private communcation (1990).

33) W.A. Rhoades and F.R. Mynett, " The DOT-III Two-Dimensional Discrete Ordinate Transport Code," ORNL-TM-4280, Oak Ridge National Laboratory (1973).

34) Y. Ikeda, et al.:" Activation Cross Section Measurements for Fusion Reactor Structural Materials at Neutron Energy from 13.3 to 15.0 MeV Using FNS Facility," JAERI 1312, Japan Atomic Energy Research Institute (1987).

35) Y. Oyama and K. Kosako: " Survey Calculation for Phase III," private communication (1989).

36) Y. Oyama, et al.: "Annular Blanket Experiment using a Line D-T Neutron Source: Phase IIIA of the JAERI/USDOE Collaborative Program on Fusion Neutronics," Fusion Technol., 19, 1879 (1991).

37) Y. Oyama, et al.: "Phase III Experimental Results of JAERI/USDOE Collaborative Program on Fusion Neutronics," Fusion Eng. Des., 18, 203 (1991).

38) M.Z. Youssef, et al.: " Post Analysis for the Line Source Phase IIIA Experiments of the USDOE/JAERI Collaborative Program on Fusion Neutronics," Fusion Eng. Des., 18, 265 (1991).

39) T. Kuroda, et al.: " ITER Plasma Facing Componenets," ITER Documentation Series, No. 30 (1991).

40) S. Yamaguchi, et al.: Nucl. Instrum. Meth., A254, 413 (1987).

41) Y. Oyama, et al.: Nucl. Instrum. Meth., A256, 333 (1987).

42) E.F. Bennett and T.J. Yule:" Techniques and Analyses of Fast Reactor Neutron Spectroscopy with Proton-Recoil Proportional Counters," ANL-7763, Argonne National Laboratory (1971).

43) Y. Oyama and K. Sekiyama: " Application of Spectrum Weighting Function Method using a Miniture NE213 Detector for Nuclear Parameter Measurements," private communication (1989).

44) R.H. Johnson: "A User's Manual of COOLC and FORIST," PSR-92, Radiation Shielding Infomation Center, Oak Ridge National Laboratory (1975).

Appendix 1 Calculated Angle Dependent Neutron Spectra emitted from Long Tube Water Cooled Target Assembly (neutrons/group/total emission)

Energy boundary for 125 group structure (eV)

1.64870E+07	1.62310E+07	1.59800E+07	1.57320E+07	1.54880E+07	1.52480E+07
1.50120E+07	1.47790E+07	1.45500E+07	1.43240E+07	1.41020E+07	1.38830E+07
1.36680E+07	1.34560E+07	1.32480E+07	1.30420E+07	1.28400E+07	1.26410E+07
1.24450E+07	1.22520E+07	1.20620E+07	1.18750E+07	1.16910E+07	1.15100E+07
1.13310E+07	1.11560E+07	1.09830E+07	1.08120E+07	1.06450E+07	1.04800E+07
1.03170E+07	1.01570E+07	9.99990E+06	9.39400E+06	8.82490E+06	8.29020E+06
7.78790E+06	7.31610E+06	6.87280E+06	6.45640E+06	6.06520E+06	5.69780E+06
5.35250E+06	5.02820E+06	4.72360E+06	4.43740E+06	4.16860E+06	3.91600E+06
3.67870E+06	3.45590E+06	3.24650E+06	3.04980E+06	2.86500E+06	2.69140E+06
2.52840E+06	2.37520E+06	2.23130E+06	2.09610E+06	1.96910E+06	1.84980E+06
1.73770E+06	1.53350E+06	1.35330E+06	1.19430E+06	1.05400E+06	9.30130E+05
8.20840E+05	7.24380E+05	6.39270E+05	5.64150E+05	4.97860E+05	4.39360E+05
3.87740E+05	3.42170E+05	3.01970E+05	2.66490E+05	2.35170E+05	2.07540E+05
1.83150E+05	1.61630E+05	1.42640E+05	1.25880E+05	1.11090E+05	9.80350E+04
8.65150E+04	7.63490E+04	6.73780E+04	5.94610E+04	5.24740E+04	4.63080E+04
4.08670E+04	3.60650E+04	3.18270E+04	2.80870E+04	2.47870E+04	2.18740E+04
1.93040E+04	1.50340E+04	1.17090E+04	9.11860E+03	7.10160E+03	5.53070E+03
4.30730E+03	3.35460E+03	2.61250E+03	2.03460E+03	1.58460E+03	1.23410E+03
9.61100E+02	5.82930E+02	3.53570E+02	2.14450E+02	1.30070E+02	7.88910E+01
4.78500E+01	2.90230E+01	1.76030E+01	1.06770E+01	6.47580E+00	3.92780E+00
2.38230E+00	1.44490E+00	8.76400E-01	5.31560E-01	3.22410E-01	1.00100E-05

No.1 Angle=180 degree Flux/Group

0.0	0.0	0.0	0.0	0.0	0.0
0.0	2.8133E-07	1.1132E-05	7.0699E-05	2.9725E-04	5.8035E-03
1.1174E-01	5.0083E-01	2.9325E-01	3.5848E-02	1.9167E-03	2.2345E-03
2.1223E-03	1.5259E-03	9.3736E-04	7.3617E-04	5.2773E-04	2.7017E-04
1.7811E-04	1.8328E-04	2.3002E-04	2.9362E-04	4.2296E-04	2.8769E-04
2.2497E-04	2.1734E-04	8.6941E-04	1.1876E-03	1.5784E-03	1.3262E-03
1.4116E-03	1.4346E-03	2.1877E-03	2.2324E-03	2.4385E-03	2.5503E-03
2.5201E-03	2.8233E-03	2.9695E-03	3.1546E-03	3.6912E-03	3.6241E-03
3.5154E-03	4.0251E-03	4.0676E-03	4.2225E-03	4.3285E-03	4.1782E-03
4.0598E-03	3.8551E-03	3.7352E-03	3.8356E-03	4.0109E-03	4.0103E-03
7.3721E-03	7.7382E-03	7.6206E-03	7.2109E-03	6.8743E-03	6.8912E-03
6.9001E-03	6.5590E-03	5.9411E-03	5.7141E-03	5.3731E-03	4.8503E-03
4.5656E-03	3.9063E-03	3.5676E-03	3.1742E-03	2.8645E-03	2.5666E-03
2.1491E-03	1.6690E-03	1.5367E-03	1.4715E-03	1.1850E-03	7.2317E-04
6.0680E-04	4.8332E-04	4.6588E-04	4.9846E-04	3.4556E-04	2.2581E-04
1.7049E-04	1.9573E-04	1.3066E-04	1.1007E-04	1.4885E-04	9.4420E-05
1.7731E-04	9.3409E-05	7.5281E-05	4.8565E-05	1.4022E-04	5.9894E-05
3.6855E-05	4.8798E-05	1.7405E-05	2.5103E-05	2.5085E-05	2.4342E-05
3.7830E-05	1.1205E-05	4.9533E-06	2.2206E-05	5.0575E-06	1.4315E-06
4.4221E-07	2.1665E-07	1.2984E-07	1.1197E-07	1.2533E-07	7.9222E-08
4.8207E-08	2.9786E-08	1.7825E-08	1.0563E-08	1.7191E-08	

No.2 Angle=175 degree Flux/Group

0.0	0.0	0.0	0.0	0.0	0.0
0.0	3.7835E-07	1.1441E-05	7.1589E-05	3.2069E-04	5.9072E-03
1.1362E-01	5.0424E-01	2.9650E-01	3.6687E-02	2.1034E-03	2.3824E-03
2.3643E-03	1.5373E-03	1.0950E-03	9.0216E-04	5.8232E-04	3.0937E-04
1.9418E-04	2.2513E-04	2.5174E-04	3.7938E-04	3.7668E-04	3.6816E-04
2.6841E-04	2.4088E-04	9.4038E-04	1.2670E-03	2.5181E-03	1.6416E-03
1.5187E-03	1.5842E-03	2.2275E-03	2.2738E-03	2.5485E-03	2.6521E-03
2.7587E-03	2.9765E-03	3.1518E-03	3.3321E-03	3.8155E-03	3.8634E-03
3.8329E-03	4.2131E-03	4.2484E-03	4.3953E-03	4.5454E-03	4.4384E-03
4.3055E-03	4.0501E-03	3.9252E-03	3.9979E-03	4.2933E-03	4.2104E-03
7.8070E-03	8.1364E-03	8.0414E-03	7.6252E-03	7.1929E-03	7.2062E-03
7.1945E-03	6.8679E-03	6.1286E-03	5.7872E-03	5.8984E-03	5.1840E-03
4.6260E-03	4.0971E-03	3.6996E-03	3.2870E-03	3.2319E-03	2.6774E-03
2.2376E-03	1.7009E-03	1.5526E-03	1.6186E-03	1.2897E-03	7.4667E-04
5.9701E-04	4.7018E-04	4.7219E-04	4.6062E-04	3.4094E-04	2.4816E-04
1.6731E-04	1.9320E-04	1.3040E-04	1.0584E-04	1.4500E-04	9.1075E-05
1.5279E-04	9.8490E-05	7.8313E-05	5.6966E-05	1.2022E-04	5.5179E-05
3.4974E-05	4.1840E-05	1.7134E-05	2.4323E-05	2.4930E-05	1.8584E-05
4.2462E-05	1.3667E-05	4.8839E-06	1.7358E-05	4.4998E-06	5.5091E-07
3.9295E-07	2.9448E-07	2.7264E-07	2.3974E-07	2.0566E-07	1.2782E-07
7.7551E-08	4.7355E-08	2.8479E-08	1.6972E-08	2.6943E-08	

No.3 Angle=170 degree Flux/Group

0.0	0.0	0.0	0.0	0.0	0.0
0.0	3.6185E-07	9.5040E-06	5.8872E-05	2.8999E-04	4.7439E-03
1.5019E-01	3.5413E-01	2.5513E-01	2.4816E-02	1.7208E-03	1.9255E-03
1.9925E-03	1.2381E-03	1.2442E-03	8.6672E-04	5.0687E-04	2.7164E-04
2.0134E-04	1.9040E-04	1.9574E-04	2.9987E-04	2.9225E-04	3.6524E-04
2.8297E-04	2.3123E-04	7.8890E-04	1.0449E-03	1.3277E-03	1.1490E-03
1.1557E-03	1.2977E-03	1.6929E-03	1.7493E-03	2.0090E-03	2.0004E-03
2.1562E-03	2.3733E-03	2.7334E-03	2.7047E-03	2.9446E-03	3.2352E-03
4.5391E-03	3.3228E-03	3.3184E-03	3.7626E-03	3.6943E-03	3.5435E-03
4.8576E-03	3.3648E-03	3.3153E-03	3.2196E-03	3.5733E-03	3.3254E-03
6.7419E-03	6.7177E-03	7.3722E-03	6.3825E-03	6.0115E-03	5.9379E-03
5.6789E-03	5.7026E-03	5.1413E-03	4.6794E-03	5.7318E-03	3.8717E-03
3.7424E-03	3.3807E-03	3.0274E-03	2.6121E-03	2.6261E-03	1.8869E-03
1.7138E-03	1.1776E-03	1.1197E-03	1.7472E-03	1.2439E-03	5.9356E-04
4.4854E-04	3.3661E-04	3.3863E-04	3.3456E-04	2.4365E-04	1.8998E-04
1.1907E-04	1.1157E-04	4.0102E-05	3.6947E-05	1.1068E-04	6.7082E-05
8.6911E-05	4.8253E-05	4.7431E-05	6.2276E-05	7.4372E-05	3.5246E-05
1.7196E-05	2.2051E-05	9.4176E-06	1.8920E-05	1.7962E-05	9.0355E-06
3.3089E-05	8.9171E-06	1.6759E-06	7.9120E-06	1.8300E-06	6.4386E-07
2.3745E-07	1.2144E-07	1.1283E-07	7.6016E-08	4.5987E-08	2.7550E-08
1.6531E-08	9.9574E-09	5.8651E-09	3.3952E-09	4.5389E-09	

No.4 Angle=165 degree Flux/Group

0.0	0.0	0.0	0.0	0.0	0.0
0.0	5.1082E-07	1.1670E-05	7.0606E-05	4.2223E-04	6.0348E-03
2.1281E-01	3.4467E-01	2.7046E-01	1.5885E-02	1.7828E-03	1.8549E-03
1.7356E-03	1.1338E-03	7.8382E-04	6.0876E-04	4.0911E-04	2.3795E-04
1.9771E-04	1.5310E-04	1.7963E-04	2.1663E-04	2.7483E-04	3.0444E-04
2.4874E-04	2.1519E-04	7.7115E-04	1.0766E-03	1.3226E-03	1.0973E-03
1.0457E-03	1.2748E-03	1.7166E-03	1.7760E-03	1.8308E-03	1.9160E-03
2.1251E-03	2.2543E-03	2.5858E-03	2.5611E-03	2.8428E-03	2.9902E-03
2.9110E-03	3.1924E-03	3.2355E-03	3.7441E-03	3.6503E-03	3.3356E-03
3.3900E-03	3.1860E-03	3.0971E-03	3.1019E-03	3.3434E-03	3.1527E-03
6.2305E-03	6.4802E-03	6.4301E-03	6.0320E-03	5.7398E-03	5.7555E-03
5.6117E-03	5.5303E-03	4.9000E-03	4.6177E-03	4.9295E-03	4.0625E-03
3.6606E-03	3.2393E-03	2.9173E-03	2.5212E-03	2.3047E-03	1.9101E-03
1.6915E-03	1.2459E-03	1.1716E-03	1.3675E-03	9.7259E-04	5.6789E-04
4.6392E-04	3.5134E-04	3.2277E-04	2.9870E-04	2.1404E-04	1.7976E-04
1.1890E-04	1.1646E-04	5.0052E-05	5.5373E-05	1.1692E-04	6.9411E-05
1.0414E-04	6.2000E-05	5.1281E-05	8.9099E-05	9.3171E-05	4.3286E-05
2.3677E-05	3.2742E-05	1.0195E-05	2.2316E-05	2.0126E-05	1.3144E-05
3.2913E-05	9.9547E-06	2.7943E-06	7.1506E-06	1.9256E-06	7.2235E-07
6.9051E-07	4.3253E-07	1.8998E-07	5.8739E-08	3.5327E-08	2.1339E-08
1.2501E-08	7.0390E-09	4.0867E-09	2.3189E-09	3.6063E-09	

No.5 Angle=160 degree Flux/Group

0.0	0.0	0.0	0.0	0.0	0.0
0.0	6.7487E-07	1.3181E-05	8.1451E-05	5.1859E-04	9.0841E-03
2.1863E-01	3.9434E-01	2.1507E-01	4.7857E-03	1.3917E-03	1.5682E-03
1.4746E-03	9.7756E-04	7.3315E-04	5.3407E-04	3.6160E-04	1.9848E-04
1.8629E-04	1.4586E-04	1.6584E-04	2.0129E-04	2.0772E-04	2.3660E-04
1.8806E-04	1.9433E-04	6.8231E-04	1.0178E-03	1.2018E-03	9.7392E-04
9.2581E-04	1.1802E-03	1.5383E-03	1.6285E-03	1.5696E-03	1.7448E-03
1.7410E-03	2.0592E-03	2.1806E-03	2.2943E-03	2.4707E-03	2.6902E-03
2.5402E-03	2.8614E-03	2.9290E-03	3.4241E-03	3.2323E-03	2.8926E-03
2.9612E-03	2.8695E-03	2.7537E-03	2.7800E-03	2.9559E-03	2.8356E-03
5.4665E-03	5.8099E-03	5.7228E-03	5.4298E-03	5.2356E-03	5.1995E-03
5.1038E-03	4.9578E-03	4.4405E-03	4.2069E-03	3.8507E-03	3.5177E-03
3.3137E-03	2.8949E-03	2.6330E-03	2.2811E-03	2.0353E-03	1.7130E-03
1.5128E-03	1.1546E-03	1.0909E-03	1.1571E-03	8.3544E-04	5.1003E-04
4.1292E-04	3.1477E-04	2.7525E-04	2.5511E-04	1.8714E-04	1.6139E-04
1.1163E-04	1.1493E-04	4.8959E-05	5.5486E-05	1.1391E-04	6.5659E-05
1.0277E-04	6.4725E-05	5.0868E-05	7.0970E-05	8.3075E-05	4.1826E-05
2.1846E-05	2.7435E-05	8.8435E-06	2.4692E-05	1.9525E-05	1.3839E-05
2.6915E-05	1.1308E-05	3.5200E-06	6.7376E-06	2.1735E-06	3.9223E-07
2.3959E-07	1.4161E-07	7.7039E-08	7.7988E-08	5.0946E-08	3.0675E-08
1.8100E-08	1.0424E-08	6.0555E-09	3.4685E-09	5.3803E-09	

No.6 Angle=155 degree Flux/Group

0.0	0.0	0.0	0.0	0.0	0.0
0.0	8.9791E-07	1.4586E-05	9.5698E-05	5.6608E-04	2.6967E-02
1.9132E-01	3.9240E-01	1.6671E-01	3.8048E-03	1.3617E-03	1.3263E-03
1.2102E-03	8.8958E-04	7.5102E-04	4.8041E-04	3.2739E-04	1.8630E-04
1.9849E-04	1.3412E-04	1.5276E-04	1.7149E-04	1.6488E-04	1.8827E-04
1.4737E-04	1.4125E-04	5.8666E-04	9.2285E-04	1.1113E-03	8.3773E-04
8.4104E-04	1.0331E-03	1.3060E-03	1.4303E-03	1.3361E-03	1.5202E-03
1.5421E-03	1.8882E-03	1.9012E-03	2.0756E-03	2.1427E-03	2.3393E-03
2.3223E-03	2.5239E-03	2.6140E-03	2.9561E-03	2.8357E-03	2.5353E-03
2.6349E-03	2.5420E-03	2.4548E-03	2.4387E-03	2.6031E-03	2.5276E-03
4.8102E-03	5.1441E-03	5.0666E-03	4.8717E-03	4.7288E-03	4.6509E-03
4.5458E-03	4.4021E-03	3.9861E-03	3.7728E-03	3.3999E-03	3.0991E-03
2.9660E-03	2.5794E-03	2.3559E-03	2.0478E-03	1.7990E-03	1.5004E-03
1.3428E-03	1.0309E-03	9.7457E-04	1.0035E-03	7.1358E-04	4.4090E-04
3.6019E-04	2.8148E-04	2.3747E-04	2.1923E-04	1.6562E-04	1.3953E-04
9.6636E-05	1.0480E-04	4.7050E-05	4.9619E-05	1.0190E-04	6.0504E-05
9.2283E-05	5.7845E-05	4.5599E-05	4.8541E-05	6.9290E-05	3.9698E-05
2.0074E-05	2.2337E-05	7.0312E-06	2.2823E-05	1.6930E-05	1.4584E-05
2.2601E-05	8.4404E-06	3.3708E-06	5.5248E-06	1.9803E-06	3.1467E-07
1.1544E-07	1.1136E-07	6.8319E-08	4.0515E-08	3.0920E-08	2.0354E-08
1.3326E-08	6.5807E-09	3.7466E-09	2.0959E-09	2.9469E-09	

No.7 Angle=150 degree Flux/Group

0.0	0.0	0.0	0.0	0.0	0.0
0.0	1.1210E-06	1.5006E-05	1.0060E-04	5.2316E-04	2.2578E-02
2.2494E-01	2.7657E-01	9.8913E-02	3.5616E-03	1.3244E-03	1.1043E-03
9.6955E-04	7.9390E-04	6.9932E-04	4.4349E-04	3.4276E-04	1.8292E-04
2.4814E-04	1.3386E-04	1.4963E-04	1.8128E-04	1.3764E-04	1.6132E-04
1.2904E-04	1.1531E-04	4.8660E-04	8.5456E-04	1.0188E-03	6.9732E-04
7.4484E-04	9.3855E-04	1.1452E-03	1.2785E-03	1.1886E-03	1.3201E-03
1.3301E-03	1.6687E-03	1.6385E-03	1.8017E-03	1.8697E-03	2.0389E-03
2.0579E-03	2.2140E-03	2.3498E-03	2.6237E-03	2.4751E-03	2.2369E-03
2.3388E-03	2.2566E-03	2.1950E-03	2.1379E-03	2.2828E-03	2.2342E-03
4.2100E-03	4.5225E-03	4.4508E-03	4.3349E-03	4.2050E-03	4.1278E-03
3.9950E-03	3.8727E-03	3.5175E-03	3.3076E-03	2.9602E-03	2.6811E-03
2.6115E-03	2.2597E-03	2.0636E-03	1.8064E-03	1.5735E-03	1.2990E-03
1.1844E-03	9.0201E-04	8.5816E-04	8.6443E-04	6.0849E-04	3.8430E-04
3.1181E-04	2.4748E-04	2.0782E-04	1.8709E-04	1.5327E-04	1.2630E-04
8.5958E-05	9.1331E-05	4.4863E-05	4.5554E-05	8.6432E-05	5.3778E-05
7.8548E-05	4.9696E-05	3.7560E-05	3.3195E-05	5.9252E-05	3.5652E-05
1.7451E-05	2.0285E-05	4.7895E-06	1.8249E-05	1.5183E-05	1.4572E-05
1.9134E-05	7.6785E-06	2.8089E-06	3.6283E-06	1.4016E-06	2.6963E-07
1.1540E-07	4.7313E-08	3.6275E-08	3.7447E-08	3.0101E-08	1.6947E-08
6.5259E-09	2.4384E-09	1.3198E-09	6.9724E-10	1.0038E-09	

No.8 Angle=145 degree Flux/Group

0.0	0.0	0.0	0.0	0.0	0.0
0.0	1.6949E-06	2.1978E-05	1.3643E-04	6.0091E-04	2.3480E-02
2.6318E-01	2.7600E-01	5.4050E-02	3.2500E-03	1.2919E-03	1.0160E-03
8.5611E-04	7.1990E-04	6.3299E-04	4.2210E-04	3.4271E-04	1.9814E-04
2.3532E-04	1.4259E-04	1.4960E-04	1.7688E-04	1.2743E-04	1.2620E-04
1.2203E-04	1.0976E-04	4.6639E-04	8.1490E-04	9.8662E-04	6.6162E-04
7.6308E-04	9.2414E-04	1.1079E-03	1.2367E-03	1.1609E-03	1.2308E-03
1.2418E-03	1.5900E-03	1.5373E-03	1.7221E-03	1.7437E-03	1.8929E-03
1.9941E-03	2.1000E-03	2.2515E-03	2.5008E-03	2.3070E-03	2.1394E-03
2.2162E-03	2.1584E-03	2.1062E-03	2.0473E-03	2.1780E-03	2.1356E-03
4.0013E-03	4.3099E-03	4.2048E-03	4.1103E-03	3.9833E-03	3.9063E-03
3.7788E-03	3.6355E-03	3.3137E-03	3.1030E-03	2.7784E-03	2.5073E-03
2.4569E-03	2.1258E-03	1.9309E-03	1.6933E-03	1.4796E-03	1.2275E-03
1.1158E-03	8.5627E-04	8.1476E-04	8.0224E-04	5.6604E-04	3.5453E-04
2.8569E-04	2.3434E-04	1.9996E-04	1.7166E-04	1.5059E-04	1.1994E-04
8.3085E-05	8.4877E-05	4.9478E-05	4.6774E-05	8.0741E-05	5.2202E-05
7.5314E-05	4.2304E-05	3.3567E-05	2.8351E-05	5.3527E-05	3.0993E-05
1.6388E-05	1.8109E-05	6.9901E-06	1.7221E-05	1.4210E-05	1.3371E-05
1.7076E-05	4.4784E-06	1.5095E-06	4.4346E-06	1.6978E-06	2.6603E-07
8.8200E-08	1.0072E-07	1.4891E-07	1.3208E-07	8.9108E-08	4.9790E-08
2.1794E-08	1.1539E-08	6.7703E-09	3.9349E-09	6.0322E-09	

No.9 Angle=140 degree Flux/Group

0.0	0.0	0.0	0.0	0.0	0.0
8.3758E-09	3.2259E-06	3.6848E-05	1.9696E-04	7.5786E-04	2.8071E-02
3.6635E-01	2.6706E-01	1.7009E-02	2.9138E-03	1.3014E-03	9.8912E-04
7.9827E-04	6.6673E-04	6.0671E-04	4.1567E-04	3.3070E-04	2.1432E-04
2.4904E-04	1.5170E-04	1.5436E-04	1.4332E-04	1.2830E-04	1.1970E-04
1.1459E-04	1.1102E-04	4.7404E-04	8.0617E-04	9.7136E-04	6.5863E-04
8.2244E-04	9.7565E-04	1.0950E-03	1.2550E-03	1.1613E-03	1.2151E-03
1.2302E-03	1.5517E-03	1.5489E-03	1.7214E-03	1.7282E-03	1.8651E-03
2.0120E-03	2.1197E-03	2.2769E-03	2.4929E-03	2.2883E-03	2.1430E-03
2.2366E-03	2.1648E-03	2.0825E-03	2.0127E-03	2.1776E-03	2.1173E-03
3.9451E-03	4.2898E-03	4.1755E-03	4.0607E-03	3.9507E-03	3.8711E-03
3.7580E-03	3.5891E-03	3.2842E-03	3.0715E-03	2.7721E-03	2.4871E-03
2.4433E-03	2.1114E-03	1.9100E-03	1.6739E-03	1.4647E-03	1.2191E-03
1.1111E-03	8.6411E-04	8.1556E-04	7.8804E-04	5.6044E-04	3.4677E-04
2.7549E-04	2.3238E-04	2.0242E-04	1.6774E-04	1.4996E-04	1.1996E-04
8.8578E-05	8.9432E-05	6.1748E-05	5.2939E-05	7.9992E-05	5.4394E-05
7.6257E-05	4.5755E-05	3.6237E-05	3.1611E-05	5.1836E-05	2.7927E-05
1.9274E-05	1.6869E-05	7.9097E-06	1.8214E-05	1.4095E-05	1.1872E-05
1.8913E-05	4.2903E-06	1.3943E-06	6.0019E-06	1.6842E-06	3.9013E-07
2.0573E-07	3.0670E-07	2.9182E-07	1.2486E-07	7.4879E-08	4.5499E-08
2.6566E-08	1.4635E-08	8.5884E-09	4.9522E-09	7.6450E-09	

No.10 Angle=135 degree Flux/Group

0.0	0.0	0.0	0.0	0.0	0.0
6.6301E-08	7.0022E-06	6.0610E-05	3.0120E-04	1.1054E-03	8.7910E-02
4.5054E-01	2.2314E-01	8.7039E-03	2.5413E-03	1.3146E-03	1.0274E-03
7.7033E-04	6.4257E-04	5.1682E-04	3.9690E-04	3.3611E-04	2.2998E-04
2.7166E-04	1.6956E-04	1.6884E-04	1.4875E-04	1.4038E-04	1.3160E-04
1.2650E-04	1.2339E-04	5.1868E-04	8.3099E-04	9.5169E-04	6.6309E-04
8.2152E-04	9.6828E-04	1.1113E-03	1.2520E-03	1.1899E-03	1.2335E-03
1.2741E-03	1.5875E-03	1.6245E-03	1.8029E-03	1.7928E-03	1.9302E-03
2.0497E-03	2.1811E-03	2.3036E-03	2.5041E-03	2.3271E-03	2.1892E-03
2.2790E-03	2.1897E-03	2.0963E-03	2.0463E-03	2.2020E-03	2.1441E-03
3.9834E-03	4.3372E-03	4.2133E-03	4.0817E-03	3.9724E-03	3.9057E-03
3.8220E-03	3.6130E-03	3.3144E-03	3.1137E-03	2.8229E-03	2.5167E-03
2.4615E-03	2.1303E-03	1.9255E-03	1.6999E-03	1.4891E-03	1.2549E-03
1.1354E-03	8.9488E-04	8.3718E-04	7.9595E-04	5.7350E-04	3.4863E-04
2.6964E-04	2.2675E-04	2.0970E-04	1.7849E-04	1.6461E-04	1.2741E-04
9.9796E-05	9.6615E-05	7.5223E-05	5.9055E-05	7.8031E-05	5.5161E-05
7.8496E-05	5.2523E-05	4.4599E-05	3.7881E-05	5.6352E-05	2.7468E-05
1.9952E-05	1.7650E-05	1.0450E-05	1.7764E-05	1.3308E-05	1.2003E-05
1.9138E-05	4.9426E-06	1.1253E-06	6.6121E-06	2.0351E-06	7.2957E-07
1.2222E-06	6.9884E-07	2.5650E-07	1.2777E-07	8.1596E-08	4.9696E-08
2.9194E-08	1.6330E-08	9.6405E-09	5.6648E-09	8.9422E-09	

No.11 Angle=130 degree Flux/Group

0.0	0.0	0.0	0.0	0.0	0.0
2.2355E-07	1.3946E-05	9.7231E-05	4.9304E-04	4.3809E-03	1.5888E-01
5.9957E-01	1.2934E-01	5.9629E-03	2.2007E-03	1.3389E-03	1.0226E-03
7.5445E-04	5.9669E-04	5.2290E-04	3.8106E-04	3.1829E-04	2.3544E-04
2.5732E-04	1.7797E-04	1.7706E-04	1.5935E-04	1.5720E-04	1.4166E-04
1.3660E-04	1.3429E-04	5.6647E-04	8.3879E-04	9.1136E-04	6.5701E-04
8.6825E-04	9.8927E-04	1.1826E-03	1.3017E-03	1.2510E-03	1.2741E-03
1.3552E-03	1.6826E-03	1.7276E-03	1.9284E-03	1.8946E-03	2.0313E-03
2.1083E-03	2.2246E-03	2.3216E-03	2.5221E-03	2.3616E-03	2.2390E-03
2.3086E-03	2.2094E-03	2.1091E-03	2.0756E-03	2.2469E-03	2.1756E-03
4.0428E-03	4.4142E-03	4.2691E-03	4.1176E-03	4.0365E-03	3.9712E-03
3.9220E-03	3.6633E-03	3.3799E-03	3.1996E-03	2.9137E-03	2.5972E-03
2.5078E-03	2.1761E-03	1.9691E-03	1.7425E-03	1.5346E-03	1.2927E-03
1.1557E-03	9.3503E-04	8.6925E-04	8.1876E-04	6.0651E-04	3.6738E-04
2.8595E-04	2.3679E-04	2.0954E-04	1.7714E-04	1.7163E-04	1.3969E-04
1.1067E-04	1.0034E-04	8.4935E-05	6.6903E-05	7.9046E-05	5.6364E-05
8.5317E-05	5.9717E-05	5.2391E-05	4.5358E-05	5.7759E-05	3.0117E-05
2.6913E-05	2.0625E-05	1.2185E-05	1.8492E-05	1.4476E-05	9.8925E-06
1.8589E-05	5.0499E-06	2.0118E-06	8.0632E-06	3.2367E-06	3.1658E-06
1.1346E-06	3.5995E-07	1.2803E-07	7.6927E-08	5.1571E-08	3.1477E-08
1.8237E-08	9.7204E-09	5.6876E-09	3.2586E-09	5.5706E-09	

No.12 Angle=125 degree Flux/Group

0.0	0.0	0.0	0.0	0.0	0.0
8.5582E-07	2.2739E-05	1.3161E-04	7.7918E-04	6.1183E-03	3.1671E-01
5.9319E-01	1.9254E-02	4.2549E-03	1.8912E-03	1.2685E-03	9.9572E-04
7.1559E-04	5.6036E-04	5.0357E-04	3.6113E-04	2.8606E-04	2.4805E-04
2.5531E-04	1.8159E-04	1.6519E-04	1.5199E-04	1.6071E-04	1.4352E-04
1.3665E-04	1.4310E-04	5.7015E-04	8.1935E-04	9.1369E-04	6.8028E-04
8.9815E-04	1.0154E-03	1.2839E-03	1.3774E-03	1.3314E-03	1.3337E-03
1.4193E-03	1.6868E-03	1.7090E-03	1.9331E-03	1.8861E-03	2.0201E-03
2.0664E-03	2.2012E-03	2.2858E-03	2.4728E-03	2.3247E-03	2.2206E-03
2.2796E-03	2.1704E-03	2.0723E-03	2.0613E-03	2.2326E-03	2.1488E-03
3.9762E-03	4.3459E-03	4.2034E-03	4.0661E-03	3.9872E-03	3.9286E-03
3.8897E-03	3.6131E-03	3.3366E-03	3.1493E-03	2.8801E-03	2.5846E-03
2.4904E-03	2.1592E-03	1.9439E-03	1.7274E-03	1.5326E-03	1.3002E-03
1.1447E-03	9.3905E-04	8.6726E-04	8.1126E-04	6.1134E-04	3.6682E-04
2.8080E-04	2.3767E-04	2.1721E-04	1.8225E-04	1.7178E-04	1.3597E-04
1.0931E-04	1.0084E-04	9.0884E-05	7.4498E-05	8.6072E-05	5.9279E-05
8.6327E-05	5.7765E-05	5.9750E-05	4.8184E-05	5.8773E-05	3.7165E-05
3.1479E-05	1.8343E-05	1.0464E-05	1.7527E-05	1.5228E-05	1.1005E-05
1.9083E-05	5.1425E-06	2.2032E-06	1.0534E-05	6.3183E-06	2.2495E-06
6.1526E-07	1.8923E-07	4.3189E-08	2.6625E-08	2.0829E-08	1.2829E-08
6.9631E-09	2.9984E-09	1.6296E-09	8.2994E-10	1.6024E-09	

No.13 Angle=120 degree Flux/Group

0.0	0.0	0.0	0.0	0.0	0.0
2.2944E-06	3.3811E-05	2.0585E-04	1.5900E-03	7.8871E-03	5.6856E-01
3.4946E-01	7.6500E-03	3.1351E-03	1.6418E-03	1.2196E-03	9.4631E-04
6.8750E-04	5.2345E-04	4.6385E-04	3.3053E-04	2.6771E-04	2.3717E-04
2.3658E-04	1.8547E-04	1.5747E-04	1.4898E-04	1.5736E-04	1.4089E-04
1.3291E-04	1.4087E-04	5.5408E-04	8.4586E-04	9.6960E-04	7.7944E-04
9.8683E-04	1.0752E-03	1.2825E-03	1.3533E-03	1.3243E-03	1.3264E-03
1.4078E-03	1.6601E-03	1.6755E-03	1.8912E-03	1.8535E-03	1.9788E-03
1.9998E-03	2.1421E-03	2.1830E-03	2.3896E-03	2.2551E-03	2.1527E-03
2.2215E-03	2.1034E-03	2.0160E-03	2.0111E-03	2.1694E-03	2.0831E-03
3.8573E-03	4.2221E-03	4.0743E-03	3.9483E-03	3.8728E-03	3.8028E-03
3.7698E-03	3.4982E-03	3.2364E-03	3.0578E-03	2.7958E-03	2.5238E-03
2.4336E-03	2.1076E-03	1.8878E-03	1.6749E-03	1.4965E-03	1.2732E-03
1.1155E-03	9.3412E-04	8.5527E-04	7.7762E-04	5.8585E-04	3.4910E-04
2.7138E-04	2.4068E-04	2.1652E-04	1.7720E-04	1.6964E-04	1.3553E-04
1.0859E-04	1.0309E-04	8.9797E-05	7.1544E-05	8.7058E-05	6.2362E-05
8.9898E-05	6.3702E-05	5.9993E-05	4.5523E-05	5.5730E-05	3.6701E-05
2.9748E-05	1.5837E-05	1.1124E-05	2.2795E-05	1.4229E-05	8.8521E-06
1.9648E-05	5.1785E-06	5.5667E-06	7.2296E-06	6.5238E-06	2.9807E-06
5.7698E-07	1.8522E-07	7.1894E-08	4.5585E-08	3.1981E-08	1.9536E-08
1.0981E-08	5.5515E-09	3.1608E-09	1.7897E-09	2.8533E-09	

No.14 Angle=115 degree Flux/Group

0.0	0.0	0.0	0.0	0.0	1.4415E-08
4.4834E-06	4.7137E-05	3.0702E-04	2.8316E-03	1.8619E-02	8.4279E-01
8.1891E-02	4.7301E-03	2.4430E-03	1.5379E-03	1.1489E-03	8.7505E-04
6.4023E-04	4.8227E-04	4.3108E-04	3.0496E-04	2.5063E-04	2.3437E-04
2.3187E-04	2.0034E-04	1.5201E-04	1.5186E-04	1.6844E-04	1.4502E-04
1.3759E-04	1.4760E-04	5.7055E-04	8.7709E-04	1.0182E-03	8.6560E-04
1.0445E-03	1.1305E-03	1.2765E-03	1.3224E-03	1.3054E-03	1.3152E-03
1.3994E-03	1.6094E-03	1.6300E-03	1.8327E-03	1.8031E-03	1.9288E-03
1.9485E-03	2.0799E-03	2.1175E-03	2.3097E-03	2.2058E-03	2.1046E-03
2.1662E-03	2.0429E-03	1.9604E-03	1.9571E-03	2.0955E-03	2.0126E-03
3.7415E-03	4.1118E-03	3.9645E-03	3.8493E-03	3.7739E-03	3.7071E-03
3.6781E-03	3.4034E-03	3.1671E-03	3.0000E-03	2.7342E-03	2.4611E-03
2.3599E-03	2.0534E-03	1.8559E-03	1.6405E-03	1.4539E-03	1.2337E-03
1.0920E-03	9.2547E-04	8.4566E-04	7.5657E-04	5.7723E-04	3.5307E-04
2.7371E-04	2.2411E-04	1.9684E-04	1.7383E-04	1.7130E-04	1.3713E-04
1.0535E-04	1.0217E-04	9.1919E-05	7.0141E-05	8.3613E-05	6.3252E-05
9.2454E-05	6.7626E-05	5.7599E-05	4.4719E-05	5.5483E-05	3.7441E-05
2.8970E-05	1.6255E-05	1.2075E-05	2.3158E-05	1.5932E-05	9.1442E-06
2.0923E-05	7.3523E-06	7.5554E-06	7.5417E-06	6.3468E-06	1.4703E-06
4.2676E-07	2.5603E-07	1.2244E-07	7.5931E-08	4.9930E-08	3.0287E-08
1.7540E-08	9.4677E-09	5.5093E-09	3.1850E-09	5.2187E-09	

No.15 Angle=110 degree Flux/Group

0.0	0.0	0.0	0.0	0.0	2.8857E-08
8.4050E-06	6.7246E-05	4.9937E-04	6.4064E-03	6.9774E-02	8.8061E-01
6.3306E-03	3.1939E-03	1.9961E-03	1.4631E-03	1.1140E-03	8.1587E-04
5.9222E-04	4.5432E-04	4.0108E-04	2.8284E-04	2.3983E-04	2.5734E-04
2.4407E-04	2.2296E-04	1.8480E-04	1.7862E-04	1.9698E-04	1.7189E-04
1.6452E-04	1.7347E-04	6.6770E-04	9.1612E-04	9.8309E-04	8.9031E-04
1.0275E-03	1.1093E-03	1.2229E-03	1.2982E-03	1.2804E-03	1.2930E-03
1.3701E-03	1.5650E-03	1.6012E-03	1.7724E-03	1.7565E-03	1.8926E-03
1.9026E-03	2.0189E-03	2.0568E-03	2.2317E-03	2.1508E-03	2.0385E-03
2.1040E-03	1.9729E-03	1.9102E-03	1.9021E-03	2.0363E-03	1.9592E-03
3.6355E-03	4.0035E-03	3.8620E-03	3.7363E-03	3.6580E-03	3.5985E-03
3.5666E-03	3.2867E-03	3.0703E-03	2.9282E-03	2.6590E-03	2.3968E-03
2.3009E-03	2.0002E-03	1.7962E-03	1.5949E-03	1.4262E-03	1.2106E-03
1.0581E-03	8.9560E-04	8.0717E-04	7.3452E-04	5.5559E-04	3.4747E-04
2.7755E-04	2.2014E-04	1.9227E-04	1.7518E-04	1.6971E-04	1.3485E-04
1.0288E-04	9.6823E-05	8.8290E-05	6.5954E-05	8.0897E-05	6.1697E-05
9.1331E-05	7.1904E-05	5.6933E-05	4.5038E-05	5.0421E-05	3.4796E-05
3.6050E-05	1.9702E-05	1.4569E-05	2.2191E-05	1.3973E-05	8.5006E-06
2.0144E-05	8.7232E-06	6.8648E-06	6.3568E-06	3.9782E-06	2.5051E-06
1.0405E-06	2.5855E-07	1.0838E-07	6.6257E-08	4.3805E-08	2.6631E-08
1.5380E-08	8.2296E-09	4.7720E-09	2.7969E-09	4.7150E-09	

No.16 Angle=105 degree Flux/Group

0.0	0.0	0.0	0.0	0.0	2.4873E-07
1.3231E-05	9.2865E-05	8.7947E-04	1.3776E-02	5.4827E-01	4.0248E-01
4.2705E-03	2.3001E-03	1.7099E-03	1.4454E-03	1.0989E-03	7.5577E-04
5.4657E-04	4.3171E-04	3.7012E-04	2.7472E-04	2.4669E-04	2.6774E-04
2.4633E-04	2.3636E-04	2.0276E-04	1.9019E-04	2.0703E-04	1.8552E-04
1.7636E-04	1.9123E-04	7.1085E-04	8.9644E-04	9.4240E-04	8.7186E-04
9.8223E-04	1.0780E-03	1.1703E-03	1.2653E-03	1.2398E-03	1.2590E-03
1.3328E-03	1.5008E-03	1.5371E-03	1.7079E-03	1.6953E-03	1.8319E-03
1.8430E-03	1.9497E-03	1.9829E-03	2.1372E-03	2.0793E-03	1.9679E-03
2.0431E-03	1.9088E-03	1.8442E-03	1.8315E-03	1.9621E-03	1.8867E-03
3.5061E-03	3.8795E-03	3.7337E-03	3.6138E-03	3.5382E-03	3.4833E-03
3.4601E-03	3.1937E-03	2.9823E-03	2.8333E-03	2.5601E-03	2.3144E-03
2.2220E-03	1.9272E-03	1.7283E-03	1.5299E-03	1.3665E-03	1.1669E-03
1.0239E-03	8.7194E-04	7.8028E-04	7.0345E-04	5.4430E-04	3.3167E-04
2.6637E-04	2.1845E-04	1.8906E-04	1.6148E-04	1.5728E-04	1.3204E-04
9.6734E-05	8.4057E-05	8.5157E-05	6.6669E-05	7.7763E-05	5.9391E-05
9.3587E-05	6.9867E-05	5.6188E-05	4.3179E-05	4.9298E-05	3.1133E-05
2.9982E-05	2.0273E-05	1.5702E-05	2.0473E-05	1.5198E-05	9.2796E-06
1.8551E-05	1.0498E-05	4.8483E-06	8.7398E-06	2.1959E-06	2.5108E-06
1.0289E-06	1.7426E-07	5.2550E-08	3.2498E-08	2.3054E-08	1.4153E-08
7.8995E-09	3.8570E-09	2.1661E-09	1.1424E-09	2.1773E-09	

No.17 Angle=100 degree Flux/Group

0.0	0.0	0.0	0.0	0.0	6.7023E-07
2.9288E-05	1.7547E-04	1.8057E-03	2.0560E-02	9.4450E-01	8.1780E-03
2.9787E-03	1.8119E-03	1.5798E-03	1.4520E-03	1.1037E-03	7.3572E-04
5.3950E-04	4.3129E-04	3.7038E-04	2.9151E-04	2.7802E-04	2.6086E-04
2.4018E-04	2.2862E-04	2.0259E-04	1.8758E-04	2.0163E-04	1.8093E-04
1.7206E-04	1.8755E-04	6.9083E-04	8.4623E-04	9.0626E-04	8.6180E-04
9.5096E-04	1.0568E-03	1.1042E-03	1.1929E-03	1.1642E-03	1.2073E-03
1.2854E-03	1.4376E-03	1.5100E-03	1.6570E-03	1.6449E-03	1.7720E-03
1.7847E-03	1.8966E-03	1.9153E-03	2.0644E-03	2.0157E-03	1.9035E-03
1.9710E-03	1.8495E-03	1.7900E-03	1.7761E-03	1.8985E-03	1.8279E-03
3.3926E-03	3.7559E-03	3.6132E-03	3.4788E-03	3.4071E-03	3.3684E-03
3.3436E-03	3.0840E-03	2.8801E-03	2.7284E-03	2.4570E-03	2.2382E-03
2.1482E-03	1.8546E-03	1.6710E-03	1.4796E-03	1.3114E-03	1.1202E-03
9.7835E-04	8.3622E-04	7.5337E-04	6.7702E-04	5.2798E-04	3.1833E-04
2.4811E-04	2.0853E-04	1.8748E-04	1.5595E-04	1.4416E-04	1.2448E-04
9.1237E-05	7.7455E-05	8.2274E-05	6.6356E-05	7.3316E-05	5.3120E-05
8.4060E-05	7.3440E-05	6.0267E-05	4.3339E-05	4.4719E-05	2.7196E-05
2.7864E-05	1.8710E-05	1.5473E-05	1.9280E-05	1.4095E-05	8.9170E-06
1.7487E-05	1.0095E-05	4.8414E-06	8.2697E-06	2.2037E-06	2.5050E-06
1.0648E-06	2.2204E-07	8.2837E-08	5.0716E-08	3.3780E-08	2.0615E-08
1.1878E-08	6.3301E-09	3.6336E-09	2.0456E-09	3.5337E-09	

No.18 Angle=95 degree Flux/Group

0.0	0.0	0.0	0.0	0.0	1.4046E-06
3.9778E-05	2.5477E-04	3.3630E-03	2.5387E-02	9.5634E-01	6.4895E-03
2.1419E-03	1.4871E-03	1.4673E-03	1.4270E-03	1.0912E-03	7.1690E-04
5.2895E-04	4.2708E-04	3.6821E-04	3.0136E-04	2.8958E-04	2.4770E-04
2.2306E-04	2.2121E-04	1.9980E-04	1.8731E-04	1.9661E-04	1.7747E-04
1.6918E-04	1.8426E-04	6.7558E-04	8.0302E-04	8.5648E-04	8.1939E-04
8.9015E-04	9.9780E-04	1.0439E-03	1.1423E-03	1.1137E-03	1.1570E-03
1.2344E-03	1.3704E-03	1.4148E-03	1.5532E-03	1.5615E-03	1.6768E-03
1.7000E-03	1.8129E-03	1.8290E-03	1.9551E-03	1.9263E-03	1.8264E-03
1.8945E-03	1.7729E-03	1.7197E-03	1.6925E-03	1.8124E-03	1.7424E-03
3.2420E-03	3.5927E-03	3.4370E-03	3.3142E-03	3.2422E-03	3.2039E-03
3.1738E-03	2.9484E-03	2.7409E-03	2.5879E-03	2.3215E-03	2.1129E-03
2.0258E-03	1.7507E-03	1.5692E-03	1.3886E-03	1.2308E-03	1.0486E-03
9.1460E-04	7.8486E-04	7.0981E-04	6.4303E-04	5.0014E-04	2.8954E-04
2.2995E-04	1.9871E-04	1.8200E-04	1.4800E-04	1.2882E-04	1.0521E-04
8.2438E-05	7.8330E-05	7.9630E-05	6.2280E-05	7.0263E-05	5.1060E-05
7.5034E-05	6.2809E-05	5.5296E-05	4.0284E-05	4.1991E-05	2.6341E-05
2.6509E-05	1.4645E-05	1.2265E-05	2.0126E-05	1.3817E-05	7.4286E-06
1.8492E-05	6.2082E-06	5.5262E-06	7.6592E-06	1.6990E-06	9.9804E-07
1.3780E-06	1.0828E-06	2.0834E-07	8.5500E-08	5.1594E-08	3.1123E-08
1.9026E-08	1.2006E-08	7.0108E-09	4.1456E-09	6.9302E-09	

No.19 Angle=90 degree Flux/Group

0.0	0.0	0.0	0.0	0.0	2.6828E-06
4.9304E-05	4.3044E-04	4.5219E-03	3.6843E-01	6.2044E-01	4.4165E-03
1.6714E-03	1.2353E-03	1.3836E-03	1.3818E-03	1.0702E-03	7.2665E-04
5.2066E-04	4.2389E-04	3.6410E-04	3.2302E-04	3.0313E-04	2.3882E-04
2.1967E-04	2.1217E-04	1.8963E-04	1.8142E-04	1.8838E-04	1.6722E-04
1.5826E-04	1.6668E-04	6.3204E-04	7.3883E-04	8.1574E-04	8.0422E-04
8.5016E-04	9.6558E-04	9.6664E-04	1.0409E-03	1.0134E-03	1.0532E-03
1.1208E-03	1.2207E-03	1.2703E-03	1.3965E-03	1.4004E-03	1.5054E-03
1.5289E-03	1.6224E-03	1.6339E-03	1.7429E-03	1.7278E-03	1.6368E-03
1.6871E-03	1.5817E-03	1.5405E-03	1.5197E-03	1.6182E-03	1.5665E-03
2.9085E-03	3.1983E-03	3.0694E-03	2.9755E-03	2.8787E-03	2.8382E-03
2.7967E-03	2.6078E-03	2.4184E-03	2.2669E-03	2.0277E-03	1.8401E-03
1.7767E-03	1.5362E-03	1.3773E-03	1.2101E-03	1.0562E-03	8.9893E-04
8.0050E-04	6.8155E-04	6.1733E-04	5.5606E-04	4.2983E-04	2.5980E-04
2.0319E-04	1.7180E-04	1.5901E-04	1.3691E-04	1.2339E-04	9.7985E-05
7.1828E-05	6.9509E-05	6.9588E-05	5.2570E-05	6.2568E-05	4.8259E-05
6.8236E-05	5.5222E-05	4.2500E-05	3.1273E-05	3.7422E-05	2.3115E-05
2.2281E-05	1.5281E-05	1.0289E-05	1.5313E-05	1.2484E-05	9.1578E-06
1.6309E-05	6.0638E-06	4.8678E-06	6.7599E-06	1.4570E-06	9.0732E-07
1.3230E-06	1.0470E-06	1.9881E-07	8.0852E-08	4.8765E-08	2.9420E-08
1.7933E-08	1.1210E-08	6.6058E-09	3.9022E-09	6.5140E-09	

No.20 Angle=85 degree Flux/Group

0.0	0.0	0.0	0.0	1.0166E-08	5.5161E-06
8.9111E-05	9.0599E-04	6.8726E-03	6.4966E-01	7.3033E-02	3.1960E-03
1.4338E-03	1.1701E-03	1.3489E-03	1.3599E-03	1.0767E-03	7.2983E-04
5.3264E-04	4.1977E-04	3.6503E-04	3.2931E-04	3.0611E-04	2.3516E-04
2.1871E-04	2.1070E-04	1.8664E-04	1.8397E-04	1.9202E-04	1.6646E-04
1.5757E-04	1.6826E-04	6.3366E-04	7.3237E-04	8.3473E-04	8.2533E-04
8.5153E-04	9.8543E-04	9.8212E-04	1.0595E-03	1.0410E-03	1.0816E-03
1.1654E-03	1.2663E-03	1.3201E-03	1.4170E-03	1.4354E-03	1.5281E-03
1.5546E-03	1.6281E-03	1.6405E-03	1.7547E-03	1.7367E-03	1.6520E-03
1.6955E-03	1.6004E-03	1.5535E-03	1.5316E-03	1.6141E-03	1.5723E-03
2.9170E-03	3.1741E-03	3.0198E-03	2.9366E-03	2.7976E-03	2.8100E-03
2.7606E-03	2.5510E-03	2.3652E-03	2.2246E-03	1.9448E-03	1.7463E-03
1.7303E-03	1.5038E-03	1.3386E-03	1.1876E-03	1.0354E-03	8.7665E-04
7.7155E-04	6.5809E-04	6.0815E-04	5.4971E-04	4.2063E-04	2.6302E-04
2.0267E-04	1.7238E-04	1.6174E-04	1.4221E-04	1.2788E-04	1.0105E-04
7.0055E-05	6.7549E-05	7.2033E-05	5.6457E-05	6.5195E-05	4.7695E-05
7.9798E-05	6.1868E-05	4.2659E-05	3.0063E-05	3.6289E-05	2.6279E-05
2.0017E-05	1.5513E-05	1.2495E-05	1.6743E-05	1.0830E-05	7.9878E-06
2.1308E-05	5.9946E-06	5.1503E-06	8.1263E-06	1.2702E-06	7.2907E-07
4.4338E-07	3.6439E-07	5.5582E-07	3.7402E-07	1.8067E-07	2.8611E-08
1.5286E-08	9.5458E-09	5.6370E-09	3.3185E-09	5.5899E-09	

No.21 Angle=80 degree Flux/Group

0.0	0.0	0.0	0.0	2.3878E-08	1.0544E-05
1.8159E-04	1.6538E-03	1.0816E-01	7.1456E-01	1.5762E-02	2.6287E-03
1.3261E-03	1.1602E-03	1.3148E-03	1.3167E-03	1.0841E-03	7.5529E-04
5.5354E-04	4.3299E-04	3.7586E-04	3.4959E-04	3.1741E-04	2.4063E-04
2.3158E-04	2.1510E-04	1.9088E-04	1.9297E-04	1.9441E-04	1.7414E-04
1.6386E-04	1.7360E-04	6.6292E-04	7.4120E-04	8.4013E-04	8.5734E-04
8.7795E-04	1.0191E-03	1.0347E-03	1.1174E-03	1.1055E-03	1.1517E-03
1.2447E-03	1.3279E-03	1.3772E-03	1.4707E-03	1.4973E-03	1.5992E-03
1.6204E-03	1.7024E-03	1.7138E-03	1.8177E-03	1.8126E-03	1.7223E-03
1.7587E-03	1.6764E-03	1.6192E-03	1.5907E-03	1.6772E-03	1.6316E-03
3.0416E-03	3.3236E-03	3.1819E-03	3.0740E-03	2.9742E-03	2.9831E-03
2.9305E-03	2.7131E-03	2.5184E-03	2.3636E-03	2.0752E-03	1.8659E-03
1.8309E-03	1.5909E-03	1.4219E-03	1.2679E-03	1.1063E-03	9.3905E-04
8.2479E-04	7.0931E-04	6.4839E-04	5.8755E-04	4.5714E-04	2.8884E-04
2.2711E-04	1.8667E-04	1.5855E-04	1.3488E-04	1.2288E-04	1.0976E-04
8.7947E-05	8.0806E-05	7.6735E-05	6.2897E-05	7.1697E-05	5.2502E-05
8.7301E-05	6.5613E-05	5.3394E-05	3.8823E-05	3.9314E-05	2.8753E-05
2.3133E-05	1.8132E-05	1.4915E-05	1.9154E-05	1.1728E-05	7.5911E-06
2.0805E-05	9.6445E-06	5.7105E-06	8.5326E-06	1.6539E-06	9.4138E-07
5.5908E-07	2.8838E-07	4.9062E-07	3.3325E-07	1.5755E-07	1.7383E-08
8.5610E-09	5.3897E-09	3.0829E-09	1.7877E-09	3.4571E-09	

No.22 Angle=75 degree Flux/Group

0.0	0.0	0.0	0.0	2.2318E-07	2.2255E-05
3.9825E-04	2.5265E-03	3.5056E-01	5.5144E-01	1.3327E-02	2.3236E-03
1.2385E-03	1.1170E-03	1.2420E-03	1.2400E-03	1.0749E-03	7.8256E-04
5.6608E-04	4.3968E-04	3.7872E-04	3.5368E-04	3.1739E-04	2.4216E-04
2.4465E-04	2.1454E-04	1.9569E-04	2.0039E-04	2.0182E-04	1.7927E-04
1.6839E-04	1.7827E-04	6.7726E-04	7.3764E-04	8.2728E-04	8.5409E-04
8.6874E-04	1.0237E-03	1.0587E-03	1.1269E-03	1.1190E-03	1.1638E-03
1.2530E-03	1.3543E-03	1.3971E-03	1.5003E-03	1.5241E-03	1.6261E-03
1.6411E-03	1.7332E-03	1.7295E-03	1.8282E-03	1.8336E-03	1.7555E-03
1.7895E-03	1.7023E-03	1.6464E-03	1.6209E-03	1.7131E-03	1.6620E-03
3.1089E-03	3.4109E-03	3.2748E-03	3.1455E-03	3.0663E-03	3.0608E-03
3.0054E-03	2.7878E-03	2.5995E-03	2.4583E-03	2.1692E-03	1.9486E-03
1.8820E-03	1.6456E-03	1.4709E-03	1.3131E-03	1.1472E-03	9.8646E-04
8.6628E-04	7.4817E-04	6.8025E-04	6.1160E-04	4.8038E-04	2.9675E-04
2.3276E-04	1.9360E-04	1.6598E-04	1.4068E-04	1.2654E-04	1.1221E-04
9.0381E-05	8.2116E-05	8.0541E-05	6.9845E-05	8.0983E-05	6.1836E-05
9.3860E-05	6.5677E-05	5.6538E-05	4.1692E-05	4.3132E-05	3.1265E-05
2.5027E-05	1.8536E-05	1.9040E-05	1.9259E-05	1.0511E-05	7.5556E-06
2.1955E-05	9.3876E-06	6.5787E-06	9.0364E-06	2.0560E-06	1.1151E-06
6.5154E-07	2.5708E-07	1.0707E-07	6.4376E-08	8.1014E-08	1.2122E-07
7.7811E-08	4.7237E-08	2.8465E-08	1.7090E-08	2.6844E-08	

No.23 Angle=70 degree Flux/Group

0.0	0.0	0.0	0.0	7.7782E-07	5.2595E-05
7.5123E-04	4.7888E-02	5.7281E-01	3.3010E-01	8.9590E-03	2.0751E-03
1.1994E-03	1.0713E-03	1.1364E-03	1.1560E-03	1.0542E-03	7.9346E-04
5.4692E-04	4.3020E-04	3.7762E-04	3.5515E-04	3.0422E-04	2.3629E-04
2.3976E-04	1.9646E-04	1.9345E-04	2.0040E-04	1.9935E-04	1.8046E-04
1.6845E-04	1.7878E-04	6.7576E-04	7.5044E-04	8.4707E-04	8.6777E-04
8.9037E-04	1.0131E-03	1.0346E-03	1.1089E-03	1.1141E-03	1.1598E-03
1.2446E-03	1.3627E-03	1.4025E-03	1.5033E-03	1.5299E-03	1.6211E-03
1.6494E-03	1.7320E-03	1.7293E-03	1.8182E-03	1.8307E-03	1.7591E-03
1.7849E-03	1.7087E-03	1.6499E-03	1.6295E-03	1.7217E-03	1.6746E-03
3.1275E-03	3.4198E-03	3.2991E-03	3.1711E-03	3.1125E-03	3.0912E-03
3.0324E-03	2.8076E-03	2.6166E-03	2.4834E-03	2.2050E-03	1.9859E-03
1.8982E-03	1.6671E-03	1.4915E-03	1.3296E-03	1.1674E-03	1.0062E-03
8.8371E-04	7.6388E-04	6.8899E-04	6.1848E-04	4.9084E-04	2.9260E-04
2.3361E-04	2.0547E-04	1.7987E-04	1.4753E-04	1.2821E-04	1.1149E-04
9.1668E-05	8.1336E-05	7.8904E-05	7.1644E-05	8.0441E-05	6.0722E-05
9.3289E-05	6.9941E-05	6.5292E-05	4.6837E-05	4.3983E-05	3.1640E-05
2.0825E-05	1.8432E-05	1.9671E-05	2.3562E-05	1.2986E-05	9.0666E-06
2.3192E-05	7.9816E-06	6.9761E-06	9.6681E-06	2.0929E-06	1.1084E-06
5.9873E-07	2.9006E-07	1.3132E-07	7.9156E-08	8.8177E-08	1.2256E-07
7.8423E-08	4.7559E-08	2.8614E-08	1.7126E-08	2.6742E-08	

No.24 Angle=65 degree Flux/Group

0.0	0.0	0.0	0.0	1.9562E-06	1.2755E-04
1.2063E-03	1.9135E-01	6.1978E-01	1.6045E-01	6.3671E-03	1.8480E-03
1.1307E-03	1.0451E-03	1.0358E-03	1.0666E-03	1.0362E-03	8.0016E-04
5.3339E-04	4.1712E-04	3.6654E-04	3.4455E-04	2.8471E-04	2.3380E-04
2.3689E-04	1.9314E-04	1.9577E-04	2.0532E-04	2.0731E-04	1.9018E-04
1.7325E-04	1.8417E-04	6.9621E-04	7.4204E-04	8.3368E-04	8.5276E-04
8.7532E-04	1.0034E-03	1.0412E-03	1.1091E-03	1.1107E-03	1.1556E-03
1.2319E-03	1.3513E-03	1.3846E-03	1.4856E-03	1.5137E-03	1.6017E-03
1.6308E-03	1.7277E-03	1.7248E-03	1.8110E-03	1.8121E-03	1.7514E-03
1.7725E-03	1.7052E-03	1.6309E-03	1.6149E-03	1.7132E-03	1.6658E-03
3.1046E-03	3.4110E-03	3.2979E-03	3.1550E-03	3.1200E-03	3.0953E-03
3.0338E-03	2.8070E-03	2.6136E-03	2.4853E-03	2.2143E-03	1.9892E-03
1.8933E-03	1.6677E-03	1.5037E-03	1.3422E-03	1.1744E-03	1.0117E-03
8.8660E-04	7.7632E-04	7.0185E-04	6.1751E-04	4.8891E-04	2.8975E-04
2.3363E-04	2.1094E-04	1.8258E-04	1.5218E-04	1.2861E-04	1.0813E-04
9.7056E-05	8.6960E-05	8.0155E-05	7.1826E-05	7.8111E-05	6.1098E-05
9.2801E-05	7.0573E-05	6.4900E-05	4.7292E-05	4.2566E-05	3.2921E-05
2.4179E-05	1.9804E-05	1.9515E-05	2.3860E-05	1.4156E-05	1.0367E-05
2.0492E-05	1.0410E-05	7.4388E-06	8.5969E-06	1.5732E-06	8.5457E-07
5.1938E-07	2.4669E-07	1.0740E-07	6.4748E-08	3.9023E-08	2.3383E-08
1.4071E-08	8.5408E-09	4.9476E-09	2.7333E-09	4.7424E-09	

No.25 Angle=60 degree Flux/Group

0.0	0.0	0.0	0.0	5.9532E-06	2.6198E-04
1.4414E-02	3.3191E-01	5.5806E-01	7.9752E-02	4.7307E-03	1.6740E-03
1.0805E-03	1.0206E-03	9.3813E-04	9.9104E-04	1.0087E-03	7.8931E-04
5.1065E-04	3.8443E-04	3.4150E-04	3.2008E-04	2.6003E-04	2.4655E-04
2.4155E-04	2.0105E-04	1.9932E-04	2.1921E-04	2.2135E-04	2.0344E-04
1.8524E-04	1.9041E-04	7.4509E-04	7.5728E-04	8.3953E-04	8.5940E-04
8.8859E-04	9.9778E-04	1.0280E-03	1.0903E-03	1.1018E-03	1.1433E-03
1.2263E-03	1.3371E-03	1.3819E-03	1.4658E-03	1.5080E-03	1.5765E-03
1.6227E-03	1.7199E-03	1.7083E-03	1.7803E-03	1.7907E-03	1.7470E-03
1.7588E-03	1.6962E-03	1.6207E-03	1.6113E-03	1.7090E-03	1.6555E-03
3.0851E-03	3.4021E-03	3.2957E-03	3.1183E-03	3.0875E-03	3.0743E-03
3.0192E-03	2.7912E-03	2.5943E-03	2.4662E-03	2.2127E-03	1.9926E-03
1.8760E-03	1.6447E-03	1.4916E-03	1.3451E-03	1.1843E-03	1.0199E-03
8.8048E-04	7.5858E-04	6.9201E-04	6.2460E-04	4.9639E-04	2.9693E-04
2.4041E-04	2.0869E-04	1.8176E-04	1.6059E-04	1.3826E-04	1.1435E-04
1.0208E-04	9.0115E-05	8.1079E-05	7.6198E-05	7.9405E-05	5.6080E-05
8.3967E-05	6.5998E-05	6.5094E-05	4.6335E-05	4.5554E-05	2.9622E-05
2.1753E-05	1.8346E-05	2.1639E-05	2.5875E-05	1.9038E-05	1.1490E-05
2.0781E-05	1.1063E-05	4.9804E-06	9.3706E-06	1.3486E-06	7.0381E-07
4.2008E-07	2.0875E-07	8.7309E-08	5.2502E-08	3.1486E-08	1.8896E-08
1.1396E-08	6.9027E-09	3.8807E-09	2.1421E-09	3.8837E-09	

No.26 Angle=55 degree Flux/Group

0.0	0.0	0.0	0.0	1.0534E-05	4.4914E-04
1.0360E-01	3.9431E-01	4.5995E-01	4.1881E-02	3.7296E-03	1.5312E-03
1.0673E-03	9.6853E-04	8.6461E-04	9.1042E-04	9.7229E-04	7.8333E-04
4.9395E-04	3.5350E-04	3.1187E-04	2.9130E-04	2.3041E-04	2.4749E-04
2.3849E-04	2.0849E-04	2.0425E-04	2.2271E-04	2.3291E-04	2.1382E-04
1.9354E-04	1.9858E-04	7.6865E-04	7.7927E-04	8.7092E-04	8.8183E-04
9.2347E-04	1.0026E-03	1.0176E-03	1.0749E-03	1.0825E-03	1.1210E-03
1.1982E-03	1.3280E-03	1.3668E-03	1.4442E-03	1.4927E-03	1.5537E-03
1.6002E-03	1.7090E-03	1.6875E-03	1.7623E-03	1.7645E-03	1.7236E-03
1.7336E-03	1.6827E-03	1.6075E-03	1.6019E-03	1.6981E-03	1.6504E-03
3.0738E-03	3.3814E-03	3.2615E-03	3.0775E-03	3.0590E-03	3.0505E-03
3.0073E-03	2.7769E-03	2.5694E-03	2.4419E-03	2.1988E-03	1.9854E-03
1.8687E-03	1.6393E-03	1.4838E-03	1.3380E-03	1.1798E-03	1.0063E-03
8.6956E-04	7.5608E-04	6.9336E-04	6.3247E-04	5.0724E-04	2.9806E-04
2.3863E-04	2.0210E-04	1.7402E-04	1.5606E-04	1.3090E-04	1.1074E-04
9.9812E-05	8.8783E-05	8.6213E-05	8.1647E-05	7.6750E-05	5.2700E-05
8.1286E-05	6.8496E-05	7.2987E-05	4.9490E-05	4.5489E-05	2.9095E-05
2.3067E-05	1.9540E-05	2.0037E-05	2.3146E-05	1.7797E-05	1.3401E-05
2.2731E-05	9.6903E-06	6.8688E-06	8.7348E-06	1.2134E-06	3.5725E-07
2.4049E-07	2.1997E-07	1.6912E-07	1.0378E-07	6.2541E-08	3.7647E-08
2.2737E-08	1.3700E-08	7.9958E-09	4.6399E-09	7.7541E-09	

No.27 Angle=50 degree Flux/Group

0.0	0.0	0.0	0.0	2.9960E-05	1.0799E-03
2.0287E-01	4.2829E-01	3.4188E-01	3.1311E-02	2.8746E-03	1.4187E-03
1.0827E-03	9.3500E-04	8.0656E-04	8.5483E-04	9.4226E-04	7.7785E-04
4.7988E-04	3.3737E-04	2.8232E-04	2.6826E-04	2.2865E-04	2.3055E-04
2.2224E-04	1.9600E-04	1.8977E-04	2.0760E-04	2.2084E-04	2.0433E-04
1.8394E-04	1.9514E-04	7.3193E-04	7.6984E-04	9.0637E-04	9.0276E-04
9.5760E-04	1.0159E-03	1.0244E-03	1.0765E-03	1.0786E-03	1.1123E-03
1.1828E-03	1.3297E-03	1.3569E-03	1.4346E-03	1.4856E-03	1.5516E-03
1.5901E-03	1.6960E-03	1.6715E-03	1.7349E-03	1.7403E-03	1.7009E-03
1.7139E-03	1.6615E-03	1.5935E-03	1.5962E-03	1.6924E-03	1.6419E-03
3.0607E-03	3.3648E-03	3.2370E-03	3.0458E-03	3.0329E-03	3.0235E-03
2.9858E-03	2.7584E-03	2.5523E-03	2.4249E-03	2.1785E-03	1.9525E-03
1.8354E-03	1.6336E-03	1.4832E-03	1.3306E-03	1.1709E-03	1.0042E-03
8.7870E-04	7.5714E-04	6.8492E-04	6.2603E-04	5.1249E-04	2.9945E-04
2.2841E-04	1.9410E-04	1.7445E-04	1.5113E-04	1.2869E-04	1.1623E-04
1.0409E-04	9.4238E-05	8.6824E-05	7.7165E-05	7.4482E-05	5.7007E-05
9.1044E-05	7.2310E-05	6.3841E-05	4.5727E-05	4.5969E-05	3.2256E-05
2.3603E-05	1.7262E-05	2.1740E-05	2.3276E-05	1.5754E-05	1.6049E-05
2.4448E-05	8.9675E-06	6.5154E-06	8.4586E-06	1.3307E-06	4.0630E-07
2.6942E-07	2.3497E-07	1.7611E-07	1.0784E-07	6.5000E-08	3.9156E-08
2.3556E-08	1.4243E-08	8.3154E-09	4.8047E-09	8.0264E-09	

No.28 Angle=45 degree Flux/Group

0.0	0.0	0.0	0.0	5.9828E-05	3.1221E-02
2.6880E-01	4.4411E-01	2.6127E-01	8.6141E-03	2.3038E-03	1.3610E-03
1.1030E-03	8.9468E-04	7.4529E-04	8.1224E-04	9.1756E-04	7.7524E-04
4.7823E-04	3.0710E-04	2.6233E-04	2.4956E-04	2.2194E-04	2.0771E-04
2.0422E-04	1.7785E-04	1.7364E-04	1.9002E-04	2.0733E-04	1.8931E-04
1.7044E-04	1.7926E-04	6.8096E-04	7.4221E-04	9.0116E-04	8.9378E-04
9.5723E-04	1.0062E-03	1.0498E-03	1.0997E-03	1.0933E-03	1.1347E-03
1.1933E-03	1.3269E-03	1.3579E-03	1.4277E-03	1.4841E-03	1.5452E-03
1.5858E-03	1.6852E-03	1.6446E-03	1.7124E-03	1.7103E-03	1.6780E-03
1.6951E-03	1.6444E-03	1.5752E-03	1.5845E-03	1.6794E-03	1.6312E-03
3.0316E-03	3.3351E-03	3.2137E-03	3.0248E-03	3.0167E-03	2.9925E-03
2.9527E-03	2.7297E-03	2.5412E-03	2.4071E-03	2.1436E-03	1.9214E-03
1.8109E-03	1.6221E-03	1.4795E-03	1.3335E-03	1.1622E-03	9.9937E-04
8.7974E-04	7.6241E-04	6.9005E-04	6.1246E-04	4.9454E-04	2.9491E-04
2.3394E-04	1.9833E-04	1.7511E-04	1.4793E-04	1.2522E-04	1.1638E-04
1.0237E-04	9.5500E-05	8.6911E-05	8.0443E-05	7.8750E-05	5.7068E-05
8.3543E-05	7.4430E-05	6.7446E-05	5.1181E-05	4.6957E-05	3.1365E-05
2.3033E-05	1.6642E-05	2.0401E-05	2.0789E-05	1.5248E-05	1.2511E-05
2.5409E-05	9.0416E-06	6.0714E-06	9.0294E-06	2.6953E-06	9.3249E-07
2.5819E-07	1.7280E-07	1.3520E-07	8.3016E-08	5.0045E-08	3.0050E-08
1.8023E-08	1.0855E-08	6.3268E-09	3.6719E-09	6.0908E-09	

No.29 Angle=40 degree Flux/Group

0.0	0.0	0.0	0.0	1.3996E-04	1.0331E-01
2.8163E-01	4.6378E-01	1.6850E-01	7.1715E-03	1.9089E-03	1.3190E-03
1.1338E-03	8.5898E-04	6.9993E-04	7.8126E-04	8.9814E-04	7.6692E-04
4.7796E-04	2.9565E-04	2.5043E-04	2.4040E-04	2.1936E-04	1.9152E-04
1.9310E-04	1.6345E-04	1.6161E-04	1.7706E-04	1.9853E-04	1.7757E-04
1.5871E-04	1.7462E-04	6.4380E-04	7.1504E-04	8.6012E-04	8.5586E-04
9.2161E-04	9.7908E-04	1.0783E-03	1.1219E-03	1.1054E-03	1.1444E-03
1.1942E-03	1.3285E-03	1.3615E-03	1.4330E-03	1.4852E-03	1.5481E-03
1.5741E-03	1.6717E-03	1.6370E-03	1.6978E-03	1.6889E-03	1.6592E-03
1.6804E-03	1.6353E-03	1.5566E-03	1.5768E-03	1.6708E-03	1.6243E-03
3.0117E-03	3.3042E-03	3.1761E-03	2.9987E-03	2.9907E-03	2.9598E-03
2.9280E-03	2.7098E-03	2.5171E-03	2.3856E-03	2.1321E-03	1.9087E-03
1.8036E-03	1.6182E-03	1.4688E-03	1.3150E-03	1.1414E-03	9.7603E-04
8.6670E-04	7.7426E-04	6.9665E-04	6.0340E-04	4.8056E-04	2.8773E-04
2.3921E-04	2.0155E-04	1.7450E-04	1.5123E-04	1.2805E-04	1.1154E-04
9.3509E-05	8.7624E-05	8.4361E-05	8.2482E-05	8.0636E-05	5.8733E-05
9.2101E-05	7.4686E-05	6.7448E-05	4.8317E-05	4.7162E-05	3.4191E-05
2.3325E-05	1.7143E-05	2.0718E-05	2.1674E-05	1.3023E-05	1.2117E-05
2.4798E-05	1.3958E-05	6.1917E-06	8.2243E-06	2.4272E-06	8.3598E-07
2.0562E-07	2.0224E-07	1.5484E-07	9.4669E-08	5.7097E-08	3.4255E-08
2.0626E-08	1.2315E-08	7.1074E-09	4.0827E-09	6.8717E-09	

No.30 Angle=35 degree Flux/Group

0.0	0.0	0.0	0.0	4.1913E-04	1.5996E-01
3.0105E-01	4.3809E-01	1.1940E-01	6.4152E-03	1.6222E-03	1.3283E-03
1.1491E-03	8.1603E-04	6.8095E-04	7.4528E-04	8.9898E-04	7.6990E-04
4.7809E-04	2.9282E-04	2.4285E-04	2.3599E-04	2.0814E-04	1.7588E-04
1.7058E-04	1.5014E-04	1.4986E-04	1.6306E-04	1.8668E-04	1.6549E-04
1.4603E-04	1.6300E-04	5.9247E-04	6.9080E-04	8.1929E-04	8.1899E-04
8.9359E-04	9.4978E-04	1.0647E-03	1.0973E-03	1.0853E-03	1.1233E-03
1.1846E-03	1.3391E-03	1.3924E-03	1.4501E-03	1.5003E-03	1.5621E-03
1.5794E-03	1.6683E-03	1.6326E-03	1.6905E-03	1.6764E-03	1.6491E-03
1.6659E-03	1.6197E-03	1.5347E-03	1.5594E-03	1.6564E-03	1.6091E-03
2.9835E-03	3.2754E-03	3.1564E-03	2.9920E-03	2.9681E-03	2.9339E-03
2.9043E-03	2.6837E-03	2.4896E-03	2.3512E-03	2.1032E-03	1.8944E-03
1.7980E-03	1.6152E-03	1.4551E-03	1.2959E-03	1.1272E-03	9.6810E-04
8.5145E-04	7.4843E-04	6.8634E-04	6.0530E-04	4.8117E-04	2.8667E-04
2.3559E-04	2.0274E-04	1.7747E-04	1.5195E-04	1.2465E-04	1.0979E-04
9.5892E-05	8.3639E-05	7.6711E-05	7.8702E-05	8.0279E-05	6.3120E-05
1.0108E-04	7.9701E-05	6.9887E-05	4.6751E-05	3.9903E-05	3.0345E-05
2.4885E-05	2.1616E-05	2.0341E-05	2.4461E-05	1.3215E-05	8.7597E-06
2.2180E-05	9.7950E-06	7.7113E-06	8.9265E-06	3.5902E-06	1.1282E-06
3.5944E-07	1.5413E-07	1.1587E-07	7.1016E-08	4.2723E-08	2.5589E-08
1.5301E-08	8.8523E-09	5.1182E-09	2.8637E-09	4.8088E-09	

No.31 Angle=30 degree Flux/Group

0.0	0.0	0.0	0.0	5.7086E-03	2.0313E-01
3.4256E-01	3.5342E-01	1.1747E-01	6.0931E-03	1.4287E-03	1.4204E-03
1.1384E-03	7.7202E-04	6.7450E-04	7.2070E-04	8.9082E-04	7.7423E-04
4.7798E-04	2.8679E-04	2.3616E-04	2.3275E-04	2.0146E-04	1.6525E-04
1.6174E-04	1.4281E-04	1.4237E-04	1.5778E-04	1.7932E-04	1.5983E-04
1.3940E-04	1.5677E-04	5.6929E-04	6.6617E-04	7.8352E-04	7.8659E-04
8.5941E-04	9.2590E-04	1.0342E-03	1.0732E-03	1.0652E-03	1.0973E-03
1.1479E-03	1.3096E-03	1.3893E-03	1.4300E-03	1.4801E-03	1.5339E-03
1.5829E-03	1.6731E-03	1.6451E-03	1.7007E-03	1.6850E-03	1.6530E-03
1.6677E-03	1.6241E-03	1.5243E-03	1.5507E-03	1.6476E-03	1.5910E-03
2.9444E-03	3.2511E-03	3.1372E-03	2.9650E-03	2.9302E-03	2.8942E-03
2.8695E-03	2.6609E-03	2.4700E-03	2.3426E-03	2.1016E-03	1.8753E-03
1.7698E-03	1.5920E-03	1.4435E-03	1.2843E-03	1.1163E-03	9.5419E-04
8.3201E-04	7.2743E-04	6.7339E-04	5.9617E-04	4.7903E-04	2.8857E-04
2.3697E-04	2.0056E-04	1.7503E-04	1.5399E-04	1.2891E-04	1.1010E-04
9.7865E-05	8.9814E-05	8.0720E-05	7.8833E-05	7.6789E-05	5.9752E-05
8.7582E-05	7.5921E-05	7.3410E-05	4.8773E-05	4.0289E-05	3.0871E-05
2.7906E-05	2.9608E-05	2.0883E-05	1.9881E-05	1.0227E-05	6.9839E-06
2.1185E-05	9.5356E-06	4.9158E-06	8.7448E-06	4.6806E-06	1.2961E-06
8.3175E-07	3.8999E-07	1.7327E-07	6.5953E-08	3.9684E-08	2.3774E-08
1.4209E-08	8.1587E-09	4.7467E-09	2.6400E-09	4.5597E-09	

No.32 Angle=25 degree Flux/Group

0.0	0.0	0.0	0.0	3.8666E-02	2.2939E-01
3.3095E-01	3.3021E-01	9.3995E-02	5.7748E-03	1.3284E-03	1.5651E-03
1.1285E-03	7.3454E-04	6.8679E-04	7.1726E-04	8.8338E-04	7.8329E-04
4.9505E-04	2.8394E-04	2.3034E-04	2.1753E-04	1.9359E-04	1.5405E-04
1.4901E-04	1.3575E-04	1.3328E-04	1.4897E-04	1.6912E-04	1.5314E-04
1.3019E-04	1.5184E-04	5.4781E-04	6.4799E-04	7.5490E-04	7.5899E-04
8.3096E-04	9.1007E-04	1.0036E-03	1.0466E-03	1.0406E-03	1.0637E-03
1.1182E-03	1.2864E-03	1.3749E-03	1.4145E-03	1.4632E-03	1.5146E-03
1.5819E-03	1.6683E-03	1.6411E-03	1.6883E-03	1.6725E-03	1.6440E-03
1.6606E-03	1.6219E-03	1.5220E-03	1.5454E-03	1.6419E-03	1.5849E-03
2.9275E-03	3.2433E-03	3.1182E-03	2.9351E-03	2.9160E-03	2.8715E-03
2.8305E-03	2.6224E-03	2.4450E-03	2.3252E-03	2.0954E-03	1.8628E-03
1.7558E-03	1.5741E-03	1.4265E-03	1.2648E-03	1.1047E-03	9.5547E-04
8.3558E-04	7.2603E-04	6.5534E-04	5.7904E-04	4.7082E-04	2.7838E-04
2.2548E-04	1.9047E-04	1.7006E-04	1.5598E-04	1.3475E-04	1.1748E-04
1.0489E-04	9.0442E-05	8.1647E-05	7.7728E-05	7.5620E-05	5.6844E-05
8.9702E-05	8.0144E-05	6.8059E-05	4.5187E-05	4.1228E-05	3.0566E-05
2.3431E-05	2.2742E-05	2.1660E-05	2.0622E-05	1.1209E-05	8.4085E-06
1.7808E-05	1.0298E-05	5.2494E-06	8.2153E-06	3.5754E-06	1.5450E-06
8.7961E-07	4.7170E-07	2.2520E-07	9.7260E-08	5.8581E-08	3.5205E-08
2.1067E-08	1.2426E-08	7.2480E-09	4.1349E-09	7.0998E-09	

No.33 Angle=20 degree Flux/Group

0.0	0.0	0.0	0.0	7.6544E-02	2.2132E-01
3.1814E-01	3.8291E-01	3.4905E-02	5.8395E-03	1.2750E-03	1.7827E-03
1.1025E-03	6.8570E-04	6.8120E-04	7.3260E-04	8.7682E-04	7.9218E-04
5.0512E-04	2.8311E-04	2.1602E-04	2.2385E-04	1.9659E-04	1.5251E-04
1.4793E-04	1.3661E-04	1.3285E-04	1.5120E-04	1.7352E-04	1.5529E-04
1.3504E-04	1.5183E-04	5.4516E-04	6.1833E-04	7.1022E-04	7.2093E-04
7.9448E-04	8.9578E-04	9.8190E-04	1.0184E-03	1.0287E-03	1.0290E-03
1.0924E-03	1.2622E-03	1.3534E-03	1.3981E-03	1.4492E-03	1.4955E-03
1.5684E-03	1.6488E-03	1.6149E-03	1.6691E-03	1.6561E-03	1.6225E-03
1.6345E-03	1.6064E-03	1.5180E-03	1.5344E-03	1.6301E-03	1.5749E-03
2.9180E-03	3.2297E-03	3.0938E-03	2.9176E-03	2.9116E-03	2.8641E-03
2.8057E-03	2.6012E-03	2.4296E-03	2.3015E-03	2.0661E-03	1.8448E-03
1.7446E-03	1.5571E-03	1.4156E-03	1.2644E-03	1.1025E-03	9.3544E-04
8.1769E-04	7.1642E-04	6.4228E-04	5.6621E-04	4.5696E-04	2.7154E-04
2.3180E-04	1.9441E-04	1.7134E-04	1.5510E-04	1.3729E-04	1.2175E-04
1.0496E-04	8.5439E-05	7.7958E-05	7.7721E-05	7.3330E-05	5.3915E-05
9.8865E-05	7.0046E-05	6.6897E-05	4.5110E-05	4.3305E-05	3.3620E-05
2.5810E-05	1.9527E-05	1.8963E-05	1.9758E-05	1.2475E-05	9.2707E-06
1.8139E-05	1.1218E-05	5.3872E-06	6.1711E-06	2.0929E-06	1.4805E-06
1.1278E-06	6.5364E-07	3.3031E-07	1.5163E-07	9.0138E-08	5.4359E-08
3.2685E-08	1.9477E-08	1.1495E-08	6.7662E-09	1.1124E-08	

No.34 Angle=15 degree Flux/Group

0.0	0.0	0.0	0.0	9.1941E-02	2.6806E-01
3.5410E-01	2.8455E-01	3.2023E-02	4.8461E-03	1.2358E-03	2.0603E-03
1.0759E-03	6.7031E-04	6.6643E-04	7.3884E-04	8.9195E-04	7.9234E-04
5.2071E-04	2.8768E-04	2.0132E-04	2.2158E-04	1.9788E-04	1.4742E-04
1.4473E-04	1.3321E-04	1.2870E-04	1.5005E-04	1.7026E-04	1.5342E-04
1.3192E-04	1.4871E-04	5.3126E-04	6.0732E-04	6.9376E-04	7.0117E-04
7.7627E-04	8.9176E-04	9.6989E-04	9.9074E-04	1.0226E-03	1.0021E-03
1.0707E-03	1.2298E-03	1.3213E-03	1.3779E-03	1.4275E-03	1.4615E-03
1.5526E-03	1.6304E-03	1.5927E-03	1.6467E-03	1.6342E-03	1.5957E-03
1.6134E-03	1.5853E-03	1.5077E-03	1.5228E-03	1.6144E-03	1.5653E-03
2.9025E-03	3.2096E-03	3.0809E-03	2.9141E-03	2.8996E-03	2.8396E-03
2.7857E-03	2.5861E-03	2.4237E-03	2.2855E-03	2.0432E-03	1.8232E-03
1.7259E-03	1.5415E-03	1.4042E-03	1.2598E-03	1.0975E-03	9.2556E-04
8.0663E-04	7.0323E-04	6.2446E-04	5.6185E-04	4.5837E-04	2.6533E-04
2.2894E-04	1.9414E-04	1.7044E-04	1.5106E-04	1.3568E-04	1.2392E-04
1.0823E-04	8.4122E-05	7.4565E-05	7.3861E-05	7.2207E-05	5.2297E-05
9.5607E-05	6.7757E-05	6.2308E-05	4.4581E-05	4.7764E-05	3.4515E-05
2.5261E-05	1.7102E-05	1.5735E-05	1.8448E-05	1.2361E-05	1.0694E-05
1.9815E-05	1.1722E-05	7.1133E-06	6.4887E-06	1.8255E-06	1.0600E-06
9.2490E-07	6.6269E-07	4.1861E-07	2.0459E-07	1.2210E-07	7.3560E-08
4.4279E-08	2.6361E-08	1.5602E-08	9.1799E-09	1.5191E-08	

No.35 Angle=10 degree Flux/Group

0.0	0.0	0.0	0.0	1.1642E-01	2.4857E-01
3.7951E-01	2.5645E-01	3.1773E-02	5.0555E-03	1.1759E-03	2.3546E-03
1.0686E-03	6.6974E-04	6.5115E-04	7.2396E-04	9.2523E-04	8.2654E-04
5.2118E-04	2.7361E-04	2.0154E-04	2.2045E-04	1.9246E-04	1.4187E-04
1.3708E-04	1.2634E-04	1.2305E-04	1.4648E-04	1.6297E-04	1.4879E-04
1.2701E-04	1.4336E-04	5.1024E-04	5.9242E-04	6.7615E-04	6.8078E-04
7.5623E-04	8.8024E-04	9.5945E-04	9.7981E-04	1.0240E-03	9.9095E-04
1.0535E-03	1.2090E-03	1.2945E-03	1.3748E-03	1.4029E-03	1.4366E-03
1.5434E-03	1.6300E-03	1.5819E-03	1.6339E-03	1.6272E-03	1.5797E-03
1.6010E-03	1.5715E-03	1.5045E-03	1.5171E-03	1.6040E-03	1.5597E-03
2.8824E-03	3.1881E-03	3.0645E-03	2.9009E-03	2.8743E-03	2.8130E-03
2.7800E-03	2.5844E-03	2.4068E-03	2.2711E-03	2.0330E-03	1.8064E-03
1.7137E-03	1.5327E-03	1.3928E-03	1.2488E-03	1.0872E-03	9.1786E-04
8.0149E-04	7.0332E-04	6.3267E-04	5.7016E-04	4.5988E-04	2.5871E-04
2.2756E-04	1.9569E-04	1.6185E-04	1.4402E-04	1.3226E-04	1.2078E-04
1.0637E-04	8.5644E-05	7.3601E-05	7.2192E-05	7.0134E-05	5.1037E-05
8.9122E-05	6.9435E-05	6.3116E-05	4.7055E-05	4.7573E-05	3.1909E-05
2.5920E-05	1.8250E-05	1.6779E-05	1.7771E-05	9.5596E-06	8.6683E-06
2.3414E-05	1.2816E-05	7.3184E-06	7.6131E-06	1.4451E-06	7.4222E-07
3.5597E-07	1.8033E-07	1.8698E-07	2.3515E-07	2.0601E-07	1.2793E-07
7.7138E-08	4.6172E-08	2.7579E-08	1.6328E-08	2.6362E-08	

No.36 Angle=5 degree Flux/Group

0.0	0.0	0.0	0.0	1.4266E-01	2.2369E-01
4.0507E-01	2.3227E-01	3.1489E-02	5.3793E-03	1.1292E-03	2.5848E-03
1.0645E-03	6.4579E-04	6.5864E-04	7.1080E-04	9.4891E-04	8.6205E-04
5.2667E-04	2.5473E-04	2.0836E-04	2.1582E-04	1.8610E-04	1.3986E-04
1.3221E-04	1.2093E-04	1.2374E-04	1.4268E-04	1.5861E-04	1.4520E-04
1.2411E-04	1.3578E-04	4.9796E-04	6.0630E-04	6.8574E-04	6.8783E-04
7.5621E-04	8.7105E-04	9.4153E-04	9.6907E-04	1.0076E-03	9.8066E-04
1.0426E-03	1.2051E-03	1.2847E-03	1.3882E-03	1.3985E-03	1.4358E-03
1.5403E-03	1.6277E-03	1.5742E-03	1.6337E-03	1.6307E-03	1.5723E-03
1.5991E-03	1.5654E-03	1.5048E-03	1.5144E-03	1.5942E-03	1.5624E-03
2.8944E-03	3.2043E-03	3.0698E-03	2.8950E-03	2.8734E-03	2.8135E-03
2.7915E-03	2.5905E-03	2.4036E-03	2.2680E-03	2.0441E-03	1.8205E-03
1.7223E-03	1.5388E-03	1.3907E-03	1.2428E-03	1.0760E-03	9.2398E-04
8.1254E-04	7.1105E-04	6.4340E-04	5.7403E-04	4.5807E-04	2.5445E-04
2.2634E-04	2.0022E-04	1.6712E-04	1.4737E-04	1.3227E-04	1.1642E-04
9.7519E-05	8.0751E-05	7.2335E-05	7.2465E-05	7.1767E-05	5.1826E-05
9.0182E-05	7.0994E-05	6.2513E-05	4.8815E-05	4.4413E-05	3.0197E-05
2.8196E-05	1.9477E-05	1.7146E-05	1.7372E-05	9.2661E-06	8.5143E-06
2.2875E-05	1.2712E-05	6.8685E-06	7.6081E-06	2.3506E-06	7.9421E-07
7.6540E-07	6.7491E-07	3.9386E-07	2.0421E-07	6.3820E-08	3.6800E-08
2.1770E-08	1.2588E-08	7.1652E-09	3.9247E-09	6.9538E-09	

No.37 Angle=0 degree Flux/Group

0.0	0.0	0.0	0.0	1.4276E-01	2.2368E-01
4.0519E-01	2.3206E-01	3.1364E-02	5.3721E-03	1.1067E-03	2.6708E-03
1.0556E-03	6.4016E-04	6.5564E-04	7.0786E-04	9.5418E-04	8.7356E-04
5.2460E-04	2.4759E-04	2.0933E-04	2.1838E-04	1.8675E-04	1.4421E-04
1.3431E-04	1.2190E-04	1.2642E-04	1.4100E-04	1.5964E-04	1.4779E-04
1.2673E-04	1.3230E-04	4.9914E-04	5.9420E-04	6.7795E-04	6.8043E-04
7.4273E-04	8.5947E-04	9.3079E-04	9.6374E-04	1.0082E-03	9.7555E-04
1.0459E-03	1.2120E-03	1.2893E-03	1.3989E-03	1.3949E-03	1.4353E-03
1.5248E-03	1.6310E-03	1.5700E-03	1.6284E-03	1.6304E-03	1.5676E-03
1.5963E-03	1.5660E-03	1.5070E-03	1.5116E-03	1.5890E-03	1.5658E-03
2.8900E-03	3.1949E-03	3.0651E-03	2.9025E-03	2.8823E-03	2.8147E-03
2.7917E-03	2.5861E-03	2.4082E-03	2.2762E-03	2.0587E-03	1.8216E-03
1.7222E-03	1.5293E-03	1.3852E-03	1.2447E-03	1.0821E-03	9.4058E-04
8.2187E-04	7.0538E-04	6.3363E-04	5.7113E-04	4.6877E-04	2.6606E-04
2.2815E-04	1.9156E-04	1.6297E-04	1.4476E-04	1.2221E-04	1.0639E-04
9.7926E-05	8.0374E-05	6.9982E-05	6.6729E-05	6.6152E-05	5.3031E-05
1.0042E-04	7.6437E-05	7.0560E-05	4.7636E-05	3.9790E-05	2.7772E-05
2.6856E-05	1.9386E-05	1.8523E-05	1.9948E-05	1.1482E-05	9.8805E-06
1.9937E-05	1.0053E-05	6.7864E-06	6.9047E-06	2.0054E-06	1.3301E-06
1.1166E-06	8.5386E-07	4.0943E-07	2.1118E-07	6.9261E-08	3.9982E-08
2.3521E-08	1.3766E-08	7.9062E-09	4.4338E-09	7.5075E-09	

Appendix 2: Neutron Spectra for the Fixed Source Measured by PRC

A proton recoil proportional counter was also applied to measure the low energy spectrum at 300 mm from the target line with a 100 mm step mode. The ramp mode high voltage supply techniques[42] was developed for this method and its technical detail is described later. The measurement was performed in a stationary mode, i.e., for a point source and along the axis at a distance of 300 mm from the line source axis. The detector was placed at the center of the assembly for the case with the reference test blanket assembly. The measured results are shown in Fig. A.2.2-10 and listed in Table A.2.1-9 at the center and at the 500 mm forward and backward to the source. There is no significant difference in spectrum shape but the flux is slightly larger for the forward.

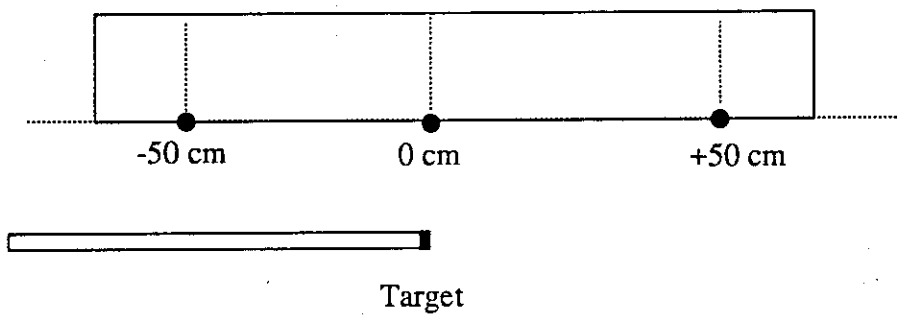

Fig. A.2.1 Relative position of the detector to the target

Table A.2.1 Measured neutron flux by the PRC spectrometer at a distance of 300 mm from the line source axis (at a position of 0 mm from the position closest to the source on the 300 mm axis)

J	Energy [keV]	Flux	Flux Error[%]	J	Energy [keV]	Flux	Flux Error[%]	J	Energy [keV]	Flux	Flux Error[%]	J	Energy [keV]	Flux	Flux Error[%]
1	2.85	5.609E-07	59.0	34	12.27	1.717E-07	97.3	66	53.95	4.842E-07	52.3	98	243.80	2.560E-06	29.2
2	2.97	3.012E-07	102.6	35	12.85	-5.347E-09	-3123.2	67	56.52	2.761E-07	91.6	99	255.49	2.616E-06	28.5
3	3.10	-9.511E-08	-312.3	36	13.45	6.501E-08	264.6	68	59.22	2.829E-07	91.9	100	267.73	2.695E-06	27.5
4	3.23	1.134E-07	262.8	37	14.08	-2.510E-08	-689.2	69	62.05	2.521E-07	104.7	101	280.57	2.335E-06	32.0
5	3.37	4.843E-07	57.6	38	14.74	-9.025E-08	-198.3	70	65.01	5.246E-07	51.8	102	294.02	2.291E-07	329.6
6	3.52	5.654E-07	48.3	39	15.43	3.017E-08	616.5	71	68.12	3.206E-08	867.1	103	308.11	3.474E-06	22.0
7	3.68	3.529E-07	71.7	40	16.16	3.483E-07	52.8	72	71.37	1.898E-08	1496.3	104	322.89	5.639E-06	13.6
8	3.84	2.663E-07	90.9	41	16.92	4.456E-08	430.9	73	74.78	6.487E-07	44.7	105	338.37	6.917E-06	10.9
9	4.01	2.530E-08	976.3	42	17.72	2.790E-08	673.8	74	78.36	-6.455E-08	-460.1	106	354.59	6.199E-06	12.2
10	4.19	2.032E-07	114.2	43	18.55	5.076E-07	38.0	75	82.10	-2.016E-07	-153.8	107	371.59	5.524E-06	13.6
11	4.37	3.463E-07	67.3	44	19.43	4.319E-07	44.5	76	86.03	6.583E-07	48.3	108	389.41	6.461E-06	11.7
12	4.57	4.591E-07	48.1	45	20.35	2.432E-07	78.1	77	90.14	5.899E-07	55.4	109	408.09	6.760E-06	11.1
13	4.77	7.160E-08	304.5	46	21.31	1.545E-07	124.9	78	94.45	9.035E-07	36.3	110	427.66	8.109E-06	9.3
14	4.99	3.457E-07	60.5	47	22.32	2.619E-07	74.5	79	98.97	8.958E-07	37.2	111	448.17	9.014E-06	8.3
15	5.21	3.558E-07	58.2	48	23.37	1.148E-07	169.9	80	103.71	5.386E-07	62.9	112	469.66	8.002E-06	9.3
16	5.45	4.606E-07	42.6	49	24.48	7.279E-07	27.1	81	108.67	4.451E-07	77.5	113	492.18	9.269E-06	8.0
17	5.70	3.701E-07	51.9	50	25.64	4.948E-07	39.6	82	113.87	4.848E-07	74.5	114	515.79	1.113E-05	6.6
18	5.95	1.166E-07	160.4	51	26.86	-1.518E-07	-131.1	83	119.32	9.176E-07	41.2	115	540.53	1.206E-05	6.1
19	6.23	8.810E-08	210.0	52	28.13	1.966E-07	101.7	84	125.03	7.786E-07	50.0	116	566.46	1.317E-05	5.5
20	6.51	4.602E-07	39.8	53	29.47	3.659E-07	56.3	85	131.02	1.417E-06	28.6	117	593.63	1.337E-05	5.3
21	6.81	3.281E-07	53.0	54	30.87	2.464E-07	83.6	86	137.29	9.070E-07	45.6	118	622.10	1.389E-05	5.1
22	7.12	1.889E-07	91.6	55	32.33	1.864E-07	113.7	87	143.87	6.985E-07	62.1	119	651.94	1.724E-05	4.1
23	7.45	4.794E-07	34.6	56	33.87	5.310E-08	404.9	88	150.76	1.161E-06	38.8	120	683.22	1.880E-05	3.8
24	7.79	1.216E-07	140.6	57	35.48	8.352E-08	265.8	89	157.98	1.295E-06	36.4	121	715.99	1.858E-05	3.7
25	8.15	-1.559E-08	-1071.2	58	37.17	2.293E-07	96.4	90	165.55	1.298E-06	37.6	122	750.34	1.893E-05	3.6
26	8.53	4.205E-07	41.1	59	38.94	7.822E-07	28.8	91	173.48	9.662E-07	52.5	123	786.33	1.714E-05	3.8
27	8.92	1.675E-07	99.7	60	40.79	1.837E-07	123.6	92	181.79	1.166E-06	44.9	124	824.05	1.522E-05	4.1
28	9.34	1.184E-07	146.1	61	42.74	1.870E-07	123.0	93	190.50	8.980E-07	62.7	125	863.59	1.254E-05	4.9
29	9.77	1.106E-07	153.7	62	44.78	3.176E-07	74.3	94	202.17	1.205E-06	63.5	126	905.02	1.074E-05	5.5
30	10.22	2.920E-07	58.9	63	46.91	-9.173E-08	-264.9	95	211.86	1.162E-06	65.2	127	948.43	1.183E-05	4.8
31	10.70	2.245E-07	76.6	64	49.15	4.369E-07	56.1	96	222.01	1.102E-06	68.5	128	993.93	1.208E-05	4.4
32	11.20	4.460E-07	38.1	65	51.49	6.787E-07	36.7	97	232.65	1.603E-06	47.0	129	1041.62	1.170E-05	4.3
33	11.72	4.654E-07	36.1												

* Flux Unit: [n/cm^2/Lethargy/Source]

Table A.2.2 Measured neutron flux by the PRC spectrometer at a distance of 300 mm from the line source axis (at a position of 500 mm backward from the position closest to the source on the 300 mm axis)

J	Energy [keV]	Flux	Flux Error[%]	J	Energy [keV]	Flux	Flux Error[%]	J	Energy [keV]	Flux	Flux Error[%]	J	Energy [keV]	Flux	Flux Error[%]
1	2.89	4.092E-08	155.9	34	12.46	1.507E-07	29.1	66	54.79	1.356E-07	47.6	98	241.09	5.377E-07	33.1
2	3.01	-1.818E-08	-352.6	35	13.04	8.651E-08	50.4	67	57.41	1.216E-07	54.3	99	252.65	3.160E-07	55.1
3	3.14	-7.323E-08	-86.4	36	13.65	-2.240E-08	-196.0	68	60.15	1.195E-07	56.1	100	264.76	5.696E-07	30.9
4	3.28	-8.709E-08	-71.8	37	14.30	-5.311E-08	-86.0	69	63.02	1.125E-07	60.8	101	277.45	6.898E-07	25.5
5	3.42	-2.925E-08	-217.1	38	14.97	3.028E-09	1542.3	70	66.03	2.566E-07	27.0	102	290.75	9.015E-07	19.4
6	3.57	3.782E-08	163.4	39	15.67	4.485E-08	106.4	71	69.18	2.688E-07	26.1	103	304.69	9.326E-07	18.9
7	3.73	4.802E-08	127.4	40	16.41	6.513E-08	74.6	72	72.49	9.209E-08	76.8	104	319.30	1.179E-06	14.9
8	3.89	7.216E-08	81.3	41	17.18	8.308E-08	58.0	73	75.96	1.430E-07	50.6	105	334.61	1.306E-06	13.4
9	4.07	1.630E-07	34.8	42	17.99	1.526E-07	31.8	74	79.59	2.155E-07	34.1	106	350.65	8.794E-07	19.9
10	4.25	-3.808E-08	-149.2	43	18.84	7.583E-08	64.6	75	83.39	2.126E-07	35.0	107	367.46	9.430E-07	18.6
11	4.44	3.891E-08	138.8	44	19.73	6.550E-08	75.4	76	87.38	1.969E-07	38.5	108	385.08	1.321E-06	13.3
12	4.64	5.185E-08	106.5	45	20.66	9.255E-08	52.9	77	91.56	2.302E-08	333.6	109	403.55	1.714E-06	10.3
13	4.84	1.341E-07	38.8	46	21.64	1.359E-07	36.8	78	95.94	1.150E-07	69.5	110	422.90	1.752E-06	10.0
14	5.06	1.077E-07	47.8	47	22.66	1.518E-07	32.1	79	100.53	1.656E-07	49.5	111	443.18	2.062E-06	8.5
15	5.29	4.720E-08	104.4	48	23.74	6.270E-08	80.4	80	105.34	1.192E-07	70.1	112	464.44	1.926E-06	9.0
16	5.53	1.001E-07	49.0	49	24.86	4.124E-08	120.8	81	110.38	2.235E-07	38.8	113	486.71	2.037E-06	8.5
17	5.78	7.796E-08	61.4	50	26.04	8.710E-08	58.7	82	115.66	2.788E-07	32.2	114	510.05	2.147E-06	8.1
18	6.04	9.661E-08	47.9	51	27.28	1.223E-07	42.0	83	121.20	2.489E-07	37.3	115	534.52	2.871E-06	6.0
19	6.32	1.127E-07	40.9	52	28.57	7.844E-08	66.5	84	127.00	1.133E-07	85.9	116	560.16	3.715E-06	4.5
20	6.61	4.473E-08	98.8	53	29.93	6.852E-08	76.2	85	133.08	1.547E-07	66.6	117	587.02	4.293E-06	3.8
21	6.91	1.078E-07	40.5	54	31.35	6.039E-08	88.8	86	139.45	3.035E-07	34.6	118	615.18	4.022E-06	4.0
22	7.23	7.052E-08	62.5	55	32.84	7.411E-08	72.5	87	146.13	3.984E-07	27.9	119	644.69	4.220E-06	3.7
23	7.56	3.051E-08	139.0	56	34.40	1.530E-07	35.8	88	153.13	3.668E-07	31.4	120	675.61	4.317E-06	3.6
24	7.91	5.640E-08	77.7	57	36.04	7.931E-08	70.1	89	160.46	4.313E-07	27.8	121	708.02	3.828E-06	4.0
25	8.27	7.310E-08	59.2	58	37.75	9.973E-08	56.0	90	168.15	3.614E-07	34.0	122	741.99	3.554E-06	4.2
26	8.66	8.677E-08	50.7	59	39.55	9.851E-08	58.3	91	176.20	6.044E-07	21.3	123	777.58	3.500E-06	4.2
27	9.06	4.907E-09	886.5	60	41.43	-1.933E-08	-302.1	92	184.65	8.254E-07	16.0	124	814.88	2.911E-06	4.8
28	9.48	1.261E-07	35.1	61	43.41	8.910E-08	66.3	93	193.49	2.560E-07	53.5	125	853.98	2.848E-06	4.9
29	9.92	1.247E-07	35.0	62	45.48	7.235E-08	84.9	94	199.92	3.342E-07	56.0	126	894.95	2.367E-06	5.7
30	10.38	6.713E-08	64.7	63	47.64	6.307E-08	97.7	95	209.50	7.510E-07	24.1	127	937.88	2.547E-06	5.2
31	10.86	6.801E-08	64.4	64	49.92	1.065E-07	59.0	96	219.54	7.334E-07	24.3	128	982.88	2.279E-06	5.7
32	11.37	5.650E-08	78.2	65	52.30	1.918E-07	33.6	97	230.06	4.233E-07	41.3	129	1030.03	1.656E-06	7.5
33	11.90	7.207E-08	61.6												

* Flux Unit: [n/cm^2/Lethargy/Source]

Table A.2.3 Measured neutron flux by the PRC spectrometer at a distance of 300 mm from the line source axis (at a position of 500 mm forward from the position closest to the source on the 300 mm axis)

J	Energy [keV]	Flux	Flux Error[%]	J	Energy [keV]	Flux	Flux Error[%]	J	Energy [keV]	Flux	Flux Error[%]	J	Energy [keV]	Flux	Flux Error[%]
1	2.89	2.822E-08	284.9	34	12.46	2.308E-09	2357.0	66	54.79	2.490E-07	32.0	98	243.80	5.774E-07	45.9
2	3.01	1.232E-07	62.4	35	13.04	6.074E-08	91.7	67	57.41	1.484E-07	54.9	99	255.49	9.491E-07	27.8
3	3.14	-2.277E-08	-316.6	36	13.65	3.436E-08	163.9	68	60.15	2.088E-07	38.6	100	267.73	9.508E-07	27.8
4	3.28	-1.064E-07	-70.5	37	14.30	5.804E-08	97.7	69	63.02	3.196E-07	25.7	101	280.57	2.961E-07	89.5
5	3.42	-1.497E-07	-50.3	38	14.97	1.846E-08	318.5	70	66.03	7.731E-08	107.7	102	294.02	5.340E-07	50.2
6	3.57	-4.571E-08	-165.4	39	15.67	1.188E-07	49.1	71	69.18	1.014E-07	83.6	103	308.11	1.157E-06	23.2
7	3.73	1.533E-07	49.4	40	16.41	1.510E-07	39.2	72	72.49	1.890E-07	45.8	104	322.89	1.559E-06	17.3
8	3.89	6.964E-08	102.7	41	17.18	1.199E-07	48.5	73	75.96	2.358E-07	37.4	105	338.37	1.640E-06	16.3
9	4.07	1.359E-07	51.1	42	17.99	1.141E-07	51.4	74	79.59	1.974E-07	45.3	106	354.59	2.058E-06	13.0
10	4.25	5.920E-08	115.5	43	18.84	8.665E-08	68.4	75	83.39	1.514E-07	59.8	107	371.59	2.010E-06	13.3
11	4.44	7.656E-08	85.0	44	19.73	1.385E-07	42.6	76	87.38	2.035E-07	45.3	108	389.41	2.051E-06	13.0
12	4.64	1.832E-08	357.0	45	20.66	5.072E-08	117.3	77	91.56	2.666E-07	35.3	109	408.09	2.336E-06	11.5
13	4.84	9.758E-08	65.4	46	21.64	7.704E-08	78.0	78	95.94	6.900E-08	139.7	110	427.66	2.336E-06	11.4
14	5.06	1.701E-07	36.4	47	22.66	2.879E-08	214.7	79	100.53	1.291E-07	76.2	111	448.17	2.769E-06	9.6
15	5.29	7.994E-08	76.1	48	23.74	2.262E-08	274.1	80	105.34	3.853E-07	26.2	112	469.66	2.905E-06	9.1
16	5.53	7.009E-08	84.0	49	24.86	8.070E-08	80.0	81	110.38	2.483E-07	41.5	113	492.18	2.842E-06	9.3
17	5.78	4.868E-08	118.5	50	26.04	1.137E-07	56.1	82	115.66	2.963E-07	35.8	114	515.79	3.445E-06	7.6
18	6.04	1.034E-07	54.9	51	27.28	1.221E-07	54.1	83	121.20	1.545E-07	71.2	115	540.53	3.621E-06	7.1
19	6.32	6.879E-08	82.3	52	28.57	1.683E-08	394.5	84	127.00	3.556E-07	32.3	116	566.46	4.355E-06	5.9
20	6.61	1.251E-07	44.0	53	29.93	9.529E-08	70.4	85	133.08	1.312E-07	91.5	117	593.63	4.129E-06	6.1
21	6.91	1.340E-07	40.1	54	31.35	1.807E-07	37.5	86	139.45	2.564E-07	48.8	118	622.10	4.993E-06	5.0
22	7.23	-3.279E-08	-163.2	55	32.84	1.044E-08	664.8	87	146.13	3.574E-07	36.7	119	651.94	5.343E-06	4.7
23	7.56	9.317E-08	56.2	56	34.40	1.468E-07	47.0	88	153.13	2.478E-07	54.5	120	683.22	5.521E-06	4.5
24	7.91	1.222E-07	43.4	57	36.04	2.900E-07	24.5	89	160.46	2.403E-07	59.9	121	715.99	5.420E-06	4.5
25	8.27	7.925E-08	65.9	58	37.75	7.128E-08	98.3	90	168.15	2.187E-07	68.6	122	750.34	5.361E-06	4.4
26	8.66	1.025E-07	51.2	59	39.55	6.705E-08	106.3	91	176.20	4.835E-07	32.5	123	786.33	5.184E-06	4.4
27	9.06	8.118E-08	63.8	60	41.43	1.231E-07	58.8	92	184.65	3.234E-07	51.0	124	824.05	5.042E-06	4.4
28	9.48	8.066E-08	64.8	61	43.41	1.708E-07	43.5	93	193.49	5.536E-07	30.9	125	863.59	3.966E-06	5.4
29	9.92	8.436E-08	62.2	62	45.48	1.938E-07	38.1	94	202.76	8.042E-07	22.1	126	905.02	3.718E-06	5.6
30	10.38	6.095E-08	87.3	63	47.64	1.620E-07	46.6	95	211.86	1.721E-07	156.9	127	948.43	3.381E-06	5.9
31	10.86	9.864E-08	53.2	64	49.92	5.549E-08	139.3	96	222.01	7.576E-07	35.2	128	993.93	3.050E-06	6.3
32	11.37	6.288E-08	85.4	65	52.30	6.540E-08	119.6	97	232.65	4.510E-07	58.5	129	1041.62	3.013E-06	6.0
33	11.90	7.198E-10	7446.5												

* Flux Unit: [n/cm^2/Lethargy/Source]

Table A.2.4 Measured neutron flux by the PRC spectrometer at a surface of the Phase IIIA assembly (at a position of 0 mm from the position closest to the source on the surface)

J	Energy [keV]	Flux	Flux Error[%]	J	Energy [keV]	Flux	Flux Error[%]	J	Energy [keV]	Flux	Flux Error[%]	J	Energy [keV]	Flux	Flux Error[%]
1	2.85	9.125E-06	48.4	34	12.27	1.669E-05	18.2	66	53.95	3.257E-05	11.5	98	242.51	3.361E-05	10.4
2	2.97	1.071E-05	39.2	35	12.85	1.709E-05	17.7	67	56.52	2.502E-05	15.1	99	254.13	3.329E-05	10.3
3	3.10	8.231E-06	49.3	36	13.45	1.193E-05	25.6	68	59.22	2.303E-05	16.6	100	266.31	3.696E-05	9.3
4	3.23	-4.211E-06	-92.9	37	14.08	1.514E-05	20.2	69	62.05	3.318E-05	11.5	101	279.08	3.314E-05	10.3
5	3.37	7.222E-06	53.3	38	14.74	1.425E-05	21.6	70	65.01	3.703E-05	10.4	102	292.46	3.813E-05	8.9
6	3.52	1.356E-05	27.7	39	15.43	2.012E-05	15.3	71	68.12	3.266E-05	11.8	103	306.48	4.076E-05	8.4
7	3.68	8.639E-06	41.9	40	16.16	1.304E-05	23.8	72	71.37	2.878E-05	13.5	104	321.17	5.128E-05	6.6
8	3.84	5.151E-06	68.1	41	16.92	9.610E-06	32.4	73	74.78	2.876E-05	13.6	105	336.57	6.386E-05	5.3
9	4.01	6.437E-06	53.6	42	17.72	1.625E-05	19.3	74	78.36	3.680E-05	10.7	106	352.71	6.023E-05	5.6
10	4.19	5.826E-06	57.8	43	18.55	1.591E-05	19.9	75	82.10	3.746E-05	10.6	107	369.62	6.251E-05	5.4
11	4.37	4.317E-06	76.9	44	19.43	1.219E-05	26.1	76	86.03	3.830E-05	10.4	108	387.34	6.060E-05	5.5
12	4.57	7.199E-06	46.1	45	20.35	1.364E-05	23.5	77	90.14	3.502E-05	11.4	109	405.92	5.841E-05	5.7
13	4.77	1.096E-05	29.4	46	21.31	2.016E-05	16.0	78	94.45	2.864E-05	14.1	110	425.39	5.563E-05	6.0
14	4.99	1.301E-05	24.6	47	22.32	2.535E-05	12.7	79	98.97	3.328E-05	12.2	111	445.79	4.915E-05	6.8
15	5.21	6.487E-06	47.9	48	23.37	2.626E-05	12.2	80	103.71	3.589E-05	11.4	112	467.16	4.929E-05	6.8
16	5.45	1.003E-05	30.6	49	24.48	2.472E-05	12.9	81	108.67	3.912E-05	10.6	113	489.57	5.918E-05	5.7
17	5.70	9.910E-06	30.7	50	25.64	1.719E-05	18.6	82	113.87	4.602E-05	9.1	114	513.05	7.555E-05	4.5
18	5.95	1.057E-05	28.3	51	26.86	9.851E-06	32.8	83	119.32	5.239E-05	8.1	115	537.66	8.876E-05	3.9
19	6.23	6.797E-06	43.7	52	28.13	1.811E-05	17.9	84	125.03	5.100E-05	8.4	116	563.45	8.738E-05	4.1
20	6.51	4.463E-06	66.1	53	29.47	1.239E-05	26.6	85	131.02	3.931E-05	11.2	117	590.47	9.141E-05	4.0
21	6.81	7.751E-06	37.8	54	30.87	1.034E-05	32.3	86	137.29	3.407E-05	13.2	118	618.79	9.813E-05	3.8
22	7.12	1.084E-05	26.8	55	32.33	1.511E-05	22.4	87	143.87	4.195E-05	11.0	119	648.48	9.940E-05	3.8
23	7.45	9.066E-06	31.9	56	33.87	1.652E-05	20.8	88	150.76	4.393E-05	10.7	120	679.58	8.907E-05	4.3
24	7.79	9.247E-06	31.4	57	35.48	1.277E-05	27.2	89	159.14	4.445E-05	9.9	121	712.18	6.037E-05	6.6
25	8.15	9.197E-06	32.0	58	37.17	1.819E-05	19.3	90	166.77	4.881E-05	8.6	122	746.35	4.482E-05	9.1
26	8.53	1.015E-05	28.9	59	38.94	1.958E-05	18.2	91	174.75	4.786E-05	8.4	123	782.15	5.025E-05	8.5
27	8.92	7.711E-06	38.9	60	40.79	2.094E-05	17.1	92	183.13	5.015E-05	7.8	124	819.67	8.357E-05	5.3
28	9.34	5.553E-06	53.8	61	42.74	2.847E-05	12.7	93	191.90	5.370E-05	7.0	125	858.99	1.061E-04	4.3
29	9.77	1.350E-05	22.5	62	44.78	3.038E-05	11.9	94	201.10	4.477E-05	8.2	126	900.20	9.812E-05	4.8
30	10.22	1.744E-05	17.4	63	46.91	2.539E-05	14.3	95	210.73	3.585E-05	10.0	127	943.39	9.566E-05	5.0
31	10.70	1.496E-05	20.3	64	49.15	1.832E-05	20.1	96	220.83	3.938E-05	9.0	128	988.65	1.081E-04	4.6
32	11.20	1.746E-05	17.3	65	51.49	2.235E-05	16.6	97	231.41	4.284E-05	8.1	129	1036.08	1.174E-04	4.3
33	11.72	1.815E-05	16.7												

* Flux Unit: [n/cm^2/Lethargy/Source]

Table A.2.5 Measured neutron flux by the PRC spectrometer at a surface of the Phase IIIA assembly (at a position of 500 mm forward from the position closest to the source on the surface)

J	Energy [keV]	Flux	Flux Error[%]	J	Energy [keV]	Flux	Flux Error[%]	J	Energy [keV]	Flux	Flux Error[%]	J	Energy [keV]	Flux	Flux Error[%]
1	2.73	-1.304E-06	-128.1	34	11.72	7.721E-06	14.9	67	53.95	1.178E-05	11.4	99	242.32	1.076E-05	9.8
2	2.85	4.479E-06	37.1	35	12.27	1.013E-05	11.3	68	56.52	1.460E-05	9.2	100	253.94	1.054E-05	10.0
3	2.97	3.910E-06	40.9	36	12.85	9.524E-06	12.1	69	59.22	1.321E-05	10.3	101	266.11	8.771E-06	12.0
4	3.10	1.875E-06	82.1	37	13.45	7.298E-06	15.6	70	62.05	1.542E-05	8.8	102	278.87	1.170E-05	9.0
5	3.23	2.976E-06	49.7	38	14.08	9.423E-06	12.1	71	65.01	1.438E-05	9.5	103	292.24	1.450E-05	7.2
6	3.37	4.815E-06	30.1	39	14.74	8.151E-06	14.1	72	68.12	1.595E-05	8.6	104	306.25	1.717E-05	6.1
7	3.52	8.723E-07	161.6	40	15.43	7.087E-06	16.2	73	71.37	1.530E-05	9.0	105	320.93	1.841E-05	5.6
8	3.68	1.787E-06	77.2	41	16.16	6.568E-06	17.7	74	74.78	1.499E-05	9.2	106	336.32	1.678E-05	6.1
9	3.84	2.504E-06	55.1	42	16.92	7.182E-06	16.2	75	78.36	1.695E-05	8.2	107	352.45	1.908E-05	5.3
10	4.01	2.769E-06	48.4	43	17.72	7.197E-06	16.4	76	82.10	1.702E-05	8.1	108	369.35	1.827E-05	5.5
11	4.19	4.741E-06	28.1	44	18.55	9.595E-06	12.2	77	86.03	1.533E-05	9.1	109	387.06	1.830E-05	5.5
12	4.37	2.740E-06	47.4	45	19.43	1.046E-05	11.3	78	90.14	1.473E-05	9.5	110	405.62	1.885E-05	5.4
13	4.57	4.475E-06	28.6	46	20.35	9.672E-06	12.2	79	94.45	1.418E-05	9.9	111	425.07	1.717E-05	5.9
14	4.77	5.748E-06	21.9	47	21.31	1.047E-05	11.3	80	98.97	1.557E-05	9.1	112	445.45	1.663E-05	6.1
15	4.99	4.853E-06	25.3	48	22.32	1.054E-05	11.2	81	103.71	1.739E-05	8.2	113	466.82	2.054E-05	4.9
16	5.21	5.683E-06	21.5	49	23.37	1.275E-05	9.3	82	108.67	1.935E-05	7.4	114	489.20	2.389E-05	4.3
17	5.45	5.931E-06	20.2	50	24.48	1.286E-05	9.1	83	113.87	2.202E-05	6.6	115	512.67	2.581E-05	4.0
18	5.70	5.186E-06	22.8	51	25.64	9.248E-06	12.7	84	119.32	2.095E-05	7.0	116	537.26	2.586E-05	4.1
19	5.95	5.106E-06	22.7	52	26.86	4.091E-06	28.8	85	125.03	1.941E-05	7.6	117	563.03	2.801E-05	3.9
20	6.23	5.560E-06	20.7	53	28.13	4.971E-06	24.1	86	131.02	1.852E-05	8.1	118	590.03	3.296E-05	3.3
21	6.51	2.984E-06	38.2	54	29.47	6.121E-06	19.9	87	137.29	1.900E-05	8.1	119	618.33	3.282E-05	3.4
22	6.81	4.461E-06	25.6	55	30.87	7.709E-06	16.0	88	143.87	1.989E-05	7.8	120	647.99	3.290E-05	3.4
23	7.12	6.396E-06	17.5	56	32.33	9.256E-06	13.4	89	151.76	1.851E-05	7.7	121	679.08	2.422E-05	4.7
24	7.45	5.746E-06	19.5	57	33.87	9.076E-06	13.9	90	159.02	2.008E-05	6.8	122	711.65	1.967E-05	5.8
25	7.79	4.704E-06	23.8	58	35.48	7.983E-06	15.9	91	166.64	2.089E-05	6.2	123	745.79	2.066E-05	5.8
26	8.15	5.759E-06	19.6	59	37.17	9.580E-06	13.4	92	174.62	2.493E-05	5.0	124	781.57	2.427E-05	5.0
27	8.53	5.570E-06	20.5	60	38.94	1.302E-05	9.9	93	182.99	2.020E-05	5.9	125	819.06	2.835E-05	4.4
28	8.92	7.341E-06	15.5	61	40.79	1.375E-05	9.4	94	191.76	1.619E-05	7.1	126	858.35	2.746E-05	4.6
29	9.34	7.632E-06	15.1	62	42.74	1.208E-05	10.7	95	200.95	1.436E-05	7.8	127	899.53	2.711E-05	4.8
30	9.77	8.587E-06	13.3	63	44.78	1.346E-05	9.7	96	210.57	1.609E-05	6.8	128	942.69	2.820E-05	4.7
31	10.22	8.874E-06	13.0	64	46.91	1.137E-05	11.4	97	220.67	1.388E-05	7.7	129	987.91	2.737E-05	4.9
32	10.70	8.070E-06	14.3	65	49.15	1.010E-05	13.0	98	231.24	1.103E-05	9.6	130	1035.31	2.779E-05	4.9
33	11.20	8.091E-06	14.1	66	51.49	1.132E-05	11.7								

* Flux Unit: [n/cm^2/Lethargy/Source]

Table A.2.6 Measured neutron flux by the PRC spectrometer at a surface of the Phase IIIA assembly (at a position of 500 mm backward from the position closest to the source on the surface)

J	Energy [keV]	Flux	Flux Error[%]	J	Energy [keV]	Flux	Flux Error[%]	J	Energy [keV]	Flux	Flux Error[%]	J	Energy [keV]	Flux	Flux Error[%]
1	2.73	2.512E-06	79.6	34	11.72	1.080E-05	12.6	67	53.95	1.581E-05	10.4	99	242.58	1.375E-05	9.0
2	2.85	-1.166E-06	-166.4	35	12.27	9.257E-06	14.7	68	56.52	1.553E-05	10.6	100	254.21	1.028E-05	12.0
3	2.97	2.378E-06	79.5	36	12.85	8.723E-06	15.6	69	59.22	1.707E-05	9.7	101	266.40	1.158E-05	10.6
4	3.10	1.295E-06	142.9	37	13.45	8.675E-06	15.7	70	62.05	1.588E-05	10.5	102	279.17	1.514E-05	8.1
5	3.23	1.327E-06	135.6	38	14.08	9.522E-06	14.3	71	65.01	1.524E-05	11.0	103	292.55	1.737E-05	7.0
6	3.37	1.733E-06	102.1	39	14.74	8.278E-06	16.5	72	68.12	1.555E-05	10.8	104	306.58	1.977E-05	6.2
7	3.52	5.448E-06	31.6	40	15.43	7.647E-06	18.0	73	71.37	1.671E-05	10.1	105	321.27	2.310E-05	5.2
8	3.68	8.161E-06	20.2	41	16.16	7.114E-06	19.4	74	74.78	1.819E-05	9.3	106	336.68	2.155E-05	5.6
9	3.84	3.324E-06	48.1	42	16.92	7.511E-06	18.5	75	78.36	1.923E-05	8.8	107	352.82	2.357E-05	5.0
10	4.01	2.243E-06	70.4	43	17.72	8.738E-06	16.0	76	82.10	1.653E-05	10.3	108	369.74	2.767E-05	4.3
11	4.19	3.544E-06	43.7	44	18.55	1.073E-05	13.0	77	86.03	1.590E-05	10.8	109	387.47	2.477E-05	4.7
12	4.37	2.907E-06	53.3	45	19.43	7.551E-06	18.7	78	90.14	1.799E-05	9.6	110	406.05	2.277E-05	5.1
13	4.57	4.145E-06	36.4	46	20.35	8.544E-06	16.6	79	94.45	1.507E-05	11.5	111	425.52	2.237E-05	5.2
14	4.77	5.305E-06	28.1	47	21.31	1.067E-05	13.4	80	98.97	1.682E-05	10.4	112	445.93	2.002E-05	5.8
15	4.99	4.590E-06	32.0	48	22.32	1.332E-05	10.7	81	103.71	1.996E-05	8.8	113	467.31	2.160E-05	5.4
16	5.21	4.096E-06	35.6	49	23.37	1.283E-05	11.1	82	108.67	2.296E-05	7.7	114	489.73	2.480E-05	4.7
17	5.45	6.500E-06	22.0	50	24.48	1.339E-05	10.6	83	113.87	2.235E-05	7.9	115	513.21	2.752E-05	4.3
18	5.70	5.967E-06	23.6	51	25.64	9.579E-06	14.9	84	119.32	2.493E-05	7.3	116	537.83	3.328E-05	3.6
19	5.95	8.267E-06	16.7	52	26.86	4.855E-06	29.5	85	125.03	2.388E-05	7.7	117	563.63	3.636E-05	3.4
20	6.23	5.066E-06	27.0	53	28.13	7.489E-06	19.4	86	131.02	1.983E-05	9.3	118	590.66	3.256E-05	3.8
21	6.51	4.290E-06	31.2	54	29.47	5.251E-06	28.0	87	137.29	1.891E-05	10.0	119	618.99	3.335E-05	3.8
22	6.81	4.686E-06	28.8	55	30.87	7.797E-06	19.2	88	143.87	2.037E-05	9.5	120	648.68	3.556E-05	3.7
23	7.12	3.769E-06	35.6	56	32.33	8.296E-06	18.3	89	150.76	2.120E-05	9.2	121	679.80	3.708E-05	3.6
24	7.45	3.398E-06	39.4	57	33.87	1.102E-05	13.9	90	159.19	2.216E-05	7.4	122	712.41	3.108E-05	4.3
25	7.79	6.615E-06	20.4	58	35.48	9.291E-06	16.6	91	166.82	2.328E-05	6.7	123	746.59	2.529E-05	5.5
26	8.15	6.635E-06	20.3	59	37.17	1.234E-05	12.6	92	174.81	2.392E-05	6.2	124	782.40	2.710E-05	5.3
27	8.53	5.448E-06	25.0	60	38.94	1.115E-05	14.1	93	183.18	2.539E-05	5.6	125	819.93	3.292E-05	4.5
28	8.92	1.035E-05	13.1	61	40.79	1.365E-05	11.6	94	191.96	2.574E-05	5.4	126	859.27	3.928E-05	3.8
29	9.34	8.620E-06	15.9	62	42.74	1.426E-05	11.1	95	201.16	2.194E-05	6.1	127	900.49	3.699E-05	4.1
30	9.77	8.131E-06	16.7	63	44.78	1.366E-05	11.6	96	210.80	2.017E-05	6.4	128	943.69	3.650E-05	4.2
31	10.22	1.021E-05	13.3	64	46.91	1.229E-05	12.9	97	220.90	1.739E-05	7.3	129	988.97	3.776E-05	4.2
32	10.70	7.555E-06	18.1	65	49.15	1.118E-05	14.5	98	231.49	1.831E-05	6.8	130	1036.42	3.836E-05	4.2
33	11.20	9.480E-06	14.3	66	51.49	1.332E-05	12.2								

* Flux Unit: [n/cm^2/Lethargy/Source]

Table A.2.7 Measured neutron flux by the PRC spectrometer inside of the Phase IIIA assembly (at a position of 0 mm from the position closest to the source on the surface)

J	Energy [keV]	Flux	Flux Error[%]	J	Energy [keV]	Flux	Flux Error[%]	J	Energy [keV]	Flux	Flux Error[%]	J	Energy [keV]	Flux	Flux Error[%]
1	2.73	-6.113E-07	-505.5	34	11.72	1.805E-05	12.1	67	53.95	2.535E-05	10.2	99	243.08	1.848E-05	11.3
2	2.85	2.486E-06	119.5	35	12.27	1.756E-05	12.5	68	56.52	2.843E-05	9.1	100	254.73	1.824E-05	11.3
3	2.97	3.063E-08	9500.5	36	12.85	1.641E-05	13.3	69	59.22	3.062E-05	8.6	101	266.94	1.928E-05	10.7
4	3.10	-1.060E-06	-269.8	37	13.45	1.369E-05	16.1	70	62.05	2.827E-05	9.3	102	279.74	2.121E-05	9.7
5	3.23	2.976E-06	94.4	38	14.08	1.502E-05	14.6	71	65.01	2.860E-05	9.3	103	293.15	2.259E-05	9.2
6	3.37	4.976E-06	55.5	39	14.74	1.789E-05	12.4	72	68.12	2.605E-05	10.3	104	307.20	2.772E-05	7.5
7	3.52	7.472E-06	35.9	40	15.43	1.626E-05	13.7	73	71.37	3.344E-05	8.0	105	321.93	3.123E-05	6.6
8	3.68	6.257E-06	41.7	41	16.16	1.890E-05	11.7	74	74.78	3.645E-05	7.4	106	337.36	3.613E-05	5.7
9	3.84	2.738E-06	93.9	42	16.92	1.785E-05	12.5	75	78.36	3.293E-05	8.2	107	353.54	3.710E-05	5.5
10	4.01	8.116E-06	31.0	43	17.72	1.390E-05	16.1	76	82.10	3.348E-05	8.1	108	370.49	3.936E-05	5.1
11	4.19	7.678E-06	32.4	44	18.55	1.670E-05	13.5	77	86.03	3.466E-05	7.8	109	388.26	3.581E-05	5.6
12	4.37	7.982E-06	30.7	45	19.43	1.693E-05	13.4	78	90.14	3.607E-05	7.6	110	406.88	3.308E-05	6.1
13	4.57	5.650E-06	42.7	46	20.35	1.654E-05	13.8	79	94.45	3.584E-05	7.6	111	426.39	3.259E-05	6.2
14	4.77	8.117E-06	29.4	47	21.31	1.750E-05	13.1	80	98.97	4.105E-05	6.7	112	446.84	3.251E-05	6.2
15	4.99	9.810E-06	24.0	48	22.32	1.763E-05	13.0	81	103.71	3.687E-05	7.4	113	468.27	3.337E-05	6.1
16	5.21	5.812E-06	39.9	49	23.37	2.249E-05	10.3	82	108.67	3.705E-05	7.4	114	490.73	4.337E-05	4.7
17	5.45	7.458E-06	30.8	50	24.48	2.025E-05	11.5	83	113.87	4.218E-05	6.6	115	514.26	5.505E-05	3.8
18	5.70	1.201E-05	19.0	51	25.64	1.733E-05	13.4	84	119.32	4.221E-05	6.6	116	538.93	5.624E-05	3.8
19	5.95	1.153E-05	19.6	52	26.86	1.753E-05	13.4	85	125.03	4.452E-05	6.4	117	564.78	5.733E-05	3.8
20	6.23	7.312E-06	30.4	53	28.13	2.020E-05	11.7	86	131.02	4.159E-05	6.9	118	591.87	5.463E-05	4.0
21	6.51	1.130E-05	19.6	54	29.47	2.051E-05	11.6	87	137.29	4.034E-05	7.2	119	620.26	5.884E-05	3.8
22	6.81	9.982E-06	21.9	55	30.87	1.490E-05	16.0	88	143.87	4.531E-05	6.5	120	650.01	6.038E-05	3.7
23	7.12	1.012E-05	21.3	56	32.33	1.702E-05	14.2	89	152.23	4.484E-05	6.7	121	681.19	5.290E-05	4.3
24	7.45	1.331E-05	16.2	57	33.87	2.548E-05	9.5	90	159.52	4.760E-05	5.9	122	713.87	5.147E-05	4.5
25	7.79	1.549E-05	13.9	58	35.48	2.154E-05	11.3	91	167.16	4.854E-05	5.6	123	748.11	5.121E-05	4.6
26	8.15	1.183E-05	18.3	59	37.17	1.958E-05	12.6	92	175.17	4.993E-05	5.1	124	784.00	4.592E-05	5.3
27	8.53	1.249E-05	17.4	60	38.94	1.822E-05	13.6	93	183.56	4.849E-05	5.1	125	821.61	3.667E-05	6.8
28	8.92	1.648E-05	13.3	61	40.79	2.351E-05	10.7	94	192.35	4.569E-05	5.1	126	861.02	4.280E-05	6.1
29	9.34	1.768E-05	12.3	62	42.74	2.664E-05	9.5	95	201.57	3.789E-05	5.9	127	902.33	5.083E-05	5.2
30	9.77	1.592E-05	13.7	63	44.78	2.739E-05	9.2	96	211.23	3.464E-05	6.3	128	945.62	5.701E-05	4.8
31	10.22	1.525E-05	14.4	64	46.91	2.555E-05	9.9	97	221.35	3.345E-05	6.4	129	990.99	5.286E-05	5.2
32	10.70	1.522E-05	14.4	65	49.15	2.601E-05	9.8	98	231.96	2.289E-05	9.2	130	1038.53	5.465E-05	5.2
33	11.20	2.034E-05	10.8	66	51.49	2.498E-05	10.3								

* Flux Unit: [n/cm^2/Lethargy/Source]

Table A.2.8 Measured neutron flux by the PRC spectrometer inside of the Phase IIIA assembly (at a position of 500 mm backward from the position closest to the source on the surface)

J	Energy [keV]	Flux	Flux Error[%]	J	Energy [keV]	Flux	Flux Error[%]	J	Energy [keV]	Flux	Flux Error[%]	J	Energy [keV]	Flux	Flux Error[%]
1	2.69	2.432E-06	50.6	34	11.55	8.051E-06	10.2	67	53.12	1.074E-05	8.4	99	240.46	7.159E-06	7.9
2	2.81	-1.155E-07	-1004.3	35	12.09	7.827E-06	10.5	68	55.65	1.122E-05	8.1	100	251.99	4.316E-06	13.0
3	2.93	1.328E-06	85.8	36	12.65	7.001E-06	11.8	69	58.31	1.044E-05	8.8	101	264.07	4.679E-06	12.0
4	3.06	1.383E-06	80.3	37	13.24	7.378E-06	11.2	70	61.09	1.157E-05	7.9	102	276.72	4.282E-06	13.1
5	3.19	3.429E-06	31.2	38	13.86	7.950E-06	10.4	71	64.01	1.334E-05	6.9	103	289.99	4.077E-06	13.8
6	3.33	2.845E-06	36.9	39	14.52	8.749E-06	9.5	72	67.07	1.147E-05	8.0	104	303.89	5.998E-06	9.4
7	3.47	1.873E-06	54.5	40	15.20	5.560E-06	14.8	73	70.27	1.185E-05	7.8	105	318.46	9.130E-06	6.1
8	3.62	1.978E-06	51.1	41	15.91	7.844E-06	10.5	74	73.63	1.259E-05	7.3	106	333.73	9.156E-06	6.1
9	3.78	1.699E-06	58.4	42	16.66	7.603E-06	10.9	75	77.15	1.285E-05	7.2	107	349.73	8.432E-06	6.6
10	3.95	3.562E-06	27.5	43	17.45	7.571E-06	11.0	76	80.83	1.294E-05	7.1	108	366.50	1.022E-05	5.4
11	4.13	1.671E-06	57.6	44	18.27	8.568E-06	9.7	77	84.70	1.335E-05	6.9	109	384.08	1.061E-05	5.1
12	4.31	3.500E-06	27.0	45	19.13	7.681E-06	10.8	78	88.75	1.237E-05	7.4	110	402.49	9.930E-06	5.4
13	4.50	4.872E-06	19.0	46	20.04	7.852E-06	10.6	79	93.00	1.255E-05	7.3	111	421.80	8.073E-06	6.7
14	4.70	3.243E-06	28.2	47	20.98	7.361E-06	11.4	80	97.44	1.324E-05	6.9	112	442.02	7.849E-06	6.8
15	4.91	2.322E-06	38.9	48	21.98	7.066E-06	11.9	81	102.11	1.368E-05	6.7	113	463.22	9.481E-06	5.7
16	5.14	4.874E-06	18.4	49	23.02	9.387E-06	9.0	82	106.99	1.509E-05	6.0	114	485.44	9.593E-06	5.6
17	5.37	3.278E-06	27.1	50	24.11	9.132E-06	9.2	83	112.11	1.451E-05	6.3	115	508.72	1.149E-05	4.8
18	5.61	4.681E-06	18.7	51	25.25	9.046E-06	9.3	84	117.48	1.419E-05	6.4	116	533.12	1.370E-05	4.1
19	5.87	4.563E-06	19.0	52	26.45	7.224E-06	11.8	85	123.10	1.510E-05	6.1	117	558.69	1.478E-05	3.8
20	6.13	4.831E-06	17.7	53	27.70	7.212E-06	11.8	86	128.99	1.429E-05	6.5	118	585.49	1.547E-05	3.7
21	6.41	5.005E-06	16.9	54	29.01	8.247E-06	10.4	87	135.17	1.621E-05	5.7	119	613.57	1.647E-05	3.5
22	6.71	6.243E-06	13.3	55	30.39	7.290E-06	11.9	88	141.64	1.550E-05	6.0	120	643.01	1.650E-05	3.5
23	7.01	5.426E-06	15.1	56	31.84	6.896E-06	12.6	89	148.43	1.373E-05	6.8	121	673.85	1.658E-05	3.5
24	7.34	5.141E-06	15.8	57	33.35	8.614E-06	10.2	90	157.80	1.490E-05	5.7	122	706.17	1.390E-05	4.2
25	7.68	5.172E-06	15.7	58	34.94	9.422E-06	9.4	91	165.36	1.529E-05	5.2	123	740.05	1.356E-05	4.3
26	8.03	5.906E-06	13.8	59	36.60	9.246E-06	9.5	92	173.28	1.480E-05	5.0	124	775.55	1.301E-05	4.5
27	8.40	6.454E-06	12.8	60	38.34	9.858E-06	9.0	93	181.58	1.510E-05	4.7	125	812.76	1.139E-05	5.3
28	8.79	6.277E-06	13.1	61	40.17	9.186E-06	9.7	94	190.28	1.369E-05	4.9	126	851.75	1.020E-05	6.0
29	9.20	7.555E-06	10.9	62	42.08	9.749E-06	9.2	95	199.40	1.252E-05	5.1	127	892.61	1.001E-05	6.2
30	9.62	7.663E-06	10.8	63	44.09	9.385E-06	9.5	96	208.96	1.160E-05	5.3	128	935.43	1.026E-05	6.2
31	10.07	8.233E-06	10.0	64	46.19	1.115E-05	8.1	97	218.97	9.748E-06	6.1	129	980.31	1.129E-05	5.7
32	10.54	6.926E-06	11.9	65	48.39	1.034E-05	8.7	98	229.46	8.941E-06	6.4	130	1027.34	1.178E-05	5.6
33	11.03	6.738E-06	12.2	66	50.70	9.527E-06	9.5								

* Flux Unit: [n/cm^2/Lethargy/Source]

Table A.2.9 Measured neutron flux by the PRC spectrometer inside of the Phase IIIA assembly (at a position of 500 mm forward from the position closest to the source on the surface)

J	Energy [keV]	Flux	Flux Error[%]	J	Energy [keV]	Flux	Flux Error[%]	J	Energy [keV]	Flux	Flux Error[%]	J	Energy [keV]	Flux	Flux Error[%]
1	2.77	-2.419E-07	-698.6	34	11.90	1.026E-05	11.5	67	54.79	1.610E-05	8.3	99	242.56	8.254E-06	9.5
2	2.89	7.045E-07	234.2	35	12.46	1.186E-05	9.9	68	57.41	1.573E-05	8.6	100	254.19	7.496E-06	10.4
3	3.01	4.263E-07	377.7	36	13.04	1.100E-05	10.6	69	60.15	1.517E-05	8.9	101	266.37	6.501E-06	12.0
4	3.14	4.599E-06	33.9	37	13.65	8.416E-06	14.0	70	63.02	1.610E-05	8.4	102	279.14	8.514E-06	9.2
5	3.28	4.429E-06	34.1	38	14.30	9.941E-06	11.9	71	66.03	1.707E-05	8.0	103	292.52	9.200E-06	8.5
6	3.42	1.982E-06	74.2	39	14.97	9.585E-06	12.4	72	69.18	1.832E-05	7.4	104	306.55	1.196E-05	6.5
7	3.57	2.106E-06	68.9	40	15.67	8.910E-06	13.4	73	72.49	1.680E-05	8.1	105	321.24	1.432E-05	5.4
8	3.73	4.012E-06	35.4	41	16.41	9.425E-06	12.6	74	75.96	1.700E-05	8.0	106	336.64	1.529E-05	5.1
9	3.89	4.471E-06	31.3	42	17.18	9.326E-06	12.9	75	79.59	1.828E-05	7.5	107	352.79	1.522E-05	5.0
10	4.07	3.649E-06	37.5	43	17.99	1.103E-05	10.9	76	83.39	1.833E-05	7.4	108	369.70	1.526E-05	5.0
11	4.25	2.247E-06	60.1	44	18.84	1.034E-05	11.7	77	87.38	2.024E-05	6.7	109	387.43	1.439E-05	5.3
12	4.44	5.667E-06	23.5	45	19.73	9.002E-06	13.4	78	91.56	1.668E-05	8.2	110	406.01	1.348E-05	5.6
13	4.64	5.008E-06	26.2	46	20.66	1.010E-05	12.1	79	95.94	1.703E-05	8.0	111	425.48	1.344E-05	5.6
14	4.84	2.525E-06	51.5	47	21.64	1.119E-05	10.9	80	100.53	1.962E-05	7.0	112	445.89	1.253E-05	6.0
15	5.06	3.618E-06	35.4	48	22.66	1.106E-05	11.0	81	105.34	1.917E-05	7.1	113	467.27	1.492E-05	5.1
16	5.29	5.122E-06	25.0	49	23.74	1.248E-05	9.9	82	110.38	1.980E-05	6.8	114	489.68	1.772E-05	4.4
17	5.53	6.961E-06	18.0	50	24.86	1.272E-05	9.6	83	115.66	2.166E-05	6.3	115	513.16	2.297E-05	3.4
18	5.78	7.600E-06	16.3	51	26.04	1.220E-05	10.1	84	121.20	2.310E-05	6.0	116	537.78	2.255E-05	3.6
19	6.04	6.965E-06	17.5	52	27.28	7.933E-06	15.5	85	127.00	2.259E-05	6.1	117	563.57	2.368E-05	3.4
20	6.32	5.870E-06	20.4	53	28.57	8.532E-06	14.7	86	133.08	2.057E-05	6.8	118	590.60	2.442E-05	3.4
21	6.61	7.885E-06	15.1	54	29.93	9.939E-06	12.7	87	139.45	1.870E-05	7.5	119	618.93	2.303E-05	3.6
22	6.91	8.813E-06	13.3	55	31.35	1.063E-05	11.9	88	146.13	2.019E-05	7.0	120	648.62	2.375E-05	3.6
23	7.23	4.419E-06	26.3	56	32.84	1.088E-05	11.8	89	153.13	2.172E-05	6.6	121	679.74	2.524E-05	3.4
24	7.56	5.247E-06	22.1	57	34.40	1.184E-05	10.9	90	159.18	2.263E-05	4.8	122	712.34	2.675E-05	3.2
25	7.91	8.276E-06	14.1	58	36.04	1.333E-05	9.7	91	166.80	2.279E-05	4.5	123	746.52	2.669E-05	3.2
26	8.27	7.815E-06	15.1	59	37.75	1.174E-05	11.1	92	174.79	2.081E-05	4.7	124	782.33	2.201E-05	4.0
27	8.66	1.021E-05	11.6	60	39.55	1.381E-05	9.4	93	183.17	2.182E-05	4.3	125	819.86	1.588E-05	5.5
28	9.06	9.926E-06	11.8	61	41.43	1.328E-05	9.9	94	191.94	1.929E-05	4.6	126	859.19	1.618E-05	5.6
29	9.48	7.370E-06	16.0	62	43.41	1.376E-05	9.6	95	201.14	1.645E-05	5.2	127	900.41	1.785E-05	5.2
30	9.92	9.163E-06	12.9	63	45.48	1.394E-05	9.5	96	210.78	1.363E-05	6.1	128	943.60	1.780E-05	5.3
31	10.38	1.092E-05	10.8	64	47.64	1.473E-05	9.0	97	220.88	1.380E-05	5.9	129	988.87	1.842E-05	5.2
32	10.86	9.707E-06	12.2	65	49.92	1.174E-05	11.3	98	231.47	1.157E-05	6.9	130	1036.32	1.838E-05	5.3
33	11.37	9.044E-06	13.0	66	52.30	1.365E-05	9.8								

* Flux Unit: [n/cm^2/Lethargy/Source]

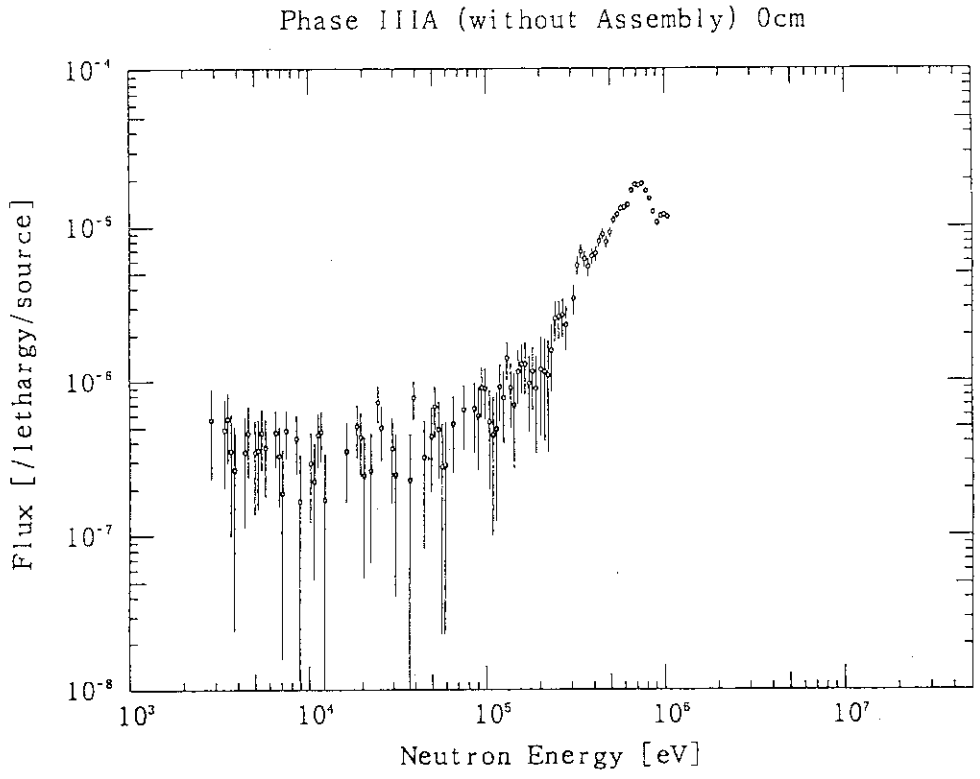

Fig. A.2.2 Measured neutron flux by the PRC spectrometer at a distance of 300 mm from the line source axis (at a position of 0 mm from the position closest to the source on the 300 mm axis)

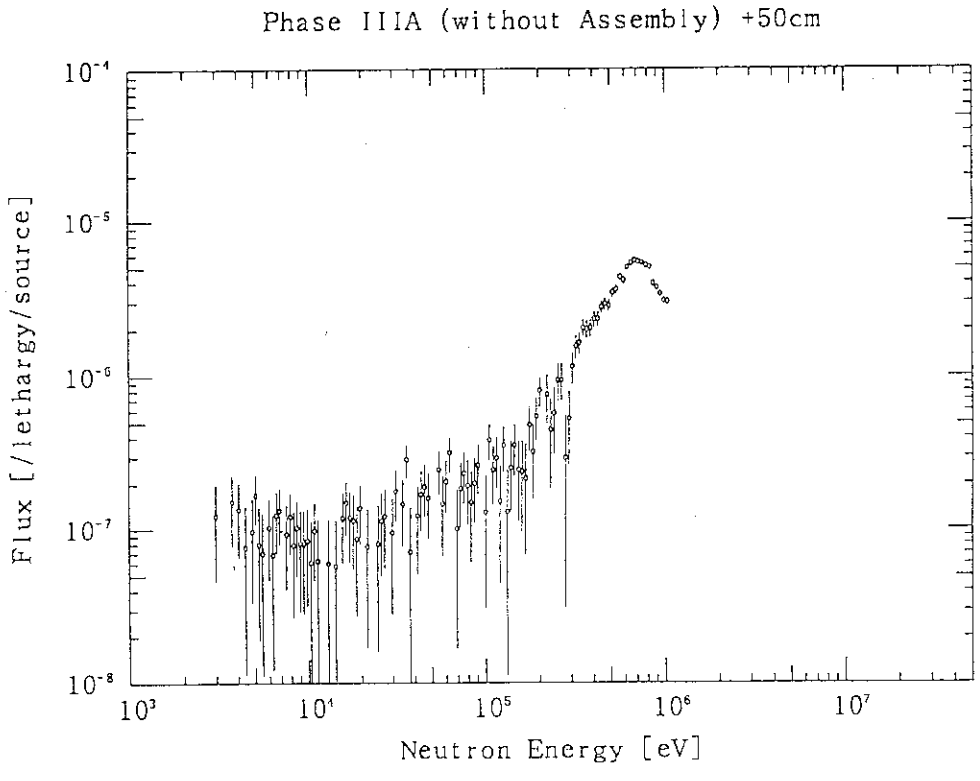

Fig. A.2.3 Measured neutron flux by the PRC spectrometer at a distance of 300 mm from the line source axis (at a position of 500 mm forward from the position closest to the source on the 300 mm axis)

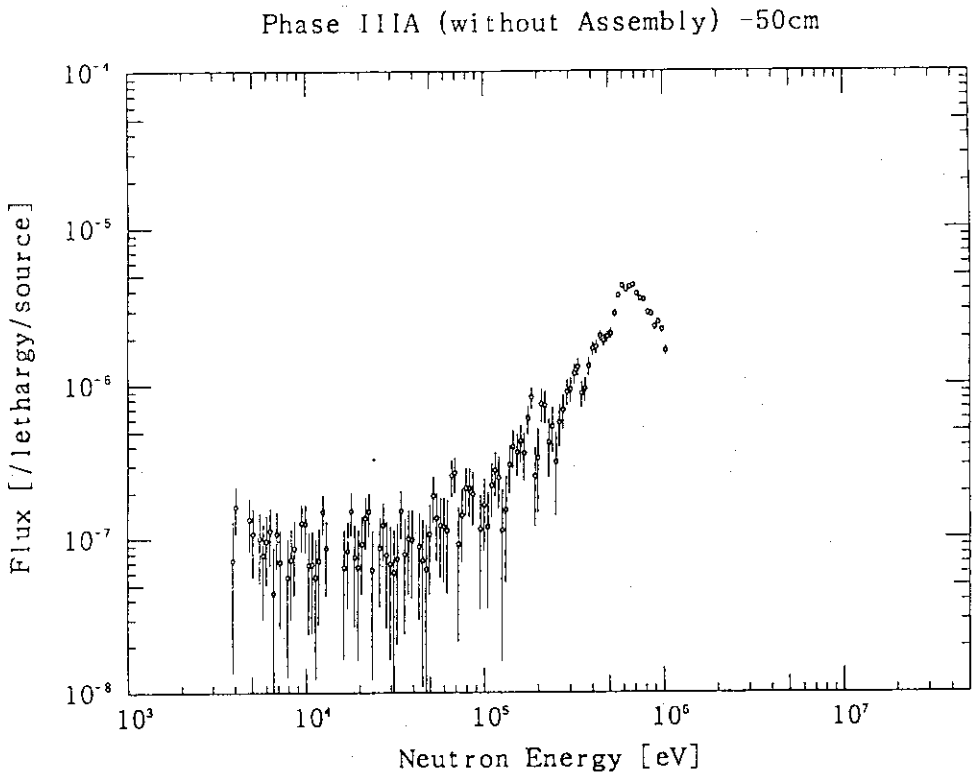

Fig. A.2.4 Measured neutron flux by the PRC spectrometer at a distance of 300 mm from the line source axis (at a position of 500 mm backward from the position closest to the source on the 300 mm axis)

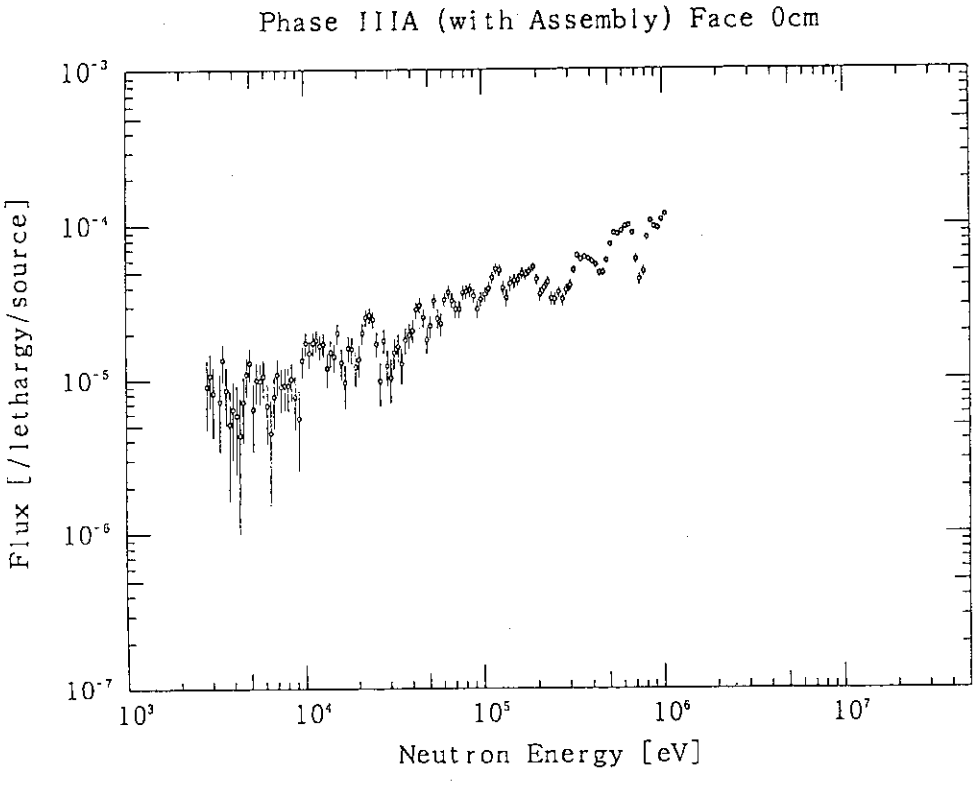

Fig. A.2.5 Measured neutron flux by the PRC spectrometer at a surface of the Phase IIIA assembly (at a position of 0 mm from the position closest to the source on the surface)

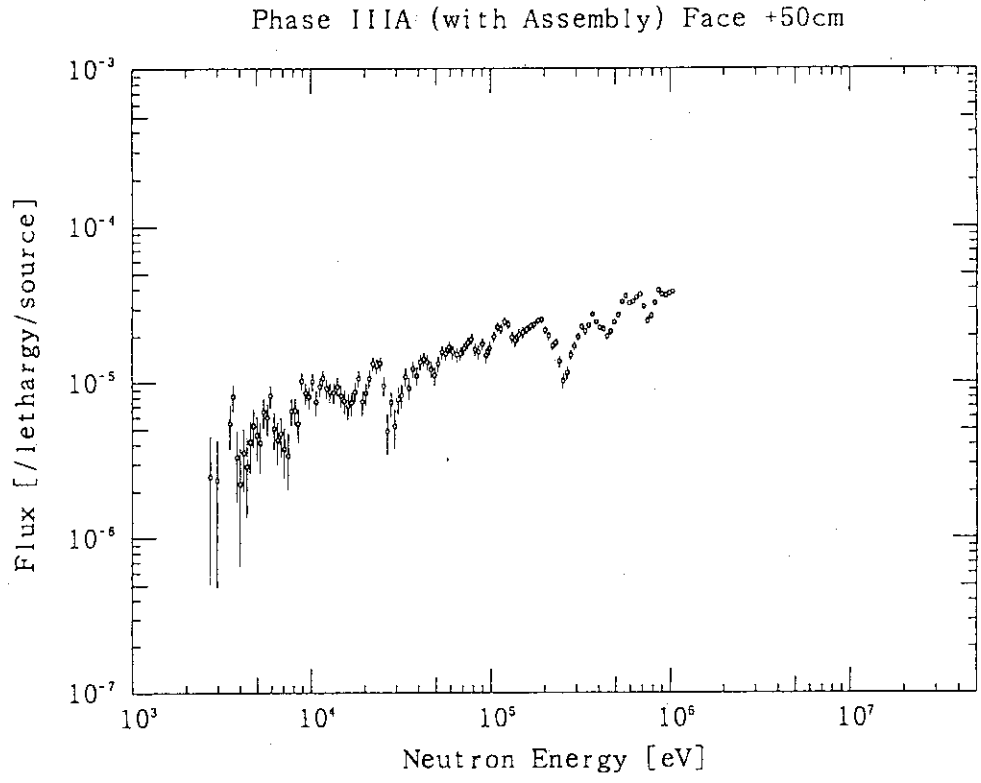

Fig. A.2.6 Measured neutron flux by the PRC spectrometer at a surface of the Phase IIIA assembly (at a position of 500 mm forward from the position closest to the source on the surface)

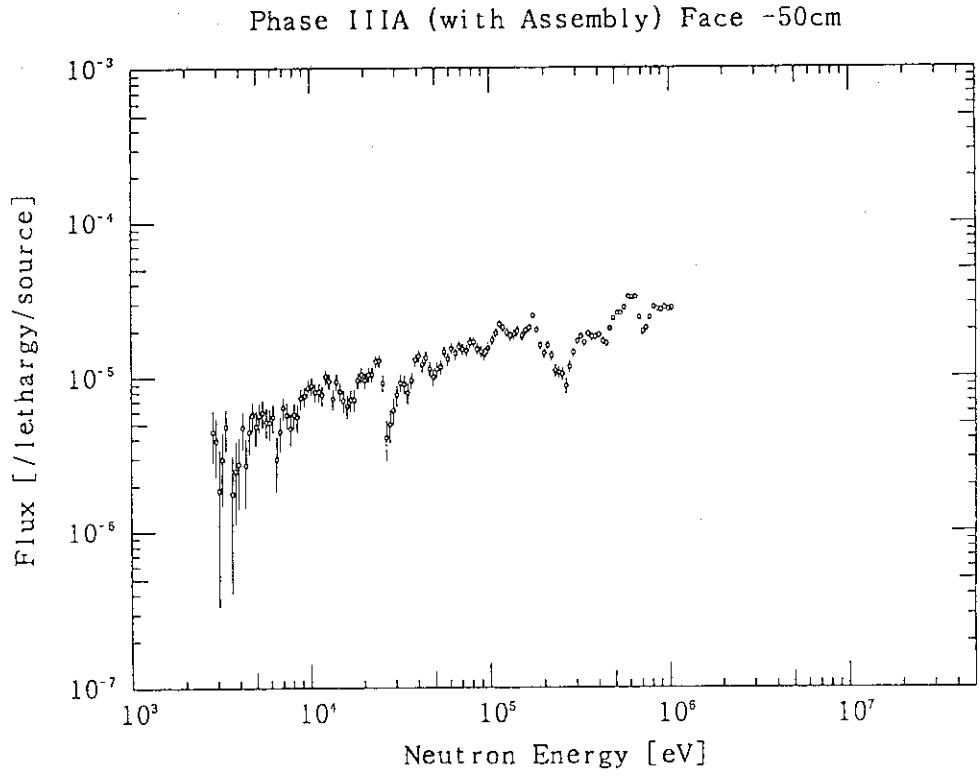

Fig. A.2.7 Measured neutron flux by the PRC spectrometer at a surface of the Phase IIIA assembly (at a position of 500 mm backward from the position closest to the source on the surface)

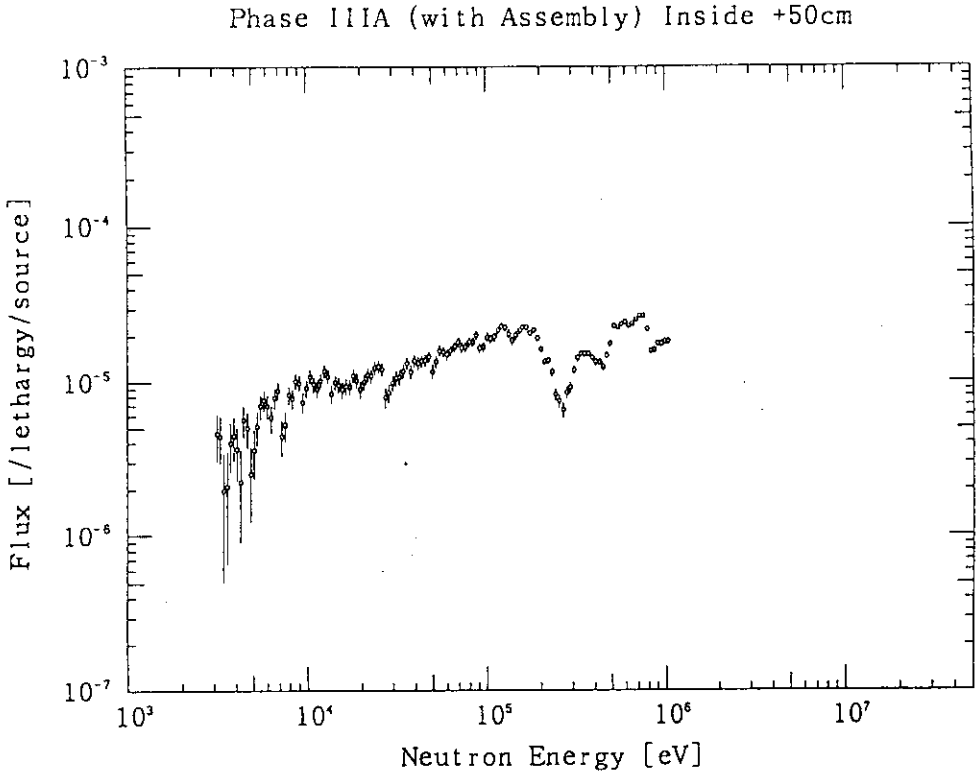

Fig. A.2.8 Measured neutron flux by the PRC spectrometer inside of the Phase IIIA assembly (at a position of 0 mm from the position closest to the source on the surface)

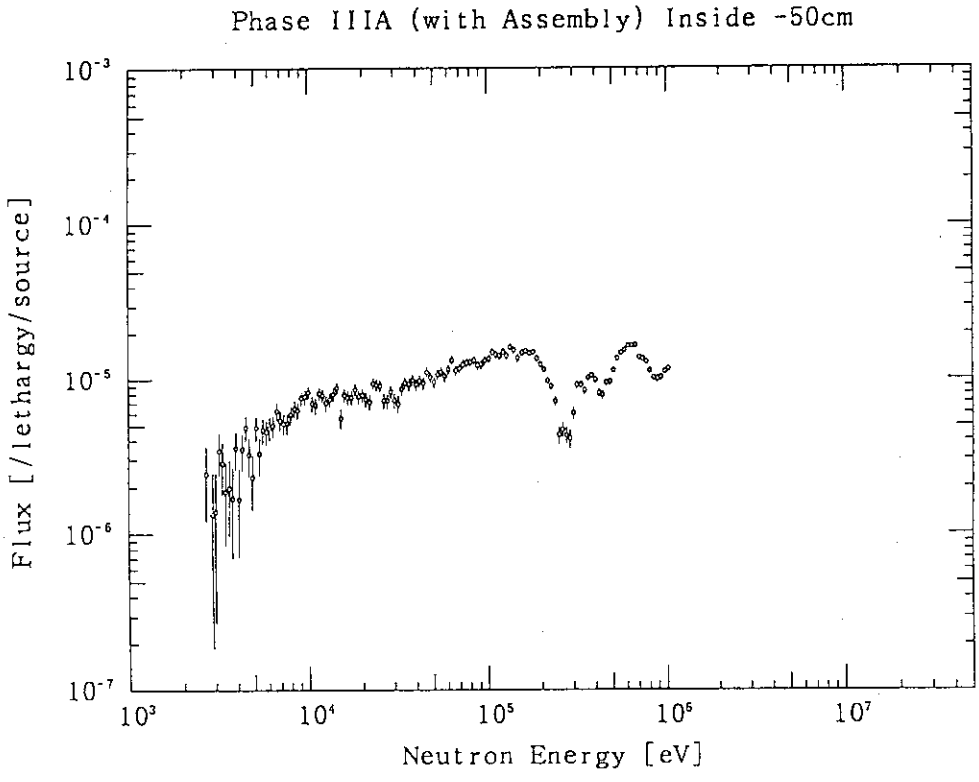

Fig. A.2.9 Measured neutron flux by the PRC spectrometer inside of the Phase IIIA assembly (at a position of 500 mm forward from the position closest to the source on the surface)

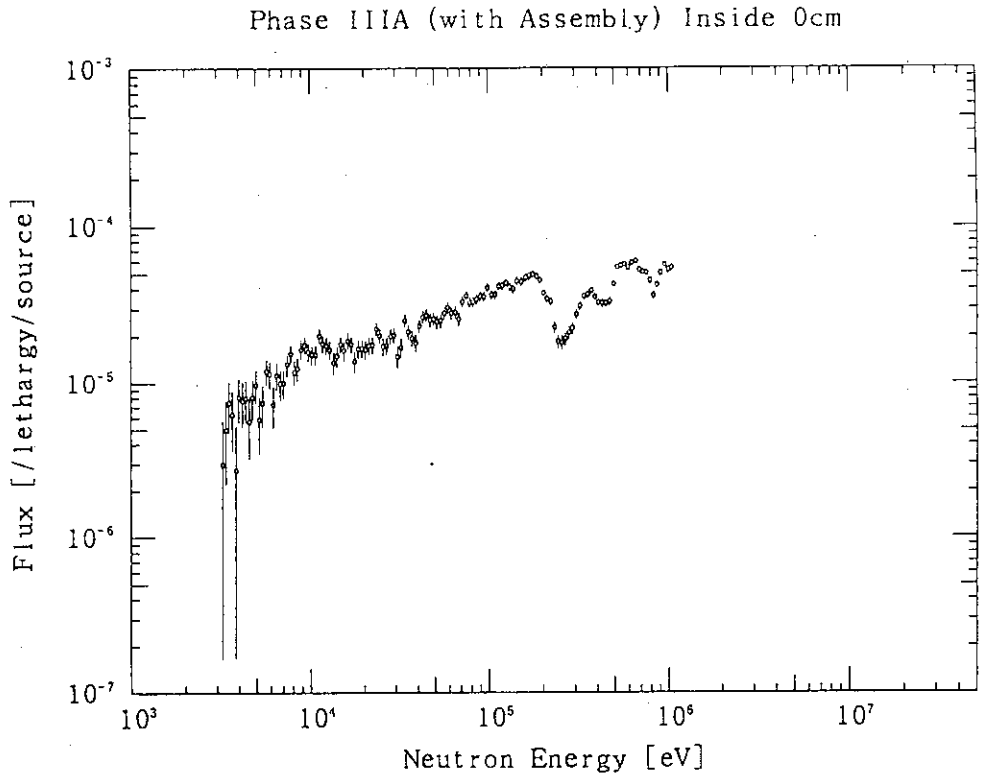

Fig. A.2.10 Measured neutron flux by the PRC spectrometer inside of the Phase IIIA assembly (at a position of 500 mm backward from the position closest to the source on the surface)

Appendix 3: Results of Tritium Production Rates Measured by Li_2O Pellets

Measurement technique of tritium production using a Li_2O pellet was applied to the Annular Blanket Experiment Phase III. However, the results obtained from that technique were inconsistent between repeated experimental runs, even though those results were expected to be first reference data. Therefore the obtained data are presented as second reference data and an example how much it does differs from each other is shown in this appendix.

A.3.1 Li_2O Pellet Technique

Preparation of Pellet

To measure tritium production rates in the Phase-III assembly, lithium oxide pellets were irradiated and number of tritium atoms produced in the pellets were counted. Lithium carbonate powder was heated about 1000 K to get lithium oxide. The powder of lithium oxide was formed into cylindrical pellets applying pressure of 400 MPa and the pellets were sintered for 4 hours at 1450 K in vacuum. Dimensions, weight and density of the obtained pellets were about ϕ12 mm x 2 mm, 0.38 g and 0.0017 g/mm^3, respectively. The apparent density corresponded to about 85 % of the theoretical density of Li_2O.

Three kinds of irradiation pellets which atomic ratios of lithium-6 and lithium-7 were different were used to measure tritium production rates of lithium-6 and -7 separately. The three atomic ratios were measured by means of the mass analysis and the results were

^{6}Li-enriched for T-6 measurement : 95.418 ± 0.002 ^{6}Li-atom %,
^{7}Li-enriched for T-7 measurement : 99.907 ± 0.001 ^{7}Li-atom % and
natural abundance for T-n measurement : 7.56 ± 0.01 ^{6}Li-atom %.

These pellets were kept in desiccators to avoid change of chemical composition absorbing H_2O, CO_2, etc.

Irradiation

The day before the irradiation, each Li_2O pellet to be irradiated was weighed and enclosed with a pair of aluminum cases of 0.2 mm thickness and sealed with bond to keep it away from tritium contamination and humidity. About thirty minutes before the irradiation, the pellets were fixed by a small amount of scotch tape between lithium oxide or lithium carbonate blocks and these blocks were inserted into the drawer which are set up in the assembly. One $^6Li_2O$, One $^7Li_2O$ and one nat-Li_2O pellets were located a measurement position.

The pellets were irradiated continuously during 5 ~ 8 hours periodically moving the assembly to simulate a line source. Total neutron yields were 2.3 ~ 7.8 x 10^{15}; the ranges of the figures depended on the different irradiation runs. About one hour after the stop of the irradiations, the pellets were collected and kept in a desiccator.

Chemical Processing for Pellet after Irradiation

After a couple of months from the irradiations, irradiated Li_2O pellets were dissolved in 8 cm^3 of distilled water. Weight of the distilled water was measured subtracting that of container between before and after adding the water. A concentration of tritium in the distilled water had been checked and it was found to be the background level. Complete solution was obtained after one week. The solution was distilled with an vacuum apparatus to obtain pure water with tritium produced. As the first step of distillation, the solution was poured into a "boiling flask" and frozen in liquid nitrogen. The apparatus was evacuated by a rotary vacuum pump. After complete evacuation about 0.1 Pa, the boiling flask was warmed up in a water bath of 80 °C while a "condensing flask" was, in turn, cooled down the another water bath of 5 °C. This resulted in transfer of most of the water, that is, hydrogens, to the condensing flask except hydrogens in LiOH. The collected water of 6 cm^3 was poured into a 20 cm^3 Teflon vial; then, 14 cm^3 of liquid scintillation cocktail, "Clear Sol", was added. The Clear Sol is a new type scintillation cocktail and makes not a two-phase state but clear solution of single phase under wide water fraction (up to 50 %). Weight of the distilled water was measured subtracting that of vial between before and after extracting the water. The vial was capped and at last samples for liquid scintillation counting were prepared.

Liquid Scintillation Counting

Tritium activity in the sample was measured by a low background scintillation counting system (Oken LSC-7100). The external standard ratio method was adapted to obtain the efficiency of each sample. The approximate efficiency was about 25 % in counts per tritium decay. The typical time chart of measurement for each sample in one cycle was as follows; three repeats of 30 seconds for the pre-ratio measurement, three repeats of 600 seconds for tritium counting and three repeats of 30 seconds for post-ratio measurement. Ten cycles were performed for each irradiation. Contents of the measurement samples were 3 NIST standard tritium water, 7 calibration samples, 3 background samples and 12 ~ 36 samples of irradiated pellets. The calibration samples were prepared for determination of a calibration curve. Four of them had several drops of carbon-tetrachloride as quencher. The calibration curve, that was relation between external standard ratio and relative efficiency,

was determined with linear fitting by the least square method. The tritium concentration was normalized to that of the standard tritium water (SRM 4926-D) which was obtained from National institute of Standards & technology (NIST), Department of Commerce, U.S.A. The background samples were made from distilled water instead of the tritium water extracted from the pellets.

Derivation of Tritium Production Rate

The obtained tritium concentrations of ten cycles for each sample were examined according to the χ^2 criterion with the Chauvenet's criterion, and sometimes one of ten data was rejected. The rest of data out of ten cycles were averaged to get tritium concentration for each sample and statistic error was estimated. Tritium production rates were calculated according to the following formula.

Tritium Production Rate [Tritiums/ Li-atom/ Source Neutron]

$$= \frac{C_T}{\lambda} \cdot \frac{W_{HTO}}{W_{H_2O}} \cdot \frac{M_{Li_2O}}{W_{Li_2O} \cdot N_{Li} \cdot N_A} \cdot \frac{1}{Y_n} \cdot \frac{1}{f_d \cdot f_e \cdot f_s}$$

C_T	:	Tritium concentration in distilled HTO water	[Bq/ g]
λ	:	Decay constant of tritium (= 1.781×10^{-9})	[Bq/ tritium]
W_{HTO}	:	Weight of collected HTO	[g]
W_{H2O}	:	Weight of poured H_2O	[g]
M_{Li2O}	:	Molecular weight of Li_2O	[g/mol]
W_{Li2O}	:	Weight of Li_2O pellet	[g]
N_{Li}	:	Number of Li-atoms in a Li_2O molecular (= 2)	[Li-atoms/ molecular]
N_A	:	Avogadro's number (= 6.022×10^{23})	[molecules/ mol]
Y_n	:	Neutron yield	[neutrons]
f_d	:	Correction factor for decay	
f_e	:	Correction factor for tritium escape	
f_s	:	Correction factor for self-shielding effect	

Produced tritiums in a pellet could not be collected perfectly. Because some of them escaped from the pellet and stop in the aluminum cover, and some of them did not stand chemical form of HTO but HT in gas phase when the pellet is dissolved. Amount of escape tritiums due to these two effects were experimentally estimated for some pellets irradiated by

14 MeV neutrons. It was found that 0.931, 0.939 and 0.929 tritiums a produced tritium were collected without escape for nat-Li, ^{6}Li and ^{7}Li, respectively. These values were correction factors for tritium escape, f_e, mentioned in the above equation.

Since atomic density of ^{6}Li in a $^{6}Li_2O$ pellet was about 16 times higher than that in Li_2O blocks or 32 times higher than Li_2CO_3 blocks used in the assembly, self-shielding effect of neutron flux inside the pellet for low energy region where neutron absorption cross section of ^{6}Li was large. The self-shielding effect was corrected as follows. Energy-dependent self-shielding correction factors f(E) were calculated based on a Monte Carlo method assuming isotropic neutron flux. After multiplication f(E) by calculated neutron spectrum at each measurement point, $\phi(E,\mathbf{r})$, they were integrated with respect to energy to obtain the correction factor for self-shielding effect, f_s, mentioned in the above equation. The factors ranged between 0.88 and 0.97 depending on positions of pellets.

Error Estimation

The estimated errors in the measured tritium production rate are as follows:

NIST tritium water standard		0.86 %
Efficiency for scintillation counting		0.7 ~ 1.0 %
Decay constant of tritium	: λ (from 12.33 ± 0.05 y)	0.41 %
Weight of collected HTO	: W_{HTO}	0.005 %
Weight of collected H_2O	: W_{H2O}	0.005 %
Weight of Li_2O pellet	: W_{Li2O}	0.005 %
Neutron yield	: Y_n	~ 1.8 %
Correction factor for decay	: f_d (from 12.33 ± 0.05 y)	0.02 ~ 0.06 %
Correction factor for tritium escape	: f_e	1.5 %

Total except for statistical error		~ 2.7 %
Statistical error in tritium counting	for $^{6}Li_2O$ pellet	0.5 ~ 5 %
	for $^{7}Li_2O$ pellet	> 4 %
	for nat-Li_2O pellet	1 ~ 17 %

A.3.2 Results in the Annular Blanket Experiments and Discussion

The results of Li_2O pellets showed two kinds of inconsistencies: between the result of natural Li_2O and the result composed from $^7Li_2O$ and $^6Li_2O$ pellets, and with the other results such as those of the NE213 and the Li-glass in terms of ratios among three configurations of the experiment. In the former case, there was 5-10% difference between both results as shown in Fig.A.3.1, and it was case by case which result was larger. In the latter inconsistency, some case deviate more than 10% from the other results such as the NE213 and the Li-glass methods. The 5 % deviation is possible, but the deviation more than 10% seems to be impossible even if the experimental error is considered. Also a criteria to judge the validity of the experimental results is obtained from physical consideration; the decrease of T_7 in the Phase IIIB and IIIC from the Phase IIIA can be estimated to be about 10% by the total cross section of graphite armor, and the T_6 in the Phase IIIB must be larger than the Phase IIIA because of neutron moderation due to the armor. From this criteria, it is inconsistent that the T_7 difference of the Phase IIIA from the others is too large and the T_6 of the Phase IIIB and IIIC are smaller than the Phase IIIA as shown in Figs. A.3.2 and 3.

To examine the reproducibility of measurement, the measurement was repeated by three times for the Phase IIIB experiment, but the results were also scattered. Figures A.3.4-6 shows the ratios of the results to the first measurement of three equivalent runs in the graphite armor blanket (Phase IIIB) for ^6Li, ^7Li and ^{nat}Li, respectively. In third measurement, two samples were placed in the same position (#3-1 and #3-2). It is seen that three independent measurements for the T_7 and T_n agree within experimental error at the front region less than 40 cm depth, though the error is large. But the T_n shows systematic difference between two measurements in the deeper region as seen in Fig. A.3.4. However, the T_6 was separated into two groups with 10% difference, and there seems to be systematic bias.

The followings are considered as possible reasons of the above behaviors:

1) Background fluctuation

In the case of poor signal-to-noise ratio such as the T_7 and T_n data in deep positions, small fluctuation can affect the background subtraction.

2) Uncertainty of gas escape correction

Correction of tritium escaped in gas form from the pellet was estimated to be about 7%, but this number could be changed by chemical state of the pellet depending on manufacturing process, i.e., depending on the date when the sample is

made. For example, the H_2O or CO_2 molecules can be contained.

3) Weight amibiguity

The number of Li atom is reduced from sample weight, but the weight can be changed by absorption of humidity depending on storage condition. The weight measured at the time when the pellet was made was used in data reduction, but usually the weight increases by several % during storage.

4) Flux perturbation

The pellet sample was canned by aluminum case and glued by epoxy resin. The hydrogen contained in them shifts neutron spectrum to lower energy and then increase the T_6.

Although it is very difficult to imagin that all of the above reasons made the present systematic biases, the obtained results deviated more than the experimental error estimated in Sec. A.3.1. Therefore the data of Li_2O pellets are judged as second reference data and for the Phase IIIB the results of three measurement were averaged by weighting for each error. The additional error of 5-10% should be accounted for those results by the above discussion. The results are listed in Tables A.3.1-3.

The existense of the unresolved error source was not found in the zonal method applied in the previous experiment. Since the zonal method uses large block of Li_2O and then an amount of tritium to be measured is large, the error sources considered above are very small factor. This should be noticed in difference of two methods. The method of small sample has the different situation and the techniques may be not established. There still exists problems as reported in Ref. (F. Maekawa, H. Maekawa, " 2nd International Comparison on Measuring Techniques of Tritium Production Rate for Fusion Neutronics Experiments (ICMT-2), JAERI-M 93-017 (1993)).

Table A.3.1 Tritium production rate measured by the $^{6}Li_2O$ pellet

	Drawer	Position (mm)	TPR-6/Li	Error(%)
Phase-3A	drawer-B	252.10	1.3162e-28	5.6303
		302.80	1.1788e-28	5.6800
		353.40	1.0720e-28	5.6619
		404.10	9.8442e-29	5.6896
Phase-3B	drawer-B	251.30	1.4771e-28	5.3309
		302.30	1.1410e-28	5.3836
		353.00	9.7003e-29	5.3040
		402.20	8.7004e-29	5.2453
		427.50	8.5018e-29	5.5541
		479.10	7.9176e-29	5.5724
		530.10	6.3881e-29	5.8959
		581.30	4.5646e-29	5.6453
	drawer-C	251.70	1.4295e-28	6.2953
		302.60	1.1502e-28	6.0901
		353.30	9.6352e-29	5.9520
		404.30	8.5138e-29	6.5033
Phase-3C	drawer-B	251.00	1.4038e-28	6.1566
		301.00	1.1504e-28	6.3952
		353.00	9.9157e-29	6.1468
		403.00	8.8122e-29	6.5806
		429.00	8.9748e-29	6.2526
		480.00	8.3668e-29	6.7207
		530.00	6.9392e-29	6.6942
		582.00	5.0724e-29	7.2004
	drawer-C	252.00	1.4110e-28	6.3509
		302.00	1.1429e-28	5.9811
		353.00	9.8940e-29	6.2996
		404.00	9.2424e-29	6.3678
	drawer-D	251.00	1.5314e-28	5.9721
		301.00	1.2676e-28	6.3070
		352.00	1.0809e-28	5.9498
		403.00	1.0163e-28	6.3841
		429.00	1.0333e-28	6.1270
		479.00	9.9080e-29	6.2226
		531.00	8.7591e-29	6.1114
		582.00	6.9230e-29	6.4519

Experimental error includes both statistical and systematical errors of detector and neutron yield monitor.

Table A.3.2 Tritium production rate measured by the $^{7}Li_2O$ pellet

	Drawer	Position (mm)	TPR-7/Li	Error(%)
Phase-3A	drawer-B	252.10	1.1274e-29	7.6703
		302.80	7.1844e-30	6.8401
		353.40	4.1064e-30	7.7700
		404.10	2.4279e-30	11.009
Phase-3B	drawer-B	251.30	8.3058e-30	6.8585
		302.30	4.8611e-30	7.5533
		353.00	3.1055e-30	9.0895
		402.20	1.7419e-30	8.1275
	drawer-C	251.70	8.8488e-30	7.7676
		302.60	5.1707e-30	7.4139
		353.30	3.1370e-30	13.500
		404.30	1.8584e-30	24.205
Phase-3C	drawer-B	251.00	7.7469e-30	11.446
		301.00	4.6773e-30	16.314
		353.00	2.6396e-30	15.790
		403.00	1.4879e-30	44.076
	drawer-C	252.00	8.4332e-30	20.872
		302.00	4.6359e-30	18.517
		353.00	2.7198e-30	22.222
		404.00	1.7599e-30	41.262
	drawer-D	251.00	9.2916e-30	8.6422
		301.00	5.8976e-30	18.142
		352.00	4.6907e-30	12.136
		403.00	2.9116e-30	22.554
		429.00	2.7110e-30	22.347
		479.00	1.8549e-30	30.250
		531.00	1.8502e-30	45.484
		582.00	7.5015e-31	94.097

Experimental error includes both statistical and systematical errors of detector and neutron yield monitor.

Table A.3.3 Tritium production rate measured by the $^{n}Li_2O$ pellet

Drawer	Position (mm)	TPR-n/Li (Composed)	Error (%)	TPR-n/Li (n-Li)	Error (%)
Phase-3A					
drawer-B	252.10	2.0357e-29	4.7929	1.8170e-29	6.0534
	302.80	1.5539e-29	4.3732	1.4311e-29	5.8991
	353.40	1.1890e-29	4.5835	1.1013e-29	6.3050
	404.10	9.6751e-30	5.0613	9.0239e-30	5.7902
Phase-3B					
drawer-B	251.30	1.8828e-29	4.2177	1.8955e-29	5.6658
	302.30	1.3108e-29	4.3844	1.3859e-29	5.9953
	353.00	1.0193e-29	4.5903	1.0326e-29	5.7104
	402.20	8.1775e-30	4.5062	8.4387e-30	6.2714
	427.50	8.0123e-30*	11.283	8.2108e-30	7.3871
	479.10	6.9397e-30*	8.7942	7.3774e-30	6.9959
	530.10	5.4017e-30*	7.8335	5.4913e-30	7.9925
	581.30	3.7900e-30*	7.1540	4.4101e-30	10.986
drawer-C	251.70	1.8971e-29	4.9031	1.7486e-29	7.7757
	302.60	1.3462e-29	4.7282	1.2381e-29	6.6934
	353.30	1.0173e-29	5.7375	9.7097e-30	9.4680
	404.30	8.1443e-30	7.2392	7.7783e-30	7.3668
Phase-3C					
drawer-B	251.00	1.7758e-29	5.8997	1.9420e-29	8.8251
	301.00	1.3008e-29	6.9021	1.4138e-29	8.2715
	353.00	9.9247e-30	6.0466	1.1274e-29	8.7784
	403.00	8.0270e-30	9.3160	9.2976e-30	13.844
	429.00	8.3309e-30*	11.006	9.0960e-30	10.188
	480.00	7.2655e-30*	9.0934	7.5844e-30	15.292
	530.00	5.8066e-30*	8.0572	6.7499e-30	10.101
	582.00	4.1706e-30*	8.0187	5.5460e-30	18.220
drawer-C	252.00	1.8447e-29	9.5532	1.9393e-29	7.5074
	302.00	1.2913e-29	7.3308	1.3906e-29	8.1229
	353.00	9.9825e-30	7.3173	1.0918e-29	8.8787
	404.00	8.6033e-30	9.3572	9.4895e-30	11.079
drawer-D	251.00	2.0149e-29	5.0312	1.9362e-29	7.7407
	301.00	1.5020e-29	7.7145	1.5965e-29	8.9834
	352.00	1.2495e-29	5.7299	1.4293e-29	10.082
	403.00	1.0363e-29	7.5270	1.1789e-29	12.248
	429.00	1.0306e-29	7.1441	1.1941e-29	12.289
	479.00	9.1934e-30	7.5803	1.0126e-29	11.808
	531.00	8.3219e-30	10.534	9.5243e-30	9.7426
	582.00	5.9190e-30	12.410	6.6270e-30	12.140

+Experimental error includes both statistical and systematical errors of detector and neutron yield monitor.
* Calculated TPR-7 data was used to compose TPR-n from TPR-6 and TPR-7.

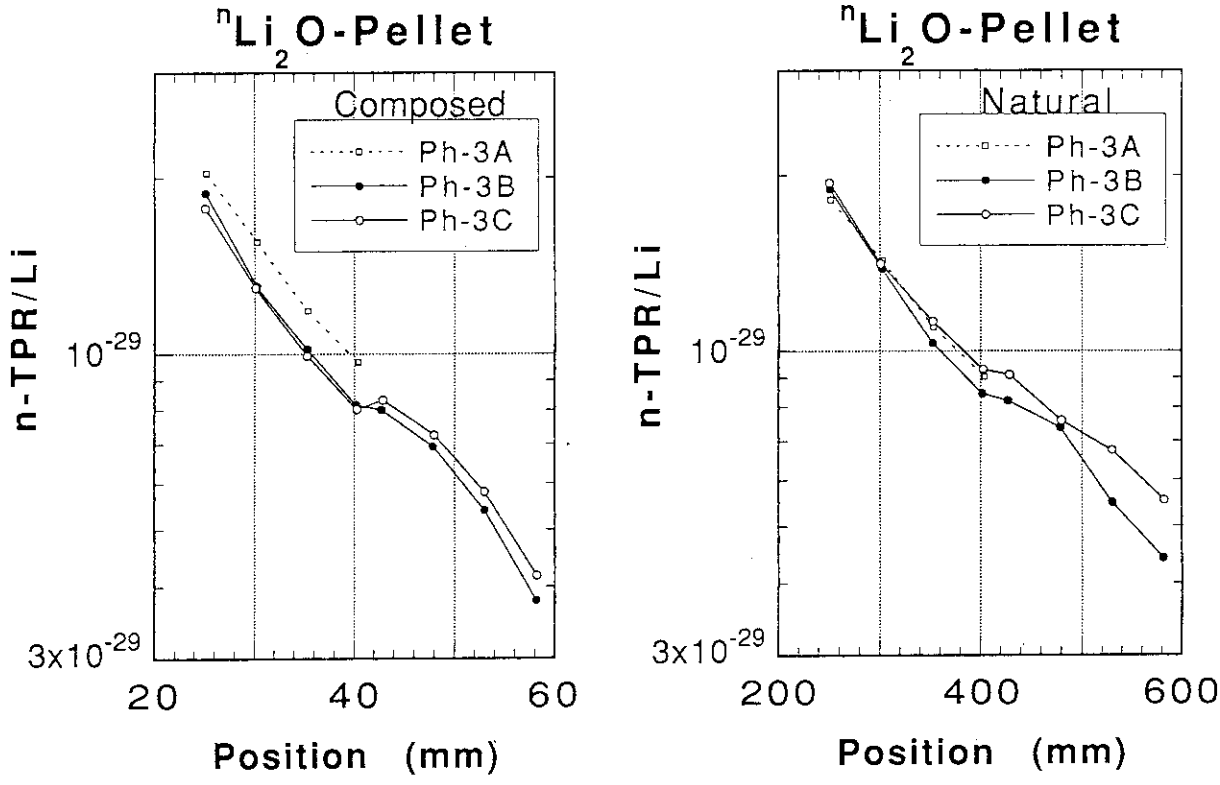

Fig. A.3.1 Comparison of the results from $^{n}Li_2O$ pellet and the results composed from the results of $^{7}Li_2O$ and $^{6}Li_2O$ pellets

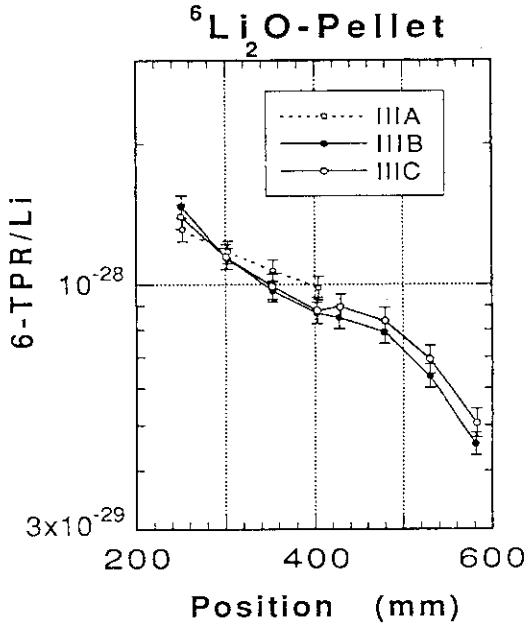

Fig. A.3.2 The results obtained from $^{6}Li_2O$ pellets

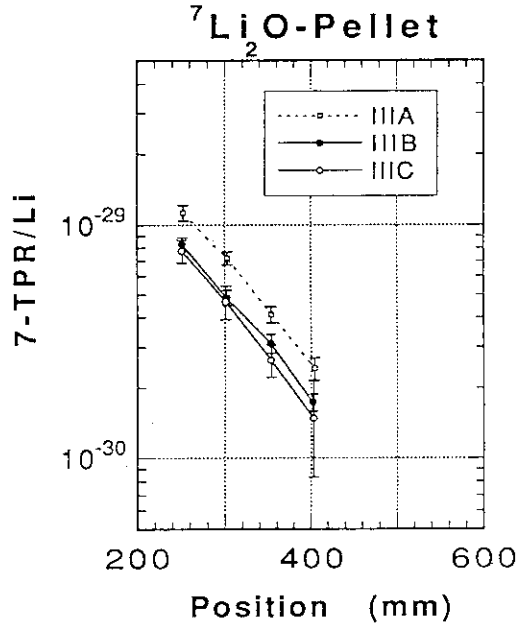

Fig. A.3.3 The results obtained from $^{7}Li_2O$ pellets

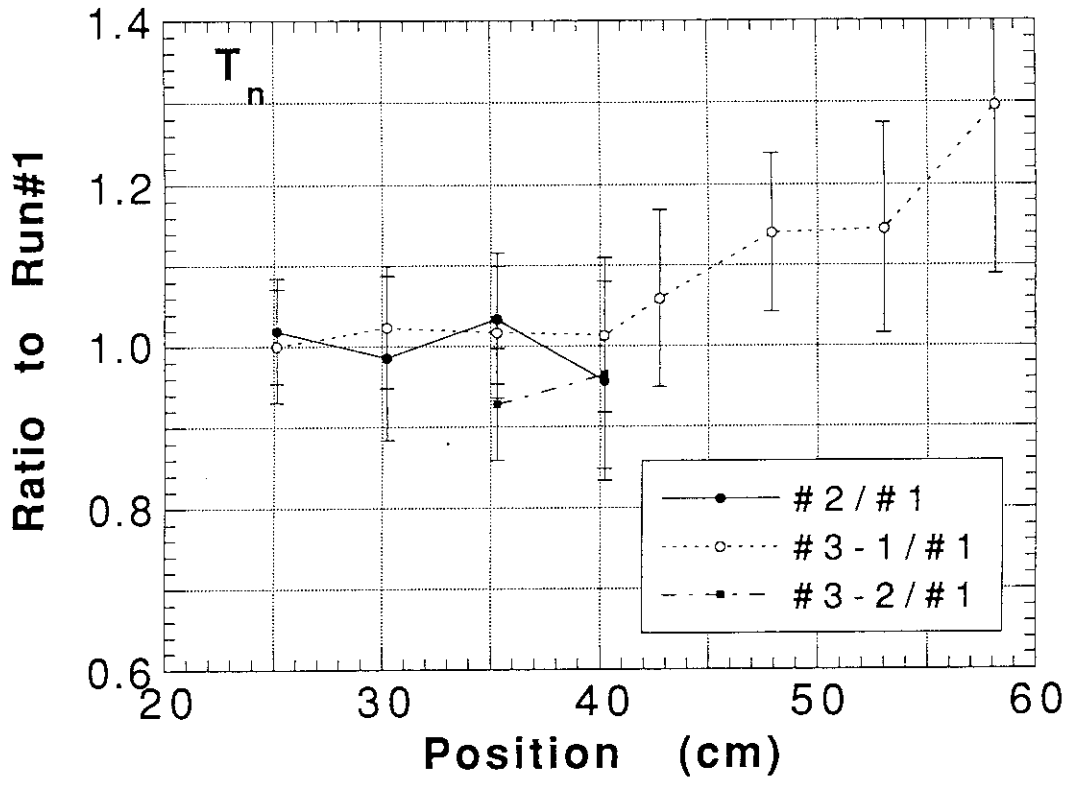

Fig. A.3.4 Relative ratio of the T_n results of each experimental run to the first measurement in the armor blanket experiment (Phase IIIB)

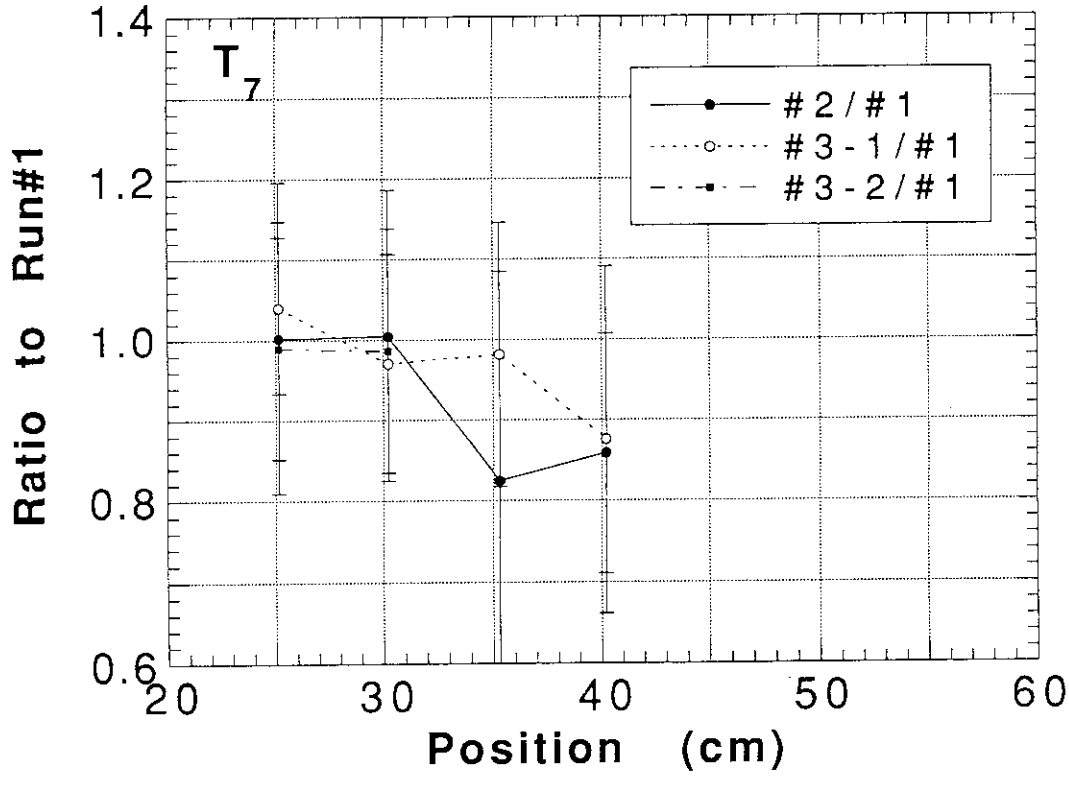

Fig. A.3.5 Relative ratio of the T_7 results of each experimental run to the first measurement in the armor blanket experiment (Phase IIIB)

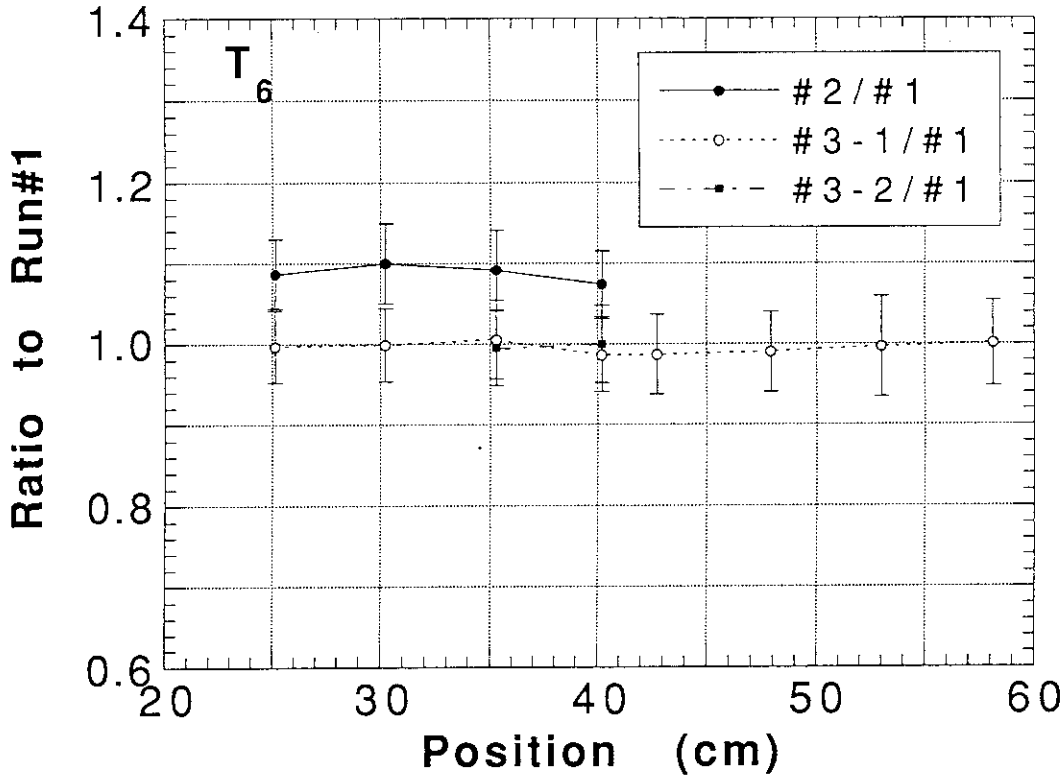

Fig. A.3.6 Relative ratio of the T_6 results of each experimental run to the first measurement in the armor blanket experiment (Phase IIIB)

Appendix 4 Measurements of Gamma-ray Responses

Gamma-ray responses were measured for some of the experimental assemblies in the annular test blankets. Measurements were performed by an NE213 recoil electron spectrometer and TLD detectors.

A.4.1 Measurements of In-situ Gamma-ray Spectrum for Phase IIIB Experiment[1]

In-situ gamma-ray spectrum was measured by using a spherical NE213 scintillation detector with 40 mm diameter. The gamma-ray spectrum is obtained by unfolding the measured recoil electron spectrum mostly produced by Compton scattering process. The scintillator size is larger than that used for neutron spectrum measurement, because the range of scattered electrons is longer than that of recoil protons. The cross section of the detector is shown in Fig. A.4.1. The gamma-ray response matrix of the detector was calculated by the Monte Carlo code MARTHA[2]. The spectrum unfolding was performed with the FORIST code.

The measurement was carried out by using step-wise mode operation of the line source. Three measurement positions are selected as shown in Fig. A.4.2. As shown in the figure, the detector size is rather large compared to the test blanket size, so the perturbation due to the detector would be large. Nevertheless the spectrum shape is expected to the same as the unperturbed spectrum, because the mean free path of high energy gamma-ray is rather long. The measured gamma-ray spectra are shown in Figs. A.4.3-5. It can be seen in the figures that several peaks and edges around 0.8 MeV, 1.4 MeV and 4.5 MeV corresponds to the gamma-rays from inelastic reactions on Fe, Ni, Cr and C. The low energy peaks from Fe, Ni and Cr in the first wall disappear with increase of depth, i.e., for the spectrum at 517 mm position.

A.4.2 Measurements of Gamma-ray Heating in the Phase IIIA and IIIB Test Blankets

Measurement of gamma-ray heating was performed by an interpolation method with plural kinds of TLD detectors.[3] The used TLDs are BeO, ^{7}LiF, Mg_2SiO_4 (hereafter abreviated as MSO), Sr_2SiO_4 (SSO) and Ba_2SiO_4 (BSO). The effective atomic numbers of these TLDs are 7.12, 8.24, 11.1, 32.5 and 49.9, respectively. Hence the gamma-ray heating of stainless steel (304SS) with effective atomic number of 25.9 can be interpolated with respect to the effective atomic number axis by using these TLD responses. However, since most of TLD detectors are sensitive not only to gamma-rays but also to neutrons, the measured TL should be corrected by the neutron contribution. This correction is made by subtracting neutron response of the TLD detector and neutron spectrum with assist of transport calculation. The neutron response of TLD detectors is also calculated with

responses for electrons and the other charged particles.[4] The calculated responses for the used TL detectors are given in Table A.4.1.

The measured TL responses were calibrated to exposure dose in unit of C/kg for ^{60}Co gamma-ray field and normalized by source neutron emission. Using the conversion factor from exposure dose to absorbed dose and subtracting neutron TL, the gamma-ray heating $\mathbf{H}_\gamma$ is obtained in unit of [erg/g/source neutron]. Using conversion factor **k**, $\mathbf{H}_\gamma$ for gamma-ray heating rate is written as follows:

$$\mathbf{H}_\gamma\,[\text{ erg/g/source}] = \mathbf{k}\,(\,TL_{observed} - TL_{neutron})\,/(\text{source neutron yield}),$$

where $\mathbf{k} = 81.4$ [(erg/g)/R for ^{60}Co equivalent field].

$TL_n = \int \phi_n(E) \cdot R_n(E) dE$ and $R_n(E)$ is neutrn responsein [R/(n/cm^2)]. The R unit of exposure dose is replaced into SI unit of [C/kg] by a factor of 2.58×10^{-4} [(C/kg)/R].

The irradiation was performed by the continuous operation mode of line source. The measured positions are illustrated in Figs. A.4.6-8 for each assemblies. Figures A.4.9-11 show the dose distribution measured by each TLD detector for the line source, the positions inside FW of the reference and armor blankets. The results without the assembly represent the response of gamma-rays emitted from the target assembly produced by inelastic reation on the target backing materials. The results obtained inside the FW are consistent with each other among the TLDs. This is explained as the gamma-ray response inside the stainless steel is larger than the irradiation in free space, because some of TLDs such as LiF, Mg_2SiO_4 are also sensitive to neutrons as shown in Fig. A.4.12. The measured results for all positions are summarized in Tables A.4.2-4. The error includes only staistical standard deviations among TLD samples irradiated at the same time.

References

1) F. Maekawa and Y. Oyama : "In-situ gamma-ray spectrometer with 40 mm diameter spherical scintillator," private communivcation. (1992)

2) K. Saito and S. Moriuchi: Nucl. Instrum. Meth., A251, 144 (1986)

3) S. Tanaka and N. Sasamoto: " J. Nucl. Sci. Technol., 22, 109 (1985)

4) H. Hashikura, et al.: " Calculation of Neutron Response of ThermoLuminescent Dosimetors," J. Faculty of Eng., 39, Univ. of Tokyo, pp7-16 (1987)

Table A.4.1 Calculated neutron response of TLDs (1/5)
[(C/kg)/(n/cm^2)]

No.	Neutron Energy [MeV]	BeO	7LiF	MSO	SSO	BSO
1.0000	1.6487e+01	0.0000e+00	2.4962e-13	1.4919e-13	7.0279e-14	5.7673e-14
2.0000	1.6231e+01	0.0000e+00	2.4962e-13	1.4919e-13	7.0279e-14	5.7673e-14
3.0000	1.6231e+01	0.0000e+00	2.4962e-13	1.4919e-13	7.0279e-14	5.7673e-14
4.0000	1.5980e+01	0.0000e+00	2.4962e-13	1.4919e-13	7.0279e-14	5.7673e-14
5.0000	1.5980e+01	0.0000e+00	2.4962e-13	1.4919e-13	7.0279e-14	5.7673e-14
6.0000	1.5732e+01	0.0000e+00	2.4962e-13	1.4919e-13	7.0279e-14	5.7673e-14
7.0000	1.5732e+01	0.0000e+00	2.4962e-13	1.4919e-13	7.0279e-14	5.7673e-14
8.0000	1.5488e+01	0.0000e+00	2.4962e-13	1.4919e-13	7.0279e-14	5.7673e-14
9.0000	1.5488e+01	1.2148e-13	2.4962e-13	1.4919e-13	7.0279e-14	5.7673e-14
10.000	1.5248e+01	1.2148e-13	2.4962e-13	1.4919e-13	7.0279e-14	5.7673e-14
11.000	1.5248e+01	1.2148e-13	2.4962e-13	1.4919e-13	7.0279e-14	5.7673e-14
12.000	1.5012e+01	1.2148e-13	2.4962e-13	1.4919e-13	7.0279e-14	5.7673e-14
13.000	1.5012e+01	1.2148e-13	2.4962e-13	1.4919e-13	7.0279e-14	5.7673e-14
14.000	1.4779e+01	1.2148e-13	2.4962e-13	1.4919e-13	7.0279e-14	5.7673e-14
15.000	1.4779e+01	1.2148e-13	2.4962e-13	1.4919e-13	7.0279e-14	5.7673e-14
16.000	1.4550e+01	1.2148e-13	2.4962e-13	1.4919e-13	7.0279e-14	5.7673e-14
17.000	1.4550e+01	1.0964e-13	2.1916e-13	1.3563e-13	6.4025e-14	5.2286e-14
18.000	1.4324e+01	1.0964e-13	2.1916e-13	1.3563e-13	6.4025e-14	5.2286e-14
19.000	1.4324e+01	1.0964e-13	2.1916e-13	1.3563e-13	6.4025e-14	5.2286e-14
20.000	1.4102e+01	1.0964e-13	2.1916e-13	1.3563e-13	6.4025e-14	5.2286e-14
21.000	1.4102e+01	1.0964e-13	2.1916e-13	1.3563e-13	6.4025e-14	5.2286e-14
22.000	1.3883e+01	1.0964e-13	2.1916e-13	1.3563e-13	6.4025e-14	5.2286e-14
23.000	1.3883e+01	1.0964e-13	2.1916e-13	1.3563e-13	6.4025e-14	5.2286e-14
24.000	1.3668e+01	1.0964e-13	2.1916e-13	1.3563e-13	6.4025e-14	5.2286e-14
25.000	1.3668e+01	1.0964e-13	2.1916e-13	1.3563e-13	6.4025e-14	5.2286e-14
26.000	1.3456e+01	1.0964e-13	2.1916e-13	1.3563e-13	6.4025e-14	5.2286e-14
27.000	1.3456e+01	1.0964e-13	2.1916e-13	1.3563e-13	6.4025e-14	5.2286e-14
28.000	1.3248e+01	1.0964e-13	2.1916e-13	1.3563e-13	6.4025e-14	5.2286e-14
29.000	1.3248e+01	1.0964e-13	2.1916e-13	1.3563e-13	6.4025e-14	5.2286e-14
30.000	1.3042e+01	1.0964e-13	2.1916e-13	1.3563e-13	6.4025e-14	5.2286e-14
31.000	1.3042e+01	1.0964e-13	2.1916e-13	1.3563e-13	6.4025e-14	5.2286e-14
32.000	1.2840e+01	1.0964e-13	2.1916e-13	1.3563e-13	6.4025e-14	5.2286e-14
33.000	1.2840e+01	9.7906e-14	2.0143e-13	1.1375e-13	5.5563e-14	4.5258e-14
34.000	1.2641e+01	9.7906e-14	2.0143e-13	1.1375e-13	5.5563e-14	4.5258e-14
35.000	1.2641e+01	9.7906e-14	2.0143e-13	1.1375e-13	5.5563e-14	4.5258e-14
36.000	1.2445e+01	9.7906e-14	2.0143e-13	1.1375e-13	5.5563e-14	4.5258e-14
37.000	1.2445e+01	9.7906e-14	2.0143e-13	1.1375e-13	5.5563e-14	4.5258e-14
38.000	1.2252e+01	9.7906e-14	2.0143e-13	1.1375e-13	5.5563e-14	4.5258e-14
39.000	1.2252e+01	9.7906e-14	2.0143e-13	1.1375e-13	5.5563e-14	4.5258e-14
40.000	1.2062e+01	9.7906e-14	2.0143e-13	1.1375e-13	5.5563e-14	4.5258e-14
41.000	1.2062e+01	9.7906e-14	2.0143e-13	1.1375e-13	5.5563e-14	4.5258e-14
42.000	1.1875e+01	9.7906e-14	2.0143e-13	1.1375e-13	5.5563e-14	4.5258e-14
43.000	1.1875e+01	9.7906e-14	2.0143e-13	1.1375e-13	5.5563e-14	4.5258e-14
44.000	1.1691e+01	9.7906e-14	2.0143e-13	1.1375e-13	5.5563e-14	4.5258e-14
45.000	1.1691e+01	9.7906e-14	2.0143e-13	1.1375e-13	5.5563e-14	4.5258e-14
46.000	1.1510e+01	9.7906e-14	2.0143e-13	1.1375e-13	5.5563e-14	4.5258e-14
47.000	1.1510e+01	9.7906e-14	2.0143e-13	1.1375e-13	5.5563e-14	4.5258e-14
48.000	1.1331e+01	9.7906e-14	2.0143e-13	1.1375e-13	5.5563e-14	4.5258e-14
49.000	1.1331e+01	9.0930e-14	1.8146e-13	8.9129e-14	4.7498e-14	3.8457e-14
50.000	1.1156e+01	9.0930e-14	1.8146e-13	8.9129e-14	4.7498e-14	3.8457e-14
51.000	1.1156e+01	9.0930e-14	1.8146e-13	8.9129e-14	4.7498e-14	3.8457e-14
52.000	1.0983e+01	9.0930e-14	1.8146e-13	8.9129e-14	4.7498e-14	3.8457e-14
53.000	1.0983e+01	9.0930e-14	1.8146e-13	8.9129e-14	4.7498e-14	3.8457e-14

Table A.4.1 Calculated neutron response of TLDs (2/5)
[(C/kg)/(n/cm^2)]

No.	Neutron Energy [MeV]	BeO	7LiF	MSO	SSO	BSO
54.000	1.0812e+01	9.0930e-14	1.8146e-13	8.9129e-14	4.7498e-14	3.8457e-14
55.000	1.0812e+01	9.0930e-14	1.8146e-13	8.9129e-14	4.7498e-14	3.8457e-14
56.000	1.0645e+01	9.0930e-14	1.8146e-13	8.9129e-14	4.7498e-14	3.8457e-14
57.000	1.0645e+01	9.0930e-14	1.8146e-13	8.9129e-14	4.7498e-14	3.8457e-14
58.000	1.0480e+01	9.0930e-14	1.8146e-13	8.9129e-14	4.7498e-14	3.8457e-14
59.000	1.0480e+01	9.0930e-14	1.8146e-13	8.9129e-14	4.7498e-14	3.8457e-14
60.000	1.0317e+01	9.0930e-14	1.8146e-13	8.9129e-14	4.7498e-14	3.8457e-14
61.000	1.0317e+01	9.0930e-14	1.8146e-13	8.9129e-14	4.7498e-14	3.8457e-14
62.000	1.0157e+01	9.0930e-14	1.8146e-13	8.9129e-14	4.7498e-14	3.8457e-14
63.000	1.0157e+01	9.0919e-14	1.8144e-13	8.9111e-14	4.7490e-14	3.8450e-14
64.000	9.9999e+00	9.0919e-14	1.8144e-13	8.9111e-14	4.7490e-14	3.8450e-14
65.000	9.9999e+00	7.3773e-14	1.5863e-13	6.1726e-14	3.4923e-14	2.8125e-14
66.000	9.3940e+00	7.3773e-14	1.5863e-13	6.1726e-14	3.4923e-14	2.8125e-14
67.000	9.3940e+00	7.3770e-14	1.5863e-13	6.1724e-14	3.4920e-14	2.8125e-14
68.000	8.8249e+00	7.3770e-14	1.5863e-13	6.1724e-14	3.4920e-14	2.8125e-14
69.000	8.8249e+00	5.7787e-14	1.3325e-13	4.3888e-14	2.5919e-14	2.0841e-14
70.000	8.2902e+00	5.7787e-14	1.3325e-13	4.3888e-14	2.5919e-14	2.0841e-14
71.000	8.2902e+00	5.7787e-14	1.3324e-13	4.3886e-14	2.5919e-14	2.0840e-14
72.000	7.7879e+00	5.7787e-14	1.3324e-13	4.3886e-14	2.5919e-14	2.0840e-14
73.000	7.7879e+00	5.2173e-14	1.1574e-13	2.9002e-14	1.9534e-14	1.5768e-14
74.000	7.3161e+00	5.2173e-14	1.1574e-13	2.9002e-14	1.9534e-14	1.5768e-14
75.000	7.3161e+00	5.2173e-14	1.1574e-13	2.8999e-14	1.9532e-14	1.5767e-14
76.000	6.8728e+00	5.2173e-14	1.1574e-13	2.8999e-14	1.9532e-14	1.5767e-14
77.000	6.8728e+00	4.6765e-14	9.7926e-14	1.8143e-14	1.2899e-14	1.0467e-14
78.000	6.4564e+00	4.6765e-14	9.7926e-14	1.8143e-14	1.2899e-14	1.0467e-14
79.000	6.4564e+00	4.6762e-14	9.7924e-14	1.8141e-14	1.2898e-14	1.0466e-14
80.000	6.0652e+00	4.6762e-14	9.7924e-14	1.8141e-14	1.2898e-14	1.0466e-14
81.000	6.0652e+00	3.9069e-14	8.4603e-14	1.1023e-14	7.6776e-15	6.3509e-15
82.000	5.6978e+00	3.9069e-14	8.4603e-14	1.1023e-14	7.6776e-15	6.3509e-15
83.000	5.6978e+00	3.9069e-14	8.4598e-14	1.1023e-14	7.6776e-15	6.3509e-15
84.000	5.3525e+00	3.9069e-14	8.4598e-14	1.1023e-14	7.6776e-15	6.3509e-15
85.000	5.3525e+00	3.8943e-14	6.6530e-14	1.1152e-14	7.9913e-15	6.5006e-15
86.000	5.0282e+00	3.8943e-14	6.6530e-14	1.1152e-14	7.9913e-15	6.5006e-15
87.000	5.0282e+00	3.8943e-14	6.6525e-14	1.1152e-14	7.9910e-15	6.5003e-15
88.000	4.7236e+00	3.8943e-14	6.6525e-14	1.1152e-14	7.9910e-15	6.5003e-15
89.000	4.7236e+00	3.5761e-14	5.9717e-14	1.4503e-14	7.2506e-15	5.8427e-15
90.000	4.4374e+00	3.5761e-14	5.9717e-14	1.4503e-14	7.2506e-15	5.8427e-15
91.000	4.4374e+00	3.5761e-14	5.9717e-14	1.4503e-14	7.2506e-15	5.8427e-15
92.000	4.1686e+00	3.5761e-14	5.9717e-14	1.4503e-14	7.2506e-15	5.8427e-15
93.000	4.1686e+00	3.2683e-14	5.0772e-14	1.2491e-14	6.3749e-15	5.1288e-15
94.000	3.9160e+00	3.2683e-14	5.0772e-14	1.2491e-14	6.3749e-15	5.1288e-15
95.000	3.9160e+00	3.2683e-14	5.0772e-14	1.2491e-14	6.3749e-15	5.1288e-15
96.000	3.6787e+00	3.2683e-14	5.0772e-14	1.2491e-14	6.3749e-15	5.1288e-15
97.000	3.6787e+00	3.2405e-14	4.7165e-14	1.2351e-14	6.4794e-15	5.1775e-15
98.000	3.4559e+00	3.2405e-14	4.7165e-14	1.2351e-14	6.4794e-15	5.1775e-15
99.000	3.4559e+00	3.2405e-14	4.7165e-14	1.2351e-14	6.4794e-15	5.1775e-15
100.00	3.2465e+00	3.2405e-14	4.7165e-14	1.2351e-14	6.4794e-15	5.1775e-15
101.00	3.2465e+00	2.8076e-14	4.5202e-14	9.0117e-15	4.4820e-15	3.5648e-15
102.00	3.0498e+00	2.8076e-14	4.5202e-14	9.0117e-15	4.4820e-15	3.5648e-15
103.00	3.0498e+00	2.8076e-14	4.5202e-14	9.0117e-15	4.4820e-15	3.5648e-15
104.00	2.8650e+00	2.8076e-14	4.5202e-14	9.0117e-15	4.4820e-15	3.5648e-15
105.00	2.8650e+00	2.5551e-14	4.4598e-14	8.4157e-15	4.0031e-15	3.1295e-15
106.00	2.6914e+00	2.5551e-14	4.4598e-14	8.4157e-15	4.0031e-15	3.1295e-15

Table A.4.1 Calculated neutron response of TLDs (3/5)
[(C/kg)/(n/cm^2)]

No.	Neutron Energy [MeV]	BeO	7LiF	MSO	SSO	BSO
107.00	2.6914e+00	2.5551e-14	4.4598e-14	8.4157e-15	4.0031e-15	3.1295e-15
108.00	2.5284e+00	2.5551e-14	4.4598e-14	8.4157e-15	4.0031e-15	3.1295e-15
109.00	2.5284e+00	1.7706e-14	4.0129e-14	5.2408e-15	2.3493e-15	1.8307e-15
110.00	2.3752e+00	1.7706e-14	4.0129e-14	5.2408e-15	2.3493e-15	1.8307e-15
111.00	2.3752e+00	1.7706e-14	4.0129e-14	5.2408e-15	2.3493e-15	1.8307e-15
112.00	2.2313e+00	1.7706e-14	4.0129e-14	5.2408e-15	2.3493e-15	1.8307e-15
113.00	2.2313e+00	1.7532e-14	3.5052e-14	5.9366e-15	3.0328e-15	2.3748e-15
114.00	2.0961e+00	1.7532e-14	3.5052e-14	5.9366e-15	3.0328e-15	2.3748e-15
115.00	2.0961e+00	1.7532e-14	3.5052e-14	5.9366e-15	3.0328e-15	2.3748e-15
116.00	1.9691e+00	1.7532e-14	3.5052e-14	5.9366e-15	3.0328e-15	2.3748e-15
117.00	1.9691e+00	1.7025e-14	3.0328e-14	6.6146e-15	3.4087e-15	2.6979e-15
118.00	1.8498e+00	1.7025e-14	3.0328e-14	6.6146e-15	3.4087e-15	2.6979e-15
119.00	1.8498e+00	1.7025e-14	3.0328e-14	6.6146e-15	3.4087e-15	2.6979e-15
120.00	1.7377e+00	1.7025e-14	3.0328e-14	6.6146e-15	3.4087e-15	2.6979e-15
121.00	1.7377e+00	1.7526e-14	1.9228e-14	6.7911e-15	3.6510e-15	2.8837e-15
122.00	1.5335e+00	1.7526e-14	1.9228e-14	6.7911e-15	3.6510e-15	2.8837e-15
123.00	1.5335e+00	1.6502e-14	1.6882e-14	6.8202e-15	3.7660e-15	2.9657e-15
124.00	1.3533e+00	1.6502e-14	1.6882e-14	6.8202e-15	3.7660e-15	2.9657e-15
125.00	1.3533e+00	1.6632e-14	1.6295e-14	7.2044e-15	4.0604e-15	3.1920e-15
126.00	1.1943e+00	1.6632e-14	1.6295e-14	7.2044e-15	4.0604e-15	3.1920e-15
127.00	1.1943e+00	1.5877e-14	1.4069e-14	6.4461e-15	3.6860e-15	2.8733e-15
128.00	1.0540e+00	1.5877e-14	1.4069e-14	6.4461e-15	3.6860e-15	2.8733e-15
129.00	1.0540e+00	1.8562e-14	1.2067e-14	8.3610e-15	5.0356e-15	3.9435e-15
130.00	9.3013e-01	1.8562e-14	1.2067e-14	8.3610e-15	5.0356e-15	3.9435e-15
131.00	9.3013e-01	1.5251e-14	1.0515e-14	6.3313e-15	3.6396e-15	2.7967e-15
132.00	8.2084e-01	1.5251e-14	1.0515e-14	6.3313e-15	3.6396e-15	2.7967e-15
133.00	8.2084e-01	1.4342e-14	9.2692e-15	5.5393e-15	3.1257e-15	2.3811e-15
134.00	7.2438e-01	1.4342e-14	9.2692e-15	5.5393e-15	3.1257e-15	2.3811e-15
135.00	7.2438e-01	1.1846e-14	7.3388e-15	4.1089e-15	2.2695e-15	1.7165e-15
136.00	6.3927e-01	1.1846e-14	7.3388e-15	4.1089e-15	2.2695e-15	1.7165e-15
137.00	6.3927e-01	1.2742e-14	7.1776e-15	3.6473e-15	2.0355e-15	1.5333e-15
138.00	5.6415e-01	1.2742e-14	7.1776e-15	3.6473e-15	2.0355e-15	1.5333e-15
139.00	5.6415e-01	9.7178e-15	6.9652e-15	3.4458e-15	1.9468e-15	1.4697e-15
140.00	4.9786e-01	9.7178e-15	6.9652e-15	3.4458e-15	1.9468e-15	1.4697e-15
141.00	4.9786e-01	1.1550e-14	6.4606e-15	5.0692e-15	2.8450e-15	2.2091e-15
142.00	4.3936e-01	1.1550e-14	6.4606e-15	5.0692e-15	2.8450e-15	2.2091e-15
143.00	4.3936e-01	1.0775e-14	6.9198e-15	4.7131e-15	2.5016e-15	1.9357e-15
144.00	3.8774e-01	1.0775e-14	6.9198e-15	4.7131e-15	2.5016e-15	1.9357e-15
145.00	3.8774e-01	9.3873e-15	6.8904e-15	4.0570e-15	2.2462e-15	1.7195e-15
146.00	3.4217e-01	9.3873e-15	6.8904e-15	4.0570e-15	2.2462e-15	1.7195e-15
147.00	3.4217e-01	8.3564e-15	7.2356e-15	3.6357e-15	1.9562e-15	1.4961e-15
148.00	3.0197e-01	8.3564e-15	7.2356e-15	3.6357e-15	1.9562e-15	1.4961e-15
149.00	3.0197e-01	7.2165e-15	9.8608e-15	3.2410e-15	1.5914e-15	1.2131e-15
150.00	2.6649e-01	7.2165e-15	9.8608e-15	3.2410e-15	1.5914e-15	1.2131e-15
151.00	2.6649e-01	6.4172e-15	9.2496e-15	2.9092e-15	1.3843e-15	1.0525e-15
152.00	2.3517e-01	6.4172e-15	9.2496e-15	2.9092e-15	1.3843e-15	1.0525e-15
153.00	2.3517e-01	5.8071e-15	4.3865e-15	2.4393e-15	1.2658e-15	9.6157e-16
154.00	2.0754e-01	5.8071e-15	4.3865e-15	2.4393e-15	1.2658e-15	9.6157e-16
155.00	2.0754e-01	5.2653e-15	2.8924e-15	2.1242e-15	1.1932e-15	9.1866e-16
156.00	1.8315e-01	5.2653e-15	2.8924e-15	2.1242e-15	1.1932e-15	9.1866e-16
157.00	1.8315e-01	4.7738e-15	2.5215e-15	1.5970e-15	9.0687e-16	6.9957e-16
158.00	1.6163e-01	4.7738e-15	2.5215e-15	1.5970e-15	9.0687e-16	6.9957e-16
159.00	1.6163e-01	4.3269e-15	2.2584e-15	1.2708e-15	6.7294e-16	5.5790e-16

Table A.4.1 Calculated neutron response of TLDs (4/5)
[(C/kg)/(n/cm^2)]

No.	Neutron Energy [MeV]	BeO	7LiF	MSO	SSO	BSO
160.00	1.4264e-01	4.3269e-15	2.2584e-15	1.2708e-15	6.7294e-16	5.5790e-16
161.00	1.4264e-01	3.9141e-15	1.7719e-15	1.1005e-15	5.8878e-16	4.9724e-16
162.00	1.2588e-01	3.9141e-15	1.7719e-15	1.1005e-15	5.8878e-16	4.9724e-16
163.00	1.2588e-01	3.5351e-15	1.7303e-15	1.0121e-15	5.2289e-16	4.4479e-16
164.00	1.1109e-01	3.5351e-15	1.7303e-15	1.0121e-15	5.2289e-16	4.4479e-16
165.00	1.1109e-01	3.1850e-15	2.7797e-15	1.0010e-15	4.6512e-16	3.9247e-16
166.00	9.8035e-02	3.1850e-15	2.7797e-15	1.0010e-15	4.6512e-16	3.9247e-16
167.00	9.8035e-02	2.8643e-15	2.4848e-15	1.3409e-15	4.1396e-16	3.4244e-16
168.00	8.6515e-02	2.8643e-15	2.4848e-15	1.3409e-15	4.1396e-16	3.4244e-16
169.00	8.6515e-02	2.5708e-15	1.3002e-15	1.5645e-15	3.6984e-16	3.0950e-16
170.00	7.6349e-02	2.5708e-15	1.3002e-15	1.5645e-15	3.6984e-16	3.0950e-16
171.00	7.6349e-02	2.3031e-15	8.8687e-16	8.0984e-16	3.3181e-16	2.8264e-16
172.00	6.7378e-02	2.3031e-15	8.8687e-16	8.0984e-16	3.3181e-16	2.8264e-16
173.00	6.7378e-02	2.0595e-15	7.2759e-16	5.6677e-16	2.9536e-16	2.4964e-16
174.00	5.9461e-02	2.0595e-15	7.2759e-16	5.6677e-16	2.9536e-16	2.4964e-16
175.00	5.9461e-02	1.8383e-15	7.2418e-16	4.5983e-16	2.5996e-16	2.2008e-16
176.00	5.2474e-02	1.8383e-15	7.2418e-16	4.5983e-16	2.5996e-16	2.2008e-16
177.00	5.2474e-02	1.6371e-15	1.3830e-15	4.0372e-16	2.2948e-16	1.9758e-16
178.00	4.6308e-02	1.6371e-15	1.3830e-15	4.0372e-16	2.2948e-16	1.9758e-16
179.00	4.6308e-02	1.4550e-15	6.6556e-16	3.6148e-16	2.0336e-16	1.7283e-16
180.00	4.0867e-02	1.4550e-15	6.6556e-16	3.6148e-16	2.0336e-16	1.7283e-16
181.00	4.0867e-02	1.2916e-15	5.5119e-16	3.1719e-16	1.8057e-16	1.5473e-16
182.00	3.6065e-02	1.2916e-15	5.5119e-16	3.1719e-16	1.8057e-16	1.5473e-16
183.00	3.6065e-02	1.1453e-15	4.4105e-16	2.7503e-16	1.6057e-16	1.4070e-16
184.00	3.1827e-02	1.1453e-15	4.4105e-16	2.7503e-16	1.6057e-16	1.4070e-16
185.00	3.1827e-02	1.0146e-15	4.6123e-16	2.3960e-16	1.4312e-16	1.2800e-16
186.00	2.8087e-02	1.0146e-15	4.6123e-16	2.3960e-16	1.4312e-16	1.2800e-16
187.00	2.8087e-02	8.9830e-16	7.8321e-16	2.1412e-16	1.2722e-16	1.1010e-16
188.00	2.4787e-02	8.9830e-16	7.8321e-16	2.1412e-16	1.2722e-16	1.1010e-16
189.00	2.4787e-02	7.9503e-16	3.7167e-16	2.0408e-16	1.1345e-16	9.8641e-17
190.00	2.1874e-02	7.9503e-16	3.7167e-16	2.0408e-16	1.1345e-16	9.8641e-17
191.00	2.1874e-02	7.0349e-16	2.9443e-16	1.9872e-16	1.0109e-16	8.9467e-17
192.00	1.9304e-02	7.0349e-16	2.9443e-16	1.9872e-16	1.0109e-16	8.9467e-17
193.00	1.9304e-02	5.8883e-16	2.5036e-16	1.5175e-16	8.5803e-17	7.5341e-17
194.00	1.5034e-02	5.8883e-16	2.5036e-16	1.5175e-16	8.5803e-17	7.5341e-17
195.00	1.5034e-02	5.1136e-16	2.2026e-16	1.2396e-16	7.5217e-17	6.6288e-17
196.00	1.1709e-02	5.1136e-16	2.2026e-16	1.2396e-16	7.5217e-17	6.6288e-17
197.00	1.1709e-02	3.8824e-16	1.7860e-16	8.8907e-17	5.5261e-17	4.9657e-17
198.00	9.1186e-03	3.8824e-16	1.7860e-16	8.8907e-17	5.5261e-17	4.9657e-17
199.00	9.1186e-03	2.8145e-16	1.4060e-16	7.0615e-17	4.4931e-17	4.2118e-17
200.00	7.1016e-03	2.8145e-16	1.4060e-16	7.0615e-17	4.4931e-17	4.2118e-17
201.00	7.1016e-03	2.2097e-16	1.1964e-16	5.6234e-17	3.6659e-17	3.3785e-17
202.00	5.5307e-03	2.2097e-16	1.1964e-16	5.6234e-17	3.6659e-17	3.3785e-17
203.00	5.5307e-03	1.7378e-16	1.0527e-16	4.4895e-17	2.9956e-17	2.7676e-17
204.00	4.3073e-03	1.7378e-16	1.0527e-16	4.4895e-17	2.9956e-17	2.7676e-17
205.00	4.3073e-03	1.3699e-16	9.5604e-17	3.5906e-17	2.4563e-17	2.2738e-17
206.00	3.3546e-03	1.3699e-16	9.5604e-17	3.5906e-17	2.4563e-17	2.2738e-17
207.00	3.3546e-03	1.0831e-16	8.9792e-17	2.8829e-17	2.0211e-17	1.8680e-17
208.00	2.6125e-03	1.0831e-16	8.9792e-17	2.8829e-17	2.0211e-17	1.8680e-17
209.00	2.6125e-03	8.5865e-17	8.7134e-17	2.3267e-17	1.6699e-17	1.5298e-17
210.00	2.0346e-03	8.5865e-17	8.7134e-17	2.3267e-17	1.6699e-17	1.5298e-17
211.00	2.0346e-03	6.8228e-17	8.7199e-17	1.8866e-17	1.3825e-17	1.2543e-17
212.00	1.5846e-03	6.8228e-17	8.7199e-17	1.8866e-17	1.3825e-17	1.2543e-17

Table A.4.1 Calculated neutron response of TLDs (5/5)
[(C/kg)/(n/cm^2)]

No.	Neutron Energy [MeV]	BeO	7LiF	MSO	SSO	BSO
213.00	1.5846e-03	5.4337e-17	8.9707e-17	1.5326e-17	1.1476e-17	1.0294e-17
214.00	1.2341e-03	5.4337e-17	8.9707e-17	1.5326e-17	1.1476e-17	1.0294e-17
215.00	1.2341e-03	4.3651e-17	9.4480e-17	1.2549e-17	9.5166e-18	8.4490e-18
216.00	9.6110e-04	4.3651e-17	9.4480e-17	1.2549e-17	9.5166e-18	8.4490e-18
217.00	9.6110e-04	3.2387e-17	1.0525e-16	9.6845e-18	7.2581e-18	6.3582e-18
218.00	5.8293e-04	3.2387e-17	1.0525e-16	9.6845e-18	7.2581e-18	6.3582e-18
219.00	5.8293e-04	2.1478e-17	1.2738e-16	6.7823e-18	4.9438e-18	4.2529e-18
220.00	3.5357e-04	2.1478e-17	1.2738e-16	6.7823e-18	4.9438e-18	4.2529e-18
221.00	3.5357e-04	1.4564e-17	1.5837e-16	4.8037e-18	3.3359e-18	2.8230e-18
222.00	2.1445e-04	1.4564e-17	1.5837e-16	4.8037e-18	3.3359e-18	2.8230e-18
223.00	2.1445e-04	1.0033e-17	1.9975e-16	3.3615e-18	2.2346e-18	1.8779e-18
224.00	1.3007e-04	1.0033e-17	1.9975e-16	3.3615e-18	2.2346e-18	1.8779e-18
225.00	1.3007e-04	6.9276e-18	2.5398e-16	2.3240e-18	1.4922e-18	1.2425e-18
226.00	7.8891e-05	6.9276e-18	2.5398e-16	2.3240e-18	1.4922e-18	1.2425e-18
227.00	7.8891e-05	4.7557e-18	3.2425e-16	1.5840e-18	9.9485e-19	8.1051e-19
228.00	4.7850e-05	4.7557e-18	3.2425e-16	1.5840e-18	9.9485e-19	8.1051e-19
229.00	4.7850e-05	3.2317e-18	4.1525e-16	1.0673e-18	6.5313e-19	5.2217e-19
230.00	2.9023e-05	3.2317e-18	4.1525e-16	1.0673e-18	6.5313e-19	5.2217e-19
231.00	2.9023e-05	2.1789e-18	5.3231e-16	7.1946e-19	4.2227e-19	3.3341e-19
232.00	1.7603e-05	2.1789e-18	5.3231e-16	7.1946e-19	4.2227e-19	3.3341e-19
233.00	1.7603e-05	1.4602e-18	6.8308e-16	4.7962e-19	2.7015e-19	2.1034e-19
234.00	1.0677e-05	1.4602e-18	6.8308e-16	4.7962e-19	2.7015e-19	2.1034e-19
235.00	1.0677e-05	9.8040e-19	8.7684e-16	3.1463e-19	1.7106e-19	1.3134e-19
236.00	6.4758e-06	9.8040e-19	8.7684e-16	3.1463e-19	1.7106e-19	1.3134e-19
237.00	6.4758e-06	6.4851e-19	1.1257e-15	2.0320e-19	1.0675e-19	8.1796e-20
238.00	3.9278e-06	6.4851e-19	1.1257e-15	2.0320e-19	1.0675e-19	8.1796e-20
239.00	3.9278e-06	4.2255e-19	1.4452e-15	1.2991e-19	6.6453e-20	5.0705e-20
240.00	2.3823e-06	4.2255e-19	1.4452e-15	1.2991e-19	6.6453e-20	5.0705e-20
241.00	2.3823e-06	2.7144e-19	1.8588e-15	8.1543e-20	4.1120e-20	3.1342e-20
242.00	1.4449e-06	2.7144e-19	1.8588e-15	8.1543e-20	4.1120e-20	3.1342e-20
243.00	1.4449e-06	1.7296e-19	2.3829e-15	5.1105e-20	2.5404e-20	1.9410e-20
244.00	8.7640e-07	1.7296e-19	2.3829e-15	5.1105e-20	2.5404e-20	1.9410e-20
245.00	8.7640e-07	1.0816e-19	3.0599e-15	3.1909e-20	1.5558e-20	1.1987e-20
246.00	5.3156e-07	1.0816e-19	3.0599e-15	3.1909e-20	1.5558e-20	1.1987e-20
247.00	5.3156e-07	6.1917e-20	4.3318e-15	1.7957e-20	8.5847e-21	6.7482e-21
248.00	3.2241e-07	6.1917e-20	4.3318e-15	1.7957e-20	8.5847e-21	6.7482e-21
249.00	3.2241e-07	2.4995e-20	6.8556e-15	7.0372e-21	3.3277e-21	2.6556e-21
250.00	1.0010e-11	2.4995e-20	6.8556e-15	7.0372e-21	3.3277e-21	2.6556e-21

Table A.4.2 TLD results for line source without assembly

Axial Position from target-side (mm)	BEO (C/kg/S)	error	LiF(C/kg/S)	error	SSO(C/kg/S)	error	MSO(C/kg/S)	error	BSO(C/kg/S)	error
200.00	5.4031e-18	4.3064e-19	1.0853e-17	1.0116e-18	5.2298e-18	6.8681e-19	6.0140e-18	8.1489e-19	3.5643e-18	1.2674e-18
400.00	5.6276e-18	5.8831e-19	1.1281e-17	1.1071e-18	5.8671e-18	1.3624e-18	6.0448e-18	5.8784e-19	2.9068e-18	6.2572e-19
600.00	5.9611e-18	5.8679e-19	1.2610e-17	4.7842e-19	6.2841e-18	9.0368e-19	7.2023e-18	4.9548e-19	3.5091e-18	6.4016e-19
800.00	6.3796e-18	2.4568e-19	1.2917e-17	4.3465e-19	5.8374e-18	2.1831e-19	6.8684e-18	7.5486e-19	4.1494e-18	8.4355e-19
900.00	5.9551e-18	3.1694e-19	1.2066e-17	6.2697e-19	5.6901e-18	1.1539e-18	6.3912e-18	3.1268e-19	3.2571e-18	1.2031e-18
1000.0	5.4139e-18	6.8230e-19	1.2878e-17	5.0495e-19	6.4114e-18	3.1425e-19	6.3026e-18	4.6585e-19	2.9068e-18	2.0581e-19
1100.0	5.2001e-18	5.6557e-19	1.1844e-17	4.4128e-19	5.3745e-18	6.2564e-19	6.0794e-18	5.9400e-19	2.3582e-18	5.8111e-19
1200.0	4.1010e-18	1.2895e-19	1.1842e-17	8.8296e-19	5.0450e-18	5.0052e-19	6.2526e-18	4.6469e-19	2.8149e-18	6.6378e-19
1400.0	4.4330e-18	2.9875e-19	1.1616e-17	4.0149e-19	5.1507e-18	3.6984e-19	5.5753e-18	1.0612e-18	2.7440e-18	1.0968e-18
1600.0	4.0115e-18	3.0481e-19	1.0961e-17	5.4341e-19	6.0863e-18	1.1678e-18	6.7721e-18	1.1719e-19	3.0117e-18	1.2110e-18
1800.0	3.8159e-18	8.4603e-19	1.0482e-17	5.6861e-19	4.6669e-18	9.1897e-19	5.1674e-18	1.9762e-19	3.2492e-18	1.5338e-18
2000.0	2.4940e-18	1.4866e-19	7.5640e-18	5.6861e-19	3.2524e-18	5.3806e-19	4.5112e-18	3.7233e-19	2.2231e-18	8.5930e-19

Radial Position (mm)	BEO (C/kg/S)	error	LiF(C/kg/S)	error	SSO(C/kg/S)	error	MSO(C/kg/S)	error	BSO(C/kg/S)	error
419.00	2.3272e-18	3.3210e-19	6.4485e-18	3.9220e-19	2.9396e-18	3.1285e-19	3.9182e-18	5.0626e-19	1.6785e-18	5.6142e-19
619.00	1.1536e-18	6.5731e-20	3.6578e-18	2.9936e-19	1.8080e-18	1.2795e-19	1.9571e-18	1.3681e-19	1.2581e-18	3.0816e-19

Table A.4.3 TLD results for the reference test blanket

Position from target-side surface (mm)	BEO (C/kg/S)	error	LiF(C/kg/S)	error	SSO(C/kg/S)	error	MSO(C/kg/S)	error	BSO(C/kg/S)	error
2013.5	1.9509e-17	8.1416e-19	1.3103e-17	3.8776e-19	9.6566e-18	7.7958e-19	1.2005e-17	3.2007e-19	1.3031e-17	3.3749e-18
1963.5	2.5336e-17	3.5080e-19	1.6351e-17	2.7550e-19	1.0967e-17	2.7788e-19	1.5728e-17	7.3626e-19	1.3978e-17	1.7213e-18
1809.5	2.4962e-17	5.8248e-19	2.1730e-17	2.7079e-18	1.6979e-17	1.6996e-18	1.9099e-17	1.7078e-19	1.6101e-17	3.0355e-18
1759.5	3.3766e-17	1.7943e-18	2.2136e-17	5.2497e-19	1.7895e-17	2.2062e-18	1.9619e-17	4.4221e-19	1.4771e-17	1.2045e-18
1605.5	3.1164e-17	3.0240e-18	2.2790e-17	7.5885e-19	1.9006e-17	1.3080e-19	2.1894e-17	4.9650e-19	1.5931e-17	8.7593e-19
1555.5	3.3552e-17	2.7923e-18	2.3835e-17	1.8191e-18	1.9169e-17	1.1440e-18	2.3432e-17	1.1434e-18	2.1037e-17	8.2648e-18
1401.5	3.2554e-17	2.4716e-18	2.5036e-17	3.5346e-19	2.0330e-17	1.8794e-18	2.4378e-17	4.0602e-19	2.0914e-17	7.4781e-18
1351.5	2.8527e-17	4.4497e-18	2.8170e-17	1.3825e-18	2.0003e-17	1.7487e-18	2.0958e-17	3.8340e-19	2.4292e-17	5.0871e-18
1251.5	2.5675e-17	3.1488e-18	2.5644e-17	1.7567e-18	2.0084e-17	1.9617e-19	2.1528e-17	5.5531e-19	1.9140e-17	1.3387e-18
1197.5	2.8170e-17	3.1666e-18	2.4396e-17	2.3337e-18	1.8516e-17	1.4382e-18	2.4640e-17	4.9650e-19	2.7778e-17	5.5345e-18
1097.5	3.1859e-17	7.9634e-19	2.4396e-17	1.7100e-18	2.0019e-17	2.2226e-18	2.4066e-17	7.0007e-19	1.4657e-17	4.9491e-19
1047.5	2.7101e-17	5.1091e-18	2.5316e-17	3.3787e-19	2.1441e-17	1.9938e-18	2.4799e-17	4.2412e-19	1.6826e-17	3.1589e-18
944.00	2.8330e-17	1.3844e-18	2.4100e-17	4.4701e-19	2.1049e-17	7.8448e-19	2.1532e-17	1.6953e-18	2.9922e-17	----------
894.00	2.6691e-17	1.8834e-18	2.7780e-17	7.2767e-19	1.8058e-17	4.2496e-19	2.2071e-17	6.2210e-20	2.0019e-17	1.5392e-18
790.00	2.7457e-17	2.4894e-18	2.5644e-17	7.9004e-19	1.9447e-17	1.0296e-18	1.9587e-17	1.4782e-18	1.9834e-17	1.8632e-18
740.00	2.4927e-17	2.4181e-18	2.4038e-17	9.1477e-19	2.1931e-17	4.0862e-19	2.1419e-17	5.7567e-19	----------	----------
577.00	2.3127e-17	1.9041e-19	2.3523e-17	4.6260e-19	1.8385e-17	2.2885e-19	2.2252e-17	1.7767e-18	2.3212e-17	6.9536e-18
537.00	2.9489e-17	3.7012e-18	2.4396e-17	1.3514e-18	1.9954e-17	1.6348e-19	2.2098e-17	---------	2.7115e-17	4.4238e-18
280.00	2.2129e-17	8.3198e-19	2.0857e-17	1.0863e-18	1.7878e-17	2.5821e-18	1.8293e-17	4.6936e-19	1.3761e-17	1.5778e-18
230.00	2.2093e-17	2.3468e-18	2.0904e-17	5.2497e-19	1.4760e-17	1.6637e-18	1.8189e-17	3.2459e-19	1.5115e-17	5.8877e-18
76.000	1.3332e-17	5.6110e-19	1.5535e-17	1.1221e-18	1.2279e-17	7.8285e-19	1.2358e-17	1.2447e-20	7.5953e-18	2.6045e-19
26.000	1.1528e-17	8.4980e-19	1.1530e-17	3.1604e-19	1.0122e-17	7.9756e-19	1.0268e-17	7.9507e-19	8.8818e-18	3.3680e-19

radial position = 220.25 mm

Radial position (mm)	BEO (C/kg/S)	error	LiF(C/kg/S)	error	SSO(C/kg/S)	error	MSO(C/kg/S)	error	BSO(C/kg/S)	error
227.75	1.8921e-17	2.1508e-18	2.1278e-17	4.7820e-19	1.8597e-17	1.7356e-18	1.7167e-17	1.4737e-18	1.8816e-17	6.8456e-18
252.75	1.8083e-17	1.8834e-18	1.5992e-17	6.1852e-19	1.4379e-17	6.9787e-19	1.3290e-17	8.7379e-19	1.2152e-17	8.2965e-19
327.75	7.1871e-18	7.4822e-19	8.8605e-18	3.6437e-19	9.6190e-18	9.6588e-18	7.8840e-18	7.4079e-19	1.0486e-17	2.0683e-18

Table A.4.4 TLD results for the armor blanket

Radial Position	Axial Position (mm)	BeO(C/kg/S)	error	^{7}LiF(C/kg/S)	error	MSO(C/kg/S)	error	SSO(C/kg/S)	error	BSO(C/kg/S)	error
D1 227.75	993.5	8.1114e-17	1.15e-17	7.0208e-17	7.09e-18	4.7543e-17	5.11e-18	5.0956e-17	7.47e-18	5.0300e-17	5.21e-18
D2 252.75	993.5	6.5335e-17	7.61e-18	5.5807e-17	6.41e-18	3.6329e-17	4.57e-18	4.0993e-17	5.20e-18	5.2201e-17	7.23e-18
D3 327.75	993.5	3.1004e-17	3.48e-18	2.8400e-17	3.07e-18	2.0563e-17	2.22e-18	2.5283e-17	3.30e-18	3.6406e-17	1.05e-17
D4 377.75	993.5	1.9420e-17	2.56e-18	2.0512e-17	2.39e-18	1.3782e-17	1.47e-18	1.9842e-17	2.38e-18	2.4455e-17	3.09e-18
F1 212.75	110.00	9.3128e-17	1.22e-17	6.7840e-17	8.40e-18	4.5408e-17	6.19e-18	4.6501e-17	5.14e-18	4.5245e-17	7.11e-18
F2 212.75	510.00	1.2908e-16	2.07e-17	9.5591e-17	1.03e-17	6.7417e-17	9.05e-18	6.2684e-17	9.45e-18	7.2298e-17	1.35e-17
F3 212.75	1010.0	1.2076e-16	1.30e-17	1.0075e-16	1.17e-17	6.3148e-17	6.72e-18	6.8050e-17	9.01e-18	7.2736e-17	1.20e-17
F4 212.75	1510.0	1.1304e-16	1.20e-17	1.0318e-16	1.08e-17	6.2995e-17	7.23e-18	7.2155e-17	8.22e-18	5.8936e-17	8.34e-18
S1 220.25	493.50					5.7555e-17	7.22e-18	5.2096e-17	6.76e-18	6.0584e-17	8.25e-18
S2 220.25	993.50					6.0860e-17	6.18e-18	5.3726e-17	6.26e-18	5.5547e-17	8.40e-18
S3 220.25	1493.5					6.0579e-17	6.52e-18	5.4199e-17	5.52e-18	5.5024e-17	1.04e-17

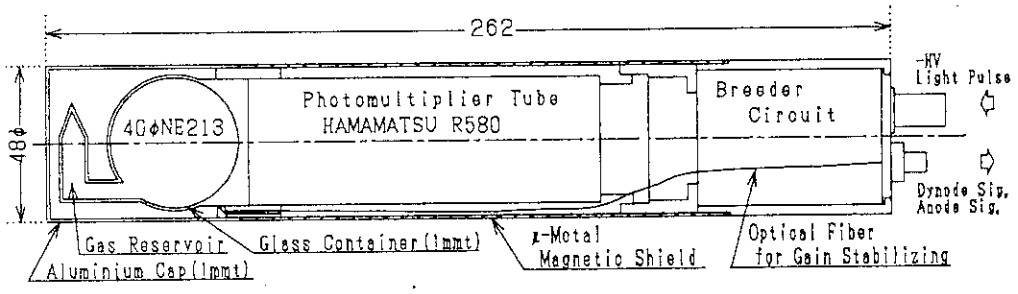

Fig. A.4.1 Cross sectional drawing of 40 mm-diameter spherical NE213 detector

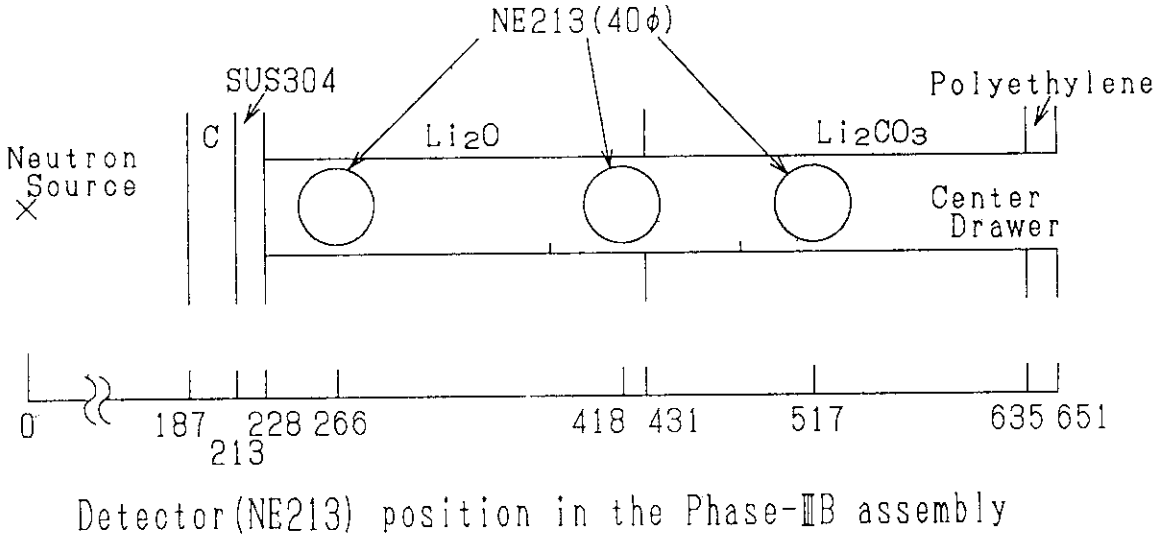

Fig. A.4.2 Detector position for gamma-ray spectrum measurement

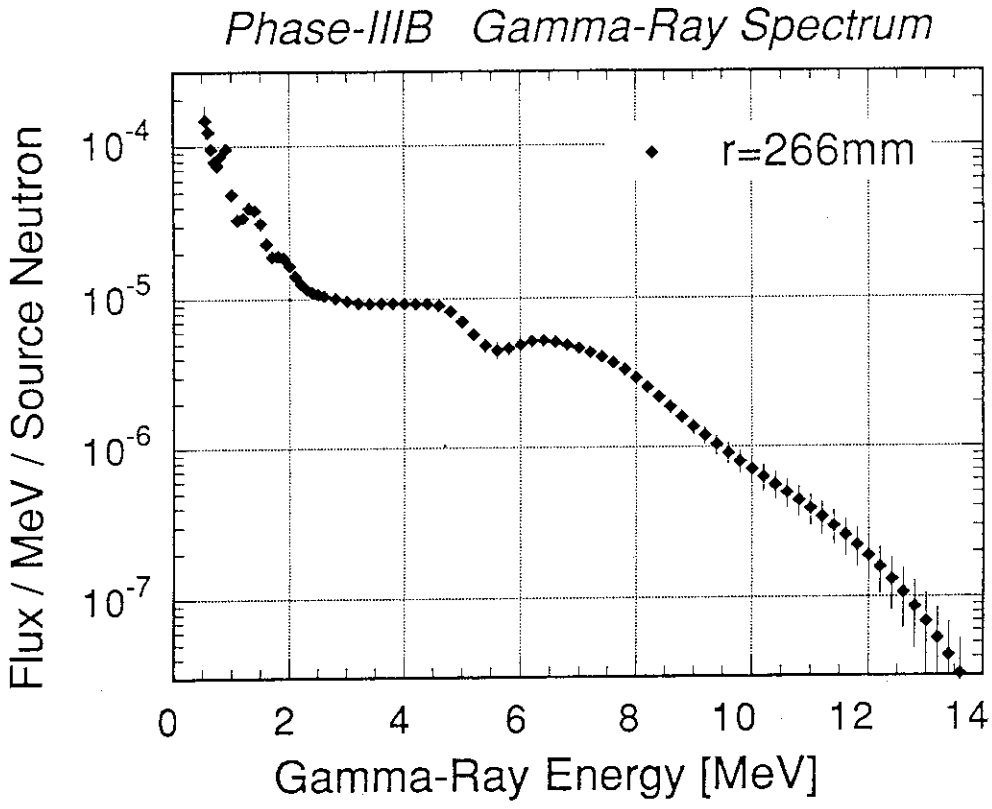

Fig. A.4.3 Measured gamma-ray spectrum at 266 mm distance from the line source in the B drawer (Phase IIIB)

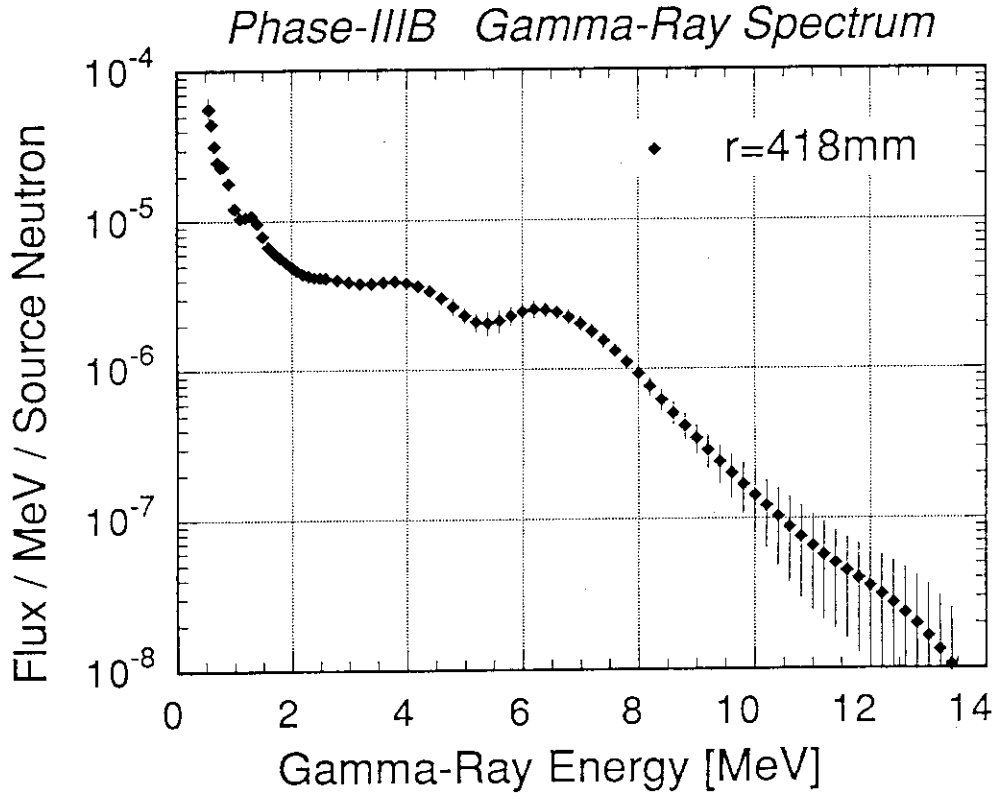

Fig. A.4.4 Measured gamma-ray spectrum at 418 mm distance from the line source in the B drawer (Phase IIIB)

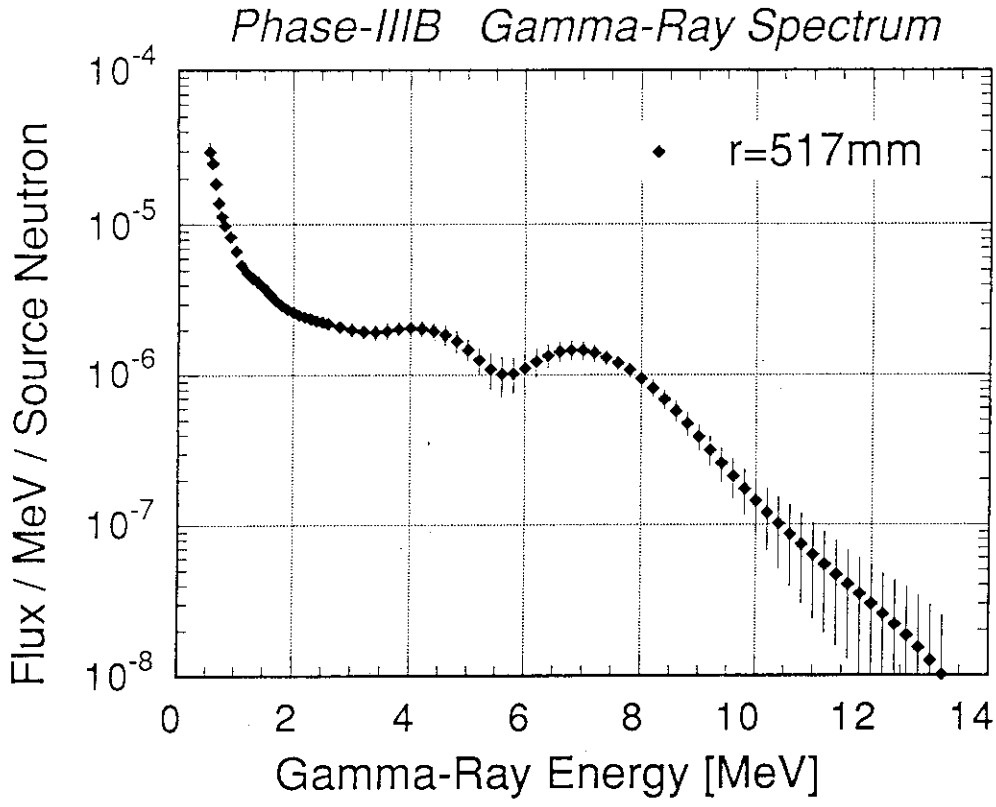

Fig. A.4.5 Measured gamma-ray spectrum at 517 mm distance from the line source in the B drawer (Phase IIIB)

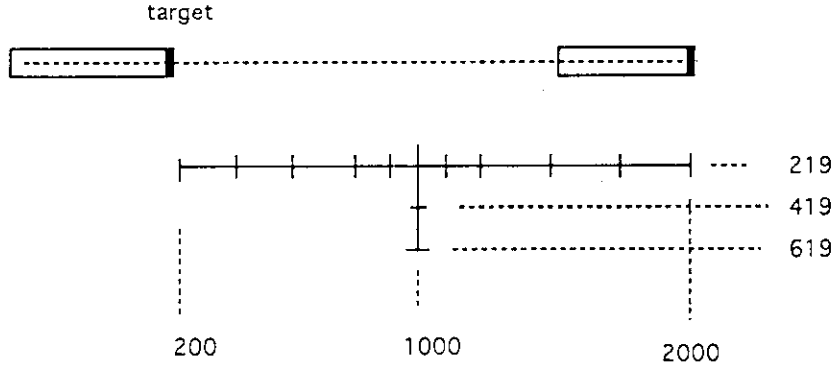

Fig. A.4.6 Positions of TLDs in gamma-ray exposure dose measurement without assembly (unit in mm)

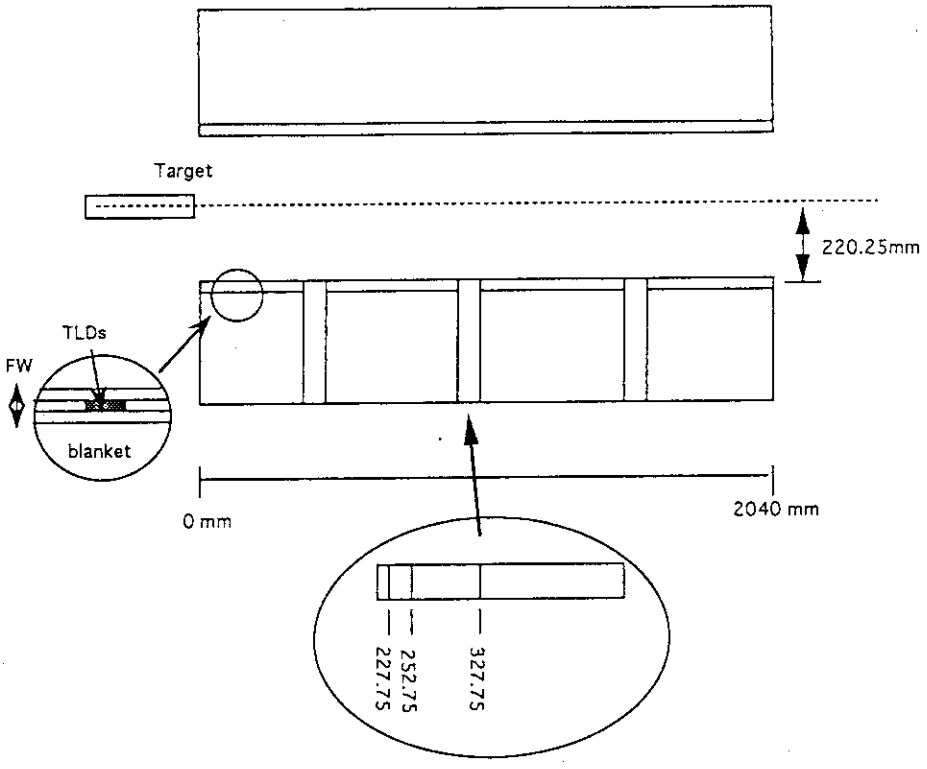

Fig. A.4.7 Positions of TLDs in gamma-ray exposure dose measurement Phase IIIA assembly (unit in mm)

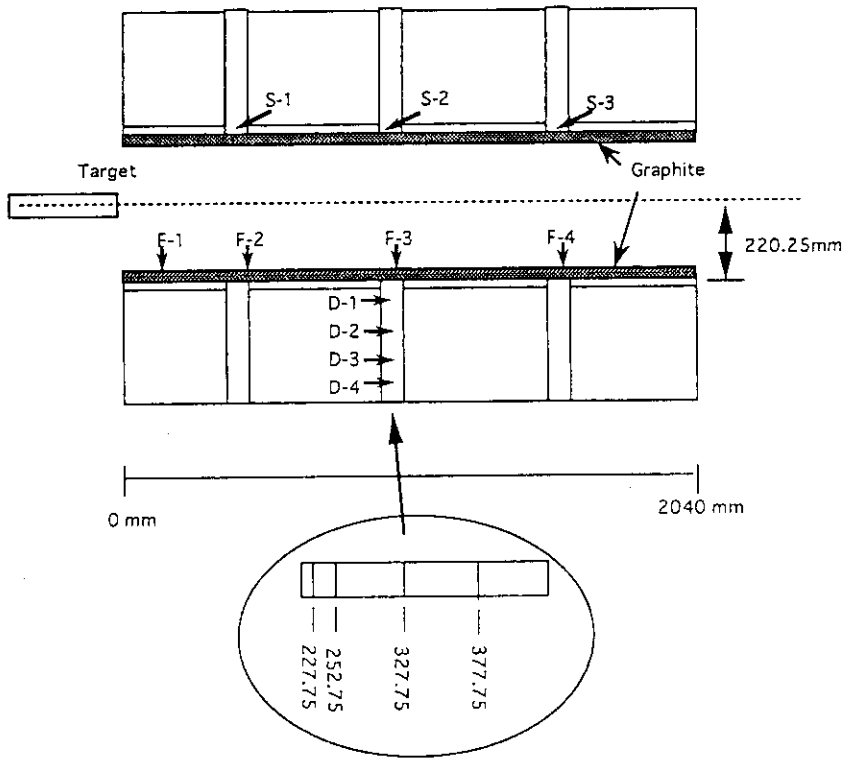

Fig. A.4.8 Positions of TLDs in gamma-ray exposure dose measurement Phase IIIB assembly (unit in mm)

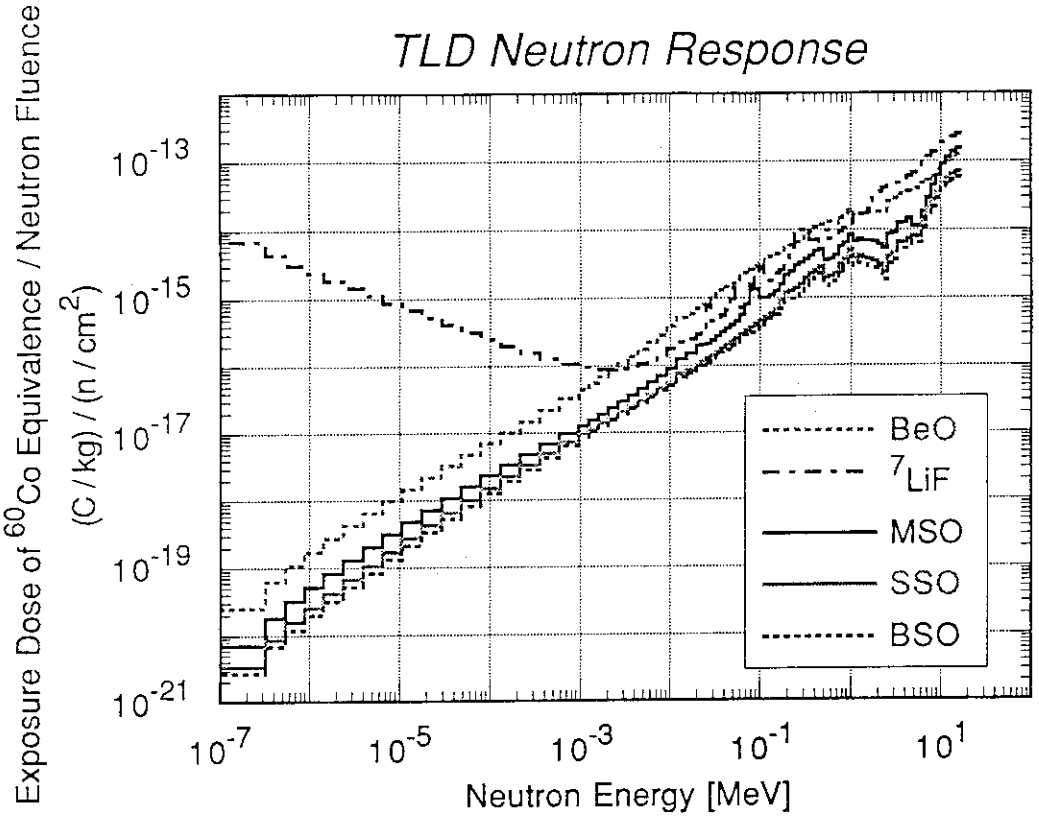

Fig. A.4.9 Neutron response calculated for various TL detectors

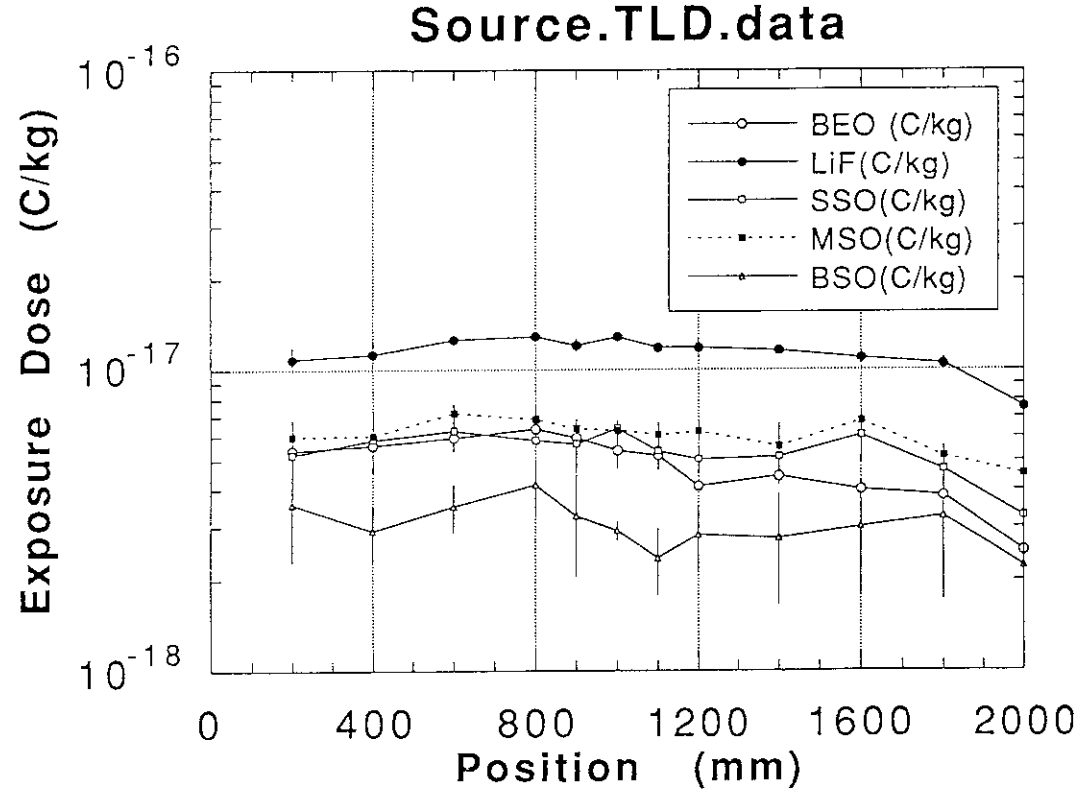

Fig. A.4.10 Exposure dose distributions measured by various TLDs for the line source without assembly

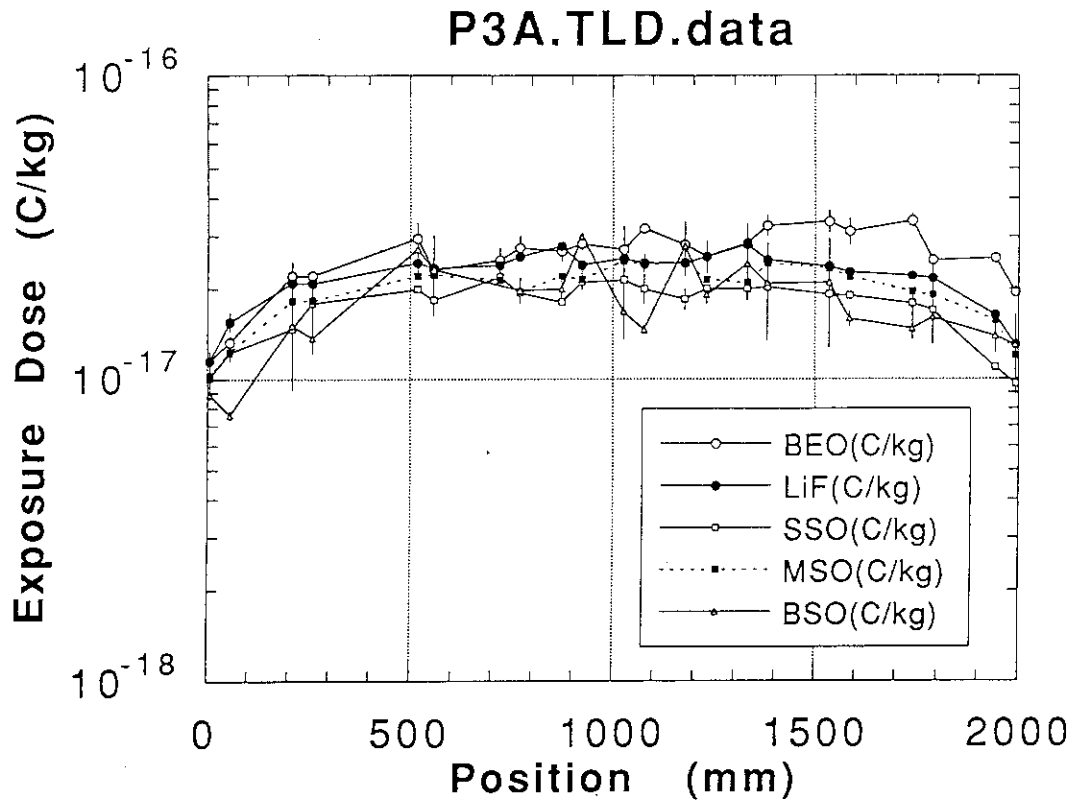

Fig. A.4.11 Exposure dose distributions measured by various TLDs for the Phase IIIA assembly

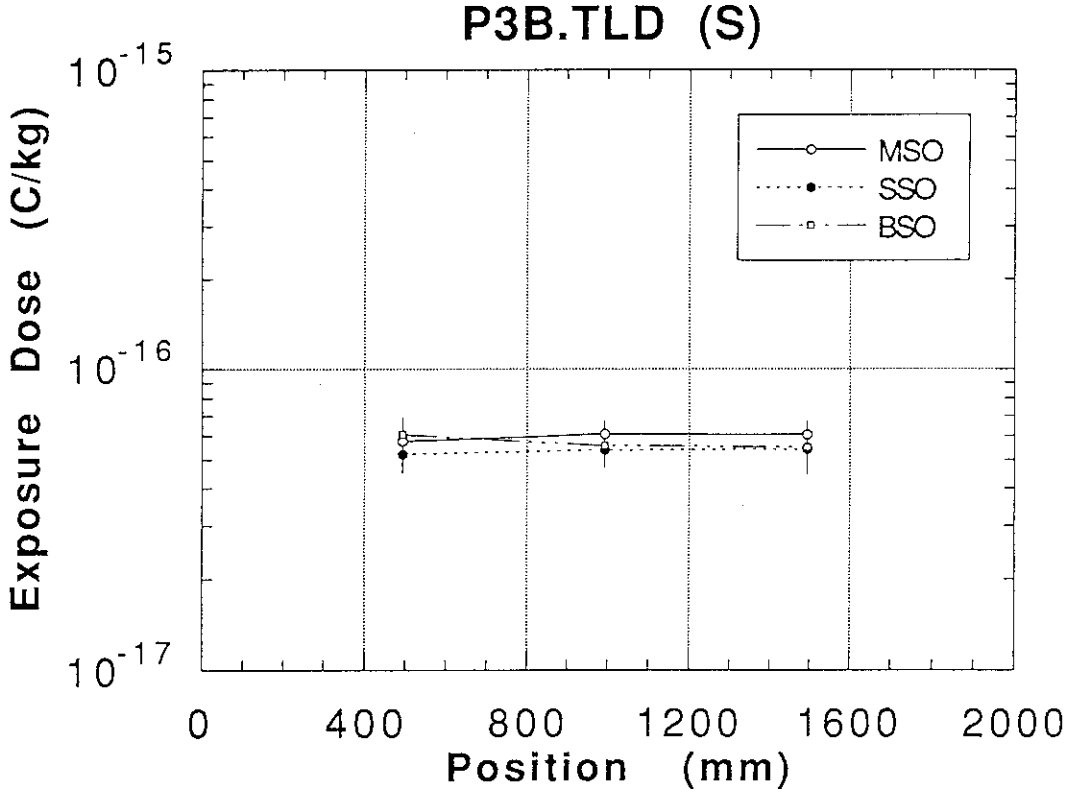

Fig. A.4.12 Exposure dose distributions measured by various TLDs for the Phase IIIA assembly